Beating ADKH-*RRAGD*:

The role of the mTORC1 signaling pathway, and therapeutic perspectives

Anastasia Adella

RADBOUD UNIVERSITY PRESS

Radboud Dissertation Series

Beating ADKH-*RRAGD*:

The role of the mTORC1 signaling pathway, and therapeutic perspectives

Anastasia Adella

Beating ADKH-*RRAGD*: The role of the mTORC1 signaling pathway, and therapeutic perspectives
Anastasia Adella

Radboud Dissertation Series
ISSN: 2950-2772 (Online); 2950-2780 (Print)

Published by RADBOUD UNIVERSITY PRESS
Postbus 9100, 6500 HA Nijmegen, The Netherlands
www.radbouduniversitypress.nl

Design: Proefschrift AIO | Annelies Lips
Cover: Anastasia Audrey & Sergio Hector
Printing: DPN Rikken/Pumbo

ISBN: 9789465151229
DOI: 10.54195/9789465151229
Free download at: https://doi.org/10.54195/9789465151229

RADBOUD
UNIVERSITY
PRESS

Beating ADKH-*RRAGD*:

The role of the mTORC1 signaling pathway, and therapeutic perspectives

Proefschrift

ter verkrijging van de graad van doctor

aan de Radboud Universiteit Nijmegen

op gezag van de rector magnificus prof. dr. J.M. Sanders,

volgens besluit van het college voor promoties

in het openbaar te verdedigen op

maandag 20 oktober 2025

om 12.30 uur precies

door

Anastasia Adella

geboren op 7 september 1996

te Jakarta, Indonesië

Promotoren:
Prof. dr. J.G.J. Hoenderop
Dr. J.H.F. de Baaij

Copromotor:
Dr. P.A. Leermakers

Manuscriptcommissie:
Prof. dr. R. Nijveldt
Prof. dr. J. van der Velden (Amsterdam UMC)
Dr. B. Smeets

Beating ADKH-*RRAGD*:

The role of the mTORC1 signaling pathway, and therapeutic perspectives

Dissertation

to obtain the degree of doctor

from Radboud University Nijmegen

on the authority of the Rector Magnificus prof. dr. J.M. Sanders,

according to the decision of the Doctorate Board

to be defended in public on

Monday, October 20, 2025

at 12:30 pm

by

Anastasia Adella

born on September 7, 1996

in Jakarta, Indonesia

PhD supervisors:
Prof. dr. J.G.J. Hoenderop
Dr. J.H.F. de Baaij

PhD co-supervisor:
Dr. P.A. Leermakers

Manuscript Committee:
Prof. dr. R. Nijveldt
Prof. dr. J. van der Velden (Amsterdam UMC)
Dr. B. Smeets

Table of contents

CHAPTER 1

General introduction

Partly adapted from:
mTOR signaling in renal ion transport

Anastasia Adella[1] and Jeroen H.F. de Baaij[1]

[1] Department of Medical BioSciences, Radboudumc, Nijmegen, The Netherlands

Acta Physiologica, 2023

A key player in intracellular nutrient sensing

The ability of cells to sense and integrate nutrients is key to their survival. In 1964, dr. Suran Sehgal and his team identified a novel compound from the soil bacteria *Streptomyces hygroscopicus* on Easter Island. This compound, named rapamycin, possesses anti-fungal, anti-tumor, and immunosuppressive properties.[1] Three decades later, in 1994, the mechanistic target of rapamycin (mTOR) was discovered as a direct target of this compound. To achieve its inhibitory effect, rapamycin has to be in complex with the 12-kilo Dalton FK506-binding protein (FKBP12).[2-4] Ever since, mTOR has been extensively characterized as a nutrient sensor due to its ability to integrate various intra- and extracellular cues, and its roles in critical cellular processes like cell growth, metabolism, and survival were established.[5] Due to this central role, dysregulation of mTOR activity is associated with the development of many diseases, such as different types of cancer, neurodegenerative diseases, and metabolic diseases.

mTOR complexes

mTOR is an evolutionary conserved serine-threonine kinase, which forms the catalytic subunit of two functionally distinct multiprotein complexes: 1) mTOR complex 1 (mTORC1) is the rapamycin-sensitive protein complex characterized by the adapter protein called Raptor, and 2) mTORC2 is the largely insensitive to rapamycin protein complex and contains the adapter protein Rictor that binds the mitogen-activated protein kinase (MAPK)-stress-activated protein kinase-interacting protein 1 (Sin1) (Figure 1).[2-4,6-11] In addition to their respective defining adapter proteins, mTORC1 and 2 also consist of the mammalian lethal SEC13 protein 8 (mLST8) that directly binds the kinase domain of mTOR and, thus, may be the stabilizing factor of this domain.[12] In addition to mTOR, Raptor, and mLST8, two endogenous inhibiting subunits proline-rich Akt substrate of 40-kilo Dalton (PRAS40) and DEP domain containing mTOR interacting protein (DEPTOR) make up mTORC1.[13,14] In mTORC2, DEPTOR and protein observed with RICTOR 1 and 2 (Protor1/2) are found in addition to the three core subunits (i.e., mTOR, Rictor, and mLST8).[15] To function, mTORC1 and -2 respond to different upstream signals; mTORC1 is sensitive to nutrients, growth factors, and stress, while mTORC2 is activated by phosphoinositide 3 kinases (PI3Ks) and protein kinase B (Akt) signaling in response to insulin and growth factor signaling (Figure 1).

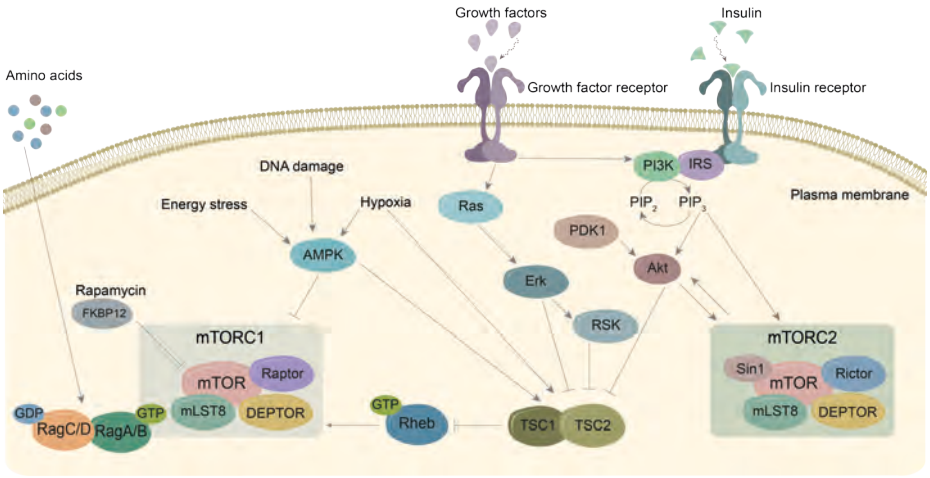

Figure 1. mTOR signaling in the cell. mTOR constitutes the kinetic subunit of two multimeric protein complexes: mTORC1 and mTORC2. mTORC1 is sensitive to stimulation by various nutrients and stress while mTORC2 is largely activated through insulin/PI3K signaling. 12-kDa FK506-binding protein (FKBP12), 5′ adenosine monophosphate-activated protein kinase (AMPK), DEP domain containing mTOR interacting protein (DEPTOR), extracellular signal-regulated kinase (Erk), insulin receptor substrate (IRS), mammalian lethal with SEC13 protein 8 (mLST8), mechanistic target of rapamycin (mTOR), mTOR complex 1 (mTORC1), mTOR complex 2 (mTORC2), phosphatidylinositol-3, 4, 5-triphosphate (PIP_3), phosphatidylinositol-4, 5-bisphosphate (PIP_2), phosphoinositide-3-kinase (PI3K), protein kinase B (Akt), pyruvate dehydrogenase kinase 1 (PDK1), rapamycin-insensitive companion of mTOR (Rictor), RAS homologue enriched in brain (Rheb), Ras-related GTP binding proteins (Rag) A-D, regulatory-associated protein of mTOR (Raptor), ribosomal s6 kinase (RSK), stress, activated protein kinase-interacting protein 1 (Sin1), tuberous sclerosis complex 1 (TSC1), tuberous sclerosis complex 1 (TSC2).

mTOR signaling

mTORC1 activation is triggered by growth factor- and nutrient-abundant states such as amino acids and insulin (Figure 1). Nutrient-depleted state, DNA damage, energy stress, and hypoxia, on the other hand, inhibit mTORC1 activation. Amino acid sensing plays an important part in mTORC1 recruitment to the lysosomal surface via the Ras-related guanine triphosphate (GTP) binding proteins (Rag GTPases; RagA-D).[16,17] Growth factors (e.g. IGF-1 and insulin) have a dual role in the regulation of mTORC1 as they can induce nutrient uptake and could directly stimulate mTORC1 via the PI3K pathway that enhances Akt signaling. This, in turn, dampens the inhibition of the GTPase RAS homolog enriched in the brain (Rheb) by the tuberous sclerosis complex (TSC) 1 and 2.[18,19] Rheb is a well-known allosteric activator of the mTORC1 that resides on the lysosomal surface.[20,21] Ultimately, mTORC1 integrates these stimuli to exert its main role in controlling cell growth and metabolism (Figure 2).

To sustain cell growth and metabolism, mTORC1 promotes anabolic activities such as nucleotide, protein, and lipid synthesis via Lipin1, sterol regulatory element binding proteins (SREBPs), S6 kinase (S6K), eukaryotic initiation factor 4E-binding protein 1 (4E-BP1), and Lipin1. Moreover, it inhibits catabolic activities such as autophagy via Unc-51 like autophagy activating kinase 1 (ULK1) and transcription factor EB (TFEB) (Figure 2).[22-28] TFEB is known as the master regulator of lysosomal biogenesis via transcription regulation of the Coordinated Lysosomal Expression and Regulation (CLEAR) network.[29-31] More recently, two distinct mTORC1 signaling pathways have been established: the canonical pathway that involves the activation of cytoplasmic targets such as S6K and 4E-BP1, and the non-canonical pathway, which involves mTORC1 lysosomal targets such as TFEB (reviewed in [32]). How and when the two distinct mTORC1 pathways are activated will be discussed in the later sections.

Unlike the extensive characterization of mTORC1, far less is known about the regulation and effectors of mTORC2, which can largely be attributed to the lack of mTORC2-specific inhibitors. Based on most recent studies, mTORC2 localizes to multiple subcellular compartments where it is differentially regulated based on its localization (discussed in more detail elsewhere [33]). The most well-characterized activator of mTORC2 at the plasma membrane is insulin through the PI3K pathway (Figure 1). Upon stimulation by growth factors, PI3K phosphorylates phosphatidylinositol-4, 5-bisphosphate (PIP_2) at the plasma membrane, producing phosphatidylinositol-3, 4, 5-triphosphate (PIP_3). PIP_3 co-recruits Akt and mTORC2 to the plasma membrane and directly releases autoinhibition of mTORC2 to stimulate Akt phosphorylation.[34,35] mTORC2 is known to phosphorylate Akt at the Ser473 site, which, together with PDK1-dependent phosphorylation of Akt at Thr308, strengthens Akt activation.[36,37] On the other hand, Angiotensin II drives mTORC2 activity to specifically phosphorylate the Ser442 site of serum and glucocorticoid-induced protein kinase 1 (SGK1) at a perinuclear compartment.[38] Other than Akt and SGK1, other mTORC2 targets that have been identified include members of the A, G, and C (AGC) kinases, such as protein kinase Cα (PKCα) and SGK3.[8,9,39,40] Through these substrates, the role of mTORC2 in regulating cell survival, cytoskeleton dynamics, and sodium and potassium homeostasis has been established (Figure 3).

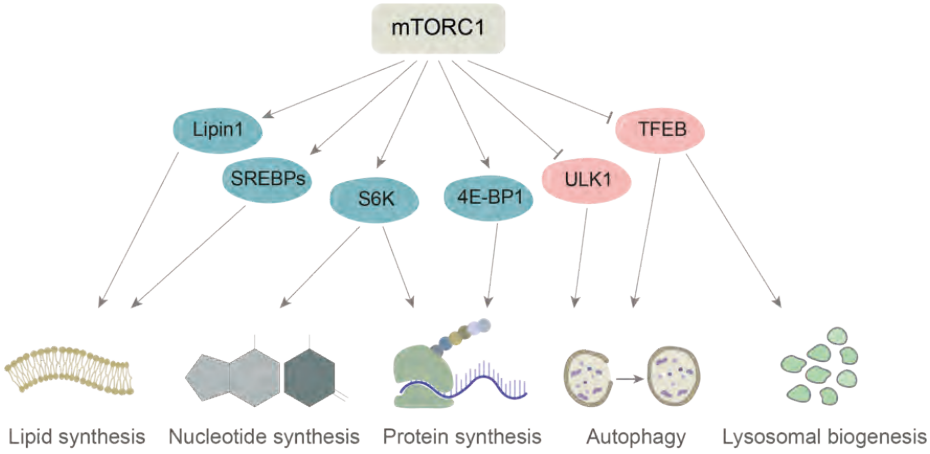

Figure 2. Downstream mTORC1 signaling. Upon activation, mTORC1 phosphorylates its downstream targets. Through this, mTORC1 activates anabolic activities (in blue) and inhibits catabolic activities (in red) to support cell growth and proliferation. Eukaryotic translation initiation factor 4E binding protein 1 (4E-BP1), mechanistic target of rapamycin complex 1 (mTORC1), ribosomal S6 kinase (S6K), sterol regulatory element binding proteins (SREBPs), transcription factor EB (TFEB), Unc-51-like autophagy activating kinase 1 (ULK1).

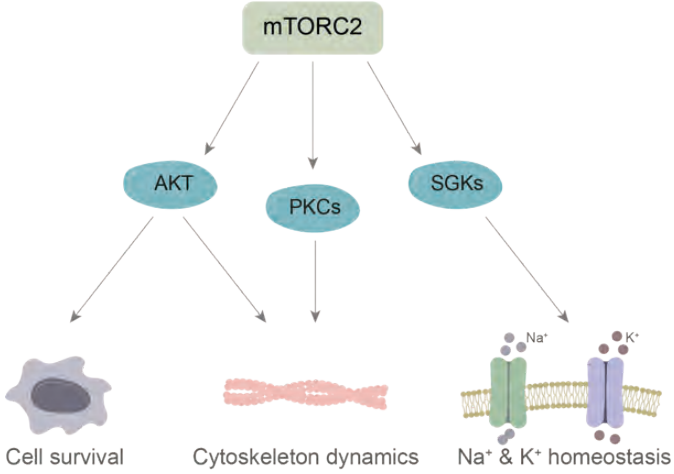

Figure 3. Downstream mTORC2 signaling. mTORC2 mainly regulates cell survival, structure and movement through cytoskeleton dynamics, and Na^+ and K^+ homeostasis via its downstream target kinases. Protein kinase B (Akt), mechanistic target of rapamycin complex 2 (mTORC2), protein kinases (PKCs), serum and glucocorticoid-induced protein kinases (SGKs).

The Rag GTPases

Interestingly, extensive recent studies into mTORC1 have changed the view on how this protein complex behaves. Originally, mTORC1 is thought to target its downstream substrates unselectively. Instead, different cues, such as specific Rag GTPases dimerization, can determine the substrate specificity of mTORC1 in a selective manner,[41,42] indicating that a delicate balance of upstream signals is needed to drive mTORC1 activity.

In mammals, four members of the Rag GTPases are present: RagA-D (Figure 4). In *Drosophila melanogaster, Caenorhabditis elegans*, and *Saccharomyces cerevisiae*, only two copies of these genes (i.e., Gtr1 and Gtr2) are found. Each Rag protein consists of a GTP-binding domain and a C-terminal roadblock domain. These Rag GTPases are tethered to the lysosomal surface through a pentameric protein complex called Ragulator (Figure 4).[43,44] Together, RagA-D work as an intracellular amino acid sensor that ultimately supports the recruitment of mTORC1 to the lysosomal surface.

In the presence of amino acids, RagA and RagB bind GTP while RagC and RagD bind GDP, subsequently forming heterodimers between RagA/B and RagC/D (Figure 4).[45-47] These heterodimers recruit mTORC1 to the lysosomal surface.[48,49] The nucleotide-binding of the Rag GTPases depends on the activity of their respective guanosine-nucleotide exchange factor (GEF) and GTPase-activating protein (GAP) activities. Leucine and arginine abundance blocks the inhibition of the GAP towards TOR (GATOR) complex 2 (GATOR2) by Sestrin2 and cellular arginine sensor of mTORC1 (CASTOR1).[50] This allows GATOR2 to inhibit GATOR complex 1 (GATOR1), a GAP for RagA/B that promotes GTP hydrolysis to GDP. RagA/B is activated by a protein complex called Ragulator, which acts as a GEF towards RagA/B by converting $RagA/B^{GDP}$ to the active $RagA/B^{GTP}$ conformation. This activation is promoted by the vacuolar H^+-ATPase (V-ATPase).[43,51] To regulate RagC/D activity, the folliculin (FLCN) forms a complex with FLCN-interacting protein (FNIP) 1 or 2. FLCN-FNIP acts as a GAP towards RagC/D and not towards RagA/B, converting $RagC/D^{GTP}$ to their active $RagC/D^{GDP}$ form under an amino acids-rich state.[52,53]

Not two peas in a pod

Initially, due to high structural similarities between RagA and RagB, as well as between RagC and RagD, these pairs are thought to be functionally redundant and are used interchangeably in experimental works. However, recent studies have demonstrated that Rag GTPases are not identical and that the presumed dimer coding does not switch mTORC1 activity in an all-or-none manner.[41,42] Instead,

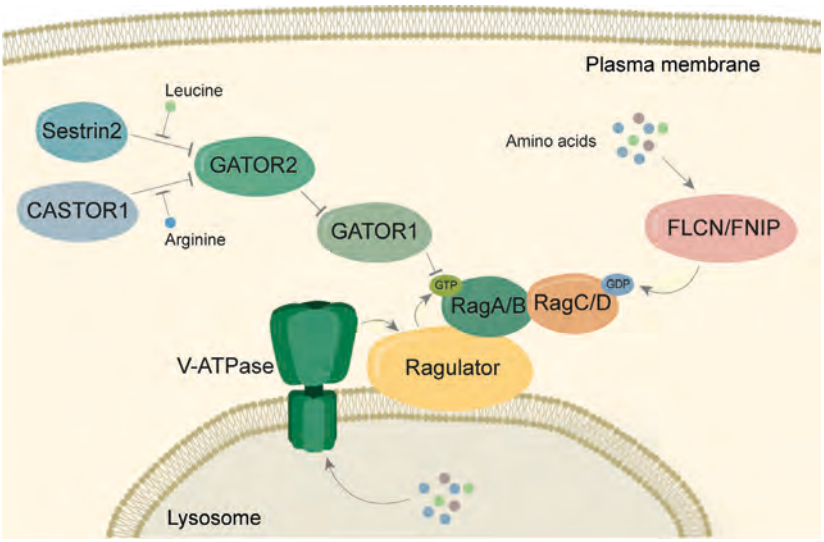

Figure 4. Regulation of Rag GTPases. Rag GTPases serve as intracellular amino acids sensors. Upon amino acids availability, a series of upstream signaling activities convert the nucleotide binding state of Rag GTPases to their active conformation (i.e., RagA/B to GTP, while RagC/D become GDP-binding). Cytosolic arginine sensor for mTORC1 subunit 1 (CASTOR1), folliculin (FLCN), folliculin interacting protein (FNIP), GTPase-activating protein (GAP) towards TOR complex 1(GATOR1), GATOR 2 (GATOR2), Ras-related GTPase A-D (RagA-D), vacuolar H^+-ATPase (V-ATPase).

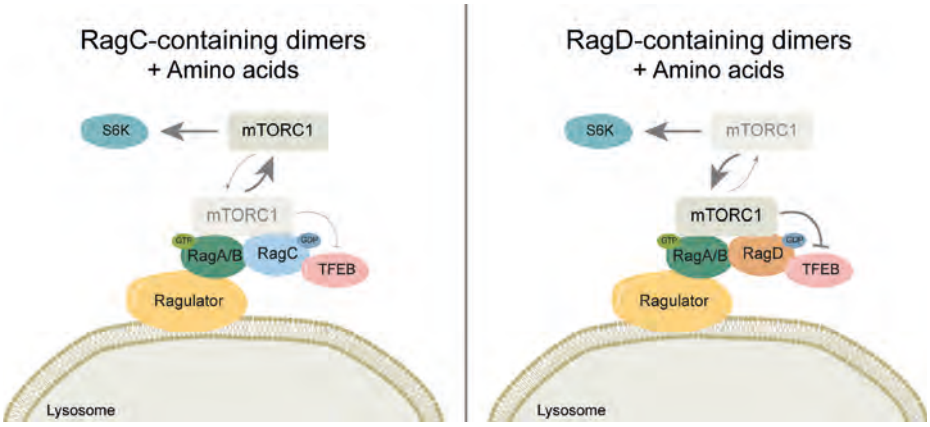

Figure 5. mTORC1 signaling specificity depends on Rag GTPase dimer coding. In nutrient-rich conditions where RagA/B is bound to GTP and RagC/D is bound to GDP, mTORC1 is recruited and activated. In dimers containing RagA/B and RagC, mTORC1 is activated but localized less to the lysosome. Here, cytosolic substrates of mTORC1 such as S6K is favored over lysosomal substrates such as TFEB. In dimers containing RagA/B and RagD, on the other hand, recruits mTORC1 to the lysosomal surface more than RagC-containing dimers. Consequently, both cytosolic and lysosomal targets of mTORC1 are equally stimulated. Mechanistic target of rapamycin complex 1 (mTORC1), Ras-related GTPase A-D (RagA-D), ribosomal S6 kinase (S6K), transcription factor EB (TFEB).

depending on which proteins make up the dimers, mTORC1 will target its substrates in a specific manner (Figure 5). Gollwitzer *et al.* showed that RagC and RagD dictate mTORC1 sensitivity towards its' substrates differently, with RagD being a more potent recruiter of mTORC1 to the lysosomes.[42] Consequently, RagD promotes phosphorylation of non-lysosomal (i.e., S6K) and lysosomal mTORC1 targets (i.e., TFEB). RagC induces phosphorylation of S6K at the same level as RagD but not TFEB (Figure 5). This study signifies that upstream signaling dictates the manner of mTORC1 activation and determines substrate specificity, further supporting the existence of distinct mTORC1 canonical and non-canonical signaling pathways.

ADKH-RRAGD

Given the key roles of the Rag GTPases in linking nutrients and mTORC1 signaling, aberrant activities of the Rag GTPases signaling have been associated with human diseases. Recently, we reported the first pathogenic *RRAGD* variants where 8 individuals and 1 large family were described (Table 1).[54] The affected individuals exhibited kidney tubulopathy, as suggested by renal salt wasting, hypomagnesemia, hypokalemia, hypercalciuria, and nephrocalcinosis, as well as dilated cardiomyopathy (DCM). This novel disease is now called autosomal dominant kidney hypomagnesemia *RRAGD* (ADKH-*RRAGD*). Another ADKH-*RRAGD* case was reported in 2023, in which a novel p.(Pro88Leu) *RRAGD* variant was identified in one family (Table 1).[55] Based on structural prediction and nucleotide binding assay, the identified *RRAGD* missense variants were found to impair the GTP binding capability of RagD, thus leaving RagD in a continuous GDP-bound or nucleotide-free state that are both active conformations of this protein.[54,55]

As a newly studied disease, the etiology and pathogenesis of ADKH-*RRAGD* are still at large. As mentioned above, the key clinical characteristic of ADKH-*RRAGD* patients is kidney tubulopathy in combination with DCM. Nonetheless, the symptoms of the patients vastly vary (Table 1). Moreover, the *RRAGD* variants seem to have variable expressivity, as not all patients exhibited the same clinical manifestations. For example, not all patients who share the same p.(Ser76Leu) variant develop DCM, and all patients with the p.(Thr97Pro) variant do not develop DCM until the most recent clinical follow-up. This suggests that the variants alone do not determine the clinical outcome in ADKH-*RRAGD* patients. Therefore, identifying more patients and understanding the disease course will be beneficial to improve future patients' diagnoses.

Aside from the genotype-phenotype correlation, the consequences of the *RRAGD* variants on mTORC1 signaling are still under debate. While it is agreed that these

variants result in mTORC1 overactivation, whether canonical and non-canonical mTORC1 signaling is involved is disputable. We reported that these variants result in the overactivation of canonical mTORC1 signaling in HEK293 cells (i.e., increased phosphorylation of S6K).[54] On the other hand, Sambri et al. suggested that the *RRAGD* variants only stimulate mTORC1 non-canonical signaling via TFEB phosphorylation.[55] Most importantly, how *RRAGD* is important in regulating renal ion transport and maintaining cardiac function is still elusive. Thus, clarification on how *RRAGD* variants found in ADKH-*RRAGD* patients affect mTORC1 signaling and how this leads to kidney tubulopathy and DCM is necessary.

This thesis focuses on understanding the etiology and pathogenesis of ADKH-*RRAGD* at the clinical and molecular levels. In the following sections, we will describe how *RRAGD* might play a role in regulating kidney and heart function and the knowledge gaps.

Table 1. Summary of patients' clinical manifestations in reported ADKH-*RRAGD* cases.

RRAGD variants	S76L[a]	P119R[a]	I221K[a]	S76L[a]	P119R[a]	S76L[a]	P119L[a]	S76W[a]	T97P[a]	S76L[b]	S76L[b]	P88L[c]	TOTAL
Patient	F1.1	F2.1	F3.1	F4.1	F5.1	F6.1	F7.1	F8.1	F8 (n=8)	F10.1	F10.2	F11 (n=8)	
Hypomagnesemia	Yes	Yes	Yes	Yes	Yes	Yes	Yes	Yes	Yes	Yes	Yes	Yes	26
Nephrocalcinosis	Yes	Yes	Yes	No	Yes	No	Yes	Yes	1/8	Yes	Yes	3/8	12
Polyuria	No	No	Yes	No	Yes	No	Yes	Yes	2/8	-	-	2/8	8
Metabolic alkalosis	No	-	Yes	Yes	No	No	No	Yes	2/8	Yes	Yes	8/8	17
DCM	Yes	Yes	Yes	No	Yes	Yes	Yes	No	No	Yes	Yes	No	6
Heart transplantation	Yes (3.3 yr)	Yes (25 yr)	Yes (15 yr)	No	No	No	No	No	No	Yes (46 yr)	Yes (41 yr)	1/8 (43 yr)	6 (29 yr)
RRAGD variants	S76L	P119R	I221K	S76L	P119R	S76L	P119L	S76W	T97P	S76L	S76L	P88L	
Patient	F1.1	F2.1	F3.1	F4.1	F5.1	F6.1	F7.1	F8.1	F8 (n=8)	F10.1	F10.2	F11 (n=8)	TOTAL
Hypomagnesemia	Yes	Yes	Yes	Yes	Yes	Yes	Yes	Yes	Yes	Yes	Yes	Yes	26
Nephrocalcinosis	Yes	Yes	Yes	No	Yes	No	Yes	Yes	1/8	Yes	Yes	3/8	12
Polyuria	No	No	Yes	No	Yes	No	Yes	Yes	2/8	-	-	2/8	8
Metabolic alkalosis	No	-	Yes	Yes	No	No	No	Yes	2/8	Yes	Yes	8/8	17
DCM	Yes	Yes	Yes	No	Yes	Yes	Yes	No	No	Yes	Yes	No	6
Heart transplantation	Yes (3.3 yr)	Yes (25 yr)	Yes (15 yr)	No	No	No	No	No	No	Yes (46 yr)	Yes (41 yr)	1/8 (43 yr)	6 (29 yr)[$]

Patients reported by [a]Schlingmann *et al.*,[54] [b] de Frutos *et al.*,[56] and [c] Sambri *et al.*[55] [$] indicates the average age of patients at heart transplantation.

Rag GTPases in the kidney

mTOR has been identified as a central player in several kidney diseases, such as acute kidney injury (AKI) and chronic kidney disease (CKD) (reviewed in [57,58]). Moreover, in the last decade, mTOR complexes have been implicated in the regulation of ion transport along the kidney tubule beyond cell metabolism and proliferation.[59] Interestingly, the kidney tubulopathies in ADKH-*RRAGD* patients are reminiscent of familial hypomagnesemia with hypercalciuria and nephrocalcinosis (FHHNC), which is caused by variants in the *CLDN16* and *CLDN19*. [60-63] *CLDN16* and *CLDN19* encode for the tight junction proteins Claudin-16 and Claudin-19, respectively. These tight junction proteins gatekeep the passive Mg^{2+} and Ca^{2+} transport in the thick ascending limb (TAL) of the nephron. A subset of patients also displayed hypomagnesemia and hypokalemia without hypercalciuria and nephrocalcinosis. These phenotypes are similar to that seen in Bartter type III and a mix with Gitelman syndrome, where defects in the distal convoluted tubule (DCT) are found.[64-66] Interestingly, RagD is most highly expressed in the TAL and DCT sections of the nephron in mouse kidneys [54], suggesting that these two regions are the most likely to be affected by the *RRAGD* variants. Nevertheless, the role of RagD in the kidney has not yet been well-studied.

Recent studies have hinted at the involvement of Rag GTPases in regulating renal cell metabolism and ion transport. For instance, variants in *FLCN* gene, the GAP of RagC and RagD, give rise to Birt Hogg-Dubé syndrome in which hyperactivation of mTORC1 is present.[52] A recent study has unveiled that constitutive activation of TFEB is the main driver of kidney abnormalities in a Birt Hogg-Dubé mouse model.[67] In addition to Birt Hogg-Dubé syndrome, TFEB function has also been associated with cystinosin expression, which is causative for nephropathic cystinosis.[68-70] Taken together, Rag GTPase regulation on TFEB activity seems to be important for maintaining normal kidney function. In ADKH-*RRAGD* patients, it is not clear whether the constitutively active RagD leads to TFEB overactivation. Therefore, it would be interesting to study whether mTORC1 and TFEB overactivation are the main culprits of kidney tubulopathies in these patients.

Rag GTPases in the heart

In addition to the kidney, the role of mTOR kinase is also widely studied in the heart. Both mTORC1 and mTORC2 are important for the physiology and pathophysiology of the heart, playing a role throughout a lifespan from embryonic development to post-natal homeostasis.[71] During embryonic development, cardiomyocytes exhibit high proliferation activity to sustain heart growth. Studies have shown that the expression of mTOR complex components and upstream regulators is crucial at

this embryonic stage for heart development and survival.[72,73] Mammalian hearts are considered mature after birth, and cardiomyocytes are considered post-mitotic. However, recent studies have revealed that mature cardiomyocytes possess limited regenerative capability.[74,75] Thus, mTOR signaling is crucial for maintaining cardiac structure and function under normal conditions and during adaptation to stress.[71]

Compared to the kidney, the role of Rag GTPases in preserving cardiac function is more established. Variants in *RRAGC* give rise to pediatric DCM, hepatopathy, and brain abnormalities.[76-78] *In vitro* and zebrafish studies revealed that the *RRAGC* p.(Ser75Tyr) variant leads to the overactivation of TFEB. This caused aberrant autophagic and lysosomal function, which culminated in heart defects.[77] RagA and RagB have also been demonstrated to be crucial for cardiac function. Deletion of RagA/B from cardiomyocytes in mice resulted in cardiac hypertrophy due to constitutive activation of TFEB and subsequent lysosomal dysfunctions.[79] In ADKH-*RRAGD* patients, whether the overactivation of mTORC1 and TFEB is responsible for DCM remains unclear. Additionally, it is still uncertain if any abnormal lysosomal and autophagic activities are associated with this condition. Based on previous studies on RagA-C, it is hypothesized that the overactivated mTORC1 caused by *RRAGD* variants leads to TFEB inhibition. Consequently, pathways downstream of TFEB (i.e., lysosomal biogenesis and autophagy) become dysregulated, ultimately resulting in cardiac dysfunction.

mTOR inhibition: a potential treatment?

Treatment for kidney tubulopathy ADKH-*RRAGD* patients has largely been symptomatic through oral magnesium and potassium supplementation.[54] To manage DCM, heart failure medications have been prescribed.[54] However, this method does not address the underlying issue, and the conditions may continue to deteriorate. Therefore, a more direct, targeted medication could improve patients' quality of life. Given the overactivation of mTORC1, it is plausible that pharmacological mTOR inhibitors could offer a potential treatment for ADKH-*RRAGD* patients.

FDA-approved mTOR inhibitors, all derivatives of rapamycin or rapalogues, are commonly used in clinical settings to treat various diseases, including renal diseases and cancers, and as immunosuppressants after kidney transplantation. Numerous preclinical studies and clinical observations have also utilized mTOR inhibitors to investigate their effects on heart and kidney function. In the kidney, inhibition of this signaling pathway influences tubular transport, among other targets.[59] For instance, prolonged use of rapalogues is known to cause hypomagnesemia and phosphaturia in kidney transplant patients. Additionally, the use of sirolimus in various cellular and

animal models has altered ion homeostasis.[59] In different heart disease models, such as aging, cardiac hypertrophy, and ischemic injury, pharmacological inhibition of mTOR has generally been beneficial and has improved cardiac function (reviewed in [80]). Based on these results, it would be intriguing to explore whether mTOR inhibition could ameliorate ion imbalance and cardiac function in ADKH-*RRAGD* patients or in animal models that carry these *RRAGD* variants.

Outline of this thesis

This thesis aimed to unravel the molecular mechanisms contributing to kidney tubulopathy and DCM in ADKH-*RRAGD* patients while identifying potential therapeutic approaches. To achieve this, the effects of *RRAGD* variants on mTORC1 signaling were examined. It is hypothesized that these variants lead to the overactivation of both canonical and non-canonical mTORC1 signaling. Subsequently, the consequences of the variants on kidney and heart function at both cellular and organismal levels were studied. Ultimately, this thesis highlights the importance of RagD in the heart and kidney, as well as in health and disease. Looking toward future patient care, the results of this thesis will assist in diagnosing more ADKH-*RRAGD* patients who may currently be undiagnosed and will further lay the groundwork for providing more precise medication for these patients.

Chapter 2 describes a new cohort of ADKH-*RRAGD* patients with various novel and previously identified *RRAGD* variants. Here, the effects of the variants on mTORC1 signaling were examined using an *in vitro* model. Moreover, patients' responses to the diuretics furosemide and hydrochlorothiazide were assessed. Lastly, as a potential treatment approach, the effects of dapagliflozin on serum Mg^{2+} levels in ADKH-*RRAGD* patients were examined. In **chapter 3**, using zebrafish embryos, the *RRAGD* p.(Ser76Leu) and p.(Pro119Arg) variants were modeled to study the effects of the variants on zebrafish heart and kidney function. Furthermore, the impact of rapamycin treatment in this model was investigated. **Chapter 4** aimed to further delineate the molecular mechanisms underlying DCM in patients with the most prevalent *RRAGD* variant, p.(Ser76Leu), using an *in vitro* model. In this chapter, a human induced pluripotent stem cell-derived cardiomyocyte (hiPSC-CM) cell line carrying the *RRAGD* p.(Ser76Leu) (c.227C>T) was generated and characterized. Furthermore, the effects of the variant on mTORC1 signaling were assessed. Together, the main findings of this thesis were discussed in **chapter 5** and summarized in **chapters 6-8**.

References

1. Powers T. The origin story of rapamycin: systemic bias in biomedical research and cold war politics. *Mol Biol Cell.* 2022;33(13).
2. Sabatini DM, Erdjument-Bromage H, Lui M, Tempst P, Snyder SH. RAFT1: a mammalian protein that binds to FKBP12 in a rapamycin-dependent fashion and is homologous to yeast TORs. *Cell.* 1994;78(1):35-43.
3. Brown EJ, Albers MW, Shin TB, et al. A mammalian protein targeted by G1-arresting rapamycin-receptor complex. *Nature.* 1994;369(6483):756-758.
4. Sabers CJ, Martin MM, Brunn GJ, et al. Isolation of a protein target of the FKBP12-rapamycin complex in mammalian cells. *J Biol Chem.* 1995;270(2):815-822.
5. Saxton RA, Sabatini DM. mTOR Signaling in Growth, Metabolism, and Disease. *Cell.* 2017;168(6):960-976.
6. Kim DH, Sarbassov DD, Ali SM, et al. mTOR interacts with raptor to form a nutrient-sensitive complex that signals to the cell growth machinery. *Cell.* 2002;110(2):163-175.
7. Hara K, Maruki Y, Long X, et al. Raptor, a binding partner of target of rapamycin (TOR), mediates TOR action. *Cell.* 2002;110(2):177-189.
8. Sarbassov DD, Ali SM, Kim DH, et al. Rictor, a novel binding partner of mTOR, defines a rapamycin-insensitive and raptor-independent pathway that regulates the cytoskeleton. *Curr Biol.* 2004;14(14):1296-1302.
9. Jacinto E, Loewith R, Schmidt A, et al. Mammalian TOR complex 2 controls the actin cytoskeleton and is rapamycin insensitive. *Nat Cell Biol.* 2004;6(11):1122-1128.
10. Loewith R, Jacinto E, Wullschleger S, et al. Two TOR complexes, only one of which is rapamycin sensitive, have distinct roles in cell growth control. *Mol Cell.* 2002;10(3):457-468.
11. Reinke A, Anderson S, McCaffery JM, et al. TOR complex 1 includes a novel component, Tco89p (YPL180w), and cooperates with Ssd1p to maintain cellular integrity in Saccharomyces cerevisiae. *J Biol Chem.* 2004;279(15):14752-14762.
12. Kim DH, Sarbassov DD, Ali SM, et al. GbetaL, a positive regulator of the rapamycin-sensitive pathway required for the nutrient-sensitive interaction between raptor and mTOR. *Mol Cell.* 2003;11(4):895-904.
13. Wang L, Harris TE, Roth RA, Lawrence JC, Jr. PRAS40 regulates mTORC1 kinase activity by functioning as a direct inhibitor of substrate binding. *J Biol Chem.* 2007;282(27):20036-20044.
14. Peterson TR, Laplante M, Thoreen CC, et al. DEPTOR is an mTOR inhibitor frequently overexpressed in multiple myeloma cells and required for their survival. *Cell.* 2009;137(5):873-886.
15. Pearce LR, Huang X, Boudeau J, et al. Identification of Protor as a novel Rictor-binding component of mTOR complex-2. *Biochem J.* 2007;405(3):513-522.
16. Kim E, Goraksha-Hicks P, Li L, Neufeld TP, Guan KL. Regulation of TORC1 by Rag GTPases in nutrient response. *Nat Cell Biol.* 2008;10(8):935-945.
17. Sancak Y, Peterson TR, Shaul YD, et al. The Rag GTPases bind raptor and mediate amino acid signaling to mTORC1. *Science.* 2008;320(5882):1496-1501.
18. Inoki K, Li Y, Zhu T, Wu J, Guan KL. TSC2 is phosphorylated and inhibited by Akt and suppresses mTOR signalling. *Nat Cell Biol.* 2002;4(9):648-657.
19. Manning BD, Tee AR, Logsdon MN, Blenis J, Cantley LC. Identification of the tuberous sclerosis complex-2 tumor suppressor gene product tuberin as a target of the phosphoinositide 3-kinase/akt pathway. *Mol Cell.* 2002;10(1):151-162.

20. Inoki K, Li Y, Xu T, Guan KL. Rheb GTPase is a direct target of TSC2 GAP activity and regulates mTOR signaling. *Genes Dev.* 2003;17(15):1829-1834.
21. Tee AR, Manning BD, Roux PP, Cantley LC, Blenis J. Tuberous sclerosis complex gene products, Tuberin and Hamartin, control mTOR signaling by acting as a GTPase-activating protein complex toward Rheb. *Curr Biol.* 2003;13(15):1259-1268.
22. Holz MK, Ballif BA, Gygi SP, Blenis J. mTOR and S6K1 mediate assembly of the translation preinitiation complex through dynamic protein interchange and ordered phosphorylation events. *Cell.* 2005;123(4):569-580.
23. Fingar DC, Blenis J. Target of rapamycin (TOR): an integrator of nutrient and growth factor signals and coordinator of cell growth and cell cycle progression. *Oncogene.* 2004;23(18):3151-3171.
24. Gingras AC, Gygi SP, Raught B, et al. Regulation of 4E-BP1 phosphorylation: a novel two-step mechanism. *Genes Dev.* 1999;13(11):1422-1437.
25. Kim J, Kundu M, Viollet B, Guan KL. AMPK and mTOR regulate autophagy through direct phosphorylation of Ulk1. *Nat Cell Biol.* 2011;13(2):132-141.
26. Martina JA, Chen Y, Gucek M, Puertollano R. MTORC1 functions as a transcriptional regulator of autophagy by preventing nuclear transport of TFEB. *Autophagy.* 2012;8(6):903-914.
27. Roczniak-Ferguson A, Petit CS, Froehlich F, et al. The transcription factor TFEB links mTORC1 signaling to transcriptional control of lysosome homeostasis. *Sci Signal.* 2012;5(228):ra42.
28. Settembre C, Zoncu R, Medina DL, et al. A lysosome-to-nucleus signalling mechanism senses and regulates the lysosome via mTOR and TFEB. *EMBO J.* 2012;31(5):1095-1108.
29. Palmieri M, Impey S, Kang H, et al. Characterization of the CLEAR network reveals an integrated control of cellular clearance pathways. *Hum Mol Genet.* 2011;20(19):3852-3866.
30. Sardiello M, Palmieri M, di Ronza A, et al. A gene network regulating lysosomal biogenesis and function. *Science.* 2009;325(5939):473-477.
31. Settembre C, Di Malta C, Polito VA, et al. TFEB links autophagy to lysosomal biogenesis. *Science.* 2011;332(6036):1429-1433.
32. Napolitano G, Di Malta C, Ballabio A. Non-canonical mTORC1 signaling at the lysosome. *Trends Cell Biol.* 2022;32(11):920-931.
33. Fu W, Hall MN. Regulation of mTORC2 Signaling. *Genes (Basel).* 2020;11(9).
34. Liu P, Gan W, Chin YR, et al. PtdIns(3,4,5)P3-Dependent Activation of the mTORC2 Kinase Complex. *Cancer Discov.* 2015;5(11):1194-1209.
35. Schroder WA, Buck M, Cloonan N, et al. Human Sin1 contains Ras-binding and pleckstrin homology domains and suppresses Ras signalling. *Cell Signal.* 2007;19(6):1279-1289.
36. Yang G, Murashige DS, Humphrey SJ, James DE. A Positive Feedback Loop between Akt and mTORC2 via SIN1 Phosphorylation. *Cell Rep.* 2015;12(6):937-943.
37. Dangelmaier C, Manne BK, Liverani E, Jin J, Bray P, Kunapuli SP. PDK1 selectively phosphorylates Thr(308) on Akt and contributes to human platelet functional responses. *Thromb Haemost.* 2014;111(3):508-517.
38. Gleason CE, Oses-Prieto JA, Li KH, et al. Phosphorylation at distinct subcellular locations underlies specificity in mTORC2-mediated activation of SGK1 and Akt. *J Cell Sci.* 2019;132(7).
39. Sarbassov DD, Guertin DA, Ali SM, Sabatini DM. Phosphorylation and regulation of Akt/PKB by the rictor-mTOR complex. *Science.* 2005;307(5712):1098-1101.

40. Garcia-Martinez JM, Alessi DR. mTOR complex 2 (mTORC2) controls hydrophobic motif phosphorylation and activation of serum- and glucocorticoid-induced protein kinase 1 (SGK1). *Biochem J.* 2008;416(3):375-385.
41. Figlia G, Muller S, Hagenston AM, et al. Brain-enriched RagB isoforms regulate the dynamics of mTORC1 activity through GATOR1 inhibition. *Nat Cell Biol.* 2022;24(9):1407-1421.
42. Gollwitzer P, Grutzmacher N, Wilhelm S, Kummel D, Demetriades C. A Rag GTPase dimer code defines the regulation of mTORC1 by amino acids. *Nat Cell Biol.* 2022;24(9):1394-1406.
43. Bar-Peled L, Schweitzer LD, Zoncu R, Sabatini DM. Ragulator is a GEF for the rag GTPases that signal amino acid levels to mTORC1. *Cell.* 2012;150(6):1196-1208.
44. Sancak Y, Bar-Peled L, Zoncu R, Markhard AL, Nada S, Sabatini DM. Ragulator-Rag complex targets mTORC1 to the lysosomal surface and is necessary for its activation by amino acids. *Cell.* 2010;141(2):290-303.
45. Sekiguchi T, Hirose E, Nakashima N, Ii M, Nishimoto T. Novel G proteins, Rag C and Rag D, interact with GTP-binding proteins, Rag A and Rag B. *J Biol Chem.* 2001;276(10):7246-7257.
46. Hirose E, Nakashima N, Sekiguchi T, Nishimoto T. RagA is a functional homologue of S. cerevisiae Gtr1p involved in the Ran/Gsp1-GTPase pathway. *J Cell Sci.* 1998;111 (Pt 1):11-21.
47. Schurmann A, Brauers A, Massmann S, Becker W, Joost HG. Cloning of a novel family of mammalian GTP-binding proteins (RagA, RagBs, RagB1) with remote similarity to the Ras-related GTPases. *J Biol Chem.* 1995;270(48):28982-28988.
48. Anandapadamanaban M, Masson GR, Perisic O, et al. Architecture of human Rag GTPase heterodimers and their complex with mTORC1. *Science.* 2019;366(6462):203-210.
49. Rogala KB, Gu X, Kedir JF, et al. Structural basis for the docking of mTORC1 on the lysosomal surface. *Science.* 2019;366(6464):468-475.
50. Bar-Peled L, Chantranupong L, Cherniack AD, et al. A Tumor suppressor complex with GAP activity for the Rag GTPases that signal amino acid sufficiency to mTORC1. *Science.* 2013;340(6136):1100-1106.
51. Zoncu R, Bar-Peled L, Efeyan A, Wang S, Sancak Y, Sabatini DM. mTORC1 senses lysosomal amino acids through an inside-out mechanism that requires the vacuolar H(+)-ATPase. *Science.* 2011;334(6056):678-683.
52. Petit CS, Roczniak-Ferguson A, Ferguson SM. Recruitment of folliculin to lysosomes supports the amino acid-dependent activation of Rag GTPases. *J Cell Biol.* 2013;202(7):1107-1122.
53. Tsun ZY, Bar-Peled L, Chantranupong L, et al. The folliculin tumor suppressor is a GAP for the RagC/D GTPases that signal amino acid levels to mTORC1. *Mol Cell.* 2013;52(4):495-505.
54. Schlingmann KP, Jouret F, Shen K, et al. mTOR-Activating Mutations in RRAGD Are Causative for Kidney Tubulopathy and Cardiomyopathy. *J Am Soc Nephrol.* 2021;32(11):2885-2899.
55. Sambri I, Ferniani M, Campostrini G, et al. RagD auto-activating mutations impair MiT/TFE activity in kidney tubulopathy and cardiomyopathy syndrome. *Nat Commun.* 2023;14(1):2775.
56. de Frutos F, Diez-Lopez C, Garcia-Romero E, et al. Dilated Cardiomyopathy With Concomitant Salt-Losing Renal Tubulopathy Caused by Heterozygous RRAGD Gene Variant. *Circ Genom Precis Med.* 2024;17(2):e004336.
57. Fantus D, Rogers NM, Grahammer F, Huber TB, Thomson AW. Roles of mTOR complexes in the kidney: implications for renal disease and transplantation. *Nat Rev Nephrol.* 2016;12(10):587-609.
58. Gui Y, Dai C. mTOR Signaling in Kidney Diseases. *Kidney360.* 2020;1(11):1319-1327.
59. Adella A, de Baaij JHF. mTOR signaling in renal ion transport. *Acta Physiol (Oxf).* 2023;238(1):e13960.
60. Praga M, Vara J, Gonzalez-Parra E, et al. Familial hypomagnesemia with hypercalciuria and nephrocalcinosis. *Kidney Int.* 1995;47(5):1419-1425.

61. Simon DB, Lu Y, Choate KA, et al. Paracellin-1, a renal tight junction protein required for paracellular Mg2+ resorption. *Science.* 1999;285(5424):103-106.
62. Konrad M, Schaller A, Seelow D, et al. Mutations in the tight-junction gene claudin 19 (CLDN19) are associated with renal magnesium wasting, renal failure, and severe ocular involvement. *Am J Hum Genet.* 2006;79(5):949-957.
63. Rodriguez-Soriano J, Vallo A, Garcia-Fuentes M. Hypomagnesaemia of hereditary renal origin. *Pediatr Nephrol.* 1987;1(3):465-472.
64. Simon DB, Nelson-Williams C, Bia MJ, et al. Gitelman's variant of Bartter's syndrome, inherited hypokalaemic alkalosis, is caused by mutations in the thiazide-sensitive Na-Cl cotransporter. *Nat Genet.* 1996;12(1):24-30.
65. Jeck N, Konrad M, Peters M, Weber S, Bonzel KE, Seyberth HW. Mutations in the chloride channel gene, CLCNKB, leading to a mixed Bartter-Gitelman phenotype. *Pediatr Res.* 2000;48(6):754-758.
66. Zelikovic I, Szargel R, Hawash A, et al. A novel mutation in the chloride channel gene, CLCNKB, as a cause of Gitelman and Bartter syndromes. *Kidney Int.* 2003;63(1):24-32.
67. Napolitano G, Di Malta C, Esposito A, et al. A substrate-specific mTORC1 pathway underlies Birt-Hogg-Dube syndrome. *Nature.* 2020;585(7826):597-602.
68. Cherqui S, Kalatzis V, Trugnan G, Antignac C. The targeting of cystinosin to the lysosomal membrane requires a tyrosine-based signal and a novel sorting motif. *J Biol Chem.* 2001;276(16):13314-13321.
69. Town M, Jean G, Cherqui S, et al. A novel gene encoding an integral membrane protein is mutated in nephropathic cystinosis. *Nat Genet.* 1998;18(4):319-324.
70. Kalatzis V, Cherqui S, Antignac C, Gasnier B. Cystinosin, the protein defective in cystinosis, is a H(+)-driven lysosomal cystine transporter. *EMBO J.* 2001;20(21):5940-5949.
71. Sciarretta S, Volpe M, Sadoshima J. Mammalian target of rapamycin signaling in cardiac physiology and disease. *Circ Res.* 2014;114(3):549-564.
72. Goorden SM, Hoogeveen-Westerveld M, Cheng C, et al. Rheb is essential for murine development. *Mol Cell Biol.* 2011;31(8):1672-1678.
73. Zhu Y, Pires KM, Whitehead KJ, et al. Mechanistic target of rapamycin (Mtor) is essential for murine embryonic heart development and growth. *PLoS One.* 2013;8(1):e54221.
74. Bergmann O, Bhardwaj RD, Bernard S, et al. Evidence for cardiomyocyte renewal in humans. *Science.* 2009;324(5923):98-102.
75. Bergmann O, Zdunek S, Felker A, et al. Dynamics of Cell Generation and Turnover in the Human Heart. *Cell.* 2015;161(7):1566-1575.
76. Long PA, Zimmermann MT, Kim M, Evans JM, Xu X, Olson TM. De novo RRAGC mutation activates mTORC1 signaling in syndromic fetal dilated cardiomyopathy. *Hum Genet.* 2016;135(8):909-917.
77. Kim M, Lu L, Dvornikov AV, et al. TFEB Overexpression, Not mTOR Inhibition, Ameliorates RagC(S75Y) Cardiomyopathy. *Int J Mol Sci.* 2021;22(11).
78. Reijnders MRF, Seibt A, Brugger M, et al. De novo missense variants in RRAGC lead to a fatal mTORopathy of early childhood. *Genet Med.* 2023;25(7):100838.
79. Kim YC, Park HW, Sciarretta S, et al. Rag GTPases are cardioprotective by regulating lysosomal function. *Nat Commun.* 2014;5:4241.
80. Sciarretta S, Forte M, Frati G, Sadoshima J. New Insights Into the Role of mTOR Signaling in the Cardiovascular System. *Circ Res.* 2018;122(3):489-505.

CHAPTER 2

Novel *RRAGD* variants in autosomal dominant kidney hypomagnesemia and therapeutic perspectives

Anastasia Adella[1], François Jouret[2,3], Leire Madariaga[4], Pieter A. Leermakers[1], Pedro Arango[5], Gema Ariceta[6], Anna Bjerre[7,8], Detlef Bockenhauer[9,10], Paula Coccia[11], Radhika Dhamija[12], Fernando de Frutos[13,14], Alejandro Garcia-Castano[15], Sara van Katwijk[1], Jesus Lucas[16], Thomas Möller[17], Dominik Müller[18], Filippo Pinto e Vairo[19], Melinda Raki[20], Hanka Venselaar[1], Matheus Vernet Machado Bressan Wilke[21], Tom Nijenhuis[22], Joost Hoenderop[1], Jeroen de Baaij[1]

[1] Department of Medical BioSciences, Radboudumc, Nijmegen, The Netherlands

[2] Laboratory of Translational Research in Nephrology, Metabolism & Cardiovascular Biology, GIGA Institute, University of Liège, Liège, Belgium

[3] Division of Nephrology-Dialysis-Transplantation, University Hospital of Liége (ULiège CHU), Liège, Belgium

[4] Pediatric Nephrology Department, Biobizkaia Health Research Institute, University of the Basque Country, CIBERDEM/CIBERER, Cruces University Hospital, Barakaldo, Spain

[5] Pediatric Nephrology and Renal Transplant Department, Hospital Sant Joan de Déu, Barcelona, Spain

[6] Pediatric Nephrology Department, Vall d'Hebron Hospital, Autonomous University of Barcelona, Barcelona, Spain

[7] Department of Transplantation and Specialized Medicine, Division of Pediatric and Adolescent Medicine, Oslo University Hospital, Oslo, Norway
[8] Institute of Clinical Medicine, University of Oslo, Oslo, Norway
[9] Department of Paediatric Nephrology, UZ Leuven and Cellular and Molecular Physiology, KUL, Leuven, Belgium
[10] Department of Renal Medicine, University College London and Paediatric Nephrology, Great Ormond Street Hospital for Children NHS Foundation Trust, London, UK
[11] Division of Pediatric Nephrology, Hospital Italiano de Buenos Aires, Buenos Aires, Argentina
[12] Department of Clinical Genomics, Mayo Clinic, Rochester, Minnesota, USA
[13] Heart Failure and Inherited Cardiac Diseases Unit, Department of Cardiology, Hospital Universitari de Bellvitge, L'Hospitalet de Llobregat, Barcelona, Spain
[14] Bioheart Group, Cardiovascular, Respiratory and Systemic Diseases and cellular aging Program, Institut d'Investigació Biomèdica de Bellvitge (IDIBELL), L'Hospitalet de Llobregat, Spain
[15] Biobizkaia Health Research Institute, CIBERDEM/CIBERER, Barakaldo, Spain
[16] Pediatric Nephrology Department, General University Hospital of Castellón, Castellón, Spain
[17] Department of Paediatric Cardiology, Division of Paediatric and Adolescent Medicine, Oslo University Hospital, Oslo, Norway
[18] Department of Pediatric Gastroenterology, Nephrology and Metabolic Diseases, Charité, University Medicine, Berlin, Germany
[19] Center for Individualized Medicine and Department of Clinical Genomics, Mayo Clinic, Rochester, Minnesota, USA
[20] Department of Pathology, Oslo University Hospital, Oslo, Norway
[21] Department of Pathology and Immunology, Washington University School of Medicine, St. Louis, Missouri, USA
[22] Department of Nephrology, Radboudumc, Nijmegen, The Netherlands

Kidney International Reports, 2025

Abstract

Introduction

Variants in the Ras-related GTPase D (*RRAGD*) have been associated with autosomal dominant kidney hypomagnesemia (ADKH) characterized by hypokalemia, nephrocalcinosis, and dilated cardiomyopathy. *RRAGD*, which encodes for RagD protein, is involved in the activation of the mechanistic target of rapamycin complex 1 (mTORC1). Due to the limited characterization of patients' phenotypes, the understanding of ADKH-RRAGD remains incomplete. Consequently, available treatment strategies are primarily symptomatic and insufficient.

Methods

In the present case series, 12 new patients and 3 novel *RRAGD* variants, *i.e.* p.(Ser77Phe), p.(Thr91Ile), and p.(Ile100Arg), are described. To assess the pathogenicity of the novel variants, an *in vitro* assay of mTORC1 activity was performed. Additionally, the clinical response to diuretics (furosemide (n=4) and thiazide, (n=4)) and SGLT2 inhibitor dapagliflozin (n=6) was evaluated in patients carrying the *RRAGD* p.(Thr97Pro) variant during routine.

Results

The patients presented with kidney tubulopathies, including hypomagnesemia, hypercalciuria, and nephrocalcinosis. Four patients also exhibited dilated cardiomyopathy. *In vitro* assays demonstrated constitutive activation of non-canonical mTORC1 signaling caused by the p.(Ser77Phe) and p.(Ile100Arg) variants. Clinically, patients remained sensitive to diuretic challenges, while dapagliflozin treatment increased serum magnesium (Mg^{2+}) concentrations by 0.04 mM but exacerbated hypokalemia.

Conclusion

To date, 36 patients with ADKH-RRAGD have been identified. Kidney tubulopathy is the most prominent feature within the phenotypic spectrum of ADKH-RRAGD. Molecularly, constitutive activation of non-canonical mTORC1 is present in most *RRAGD* variants. From a therapeutic perspective, dapagliflozin may increase serum Mg^{2+} levels in patients with *RRAGD* variants.

Keywords: dapagliflozin, dilated cardiomyopathy, kidney tubulopathy, magnesium, RRAGD, mTORC1

Introduction

Recently, we identified gain-of-function variants in Ras-related GTPase D gene (*RRAGD*) as the cause of autosomal dominant kidney hypomagnesemia (ADKH), which is associated with hypokalemia, salt wasting, hypercalciuria, and nephrocalcinosis.[1] In a subset of ADKH-*RRAGD* patients, these kidney defects co-occurred with dilated cardiomyopathy (DCM), requiring early heart transplantation.[1] Since our initial report, additional familial cases of ADKH-*RRAGD* have been reported.[2,3]

RRAGD encodes for the small GTPase RagD, one of the four Rag GTPases in mammalian cells (i.e., RagA-D) that serve as intracellular amino acids (AA) sensors.[4,5] Upon AA signaling, Rag GTPases form heterodimeric complexes composed of RagA or RagB with RagC or RagD.[6-8] In their active states, GTP-bound RagA/B and GDP-bound RagC/D recruit the mechanistic target of rapamycin complex 1 (mTORC1) to the lysosomal surface, resulting in mTORC1 activation.[9,10] From there, mTORC1 phosphorylates its downstream targets such as the canonical cytosolic targets S6 kinase (S6K) and eukaryotic initiation factor 4e-binding protein 1 (4E-BP1), and its non-canonical lysosomal targets such as the transcription factor EB (TFEB).[11-17]

mTOR inhibition has been proposed as a potential treatment strategy to prevent dilated cardiomyopathy due to pathogenic *RRAGD* variants. Overexpression of the *RRAGD-associated* variants p.(Ser76Leu) and p.(Pro119Arg) in zebrafish embryos resulted in cardiac dysfunctions.[18] Furthermore, exposure to rapamycin, an mTOR inhibitor, rescued these phenotypes.[18] Nevertheless, clinicians have been hesitant to prescribe lifelong mTOR inhibitors given their immunoinhibiting properties and the lack of supporting evidence for ADKH-*RRAGD* patients. Therefore, patients with stable heart function are treated with magnesium and potassium supplements, limiting their options to symptomatic treatment only. For those with heart failure and mildly reduced ejection fraction, standard therapy includes diuretics and Na^+-glucose cotransporter 2 (SGLT2) inhibitors.[19,20] Still, these patients are characterized by chronic ionic disturbances caused by a poorly understood tubular dysfunction, which might be pharmacologically improved or aggravated. This highlights the need for detailed phenotypic characterization and evaluation of diuretic response in ADKH-RRAGD patients.

Here, we report on a new cohort of twelve ADKH-*RRAGD* patients, including three novel *RRAGD*-associated variants: (p.(Ser77Phe), p.(Thr91Ile), and p.(Ile100Arg)). The functional effect of these variants was assessed by *in vitro* mTOR activity assays, TFEB translocation in T-REx HeLa cells stably overexpressing *RRAGD*-associated

variants, and *in silico* RagD structure analysis. Moreover, we examined the biological response to two commonly used diuretics in clinical routine, *i.e.* furosemide and hydrochlorothiazide (HCT). Finally, patients' response to SGLT2 inhibitor dapagliflozin was assessed as a potential treatment strategy in patients with ADKH-*RRAGD*.

Materials and methods

For complete methods, please refer to the Supplementary Methods section.

Study participants

The individuals included in this manuscript were identified by routine diagnostic DNA testing (see details below). Written informed consent was obtained for the genetic analysis and the publication of anonymized data, including the clinical challenges of diuretics.

Molecular assays

All *in vitro* experiments were performed using T-REx HeLa cell lines stably overexpressing *RRAGD* WT or variants described in this study. Immunoblotting was performed on protein materials of the cells under AA stimulation. Immunocytochemistry was performed on T-REx HeLa stable cell lines transfected with pcDNA3.1-TFEB-WT-MYC (Addgene plasmid #99955).[21] All HeLa T-REx cell lines were cultured in the cell culture medium (Dulbecco's Modified Eagle Medium (DMEM) containing 25 mM Hepes, 4.5 g/L glucose, and 4 mM L-glutamine (#42430082, Thermo Fisher Scientific, California, USA), supplemented with 10% FBS (Greiner Bio-One, Alphen aan den Rijn, the Netherlands), 1 mM sodium pyruvate (Thermo Fisher Scientific, California, USA), and 1% v/v MEM non-essential amino acids solution 100x (Capricorn Scientific GmbH, Ebsdorfergrund, Germany)) in a humidified 37°C incubator with 5% (v/v) CO_2 unless stated otherwise.

Furosemide and hydrochlorothiazide testing

In order to assess the effects of furosemide on urinary ion excretion in patients with the p.(Thr97Pro) *RRAGD* variant, a single oral dose of 40 mg furosemide was administered in routine renal physiology explorations after informed consent of each participant (n=4). To assess the effects of hydrochlorothiazide (HCT) on urinary ion excretion in patients with p.The97Pro *RRAGD* variant, a single oral dose of 50 mg HCT was administered in routine renal physiology explorations after informed consent of each participant (n=4). The study duration was 6 hr post-administration of HCT. To compare the patients' response to each diuretic to the healthy population, we re-analyzed Cl^- and Mg^{2+} data from furosemide testing done

by Bech et al. using the same protocol (2017).[22] Mg^{2+} levels were not reported in the original publication but were taken from the unpublished study files.

Dapagliflozin treatment

To assess the effect of dapagliflozin on serum ion levels in patients with p.(Thr97Pro) *RRAGD* variant (n=6), blood samples were collected at baseline and 15 days after a daily oral dose of 10 mg of dapagliflozin in real-life settings.

Statistics

For the *in vitro* studies, Two-way ANOVA was performed. This was followed by Dunnett multiple comparisons test for the immunocytochemistry results or Šídák multiple comparisons test for the immunoblotting results. Multiple comparisons were performed by comparing the mean of mock, *RRAGD* mutants p.(Ser77Phe), p.(Thr91Ile), and p.(Ile100Arg) to the mean of *RRAGD* WT cells, within the amino acids treatment group. Statistical significance at $P < 0.05$ was considered significant. For other studies, no statistical tests were performed. All statistical tests were performed using GraphPad Prism version 10.4.0 for MacOS, GraphPad Software (Massachusetts, USA). All image analyses were performed in Fiji, ImageJ2 version 2.14.0.[23, 24]

Results

Clinical presentation of new patients with *RRAGD* variants

Routine diagnostic screening of patients with suspected familial kidney tubulopathies resulted in the identification of 7 families consisting of 12 individuals with variants in *RRAGD* (Table 1). Clinical and laboratory findings are described in Table 1, Figure 1, and Supplementary Figure 1a-c.

Main kidney tubulopathy phenotypes in *RRAGD*-associated autosomal dominant kidney hypomagnesemia (ADKH-*RRAGD*) are present in all patients described in this study: hypomagnesemia, hypokalemia, salt-wasting, and nephrocalcinosis (Table 1, Figure 1a&b, Supplementary Figure 1a-c). Additionally, nephrolithiasis was present in F1.1, F2.2, and F3.2 individuals. In addition to the kidney tubulopathy, dilated cardiomyopathy was found in 4 individuals (F4.1, F4.2, F5.1, and F7.1) as shown by the enlargement of left ventricles (Figure 1b, Supplementary Figure 1d). Individual F4.3, daughter of F4.2, did not present with dilated cardiomyopathy but developed excessive apical trabeculations with normal left ventricular ejection fraction (LVEF) at 6 years old. Family 4 was first described by de Frutos *et al*., 2024.[3] Heart transplantation was performed in individuals F4.1, F4.2, and F7.1. In individual F7.1,

Masson trichrome staining of explanted heart ventricular samples indicated the presence of diffuse myocardial fibrosis (Figure 1c). Moreover, in the left ventricular posterior wall section, diffuse interstitial fibrosis with infiltrating lymphocytes and macrophages can be seen (Figure 1d). In Family 1, the mother and two maternal uncles of the proband individual F1.1 presented with kidney tubulopathy, while the maternal grandmother experienced nephrolithiasis. The seven families were described in more detail in the Supplementary Appendix.

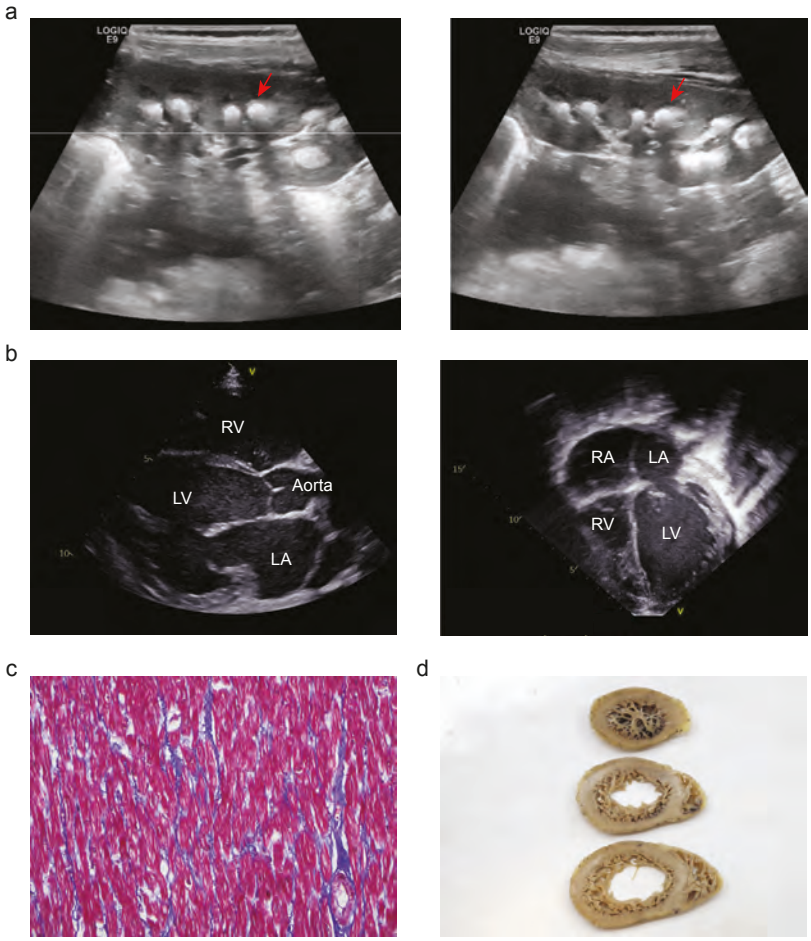

Figure 1. Renal tubulopathy and dilated cardiomyopathy in ADKH-*RRAGD* patient F7.1. (a-b) Ultrasound images: (a) left and right kidney showing nephrocalcinosis (structures pointed by red arrow), (b) left: parasternal long axis view of the heart, right: apical 4 chamber view of the heart. (c) Masson trichrome staining of the explanted left ventricle anterior wall longitudinal section, showing interstitial fibrosis with blue collagen fibers surrounding red individual cardiomyocytes (magnification 200x). (d) Macroscopy picture of the sliced left ventricle of the explanted heart showing excessive trabeculation (top to bottom: apical to basal). LA: left atrium, LV: left ventricle, RA: right atrium, RV: right ventricle.

Table 1. Clinical characteristics. DCM: dilated cardiomyopathy, EF: ejection fraction, FE: fractional excretion, FS: fractional shortening, N: no, N/A: not applicable, n.d.: not determined, S- = serum value, Y: yes, ?: unknown.

Individuals	**F1.III.1**	**F2.II.1**	**F2.II.2**	**F2.II.4**	**F3.III.1**	**F3.II.1**
Origin	Ashkenazi Jew	UK-SE Asia	UK-SE Asia	UK-SE Asia	Germany	Germany
Sex	F	F	F	M	F	F
Age at manifestation	Adulthood*	7 yr	2 yr	8 m	15 yr	20 yr
Current age	46 yr	11 yr	8 yr	1 yr	16 yr	44 yr
Cardiac symptoms						
DCM (age of finding)	N	N	N	N	N	N
FS (%)	N/A	N/A	N/A	N/A	N/A	N/A
EF (%)	N/A	N/A	N/A	N/A	N/A	N/A
LVEDD (mm)	N/A	N/A	N/A	N/A	N/A	N/A
Heart transplantation (age)	N/A	N/A	N/A	N/A	N/A	N/A
Renal symptoms						
Hypomagnesemia-related symptoms	Y - Paresthesia	N	N	N	Y - Cramps, Weakness	
Nephrocalcinosis	Y	Y	Y	Y	Y	Y
Nephrolithiasis	Y	N	Y	N	N	Y
Polyuria	N	N	N	N	N	N
Metabolic alkalosis	Y	Y	Y	N	Y	n.d.
Laboratory findings						
S-Ca (mmol/L; N=2.2-2.6)	2.4	2.39	2.46	2.68	2.28	n.d.
S-Cl (mmol/L; N=98-107)	100	102	99	106	98	
S-K (mmol/L; N=3.5-5.1)	3.5	3.4	2.9	4.2	2.8	
S-Mg (mmol/L; N=0.7-1.1)	0.41	0.61	0.62	0.93	0.52	
S-Na (mmol/L; N=136-145))	139	139	137	139	141	
S-PO_4 (mmol/L)	1.13	1.48	1.29	2.15	0.92	
S-creatinine (mg/dL; N=0.73-1.18)	0.64	0.47	0.41	0.29	0.41	
S-HCO_3 (mmol/L; N=22-31)	22	26	27	21	27.9	
FE-K (%; N=5.5-17)	17 - 77 mmol/ 24 h 55	13	19	11	n.d.	
FE-Mg (%; N=3-5)	51 - 269 mg/ 24 h 246	3.2	6.2	2.9	n.d.	
FE-Na (%=0.1-2)	41 - 227 mmol/ 24 h 106	0.3	0.1	0.4	n.d.	
Ca/Crea-ratio (mol/mol)	eGFR >60 >=60 mL/ min/1.73m2	0.26	1.03	1.4		

F4.II.1	**F4.II.2**	**F4.III.3**	**F5.II.1**	**F6.II.1**	**F7.II.1**
Spain	Spain	Spain	Argentina	Spain	Bosnian
F	F	F	M	M	F
3.5 yr	3.5 yr	6 yr	6 mo	5 yr	2.5 yr
48 yr	48 yr	8 yr	16 yr	7.5 yr	13 yr
Y (33 yr)	Y (33 yr)	N[#]	Y	N	Y (7 yr)
N/A	N/A	N/A	25	26	6
N/A	N/A	55	48	50	21
N/A	N/A	56	46	42	66
Y, 47 yr	Y, 42 yr	N/A	N	N/A	Y, 9 yr
Y - carpopedal spasms	Y - carpopedal spasms	Y - paresthesia and tetany	Y	N	N
Y	Y	Y	Y	Y	Y
N	N	N	N	N	N
?	?	Y (+ polyhydramnios)	N	Y	Y
Y	Y	Y	Y	Y	Y
1.72	1.72	2.5	2.44	2.37	2.48
92	92	105	97	99	N/A
2.8	2.8	3.76	3.4	3	3
0.45	0.53	0.62	0.33	0.37	0.63
136	135	142	136	137	134
1.55	1.55	1.58	1.3	1.36	1.2
0.8	0.8	0.34	0.38	0.37	0.38
31	30	29.4	29.8	23	N/A
n.d.	n.d.	18.7	21	17	5.6
n.d.	n.d.	13	14.2	16	8.50
n.d.	n.d.	1.4	0.3	0.5	0.13
0.14 mg/mg	0.17 mg/mg	0.44 mg/mg	0.05 mg/mg	0.42 mg/mg	0.16

Table 1. Continued

Individuals	F1.III.1	F2.II.1	F2.II.2	F2.II.4	F3.III.1	F3.II.1
Therapy						
Magnesium supplementation	MAGNESIUM-OXIDE 400 (241.3 Mg) MG tablet	N	N	N	300 mg three times daily	
Potassium supplementation	potassium chloride (K-TAB) 20 mEq CR tablet	N	N	N	315 mg = 8 mmol = 8 mval K+ twice daily	
Heart failure medication	eplerenone	N	N	N	none	
Others		laxatives	Laxatives, antibiotic prophylaxis (UTI)	N	Vit D 1000 I.U. per day	
Genetic findings (*RRAGD* variants)						
Nucleotide	c.272C>T	c.272C>T	c.272C>T	c.272C>T	c.299T>G	c.299T>G
Protein	p.(Thr91Ile)	p.(Thr91Ile)	p.(Thr91Ile)	p.(Thr91Ile)	p.(Ile100Arg)	p.(Ile100Arg)
Inheritance	?	Dominant?	Dominant?	Dominant?	Dominant	Dominant

*Patient F1.III.1 experienced nephrolithiasis since 15 months of age. Further testing was performed only in adulthood. The inheritance pattern of this patient is unknown. #Patient F4.III.3 developed apical trabeculations at 6 years old. Y: yes, N: no, N/A: not applicable, n.d.: not determined, ?: unknown.

Within this patient cohort, three novel variants, *RRAGD* p.(Ser77Phe), p.(Thr91Ile), and p.(Ile100Arg), were identified. These variants were absent in gnomAD. For three individuals (F5.1, F6.1, and F7.1), the *RRAGD* p.(Ser76Leu) and p.(Ser77Phe) variants occurred *de novo* as both parents of the patients were unaffected (Figure 2a). In Families 3 and 4, dominant inheritance is confirmed.

In silico modeling of *RRAGD* p.(Ser77Phe), p.(Thr91Ile), and p.(Ile100Arg) variants

To evaluate the consequences of the novel *RRAGD* variants on the protein structure, we generated an *in silico* modeling. All three variants are located just outside the G-box domains G1 and G2 (Figure 2b), which are predicted to mediate phosphate and Mg^{2+} binding.[25] Multiple sequence alignment analyses showed high conservation of the Ser-77, Thr-91, and Ile-100 residues (Supplementary Figure 2). Using the crystal structure of RagD in complex with a GTP analog (PDB: 2Q3F), the consequences of the p.(Ser77Phe), p.(Thr91Ile), and p.(Ile100Arg) variants were evaluated. Residue Ser-77 is located within the nucleotide-binding region in RagD

	F4.II.1	F4.II.2	F4.III.3	F5.II.1	F6.II.1	F7.II.1
	Y	Y	Y	Y	Y	Y
	Y	Y	Y	Y	Y	N
	Y	Y	N	Y	N	ACEi
	Immunosuppressives (heart transplant). Progression to renal failure, patient is being evaluated as a candidate for kidney transplant	immunosuppressives (heart transplant)	Citrate supplementation	Carvedilol	Potassium citrate + thiazides + enalapril	Immunosuppressive drugs: everolimus tacrolimus
	c.227C>T p.(Ser76Leu) Dominant	c.227C>T p.(Ser76Leu) Dominant	c.227C>T p.(Ser76Leu) Dominant	c.227C>T p.(Ser76Leu) de novo	c.227C>T p.(Ser76Leu) de novo	c.230C>T p.(Ser77Phe) de novo

(Figure 2c and d). Mutating Ser-77 to Phe-77 drastically enlarged the physical size of the residue and, therefore, would likely interfere with the nucleotide-binding capability of RagD (Figure 2d). Residue Thr-91 is positioned closely to the binding site of the nucleotide (Figure 2c and d). Thus, mutation at this residue to a larger isoleucine might affect nucleotide binding (Figure 2d). Lastly, residue Ile-100 is located in a hydrophobic pocket, surrounded by other hydrophobic residues (Figure 2c and d). Such hydrophobic sides are known to be energetically favorable for ligand binding.[26] The p.(Ile100Arg) variant, however, induced a change in properties from hydrophobic isoleucine to a larger and hydrophilic arginine (Figure 2d). Additionally, upon change to arginine, a steric clash to neighboring residues was observed (Figure 2d). Thus, this variant might result in protein binding instability. Of note, we compared the corresponding RagD residues to RagC in complex with Raptor, Ragulator, RagA, and TFEB (PDB: 7UX2) and found that Ile-100 residue is not directly interacting with any of these proteins.

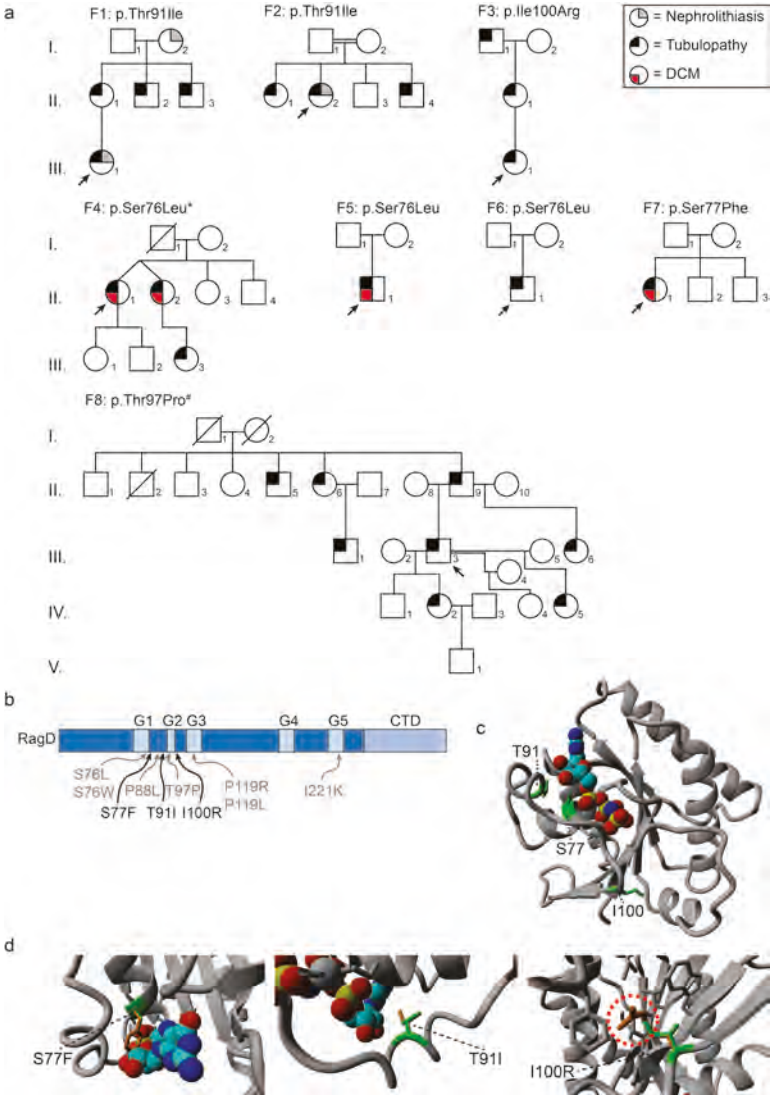

Figure 2. *In silico* modeling of the novel *RRAGD* variants. (a) Pedigrees of all families described in this study. The square shows males, while the circle shows females individuals. The crossed symbol indicates deceased individual. Filled symbols indicate affected individuals: grey indicates nephrolithiasis, black indicates kidney tubulopathy, and red indicates dilated cardiomyopathy (DCM). Proband individuals are marked with a black arrow. * Adapted from de Frutos *et al*,.[3] # Adapted from Schlingmann *et al.* and Trepiccione *et al*.,[1,27] (b) Schematic representation of RagD domain organization and the location of novel *RRAGD* variants (in black) and previously identified *RRAGD* variants (in grey). CTD: C-terminal domain. (C-F) Crystal structure of RagD in a complex with a GTP analog, GMPPNP (PDB structure: 2Q3F, shown as colored spheres). (c) Overview of RagD. Variant sites Ser-77 (S77), Thr-91 (T91), and Ile-100 (I100) are highlighted in green. (d) Close-up views of the mutated residues: (left) p.(Ser77Phe) (S77F), (middle) p.(Thr91Ile) (T91I), and (right) p.(Ile100Arg) (I100R). Mutated residues are highlighted in orange, the native residues are in green. The red dashed circle indicates a steric clash.

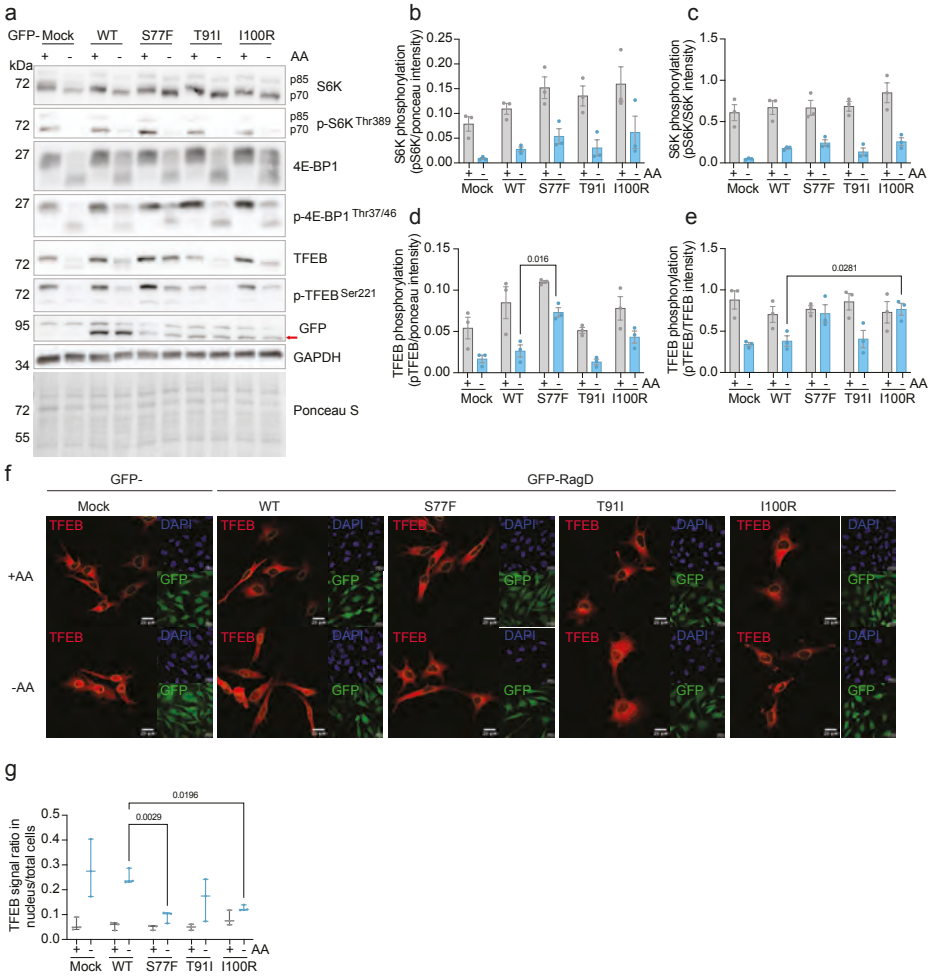

Figure 3. The effects of RagD p.(Ser77Phe), p.(Thr91Ile), and p.(Ile100Arg) variants on mTORC1 signaling. (a) Representative immunoblots of S6K, p-S6K, 4E-BP1, p-4E-BP1, TFEB, p-TFEB, GFP (RagD), GAPDH, and Ponceau S staining in T-REx HeLa cell lines overexpressing GFP-Mock, RagD-WT, -p.(Ser77Phe), -p.(Thr91Ile), and -p.(Ile100Arg) (S77F, T91I, and I100R in the figure, respectively) in the presence (+AA) or absence (-AA) of amino acids. (b-e) Graphs showing quantification of (b) p-S6K signal over ponceau, (c) p-S6K signal over S6K, (d) p-TFEB signal over ponceau, (e) p-TFEB signal over TFEB (mean ± SEM from 3 independent experiments). (f) Representative immunocytochemistry images of GFP-RagD T-REx HeLa cell lines upon TFEB transfection and subsequent AA stimulation. The cells were stained with anti-TFEB (red) and counterstained with DAPI (blue). The nuclei of TFEB-positive cells are outlined in yellow. Scale bar: 20 µm. (g) Quantification of TFEB nuclear/total cell signal from 3 independent experiments. Whiskers are extended from the maximum to the minimum points, and the middle line shows the median.

Non-canonical mTORC1 signaling is constitutively active due to *RRAGD* variants

We have previously reported that *RRAGD* variants identified in the initial cohort resulted in the overactivation of mTORC1 signaling.[1] To study the effects of the new variants described in this study on mTORC1 signaling, stable T-REx HeLa cell lines overexpressing GFP (mock), or GFP-RagD WT or mutants p.(Ser77Phe), p.(Thr91Ile), and p.(Ile100Arg) were generated. The cells were exposed to amino acids rich (+AA) or amino acids deprived (-AA) medium for 1 hr. Subsequently, phosphorylation of canonical and non-canonical mTORC1 targets, S6K, 4E-BP1, and TFEB was assessed (Figure 3a-e). Under -AA conditions, phosphorylation of TFEB in RagD-p.(Ser77Phe) and -p.(Ile100Arg) cells was significantly higher than in RagD-WT cells (mean ± SEM; p.(Ser77Phe) 0.07 ± 0.01 vs. WT 0.03 ± 0.01; p.(Ile100Arg) 0.8 ± 0.07 vs. WT 0.40 ± 0.06) (Figure 3a, d, and e). Interestingly, TFEB phosphorylation was not different in RagD-p.(Thr91Ile) cells compared to RagD-WT cells (Figure 3a-e). No significant differences in S6K and 4E-BP1 phosphorylation were detected in all cell lines, both in +AA and -AA conditions (Figure 3a-c).

Previously, TFEB was reported to be retained in the cytoplasm when RagD is constitutively active.[2] To test if TFEB subcellular localization is affected by the three novel *RRAGD* variants, all GFP-RagD T-REx HeLa cell lines were transiently transfected with TFEB and exposed to amino acid deprivation (1 hr), after which immunocytochemistry was performed for TFEB (Figure 3f & g). In line with the immunoblotting results, overexpression of RagD-p.(Ser77Phe) and -p.(Ile100Arg) resulted in a significantly reduced nuclear translocation of TFEB under -AA compared to RagD-WT cells (p.(Ser77Phe) 0.09 ± 0.01, p.(Ile100Arg) 0.13 ± 0.01 vs. WT 0.25 ± 0.02) (Figure 3f & g). Additionally, RagD-p.(Thr91Ile) overexpression did not affect TFEB nuclear translocation in -AA conditions (Figure 3f & g).

Diuretic challenges

To further characterize the renal phenotype of the *RRAGD* variants, we examined the patients' response to furosemide and HCT diuretics as measures for Na^+ reabsorption in the thick ascending limb (TAL) and distal convoluted tubule (DCT), respectively. Four patients carrying the *RRAGD* p.(Thr97Pro) variant (previously reported in[1]) were tested in hospital settings for renal physiology explorations. In healthy populations, 40 mg of furosemide causes increased urinary excretion of Na^+, K^+, Cl^-, Ca^{2+}, and Mg^{2+}.[22,28,29] As depicted in Table 2, the median [min; max] fractional excretions (FE, %) at baseline (T=0) were Na^+ (0.71 [0.1; 1]), K^+ (14.6 [6.60; 26]), Cl^- (1.03 [0.2; 2]), Ca^{2+} (0.8 [0.1; 1.1]), and Mg^{2+} (5.6 [2.5; 6.5]). These FEs increased over time after furosemide ingestion and peaked after 2 hr (Figure 4a, Supplementary Table 2, Supplementary Figure 3a-d). Accordingly, serum Mg^{2+}

concentrations decreased from 0.44 mM [0.40; 0.47] at baseline to 0.37 mM [0.36; 0.41] (Figure 4b). To compare the patients' response to furosemide to the healthy population, we re-analyzed data from Bech *et al*. (2017)[22]. The maximal increase of FE of Cl^- (i.e., maximal Δ FE Cl^-) of the ADKH-*RRAGD* patients following furosemide treatment is within the range of healthy individuals (ADKH-*RRAGD* patients 13.0% [12.4; 17.6] vs. healthy individuals 11.23% [3.9; 26.3]) (Supplementary Figure 3e, Table 2). The maximal Δ FE Mg^{2+} of ADKH-*RRAGD* patients was in the higher portion than in healthy individuals but still falls within range (ADKH-*RRAGD* patients 18.2% [17.1; 19.9] vs. healthy individuals 11.1% [7.1; 20.9]) (Figure 4c).

Table 2. Furosemide treatment. Fractional excretion (FE) of Cl^- and Mg^{2+} at baseline (T=0), maximal, maximal Δ (maximal value – baseline value), and the time of maximal FE reached. Values represent the median [min; max] of twenty-five healthy individuals[22] and four ADKH-*RRAGD* patients following p.o. 40 mg furosemide for 3 hr.

	Healthy controls (n=25)	**ADKH-*RRAGD* patients (n=4)**
Baseline FE Cl^- (%)	1.16 [0.45; 6.74]	1.0 [0.2; 2.1]
Maximal FE Cl^- (%)	12.79 [5.24; 27.5]	14.3 [13.4; 18.4]
Maximal ΔFE Cl^- (%)	11.23 [3.91; 26.29]	13.0 [12.4; 17.6]
Time max. FE Cl^- (hr)	2 [1; 3]	2 [2; 2]
Baseline FE Mg^{2+} (%)	2.8 [0.3; 6.3]	5.6 [2.5; 6.5]
Maximal FE Mg^{2+} (%)	14.5 [7.7; 25.8]	24.4 [19.6; 25.3]
Maximal ΔFE Mg^{2+} (%)	11.1 [7.1; 20.9]	18.2 [17.1; 19.9]
Time max. FE Mg^{2+} (hr)	2 [1; 3]	2 [2; 2]

The administration of 50 mg of HCT typically causes an increased urinary excretion of Na^+, K^+, and Cl^-, with decreased Ca^{2+} excretion.[22,30] Magnesium excretion physiologically remains unchanged or slightly increased after HCT. As summarized in Table 3, median [min; max] FE (%) at baseline were Na^+ (0.5 [0.2; 1.3]), K^+ (17.2 [6.3; 25.5]), Cl^- (1.2 [0.3; 2.1]), Ca^{2+} (0.6 [0.3; 1]), and Mg^{2+} (5.1 [2.9; 9.9]). The FE of Na^+, K^+, and Cl^- increased as early as 2 hr and remained stably high (Supplementary Table 3, Supplementary Figure 4a-c). FE Ca^{2+} stayed stable throughout the 6-hr (Supplementary Figure 4d). Compared to the healthy individuals cohort treated with 50 mg HCT for 6 hr,[22] the maximal median of Δ FE Cl^- after HCT administration in ADKH-*RRAGD* patients was similar to the healthy cohort (3.1% [2.5; 4.3] ADKH-*RRAGD* patients vs. 2.5% [1.3; 4.7] healthy individuals) (Supplementary Figure 4e, Table 3).[22] Furthermore, the FE of Mg^{2+} steeply increased after 2-hr oral exposure to 50 mg of HCT (24.4% [19.6; 25.3] vs. 11.6% [7.7; 18.8) in healthy controls], with no significant change in serum Mg^{2+} levels (Figure 5a&b, Table 3). The maximal median Δ FE Mg^{2+} in ADKH-*RRAGD* patients, however, was in range with that in healthy individuals (2.8% [0; 6.1] vs. 4% [0; 7.9]) (Figure 5c, Table 3).

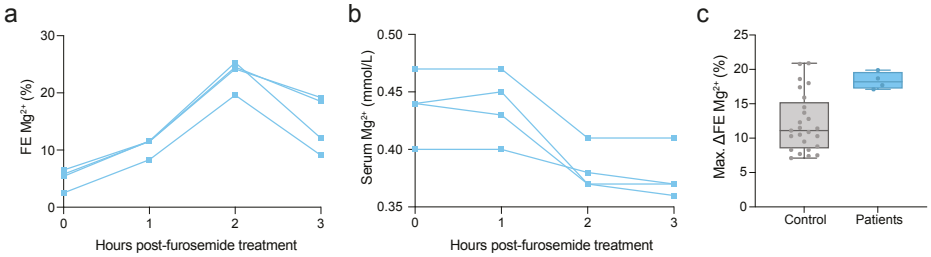

Figure 4. The effects of furosemide diuretics administration on fractional excretion of magnesium and serum magnesium in ADKH-*RRAGD* patients. Fractional excretion (FE) of Mg^{2+} (a), serum Mg^{2+} (b)) and maximal Δ FE Mg^{2+} in ADKH-*RRAGD* patients (blue, n=4) or healthy individuals (grey, n=25)[22] following p.o. 40 mg furosemide. In the box and whiskers graph (c), the box represents the 25th to the 75th quartile, the whiskers extend from the minimum to maximum points, and the middle line represents the median. Data points represent individuals.

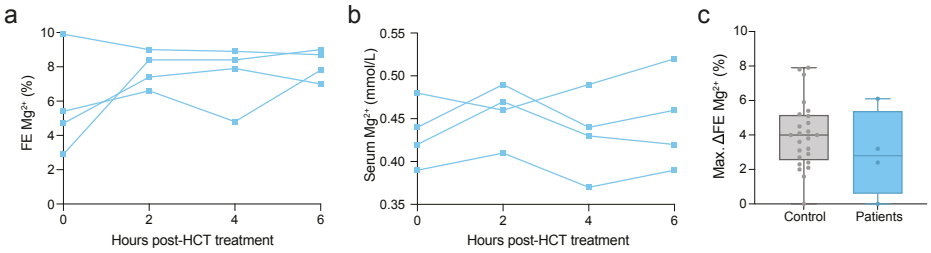

Figure 5. The effects of HCT diuretics administration on fractional excretion of magnesium and serum magnesium in ADKH-*RRAGD* patients. Fractional excretion (FE) of Mg^{2+} (a), serum Mg^{2+} (b), and maximal Δ FE Mg^{2+} in ADKH-*RRAGD* patients (blue, n=4) or healthy individuals (grey, n=25)[22] following p.o. 50 mg HCT administration. In the box and whiskers graph (c), the box represents the 25th to the 75th quartile, the whiskers extend from the minimum to maximum points, and the middle line represents the median. Data points represent individuals. HCT: hydrochlorothiazide.

Table 3. HCT treatment. Fractional excretion (FE) of Cl^- and Mg^{2+} at baseline (T=0), maximal, maximal Δ (maximal value – baseline value), and the time of maximal FE reached. Values represent the median [min; max] of twenty-five healthy individuals[22] and four ADKH-*RRAGD* patients following p.o. 50 mg HCT (hydrochlorothiazide) for 6 hr.

	Healthy controls (n=25)	**ADKH-*RRAGD* patients (n=4)**
Baseline FE Cl^- (%)	1.04 [0.26; 1.64]	1.19 [0.31; 2.1]
Maximal FE Cl^- (%)	3.47 [2.13; 5.63]	4.18 [3.65; 4.65]
Maximal ΔFE Cl^- (%)	2.53 [1.32; 4.73]	3.15 [2.46; 4.29]
Time max FE Cl^- (hr)	4 [2; 4]	3 [2; 4]
Baseline FE Mg^{2+} (%)	3.3 [0.1; 6.3]	5.05 [2.9; 9.9]
Maximal FE Mg^{2+} (%)	6.6 [4; 12.9]	8.45 [7.8; 9.9]
Maximal ΔFE Mg^{2+} (%)	4 [0; 7.9]	2.8 [0; 6.1]
Time max. FE Mg^{2+} (hr)	4 [0; 6]	5 [0; 6.1]

Therapeutic perspective

Current therapy available for patients with ADKH-*RRAGD* is limited to Mg^{2+} and K^{+} supplementation. Although SGLT2 inhibitors, including dapagliflozin, have been recommended in the management of patients with chronic cardiomyopathy,[31] no data are available on the use of SGLT2 inhibitors in ADKH-*RRAGD* patients to date. Here, we have evaluated the impact of 15 days of daily exposure to 10 mg dapagliflozin on serum ion levels in 6 patients from the p.(Thr97Pro) *RRAGD* family. After 15 days of dapagliflozin intake, serum concentration of Mg^{2+} was increased by 0.04 mM from baseline (median [min; max], 0.40 [0.34; 0.53] mM) to D15 (0.44 [0.39; 0.58] mM) (Table 4, Figure 6a). Of note, the median serum K^{+} levels dropped by 0.25 mM at D15 (3.4 [3.0; 4.1] at baseline; 3.15 [2.4; 3.7] at D15). Serum creatinine levels did not change within the 15 days of dapagliflozin treatment (0.68 mg/dL [0.5; 1] at baseline; 0.69 mg/dL [0.5; 1] at D15).

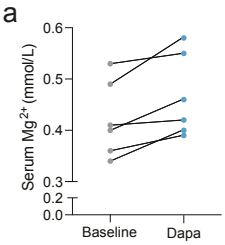

Figure 6. Dapagliflozin and serum Mg^{2+} levels in ADKH-*RRAGD* patients. Serum Mg^{2+} levels at day 0 (baseline) and after 15 days of 10 mg dapagliflozin treatment (dapa) in six ADKH-*RRAGD* patients. Data points represent individuals.

Table 4. Dapagliflozin data. Values represent the median [min; max] of six patients following p.o. 10 mg dapagliflozin for 15 days.

	Baseline	Dapa	Δ Dapa-Baseline
Blood			
Osmolarity (mosm/kg; N=281-303)	281 [281; 291]	282 [279; 288]	1.00
Na^{+} (mmol/L; N=136-145)	142 [138; 143]	141 [140; 144]	-1.00
K^{+} (mmol/L; N=3.5-5.1)	3.4 [3; 4.08]	3.15 [2.4; 3.67]	-0.25
Cl^{-} (mmol/L; N=98-107)	96 [90; 108]	95.5 [88; 106]	-0.50
Ca^{2+} (mmol/L; N=2.2-2.6)	2.4 [2.3; 2.7]	2.44 [2.3; 2.51]	0.04
Mg^{2+} (mmol/L; N=0.66-1.07)	0.41[0.34; 0.53]	0.44 [0.39; 0.58]	0.04
HCO3 (mmol/L; N=22-31)	33.75 [26; 38.4]	31.4 [27.4; 39.6]	-2.35
Creatinine (mg/dL; N=0.73-1.18)	0.68[0.47; 0.9]	0.69 [0.49; 1]	0.01
eGFR (mL/min/1.73m2; N=>60)	109.9 [88.1; 128.5]	104.65 [77.6; 128.5]	-5.25

Table 4. Continued

	Baseline	Dapa	Δ Dapa-Baseline
PTH 3rd generation (ng/L)	27.9 [18.1; 40.1]	22.9 [15.5; 33.4]	-5.00
Glucose (mg/dL; N=60-100)	91.5 [75; 142]	94 [78; 151]	2.50
Urine			
Osmolarity (mosm/kg; N=50-1200)	152.65 [88; 214.2]	112.75 [49; 214]	-39.90
Na^+ (mmol/L; N=22.3-200.1)	70.54 [42; 82.94]	64.48 [47.3; 95]	-6.07
K^+ (mmol/L; N=20.6-101.9)	100.5 [76; 125]	174 [131; 217]	73.50
Cl^- (mmol/L; N=27-225)	3.96 [2.63; 6.3]	4.3 [2.6; 8.8]	0.34
Creatinine (mg/dL; N=0-37.7)	5.06 [1.82; 6.21]	3.9 [3.1; 6.33]	-1.16
Ca/Creat (mmol/g creat; N=0.3-6.1)	0.4 [0.4; 0.4]	6.63 [1.6; 27.09]	6.23
Mg/Creat (mmol/g creat; N=0.74-4.53)	1.43 [0.7136; 2.0]	1.31 [0.673; 1.98]	-0.11

Discussion

In this study, we identified seven novel families comprising 12 patients with pathogenic variants in *RRAGD*. Pathogenicity of the novel *RRAGD* variants was confirmed by assessing mTORC1 activity in T-REx HeLa cells. The identified *RRAGD* p.(Ser77Phe) and p.(Ile100Arg) variants rendered mTORC1 insensitive to amino acids starvation, resulting in a constitutive activation of the non-canonical mTORC1 signaling pathway. Additionally, diuretic challenges revealed that Na^+ reabsorption in patients remained sensitive to furosemide and thiazide treatment. Most importantly, SGLT2 inhibition by dapagliflozin increased serum Mg^{2+} levels in a small cohort of 6 individuals with the *RRAGD* p.(Thr97Pro) variant.

RagD, one of the four small Rag GTPases, is involved in amino acid sensing by mTORC1. Using an *in vitro* model, we demonstrated that p.(Ser77Phe) and p.(Ile100Arg) *RRAGD* variants rendered mTORC1 non-canonical signaling (i.e., TFEB phosphorylation) insensitive to amino acids signaling, but not the canonical signaling (i.e., S6K and 4E-BP1 phosphorylation). Specifically, these *RRAGD* variants led to constant phosphorylation of TFEB and reduced TFEB translocation to the nuclei. This is in line with Sambri *et al.*'s study where non-canonical mTORC1 signaling was affected by the *RRAGD* variants in their *in vitro* model.[2] Concerning mTORC1 canonical signaling, we previously showed that most of the *RRAGD* variants from the initial patient cohort resulted in the overactivation of canonical mTORC1 signaling as shown by increased phosphorylation of S6K under amino acids starvation.[1] Indeed, our results showed that p.(Ser77Phe) and p.(Ile100Arg)

RRAGD variants tended towards a slight increase in S6K phosphorylation, but this was not statistically significant. Therefore, we suggest that *RRAGD* variants affect non-canonical mTORC1 signaling more strongly than canonical signaling and that the degree of overactivation of the mTORC1 canonical signaling might vary per mutation, as already previously highlighted by the *RRAGD* p.(Thr97Pro) variant.[1]

Common symptoms reported in this cohort included hypomagnesemia (11/12), nephrocalcinosis (11/12), hypokalemia (10/12), metabolic alkalosis (10/12), and dilated cardiomyopathy (4/12). These 12 new ADKH-RRAGD patients, together with previous reports, represent the most extensive phenotypic characterization of the disease to date (Table 5).[1-3,27] Across 36 identified patients, kidney tubulopathies were nearly universal, with 23 presenting in childhood and 11 developing them later in life. In all known *RRAGD* cases, cardiomyopathies are present in about half of the patients (n=17) with DCM being the most prominent form (n=12). DCM was diagnosed in childhood in 8 out of the 12 patients affected. In addition to DCM, other forms of cardiomyopathy are also found among ADKH-*RRAGD* patients, which are ventricular arrhythmia (3/17), myocardial infarction (1/17), and excessive apical trabeculations with normal LVEF (1/17). Among these cases of non-DCM cardiomyopathy, three patients were diagnosed in childhood and the other two in adulthood.

Interestingly, half of all patients (17/36) presented with isolated kidney tubulopathies, suggesting that renal and cardiac phenotypes can occur independently. While cardiomyopathies typically manifest early, four patients developed DCM in adulthood. Thus, we recommend that healthcare providers continue to monitor the cardiac health of ADKH-*RRAGD* patients, with particular attention to pediatric cases. Regarding the distribution by sex of the patients with DCM, 40% of the affected females and 21% of the affected males presented with DCM. In the future, it would be important to monitor if age and sex are determinant factors for disease outcomes and if more factors can be identified. This would require the identification of more patients and follow-up of current patients. Finally, we would like to highlight that half of all patients (17/36) presented with only kidney tubulopathy and no cardiac dysfunction, at least until the most recent follow-up, suggesting that the two key phenotypes can occur separately. Therefore, future ADKH-*RRAGD* patient screening should also be done in patient cohorts with idiopathic DCM or other cardiomyopathies with proven/frequent genetic origin.

Table 5. Summary of all identified patients with pathogenic *RRAGD* variants.

Variants	p.(Ser76Leu)	p.(Ser76Trp)	p.(Ser77Phe)	p.(Pro88Leu)	p.(Thr91Ile)
Patients (family)	8 (6)	1 (1)	1 (1)	8 (1)	4 (2)
Initial clinical presentation	KT (5), DCM (3)	KT (1)	KT (1)	KT (5), DCM (1)	KT (4)
Childhood tubulopathies[#]	Yes	Yes	Yes	3/8	3/4
Adulthood tubulopathies	No	No	No	4/8	1/4
Hypomagnesemia	Yes	Yes	Yes	Yes	Yes
Nephrocalcinosis	Yes	Yes	Yes	3/8	Yes
Nephrolithiasis	No	No	No	3/8	2/4
Polyuria	2/8	Yes	Yes	2/8	No
Metabolic alkalosis	6/8	Yes	Yes	?	3/4
Childhood DCM[#]	3/8	No	Yes	No	No
Adulthood DCM	2/8	No	No	2/8	No
Heart transplantation	3/8 (31 yr)[%]	No	Yes (9 yr)	1/8 (43 yr)	No
Other cardiomyopathies	1/8	No	No	4/8	No
***In vitro* mTORC1 activation**					
Canonical signaling	Yes	Mild	Mild	No	No
Non-canonical signaling	Yes	?	Yes	Yes	No

Summary of known patients with pathogenic *RRAGD* variants described in this study and previous reports.[1-3, 27] Kidney tubulopathy (KT), dilated cardiomyopathy (DCM), mechanistic target of rapamycin complex 1 (mTORC1). [#]Infancy – early adolescence (≤ 18 yr), [%]average age, *some family members were incidentally diagnosed in adulthood due to family screening, ? unknown number of cases or has never been investigated.

Due to the phenotypic variability in the patients (i.e., not all variants lead to the same clinical manifestations), we hypothesized that the severity of symptoms can be attributed to the degree of mTORC1 dysregulation caused by the *RRAGD* variant.[1] However, our data revealed that the effects of the variant on mTORC1 activation alone are not linear to the clinical manifestations. In this study, we described *RRAGD* p.(Thr91Ile) patients exhibiting the complete set of renal phenotypes seen in other patients without DCM. *In vitro* assessment showed that this variant did not induce mTORC1 overactivation in our stable T-REx HeLa cell line. Previously, we have observed that *RRAGD* p.(Thr97Pro) variant also induced a less pronounced mTORC1 signaling activation.[1] Interestingly, patients with p.(Ile100Arg) variant presented with the same clinical manifestations as p.(Thr91Ile) patients. However, *RRAGD* p.(Ile100Arg) variant did show an increased mTORC1 activity under amino acids starvation. Nevertheless, the effects of *RRAGD* variants on mTORC1 signaling have so far been assessed in HEK293 and HeLa cells, as well as whole zebrafish embryo lysates.[1,2,18] Future functional

p.(Thr97Pro)	p.(Ile100Arg)	p.(Pro119Leu)	p.(Pro119Arg)	p.(Ile221Lys)	Total
8 (1)	2 (1)	1 (1)	2 (2)	1 (1)	36 (17)
KT (8)	KT (2)	DCM (1)	KT (2)	DCM (1)	KT (28), DCM (6)
2/8	1/2	Yes	Yes	Yes	23
6/8*	1/2	No	No	No	11
Yes	1/2	Yes	Yes	Yes	35
No	Yes	Yes	Yes	Yes	21
1/8	1/2	?	?	No	7
2/8	No	Yes	Yes	Yes	12
4/8	1/2	No	No	Yes	17
No	No	Yes	Yes	Yes	8
No	No	No	No	No	4
No	No	No	1/2 (25 yr)	Yes (15 yr)	7 (18 yr)[%]
No	No	No	No	No	5
No	Mild	Mild	Yes	Yes	7 (4 mild)
Yes	Yes	Yes	?	Yes	7

studies to assess the effects of *RRAGD* variants on renal transport and cardiac function are necessary to fully elucidate the molecular mechanisms of this rare disease.

The renal phenotypes seen in ADKH-*RRAGD* patients resemble Bartter syndrome and Familial Hypomagnesemia, Hypercalciuria, and Nephrocalcinosis (FHHNC) in which the thick ascending limb (TAL) section of the renal tubule is affected.[32-35] In family 8, which is affected by the variant p.(Thr97Pro), the absence of hypercalciuria and nephrocalcinosis more closely resembles Gitelman syndrome where the Na^+-Cl^- cotransporter (NCC) is impaired, suggesting a defect in the distal convoluted tubule (DCT).[36] This, together with the fact that RagD is mainly expressed in the distal segments of mouse nephrons, points to a TAL and DCT defect in ADKH-*RRAGD* patients.[1] Paracellular Mg^{2+} and Ca^{2+} transport in the TAL is driven by the activity of the Na^+-K^+-2Cl cotransporter 2 (NKCC2). Thus, dysfunctional NKCC2 could affect Mg^{2+} and Ca^{2+} homeostasis.

Currently, the therapeutic management of ADKH-*RRAGD* patients focuses on symptomatic treatment with Mg^{2+} and K^{+} supplementation. According to guidelines, patients with DCM should also receive renin-angiotensin system (RAS) and SGLT2 inhibitors.[19,20] In this study, we explored the impact of dapagliflozin (SGLT2 inhibitor) treatment on serum Mg^{2+} levels: we demonstrated that dapagliflozin increased serum Mg^{2+} levels in p.(Thr97Pro) *RRAGD* patients (i.e., by 0.04 mM). Interestingly, SGLT2 inhibitors have been shown to have both renal and cardioprotective properties in both patients with and without type 2 diabetes mellitus.[37,38] More recently, SGLT2 inhibitors have been associated with a mild increase in serum Mg^{2+} levels (0.06-0.3 mM) in diabetic patients with hypomagnesemia.[39-41] The mild increase in serum magnesium level is, however, significant given the inherent difficulty to raise serum magnesium by oral supplementation in patients with a renal magnesium leak. In addition to increasing serum Mg^{2+} levels, in separate studies, the use of SGLT2 inhibitors reduced mTORC1 activation in the kidney and cardiac myocytes, further strengthening the potential benefit of this drug for ADKH-*RRAGD* patients.[42-44] Although it was not investigated if mTORC1 activation is dampened in patients upon dapagliflozin administration, this opens up a novel treatment option for ADKH-*RRAGD* patients with hypomagnesemia, DCM, and mTORC1 overactivation. However, the associated serum K^{+} reduction (median: 0.25 mM) warrants consideration when prescribing this treatment.

There are a few limitations in this study. First, HeLa cells lack the expression of relevant renal transporters, such as the claudins and NKCC2, making functional studies not feasible in these cells. Here, we have provided evidence that mTORC1 activation is not linear to the clinical manifestations in patients in HeLa cells. It is, therefore, crucial to investigate how *RRAGD* variants affect renal ion transports and cardiac functions to further unravel the molecular mechanisms underlying this disease. Second, the dapagliflozin trial was conducted in only one family. Future studies should evaluate the efficacy of SGLT2 inhibitors in larger cohorts with diverse *RRAGD* variants. Importantly, dapagliflozin is already clinically approved for managing refractory hypomagnesemia and chronic cardiomyopathy.[31,40]

In conclusion, we report a large cohort of ADKH-*RRAGD* patients comprising 12 individuals with three novel *RRAGD* variants and present the most comprehensive phenotypic characterization of this disease to date. This work highlights the potential of SGLT2 inhibitors as a novel treatment option for ADKH-RRAGD patients, particularly those with hypomagnesemia, DCM, and mTORC1 overactivation. Future studies should focus on elucidating the mechanisms of SGLT2 inhibitors and further assessing their therapeutic benefits in ADKH-RRAGD patients.

Disclosure

None declared

Acknowledgements

We would like to thank Radboudumc Technology Center Microscopy for the use of their microscopy facilities.

Grants

This work was financially supported by the IMAGEN (IMplementation of Advancements in GENetic Kidney Disease) project, which is co-funded by the PPP Allowance made available by Health~Holland, Top Sector Life Sciences & Health, to stimulate public-private partnerships (LSHM20009) and the Dutch Kidney Foundation (20OP + 018). In addition, this work was funded by the European Research Council grant 101040682 (IN-THE-KIDNEY) and Netherlands Organization for Scientific Research grants OCENW.M.21.022 and VIDI 391 09150172110040 (IMAGE-THE-KIDNEY). The study of families 4-6 was financially supported by the grant PI21/01419 from the National Institute of Health Carlos III (Spain) and the grant IT1739-22 from the Department of Education of the Basque Government (Spain).

References

1. Schlingmann KP, Jouret F, Shen K, et al. mTOR-Activating Mutations in RRAGD Are Causative for Kidney Tubulopathy and Cardiomyopathy. *J Am Soc Nephrol.* 2021;32(11):2885-2899.
2. Sambri I, Ferniani M, Campostrini G, et al. RagD auto-activating mutations impair MiT/TFE activity in kidney tubulopathy and cardiomyopathy syndrome. *Nat Commun.* 2023;14(1):2775.
3. de Frutos F, Diez-Lopez C, Garcia-Romero E, et al. Dilated Cardiomyopathy With Concomitant Salt-Losing Renal Tubulopathy Caused by Heterozygous RRAGD Gene Variant. *Circ Genom Precis Med.* 2024;17(2):e004336.
4. Kim E, Goraksha-Hicks P, Li L, Neufeld TP, Guan KL. Regulation of TORC1 by Rag GTPases in nutrient response. *Nat Cell Biol.* 2008;10(8):935-945.
5. Sancak Y, Peterson TR, Shaul YD, et al. The Rag GTPases bind raptor and mediate amino acid signaling to mTORC1. *Science.* 2008;320(5882):1496-1501.
6. Sekiguchi T, Hirose E, Nakashima N, Ii M, Nishimoto T. Novel G proteins, Rag C and Rag D, interact with GTP-binding proteins, Rag A and Rag B. *J Biol Chem.* 2001;276(10):7246-7257.
7. Hirose E, Nakashima N, Sekiguchi T, Nishimoto T. RagA is a functional homologue of S. cerevisiae Gtr1p involved in the Ran/Gsp1-GTPase pathway. *J Cell Sci.* 1998;111 (Pt 1):11-21.
8. Schurmann A, Brauers A, Massmann S, Becker W, Joost HG. Cloning of a novel family of mammalian GTP-binding proteins (RagA, RagBs, RagB1) with remote similarity to the Ras-related GTPases. *J Biol Chem.* 1995;270(48):28982-28988.
9. Anandapadamanaban M, Masson GR, Perisic O, et al. Architecture of human Rag GTPase heterodimers and their complex with mTORC1. *Science.* 2019;366(6462):203-210.
10. Rogala KB, Gu X, Kedir JF, et al. Structural basis for the docking of mTORC1 on the lysosomal surface. *Science.* 2019;366(6464):468-475.
11. Holz MK, Ballif BA, Gygi SP, Blenis J. mTOR and S6K1 mediate assembly of the translation preinitiation complex through dynamic protein interchange and ordered phosphorylation events. *Cell.* 2005;123(4):569-580.
12. Fingar DC, Blenis J. Target of rapamycin (TOR): an integrator of nutrient and growth factor signals and coordinator of cell growth and cell cycle progression. *Oncogene.* 2004;23(18):3151-3171.
13. Gingras AC, Gygi SP, Raught B, et al. Regulation of 4E-BP1 phosphorylation: a novel two-step mechanism. *Genes Dev.* 1999;13(11):1422-1437.
14. Kim J, Kundu M, Viollet B, Guan KL. AMPK and mTOR regulate autophagy through direct phosphorylation of Ulk1. *Nat Cell Biol.* 2011;13(2):132-141.
15. Martina JA, Chen Y, Gucek M, Puertollano R. MTORC1 functions as a transcriptional regulator of autophagy by preventing nuclear transport of TFEB. *Autophagy.* 2012;8(6):903-914.
16. Roczniak-Ferguson A, Petit CS, Froehlich F, et al. The transcription factor TFEB links mTORC1 signaling to transcriptional control of lysosome homeostasis. *Sci Signal.* 2012;5(228):ra42.
17. Settembre C, Zoncu R, Medina DL, et al. A lysosome-to-nucleus signalling mechanism senses and regulates the lysosome via mTOR and TFEB. *EMBO J.* 2012;31(5):1095-1108.
18. Adella A, Tengku F, Arjona FJ, et al. RRAGD variants cause cardiac dysfunction in a zebrafish model. *Am J Physiol Heart Circ Physiol.* 2024;327(5):H1187-H1197.

19. Authors/Task Force M, McDonagh TA, Metra M, et al. 2023 Focused Update of the 2021 ESC Guidelines for the diagnosis and treatment of acute and chronic heart failure: Developed by the task force for the diagnosis and treatment of acute and chronic heart failure of the European Society of Cardiology (ESC) With the special contribution of the Heart Failure Association (HFA) of the ESC. *Eur J Heart Fail.* 2024;26(1):5-17.
20. Zannad F, Ferreira JP, Pocock SJ, et al. SGLT2 inhibitors in patients with heart failure with reduced ejection fraction: a meta-analysis of the EMPEROR-Reduced and DAPA-HF trials. *Lancet.* 2020;396(10254):819-829.
21. Vega-Rubin-de-Celis S, Pena-Llopis S, Konda M, Brugarolas J. Multistep regulation of TFEB by MTORC1. *Autophagy.* 2017;13(3):464-472.
22. Bech AP, Wetzels JFM, Nijenhuis T. Reference values of renal tubular function tests are dependent on age and kidney function. *Physiol Rep.* 2017;5(23).
23. Schindelin J, Arganda-Carreras I, Frise E, et al. Fiji: an open-source platform for biological-image analysis. *Nat Methods.* 2012;9(7):676-682.
24. Rueden CT, Schindelin J, Hiner MC, et al. ImageJ2: ImageJ for the next generation of scientific image data. *BMC Bioinformatics.* 2017;18(1):529.
25. Nicastro R, Sardu A, Panchaud N, De Virgilio C. The Architecture of the Rag GTPase Signaling Network. *Biomolecules.* 2017;7(3).
26. Patil R, Das S, Stanley A, Yadav L, Sudhakar A, Varma AK. Optimized hydrophobic interactions and hydrogen bonding at the target-ligand interface leads the pathways of drug-designing. *PLoS One.* 2010;5(8):e12029.
27. Trepiccione F, Sambri I, Ruggiero B, et al. RRAGD-Associated Autosomal Dominant Kidney Hypomagnesemia with Cardiomyopathy: A Review on the Clinical Manifestations and Therapeutic Options. *Kidney Blood Press Res.* 2024;49(1):637-645.
28. Davies DL, Wilson GM. Diuretics: mechanism of action and clinical application. *Drugs.* 1975;9(3):178-226.
29. Ryan MP, Devane J, Ryan MF, Counihan TB. Effects of diuretics on the renal handling of magnesium. *Drugs.* 1984;28 Suppl 1:167-181.
30. Reyes AJ. Effects of diuretics on outputs and flows of urine and urinary solutes in healthy subjects. *Drugs.* 1991;41 Suppl 3:35-59.
31. Arbelo E, Protonotarios A, Gimeno JR, et al. 2023 ESC Guidelines for the management of cardiomyopathies. *Eur Heart J.* 2023;44(37):3503-3626.
32. Praga M, Vara J, Gonzalez-Parra E, et al. Familial hypomagnesemia with hypercalciuria and nephrocalcinosis. *Kidney Int.* 1995;47(5):1419-1425.
33. Simon DB, Lu Y, Choate KA, et al. Paracellin-1, a renal tight junction protein required for paracellular Mg2+ resorption. *Science.* 1999;285(5424):103-106.
34. Konrad M, Schaller A, Seelow D, et al. Mutations in the tight-junction gene claudin 19 (CLDN19) are associated with renal magnesium wasting, renal failure, and severe ocular involvement. *Am J Hum Genet.* 2006;79(5):949-957.
35. Rodriguez-Soriano J, Vallo A, Garcia-Fuentes M. Hypomagnesaemia of hereditary renal origin. *Pediatr Nephrol.* 1987;1(3):465-472.

36. Blanchard A, Bockenhauer D, Bolignano D, et al. Gitelman syndrome: consensus and guidance from a Kidney Disease: Improving Global Outcomes (KDIGO) Controversies Conference. *Kidney Int*. 2017;91(1):24-33.
37. Packer M. Critical Reanalysis of the Mechanisms Underlying the Cardiorenal Benefits of SGLT2 Inhibitors and Reaffirmation of the Nutrient Deprivation Signaling/Autophagy Hypothesis. *Circulation*. 2022;146(18):1383-1405.
38. Heerspink HJ, Perkins BA, Fitchett DH, Husain M, Cherney DZ. Sodium Glucose Cotransporter 2 Inhibitors in the Treatment of Diabetes Mellitus: Cardiovascular and Kidney Effects, Potential Mechanisms, and Clinical Applications. *Circulation*. 2016;134(10):752-772.
39. Tang H, Zhang X, Zhang J, et al. Elevated serum magnesium associated with SGLT2 inhibitor use in type 2 diabetes patients: a meta-analysis of randomised controlled trials. *Diabetologia*. 2016;59(12):2546-2551.
40. Ray EC, Boyd-Shiwarski CR, Liu P, Novacic D, Cassiman D. SGLT2 Inhibitors for Treatment of Refractory Hypomagnesemia: A Case Report of 3 Patients. *Kidney Med*. 2020;2(3):359-364.
41. Toto RD, Goldenberg R, Chertow GM, et al. Correction of hypomagnesemia by dapagliflozin in patients with type 2 diabetes: A post hoc analysis of 10 randomized, placebo-controlled trials. *J Diabetes Complications*. 2019;33(10):107402.
42. Schaub JA, AlAkwaa FM, McCown PJ, et al. SGLT2 inhibitors mitigate kidney tubular metabolic and mTORC1 perturbations in youth-onset type 2 diabetes. *J Clin Invest*. 2023;133(5):e164486.
43. Tuttle KR. Digging deep into cells to find mechanisms of kidney protection by SGLT2 inhibitors. *J Clin Invest*. 2023;133(5).
44. Li X, Lu Q, Qiu Y, et al. Direct Cardiac Actions of the Sodium Glucose Co-Transporter 2 Inhibitor Empagliflozin Improve Myocardial Oxidative Phosphorylation and Attenuate Pressure-Overload Heart Failure. *J Am Heart Assoc*. 2021;10(6):e018298.
45. Wilke M, Klee EW, Dhamija R, et al. Diagnostic yield of exome and genome sequencing after non-diagnostic multi-gene panels in patients with single-system diseases. *Orphanet J Rare Dis*. 2024;19(1):216.
46. Sobreira N, Schiettecatte F, Valle D, Hamosh A. GeneMatcher: a matching tool for connecting investigators with an interest in the same gene. *Hum Mutat*. 2015;36(10):928-930.
47. Karczewski KJ, Francioli LC, Tiao G, et al. The mutational constraint spectrum quantified from variation in 141,456 humans. *Nature*. 2020;581(7809):434-443.
48. Madeira F, Madhusoodanan N, Lee J, et al. The EMBL-EBI Job Dispatcher sequence analysis tools framework in 2024. *Nucleic Acids Res*. 2024;52(W1):W521-W525.
49. Land H, Humble MS. YASARA: A Tool to Obtain Structural Guidance in Biocatalytic Investigations. *Methods Mol Biol*. 2018;1685:43-67.
50. Brooks HL, de Castro Bras LE, Brunt KR, et al. Guidelines on antibody use in physiology research. *Am J Physiol Renal Physiol*. 2024;326(3):F511-F533.

Supplementary materials and methods

Sequencing

Family 1

Exome sequencing was conducted at a CLIA-certified and CAP-accredited laboratory using Illumina (Illumina, California, USA) short reads platform. Manual analysis of the raw sequencing files, was done utilizing commercial genomic prioritization tools that operate through AI-driven graphical interfaces, requiring the input of VCF or BAM files, along with information on sex, age of onset, and Human Phenotype Ontology (HPO) terms. [45]

Family 4

Genomic DNA was extracted from peripheral blood leukocytes using the MagPurix instrument (Zinexts Life Science Corp., New Taipei City, Taiwan, R.O.C.). DNA purity and concentration were determined using Qubit 2.0 fluorometer (Thermo Fisher Scientific). Library preparation was done using the Ion AmpliSeq™ Exome RDY Library Preparation kit (Thermo Fisher Scientific) according to manufacturer's instructions. Samples were then sequenced using the Ion GeneStudio S5 System (Thermo Fisher Scientific, California, USA). Base calling, read filtering, alignment to the reference human genome GRCh37/hg19, and variant calling were done using Ion Torrent Suite and Ion Reporter Software (Thermo Fisher Scientific, California, USA). Not appropriately covered amplicons (<20x) and candidate variants were assessed by Sanger sequencing after polymerase chain reaction (PCR), sequenced with fluorescent dideoxynucleotides (BigDye Terminator v3.1 Cycle Sequencing Kit, Life Technologies, Grand Island, NY, USA), and loaded onto an ABI3130xl Genetic Analyzer (Thermo Fisher Scientific, California, USA).

Families 5 and 6

Genomic DNA was extracted from peripheral blood leukocytes using the MagPurix instrument (Zinexts Life Science Corp., New Taipei City, Taiwan, R.O.C.). DNA purity and concentration were determined using Qubit 2.0 fluorometer (Thermo Fisher Scientific, California, USA). Library preparation was done using the Illumina DNA Prep with Exome 2.0 Plus Enrichment according to manufacturer's instructions. Samples were then sequenced using the NovaSeq6000 platform (Illumina, California, USA). Alignment and variant calling was carried out using Dragen 4.2.4 pipeline (Illumina, California, USA) against GRCh38 (hg38). Annotation and interpretation of identified variants was done with the Illumina Variant Interpreter Version 2.16. The variant filtering (SNV/Indel) was performed by using pre-established filters: coding

and flanking intronic variants (+/-10 bp), more than 20X read depth and less than 0.01% population frequency (GnomAD v2.1.1, https://gnomad.broadinstitute.org/). Novel DNA variant was named according to the Human Genome Variation Society guidelines (www.hgvs.org), and classified according to ACMG-AMP (American College of Medical Genetics and Genomics and the Association for Molecular Pathology) guidelines. Candidate variants were assessed by Sanger sequencing after polymerase chain reaction (PCR), sequenced with fluorescent dideoxynucleotides (BigDye Terminator v3.1 Cycle Sequencing Kit, Life Technologies, Grand Island, NY, USA), and loaded onto an ABI3130xl Genetic Analyzer (Thermo Fisher Scientific, California, USA).

Family 7

Next Generation Sequencing of relevant genes in Illumina's Trusight Cardio kit (Illumina, California, USA) was performed. Results of the sequencing revealed no known variants that cause dilated cardiomyopathy. Next, genome sequencing was performed, which included analysis of copy numbers, with filtration for variants of genes that are part of the gen panel for renal tubular disease (v2). On request from the clinician, *RRAGD* was part of the analysis.

Study participants

The individuals included in this manuscript were identified by routine diagnostic DNA testing (see details below). All patients had a clinical presentation of kidney tubulopathy and genetic screening resulted in the identification of class 3-5 *RRAGD* variants. GeneMatcher was employed to find and connect multiple cases.[46] Written informed consent was obtained for the genetic analysis and the publication of anonymized data, including the clinical challenges of diuretics.

Genetic analysis

Allele frequencies of the newly identified *RRAGD* (NM_021244.5) variants were checked in the GnomAD v4.1 [47] database in July 2024.

In silico analysis

For multiple sequence alignment analysis, the following sequences were used: Saccharomyces cerevisiae (UniProtKB ID: P53290), Caenorhabditis elegans (UniProtKB ID: G5EGB3), Drosophila melanogaster (UniProtKB ID: Q7K519), Danio rerio (UniProtKB ID: F1QIB5), Xenopus tropicalis (UniProtKB ID: Q0VFL0), Mus musculus (UniProtKB ID: Q7TT45), and Homo sapiens (UniProtKB ID: Q9NQL2). Multiple alignment analysis was performed using Clustal Omega (EMBL-BI).[48] To model the variants, a publicly available crystal structure of RagD in complex with a GTP analogue, Gmppnp, was used (PDB: 2Q3F). Analysis and visualization were done in YASARA.[49]

Cloning and plasmids

Human *RRAGD* construct (VectorBuilder GmbH, Neu-Isenburg, Germany (Vector ID: VB171030-1104zuv)) was amplified by PCR and subcloned into the pcDNA5/FRT/TO eGFP expression vector. The full *RRAGD* cDNA length was amplified using primers. Subsequently, the PCR product and the plasmid backbone were digested using restriction enzymes KpnI and XhoI (New England Biolabs, the Netherlands). The digested sequence was then ligated into the digested backbone behind eGFP sequence using T4 DNA ligase (New England Biolabs, the Netherlands). Subsequently, site-directed mutageneses were performed on the created pcDNA5/FRT/TO-eGFP-h*RRAGD* wild-type (WT) plasmid to obtain the h*RRAGD* p.Ser77Phe, p.(Thr91Ile), and p.(Ile100Arg) variant constructs using the QuikChange II XL site-directed mutagenesis kit (Agilent Technologies, USA). All obtained constructs were checked through Sanger sequencing for the full-length DNA. All primers used are available in Supplementary Table 1. pcDNA3.1-TFEB-WT-MYC was a gift from James Brugarolas (Addgene plasmid #99955).[21]

Antibodies

The following antibodies (Cell Signaling Technology, Massachusetts, USA) were used: p70-S6K (#2708S, IB: 1:1,000), p-p70-S6K^{Thr389} (#9234S, IB: 1:1,000), TFEB (#4240S, IB: 1:1,000, ICC: 1:200) , p-TFEB^{Ser211} (#37681S**,** IB: 1:1,000), 4E-BP1 (#9452S, IB: 1:1,000), p-4E-BP1$^{Thr37/46}$ (#2855S, IB: 1:1000). Additionally, anti-RagD (#NBP2-32106, IB: 1:2,000, Novius Biologicals, Colorado, USA), anti-GFP (#G1544-100UG, IB: 1:5,000, Sigma Aldrich, Missouri, USA) and anti-GAPDH (#AM4300, IB: 1:4,000, Thermo Fisher Scientific Baltics UAB, Vilnius, Lithuania) antibodies were used. For immunoblotting, the following peroxidase- (PO) conjugated secondary antibodies were used: anti-IgG mouse (#145-515-035, 1:10,000, Jackson ImmunoResearch Europe Ltd., Exeter, UK), anti-IgG rabbit (#A4914, 1:10,000, Merck Life Science N.V, Amsterdam, The Netherlands). For immunocytochemistry experiments, we applied a secondary anti-IgG rabbit antibody conjugated to Alexa Fluor 594 (#A11012, 1:300, Thermo Fisher Scientific, Orlando, USA).

Stable cell line generation and culture

300,000 T-REx™ HeLa cells (Invitrogen, Massachusetts, USA) were seeded into a 6-well plate. 6 hr later, the cells were co-transfected with the pOG44 plasmid (Invitrogen, Massachusetts, USA), and either empty pcDNA5/FRT/TO-eGFP (mock), pcDNA5/FRT/TO-eGFP h*RRAGD* WT, or h*RRAGD* mutants, at 1:1 ratio, totaling to 2 µg DNA. As a negative control, transfection with only 2 µg of pOG44 plasmid was used. 2 µL Lipofectamine 2000 (Invitrogen, Massachusetts, USA) was used per 1 µg of DNA. After ± 18 hr, transfected cells from each well were transferred to

10-cm petri dish and left to attach for approximately 6 hr. Subsequently, 3 µg/mL blasticidine (Sigma-Aldrich, Missouri, USA) and 100 µg/mL Hygromycin B (Thermo Fisher Scientific, California, USA) was added to the cell culture medium to start the selection procedure. Cell culture medium containing the antibiotics, now termed as selection medium, was replaced every 2 days until cell sorting.

9 days after the transfection, expression of GFP or fusion GFP-RagD sequence was induced in the transfected cells by adding 1 µg/mL tetracycline to the selection medium. The following day (after 24 hr), the cells were prepared for single-cell sorting using fluorescence-activated cell sorting (FACS) by the flow cytometry facility at Radboudumc. In short, on the sorting day, cells were disassociated from the Petri dishes using trypsin-EDTA solution (0.05% trypsin (w/v), 0.02% (w/v) EDTA; Sigma-Aldrich, USA) and resuspended in 1x PBS and 2% (w/v) EDTA. GFP-positive cells were sorted individually into a single 96-well plate each using 100 µm nozzle of the Cytek™ Aurora CS System (Cytek, the Netherlands). Following the cell sorting, cells were kept in the incubator to let individual clones grow. After 10 days, grown clones from each cell lines were expanded and genotyped using the subcloning primers. For each mock, RagD-WT, - p.(Ser77Phe), p.(Thr91Ile), or p.(Ile100Arg) cell line, one clone was selected and used for subsequent experiments.

Cell culture and treatments for experiments

All HeLa T-REx cell lines were cultured in the culture medium described above in a humidified 37°C incubator with 5% (v/v) CO_2 unless stated otherwise.

For immunoblotting experiments, 200,000 HeLa T-REx cells were seeded into a 6-well plate. The next day, expression of GFP or GFP-RagD was induced by adding 1 µg/mL tetracycline to the culture medium. For immunocytochemistry experiments, ± 300,000 cells were seeded into a 6-well plate. After 6 hr, cells were transfected with 0.5 µg of pcDNA3.1-WT-TFEB-MYC using FuGENE HD Transfection Reagent (Promega, Shanghai, China) at a 1:2 DNA:FuGENE ratio. The next day, these transfected cells were collected, and 20,000 cells were re-seeded on poly-L-lysine-coated 10 mm cover slips in 24-well plates. After 24 hr, tetracycline was added to the culture medium to induce the expression of GFP or GFP-RagD.

Amino acids (AA) starvation was performed 24 hr after tetracycline induction. Nutrient-rich (+AA) and starvation (-AA) media were made following the DMEM culture medium manufacturer's formulation. The -AA medium was prepared by omitting the addition of any AA's to the medium. The media were then pH-adjusted to pH 7.4 using 1 M HCl, and sterile filtered through a 0.22 µm filter device. Before

use, treatment media were supplemented with 10% (v/v) dialysed FBS (Thermo Fisher Scientific, California, USA) and 1 mM sodium pyruvate. Specifically, to +AA medium, 4 mM L-glutamine (Thermo Fisher Scientific, California, USA) and MEM non-essential amino acids solution (Capricorn Scientific GmbH, Ebsdorfergrund, Germany) were added. The cells were washed with PBS, and incubated with +AA or -AA medium for 1 hr at 37°C.

Cell lysis

Cells were washed with ice-cold PBS buffer and lysed in 200 µL Triton lysis buffer (50 mM Tris-HCl pH 7.5, 1 mM EGTA, 1 mM EDTA, 1% (v/v) Triton X-100, 10 mM Na-glycerophosphate, 50 mM NaF, 10 mM Na-pyrophosphate, 270 mM sucrose, and 150 mM NaCl) supplemented with phosphatase inhibitor (1 mM Na-orthovanadate) and protease inhibitors (1 mM PMSF, 1 µM aproptin, 0.01 mM leupeptin, 1.4 µM pepstatin) by scraping on ice. Next, samples were centrifuged at 18,000xg at 4°C for 10 minutes and the supernatant was collected. Protein concentration was measured using the Pierce BCA protein assay kit (Thermo Scientific, USA) and 1 µg/µL samples were prepared in Laemmli (60 mM Tris-HCl pH 6.8, 2% (v/v) SDS, 0.01% (v/v) bromophenol blue, 6% (v/v) glycerol, 0.1 M DTT) loading buffer. Finally, samples were denatured at 95°C for 5 mins and stored at -20°C.

Immunoblotting

Using denatured samples in Laemmli + DTT, 15 µg of protein was loaded per sample in a 12% (v/v) polyacrylamide gel and resolved through SDS-PAGE run at 50 V for 30 mins, and then 100 V for 60 mins. After this, proteins were transferred to polyvinylidene fluoride (PVDF) membranes at 100 V for 120 mins. After the transfer, similar protein loading was confirmed through Ponceau S staining (Thermo Fisher Scientific, Illinois, USA) and imaged using Gel Doc EZ Imager (Bio-Rad, California, USA). Next, the membranes were blocked in 5% (w/v) non-fat dry milk in Tris-buffered saline (TBS) containing 0.1% (v/v) Tween-20 (TBS-T; VWR, Amsterdam, the Netherlands) for 1 hr. After 1 hr, membranes were incubated in primary antibody diluted in 1% (w/v) non-fat dry milk in TBS-T at 4°C. The next day, membranes were washed 3x in TBS-T for 10 mins each, and incubated in secondary antibody diluted in 1% milk in TBS-T at RT for 1 hr. After this, the membranes were washed 3x in TBS-T and 1x in TBS for 10 mins each. To visualize the protein of interest, membranes were incubated with SuperSignal West Pico PLUS Chemiluminescent Substrate (Thermo Scientific, Illinois, USA) or SuperSignal West Femto Maximum Sensitivity Substrate (Thermo Scientific, Illinois, USA), and then imaged using the ImageQuant™ LAS 4000 (GE Healthcare, Freiburg, Germany).

To analyze the signal intensity, Fiji, ImageJ2 version 2.14.0 was used.[23, 24] To correct for protein loading, Ponceau S signal was used as the reference.[50] Ponceau S signal was quantified in the same way as immunoblot quantification with the addition of background correction using the rolling ball method using a similar radius for all independent experiments.

Immunocytochemistry

Cells were fixated with 4% (v/v) paraformaldehyde (Sigma-Aldrich) in PBS for 10 mins at RT and permeabilized with PBS containing 0.3% (v/v) Triton X-100 and 0.1% (w/v) bovine serum albumin, also for 10 mins. Next, to quench free aldehyde, samples were incubated in 50 mM NH_4Cl in PBS for 10 mins. Following 2x rinsing with PBS, samples were blocked in goat serum dilution buffer (GSDB) containing 16% (v/v) goat serum and 0.3% (v/v) Triton X-100 in PBS for 30 mins. Subsequently, samples were incubated overnight at 4°C in primary antibodies diluted in GSDB. The next day, samples were washed 3x with PBS for 10 mins each, and incubated with secondary antibodies dilutes in GSDB for 45 mins at room temperature. Samples were then washed 3x with PBS for 10 mins each. During the second wash, DAPI was added to the PBS to a final concentration of 300 nM. Finally, samples were mounted with Fluoromont-G (Southern Biotech, Alabama, USA). Images were taken with an SP8 confocal microscope with a tunable pulsed white light laser (WLL) and a fixed 405 nm laser (Leica Microsystems, Amsterdam, the Netherlands). A 63x water-based objective (NA 1.20) was used. DAPI was excited with the 405 nm diode laser with 5% laser intensity, excited at 432-474 nm wavelength, detected with PMT detector, 1000% gain. GFP acquisition parameters were: 488 argon laser with 25% intensity, 493-560 nm wavelength, HyD2 detector, and 50% gain. Alexa Fluor 594 acquisition parameters were: 594 laser with 3% intensity, 600-668 nm wavelength, HyD4 detector, and 10% gain.

To quantify TFEB nuclear translocation, an automated script was created in ImageJ2 version 2.14.0. In short, using the TFEB channel, TFEB-transfected cells were manually selected. The DAPI channel was used to determine the location and outline of the nuclei. Next, a ratio of the TFEB signal in the nuclei over the total TFEB signal in cells per image was calculated, thus, depicting the TFEB translocation to the nuclei. In each experiment, 10 images from 10 independent fields containing at least 2 TFEB-transfected cells were obtained per genotype. In the end, the average of the 10 images per genotype was calculated.

Furosemide and thiazide testing

In order to assess the effects of furosemide on urinary ion excretion in patients with the p.(Thr97Pro) *RRAGD* variant, a single oral dose of 40 mg furosemide was

administered in routine renal physiology explorations after informed consent of each participant (n=4). The study duration was 3 hr *post*-administration of furosemide. Participants were in non-fasting conditions at baseline. After furosemide administration, participants remained fasting, with *ad libitum* access to water. The first post-furosemide blood sampling and urine collection occurred at 1-hr post-furosemide intake. Subsequent samplings took place at 2 hr and 3 hr post-furosemide intake. To compare the patients' response to furosemide to the healthy population, we re-analyzed Cl^- and Mg^{2+} data from furosemide testing done by Bech et al. using the same protocol (2017).[22] For our analysis, we included healthy individuals of all age ranges. Mg^{2+} levels were not reported in the original publication but were taken from the unpublished study files.

To assess the effects of hydrochlorothiazide (HCT) on urinary ion excretion in patients with p.The97Pro *RRAGD* variant, a single oral dose of 50 mg HCT was administered in routine renal physiology explorations after informed consent of each participant (n=4). The study duration was 6 hr post-administration of HCT. Participants were in non-fasting conditions at baseline. After HCT administration, participants had *ad libitum* access to water. From T=1 (*i.e.,* 2 hr post-HCT intake), participants had the option to consume crackers, but no other food or beverages were permitted. Blood and urine samples were collected at 2, 4, and 6 hr post-HCT intake. To compare the patients' response to HCT to the healthy population, we re-analyzed Cl^- and Mg^{2+} data from thiazide testing done by Bech et al. using the same protocol (2017).[22] Healthy individuals from all age ranges were included in this study. Mg^{2+} levels were not reported in the original publication but were taken from the unpublished study files.

Detailed clinical descriptions

Family 1

A 46-year-old female of Ashkenazi Jewish descent with nephrolithiasis, hypomagnesemia, and hypokalemia. She has family history of the maternal grandmother experiencing nephrolithiasis, and her mother and two maternal uncles exhibiting electrolyte imbalances suggestive of Gitelman syndrome. Born via C-section at full term, her delivery was complicated by her mother's hypokalemia-induced cardiac arrest. At 8-10 months, she developed a urinary tract infection, with nephrolithiasis diagnosed at 15 months, necessitating a partial nephrectomy for stone removal. Throughout childhood, she frequently experienced urinary tract infections, responding well to sulfamethoxazole and trimethoprim therapy. In adulthood, recurrent severe pyelonephritis episodes ensued. Paresthesias developed,

accompanied by intermittent hypokalemia, hypomagnesemia, and occasionally hypocalcemia. Treatment with magnesium and potassium replacement therapy was initiated. At 40, pancreatitis episodes exacerbated by pyelonephritis and sepsis led to a diabetes diagnosis, prompting a switch from metformin to insulin. A kidney ultrasound at 42 revealed medullary nephrocalcinosis with bilateral renal calculi, non-obstructive. Genetic testing at 43, conducted in November 2019 via an exome-based gene panel, yielded negative results. However, a reanalysis of the ES data in January 2022 identified a VUS in *RRAGD* (Ras-related GTP binding D, HGNC:19903), (NM_021244.4:c.272C>T - p.(Thr91Ile).[45]

Family 2

The index patient was referred at the age of 4 years by her local hospital for management of extensive bilateral stone burden, after presentation with acute abdominal pain. Nephrocalcinosis and stones had been initially identified a year earlier in the context of investigations for recurrent urinary tract infections that started around the age of 2 years. Antenatal history was normal. Parents were consanguineous (first cousins). The stones were initially managed surgically and consisted of calcium phosphate, mainly as carbapatite. Subsequent metabolic analysis showed hypokalemia (3.2 mmol/l), hypomagnesemia (0.57 mmol/l), as well as hypercalciuria (calcium/creatinine ratio 1.66 mol/mol), and initially a clinical diagnosis of Familial Hypomagnesaemia with Hypercalciuria and Nephrocalcinosis was made but could not be confirmed genetically. Family screening showed that her older sister, at the age of 8 years, also had nephrocalcinosis as well as hypokalemia (3.1 mmol/L) and hypomagnesemia (0.59 mmol/L), but no hypercalciuria. Subsequent screening of a new brother at the age of 8 months demonstrated mild nephrocalcinosis but no electrolyte abnormalities. The parents both had normal electrolytes, as well as normal kidney ultrasounds. An autosomal dominant missense variant was identified in *RRAGD* (NM_021244.4, c.272C>T, p.(Thr91Ile)) by exome sequencing.

Family 3

The female patient presented at the age of 16 years for persistent muscle weakness and cramps upon activities ever since or during infections like tonsillitis. Her mother reported for herself a long history of kidney stones without ever receiving a definite diagnosis. Hypokalemia, hypomagnesemia, and hypocalcemia, together with metabolic alkalosis, were found, and substitution (was prescribed but never continuously taken). An echocardiogram at that time, was normal. An autosomal dominant missense variant was identified in *RRAGD* (NM_021244.4, c.299T>G, p.(Ile100Arg)) by whole exome sequencing. The same mutation was found in

the mother. The grandfather was diagnosed in his 30ies initially with Medullary Cystic Kidney disease and currently suffers from CKD IV. He received later in life an implantable defibrillator.

Family 4

A 47-year-old woman was diagnosed with dilated cardiomyopathy (DCM) at age 32, with a baseline left ventricular ejection fraction (LVEF) of 24%, and excessive trabeculation. She had a history of salt-losing tubulopathy and hypomagnesemia since childhood, leading to chronic electrolyte imbalances and nephrocalcinosis, and resembling Bartter syndrome but with negative genetic testing,. Despite treatment, her condition deteriorated, necessitating a cardiac resynchronization therapy-defibrillator (CRT-D) at age 39 due to further LVEF decline and atrial fibrillation (AF). She eventually underwent heart transplantation (HT) after experiencing advanced heart failure and polymorphic ventricular tachycardia. Her monozygotic twin developed in parallel an overlapping phenotype of tubulopathy since pediatric age and DCM leading to HT. Repeated genetic testing for cardiomyopathy and related renal tubulopathies was negative. Several years later, the proband's 6-year-old niece started to develop an incipient phenotype of tubulopathy and excessive ventricular trabeculation that led to a trio exome sequencing that identified the p.(Ser76Leu) variant in RRAGD that was considered as likely pathogenic. Family 4 was first reported by de Frutos et al. (2024).[3]

Family 5

A male patient of 6 months of age was sent to a pediatric center in Buenos Aires, Argentina, with a history of food rejection, intermittent vomiting, hypotonia, and growth retardation. Various clinical investigations were conducted, revealing dilated cardiomyopathy with generalized wall hypomotility and moderate deterioration of left ventricular systolic function. He was evaluated to rule out metabolic and mitochondrial diseases, with all tests returning normal results. At 12 months of age, nephrocalcinosis was detected on a renal ultrasound, initially attributed to the use of loop diuretics. At 11 years of age, the patient was referred to our center for further consultation, and a nephrology evaluation was requested to address the nephrocalcinosis. He had normal kidney function and severe hypomagnesemia and hypokalemia. Renal US showed medullary nephrocalcinosis, but serum calcium and phosphorus were within normal range, with normal calciuria.

Family 6

The patient is diagnosed of severe hypomagnesemia at 5 years of age. He is asymptomatic but has a history of delayed language development and a slight

stature-weight growth delay. He refers chronic polyuria. In the initial study, he presents with normal kidney function, hypokalemia and hypomagnesemia of renal origin, and mild hypercalciuria with normal PTH and vitamin D3 levels. The renal US shows normal-sized kidneys with medullary nephrocalcinosis. The patients showed no pathologic findings in echocardiographic evaluation. He has an older brother who is asymptomatic. The parents have no history of kidney disease.

Family 7

Prematurely born girl, gestational week 32+5, birthweight 1880 g. The oldest of three children to non-consanguineous parents with an unremarkable family history. During infancy, signs of failure to thrive and signs of tubulopathy were apparent, with severe hypomagnesemia and hypokalemia due to renal losses. There were no signs of renal failure or hypertension. The patient was referred to the tertiary care hospital for further diagnostic work-up at the age of 2,5 years. A heart examination had revealed a mitral prolapse and regular echocardiograms had shown no signs of impaired ventricular function. A kidney ultrasound showed medullary nephrocalcinosis. She received supplementation with magnesium and potassium without achieving normalizing of electrolytes. During a summer holiday at the age of seven, she had a varicella infection and was admitted to hospital due to abdominal pain and fatigue. Investigations revealed dilated cardiomyopathy and severe decompensated heart failure with compromised end organ function, non-responsive to pharmacological heart failure therapy. At the age of 7 years and 8 months, she was listed for heart transplantation and successfully transplanted 4 weeks later. Five years post-transplantation, the patient is in good clinical condition, with excellent graft function and no rejection episodes. Supplementation of magnesium is ongoing but at lower doses. Immunosuppression consists of everolimus and low-dose tacrolimus.

Family 8

Family 8 was previously described in Schlingmann *et al.,* (2021) and Trepiccione *et al*., (2024).[1, 27]

Supplementary data

Supplementary Table 1. List of mutagenesis primers.

Usage	Variants	Primer name	Sequence (5'-3')
Subcloning	All variants	Forward	GCCGGTACCAGCCAGGTGCTGG
		Reverse	GCCCTCGAGCTACAGCAGCACTCTAGG
Mutagenesis	h*RRAGD* p.(Ser77Phe)	Forward	GGAGAAGCGGCAAGTCGTTTATTCAGAAAGTTGTC
		Reverse	GACAACTTTCTGAATAAACGACTTGCCGCTTCTCC
	h*RRAGD* p.(Thr91Ile)	Forward	CACAAAATGTCTCCCAACGAAATTCTGTTCTTGGAGAGCAC
		Reverse	GTGCTCTCCAAGAACAGAATTTCGTTGGGAGACATTTTGTG
	h*RRAGD* p.(Ile100Arg)	Forward	GAGAGCACTAATAAGAGATGCCGGGAAGATGTTTC
		Reverse	GAAACATCTTCCCGGCATCTCTTATTAGTGCTCTC

Supplementary Table 2. Furosemide treatment. Values represent the median [min; max] of four ADKH-*RRAGD* patients following 3-hr p.o. 40 mg furosemide. T=0: baseline, T=1, 2, 3: number of hours post-furosemide treatment.

	T=0	T=1	T=2	T=3
Blood				
Osmolarity (mosm/kg; N=281-303)	285.5 [284; 287]	284 [282; 287]	281.5 [277; 285]	277.5 [273; 281]
Na^+ (mmol/L; N=136-145)	141 [140; 142]	141.5 [141; 142]	139.5 [138; 141]	139 [137; 140]
K^+ (mmol/L; N=3.5-5.1)	3.42 [2.96; 3.55]	3.42 [3.23; 3.6]	3.4 [3.13; 3.64]	3.22 [2.97; 3.4]
Cl^- (mmol/L; N=98-107)	97 [94; 101]	95 [90; 98]	91 [88; 95]	91 [86; 94]
Ca^{2+} (mmol/L; N=2.2-2.6)	2.3 [2.26; 2.44]	2.44 [2.32; 2.53]	2.45 [2.37; 2.62]	2.36 [2.29; 2.53]
Mg^{2+} (mmol/L; N=0.66-1.07)	0.44 [0.4; 0.47]	0.44 [0.4; 0.47]	0.38 [0.37; 0.41]	0.37 [0.36; 0.41]
HCO3 (mmol/L; N=22-31)	33.4 [31.7; 35]	35.1 [31.5; 37.1]	34.35 [31.8; 38.1]	35.1 [30.2; 36.7]
Creatinine (mg/dL; N=0.73-1.18)	0.765 [0.51; 0.93]	0.74 [0.43; 0.86]	0.75 [0.46; 0.91]	0.75 [0.42; 0.88]
Urine				
Osmolarity (mosm/kg; N=50-1200)	439.5 [140; 507]	221.5 [161; 271]	214 [177; 258]	176 [135; 226]
Na^+ (mmol/L; N=22.3-200.1)	52.5 [33; 90]	81.5 [60; 105]	90 [76; 103]	58 [50; 82]
K^+ (mmol/L; N=20.6-101.9)	52.15 [11.8; 60.3]	12.95 [9.4; 17.5]	10.75 [7.9; 17.7]	15.95 [9.3; 19.1]

Supplementary Table 2. Continued

	T=0	T=1	T=2	T=3
Cl^- (mmol/L; N=27-225)	59.5 [33; 132]	95.5 [67; 113]	101.5 [84; 120]	76.5 [60; 99]
Creatinine (mg/dL; N=0-37.7)	0.7 [0.13; 1.89]	0.1 [0.05; 0.18]	0.06 [0.03; 0.08]	0.1 [0.03; 0.16]
Ca/Creat (mmol/g creat; N=0.3-6.1)	2.64 [0.46; 2.92]	10.1 [6.38; 12.88]	18.98 [14.17; 27.67]	9.9 [6.6; 19.71]
Mg/Creat (mmol/g creat; N=0.74-4.53)	2.805 [1.71; 5.85]	6.15 [5.68; 12.88]	12.7 [9.4; 21.67]	7.47 [5.33; 17.35]
Fractional excretions				
Na^+ (%; N=0.1-2)	0.705 [0.1; 0.99]	4.3 [2.37; 5.05]	8.43 [7.17; 10.76]	4.03 [1.99; 4.66]
K^+ (%; N=5.5-17)	14.55 [6.6; 26]	25.15 [17.6; 37.8]	45.6 [34.1; 58.9]	39.9 [23.4; 46.5]
Cl^- (%; N=0.7-2)	1.0 [0.2; 2.05]	7.0 [4.32; 8.54]	14.3 [13.39; 18.41]	7.3 [4.28; 9.03]
Ca^{2+} (%; N=1-2.6)	0.78 [0.14; 1.1]	2.84 [1.78; 3.5]	5.3 [4.89; 7.09]	3.18 [1.91; 3.86]
Mg^{2+} (%; N=3-5)	5.6 [2.5; 6.5]	11.5 [8.3; 11.6]	24.35 [19.6; 25.3]	15.3 [9.1; 19.2]

Supplementary Table 3. HCT treatment. Values represent the median [min; max] of four ADKH-*RRAGD* patients following 6-hr p.o. 50 mg HCT. T=0: baseline, T=2, 4, 6: number of hours post-HCT treatment.

	T=0	T=2	T=4	T=6
Blood				
Osmolarity (mosm/kg; N=281-303)	287.5 [281; 291]	282 [277; 283]	281 [278; 285]	279.5 [275; 282]
Na^+ (mmol/L; N=136-145)	141.5 [140; 144]	140 [139; 141]	139 [138; 141]	139.5 [138; 140]
K^+ (mmol/L; N=3.5-5.1)	3.26 [3.22; 3.7]	3.63 [3.2; 4.03]	3.24 [2.99; 3.67]	3.34 [3.05; 3.65]
Cl^- (mmol/L; N=98-107)	96 [96; 103]	93.5 [92; 98]	93 [92; 98]	92.5 [90; 96]
Ca^{2+} (mmol/L; N=2.2-2.6)	2.38 [2.26; 2.63]	2.46[2.36; 2.65]	2.47 [2.39; 2.71]	2.54 [2.44; 2.79]
Mg^{2+} (mmol/L; N=0.66-1.07)	0.43 [0.39; 0.48]	0.47 [0.41; 0.49]	0.44 [0.37; 0.49]	0.44 [0.39; 0.52]
HCO3 (mmol/L; N=22-31)	32.4 [30.9; 34.8]	33.05 [30.7; 35.1]	34.45 [32.9; 37.4]	35.55 [32.3; 37.8]
Creatinine (mg/dL; N=0.73-1.18)	0.75 [0.58; 1.04]	0.73 [0.54; 0.98]	0.73 [0.55; 1]	0.75 [0.54; 0.94]
Urine				
Osmolarity (mosm/kg; N=50-1200)	351 [112; 640]	219 [117; 323]	140 [113; 211]	113 [95; 215]
Na^+ (mmol/L; N=22.3-200.1)	50.5 [14; 115]	66 [36; 100]	44 [25; 70]	34.5 [24; 66]

Supplementary Table 3. Continued

	T=0	T=2	T=4	T=6
K^+ (mmol/L; N=20.6-101.9)	40.5 [11.9; 53.6]	18.05 [11.1; 25.8]	13.4 [6.5; 14.9]	11 [7.3; 15.2]
Cl^- (mmol/L; N=27-225)	71 [23; 129]	71.5 [36; 128]	41 [32; 86]	34.5 [30; 82]
Creatinine (mg/dL; N=0-37.7)	9.25 [6.8; 11.9]	6.35 [5.9; 8.2]	7.5 [3.9; 9.6]	7.35 [5; 9.4]
Ca/Creat (mmol/g creat; N=0.3-6.1)	1.13 [0.35; 1.59]	0.4 [0.23; 0.55]	0.17 [0.12; 0.21]	0.16 [0.11; 0.25]
Mg/Creat (mmol/g creat; N=0.74-4.53)	1.86 [0.45; 4.74]	0.79 [0.35; 1.39]	0.5 [0.34; 0.69]	0.45 [0.42; 0.74]
Fractional excretions				
Na^+ (%; N=0.1-2)	0.49 [0.17; 1.26]	2.13 [2.01; 2.54]	2.085 [1.11; 3.28]	1.84 [1.47; 2.71]
K^+ (%; N=5.5-17)	17.15 [6.3; 25.5]	22.65 [19.2; 34]	22.45 [17.4; 29.8]	21.95 [19.8; 31.1]
Cl^- (%; N=0.7-2)	1.19 [0.31; 2.1]	3.7 [3.15; 4.12]	3.45 [2.04; 4.65]	3.18 [2.68; 4.02]
Ca^{2+} (%; N=1-2.6)	0.64 [0.29; 0.96]	0.77 [0.61; 0.96]	0.48 [0.24; 0.59]	0.54 [0.18; 0.82]
Mg^{2+} (%; N=3-5)	5.05 [2.9; 9.9]	7.9 [6.6; 9]	8.15 [4.8; 8.9]	8.25 [7; 9]

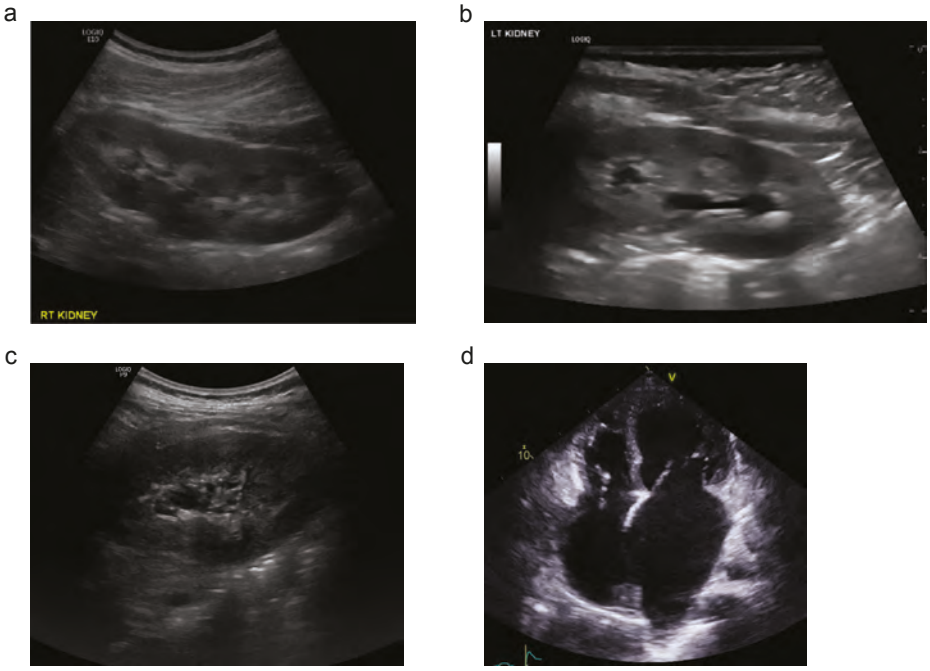

Supplementary Figure 1. Ultrasound images of patients with pathogenic *RRAGD* variants. (a-c) Ultrasound images of the kidney of patients (a) F2.II.1, (b) F2.II.3, and (c) F3.III.I.1. (d) Apical 4 chamber view of heart ultrasound in family F4.

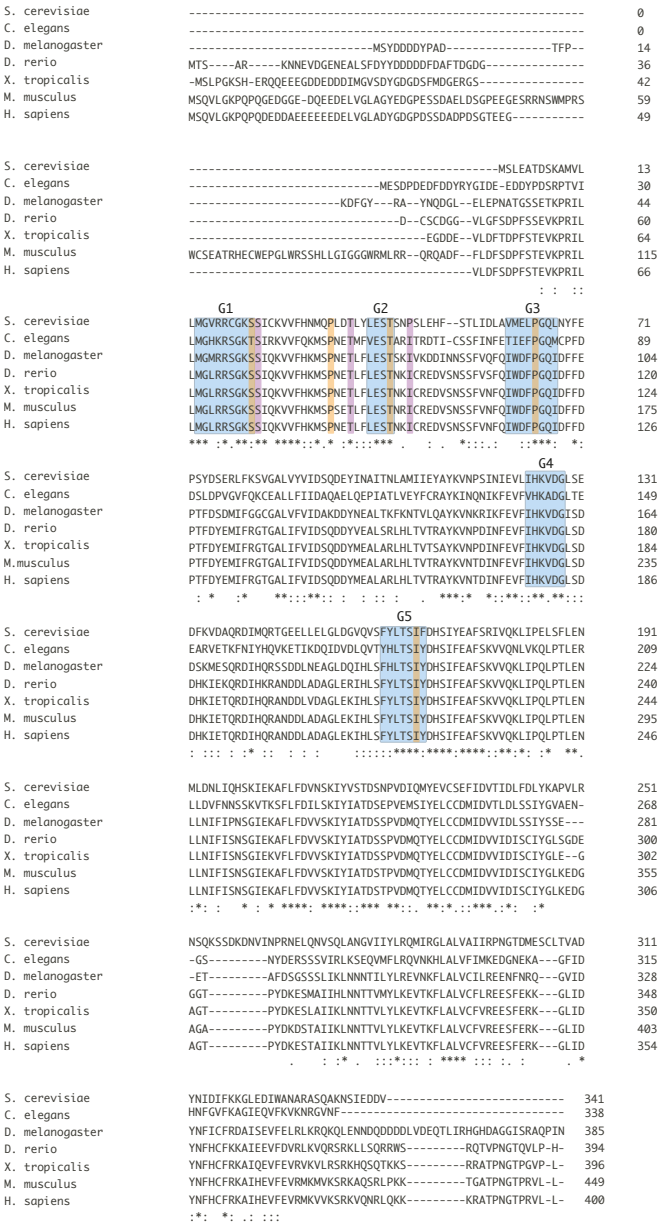

Supplementary Figure 2. Alignment of RagD sequences showed conservation of variant sites. Multiple alignment analysis of RagD protein sequences in yeast (Saccharomyces cerevisiae; P53290), round worm (Caenorhabditis elegans; G5EGB3), fruit fly (Drosophila melanogaster; Q7K519), zebrafish (Danio rerio; F1QIB5), western clawed frog (Xenopus tropicalis; Q0VFL0), mouse (Mus musculus; Q7TT45), and human (Homo sapiens; Q9NQL2). GTP-binding domains, or G-boxes, are highlighted in blue. Affected residues by variants described in this study are highlighted in purple. Residues that have been previously described are highlighted in orange.

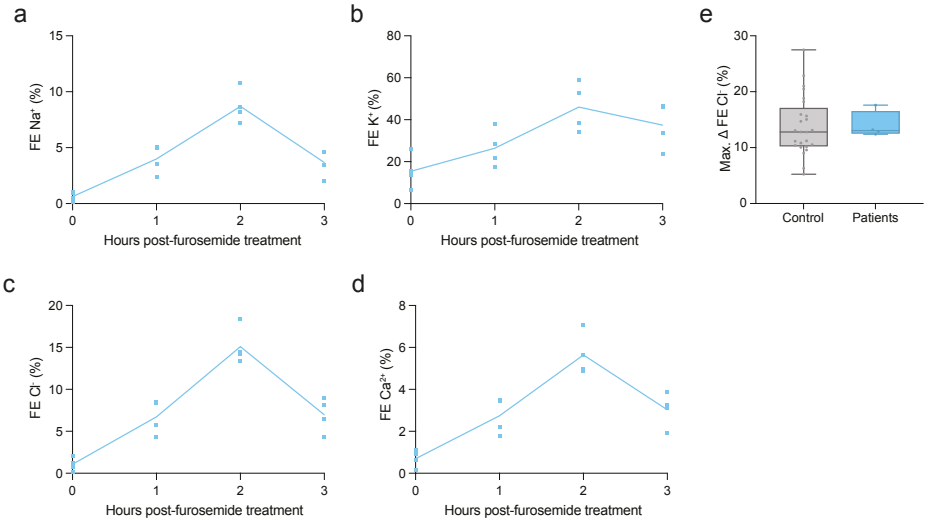

Supplementary Figure 3. Fractional excretions in ADKH-*RRAGD* patients following furosemide treatment. Fractional excretions (FE) of (a) Na^+, (b) K^+, (c) Cl^-, and (d) Ca^{2+} at 0, 1, 2, and 3 hr post- p.o. 40 mg furosemide administration. (e) Maximal Δ FE Cl^- (*i.e.,* max. FE Cl^- – baseline value) of healthy individuals (n=25, grey) and ADKH-*RRAGD* patients (n=4, blue). (a-e) Data points indicate individuals. (e) the boxes range from the 25th to the 75th quartile, the whiskers extend from max. to min. points, and the middle lines indicate the median.

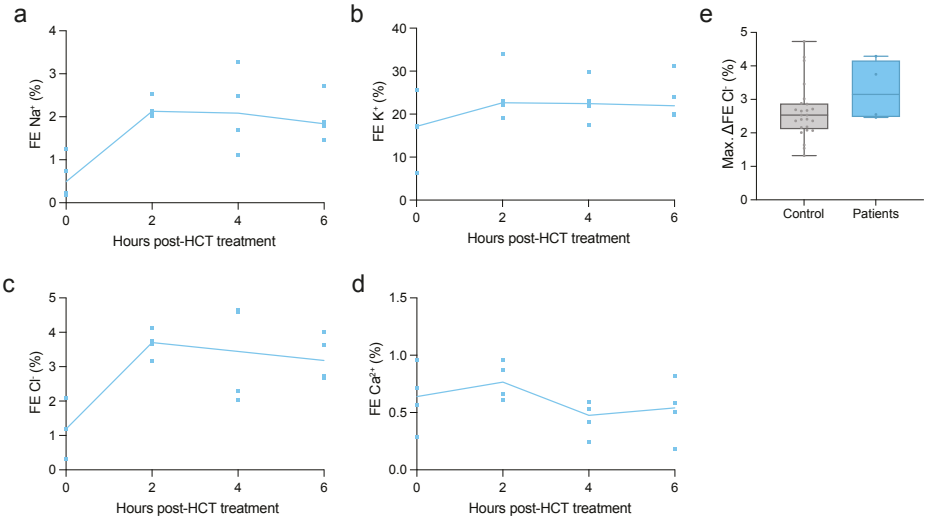

Supplementary Figure 4. Fractional excretions in ADKH-*RRAGD* patients following HCT treatment. Fractional excretions (FE) of (a) Na^+, (b) K^+, (c) Cl^-, and (d) Ca^{2+} at 0, 2, 4, and 6 hr post-p.o. 50 mg hydrochlorothiazide (HCT) administration. (e) Maximal Δ FE Cl^- (*i.e.,* max. FE Cl^- – baseline value) of healthy individuals (n=25, grey) and ADKH-*RRAGD* patients (n=4, blue). (a-e) Data points indicate individuals. (e) the boxes range from the 25th to the 75th quartile, the whiskers extend from max. to min. points, and the middle lines indicate.

CHAPTER 3

RRAGD variants cause cardiac dysfunction in a zebrafish model

Anastasia Adella[1], Faris Tengku[1], Francisco J. Arjona[1], Sanne Broekman[2], Erik de Vrieze[2], Erwin van Wijk[2], Joost G.J. Hoenderop[1], Jeroen H.F. de Baaij[1]

[1] Department of Medical BioSciences, Radboudumc, Nijmegen, The Netherlands

[2] Department of Otorhinolaryngology, Radboudumc, Nijmegen, The Netherlands

AJP Heart and Circulatory Physiology, 2024

Abstract

The Ras-related GTP-binding protein D (*RRAGD*) gene plays a crucial role in cellular processes. Recently, *RRAGD* variants found in patients have been implicated in a novel disorder with kidney tubulopathy and dilated cardiomyopathy. Currently, the consequences of *RRAGD* variants at organismal level is unknown. Therefore, this study investigated the impact of *RRAGD* variants on cardiac function using zebrafish embryo model. Furthermore, the potential usage of rapamycin, an mTOR inhibitor, as a therapy was assessed in this model. Zebrafish embryos were injected with *RRAGD* p.S76L and p.P119R cRNA and the resulting heart phenotypes were studied. Our findings reveal that overexpression of *RRAGD* mutants resulted in decreased ventricular fractional shortening, ejection fraction, and pericardial swelling. In *RRAGD* S76L-injected embryos, lower survival and heartbeat were observed, while survival was unaffected in *RRAGD* P119R embryos. These observations were reversible following therapy with the mTOR inhibitor rapamycin. Moreover, no effects on electrolyte homeostasis were observed. Together, these findings indicate a crucial role of *RRAGD* for cardiac function. In the future, the molecular mechanisms by which *RRAGD* variants result in cardiac dysfunction, and if the effects of rapamycin are specific for *RRAGD*-dependent cardiomyopathy should be studied in clinical studies.

Keywords: cardiac dysfunction; mTORC1; rapamycin; *RRAGD*; zebrafish

Introduction

Recently, we have identified Ras-related GTP binding protein D (*RRAGD*) variants as cause for a hereditary disorder comprising dilated cardiomyopathy (DCM), hypomagnesemia, hypercalciuria, and nephrocalcinosis.[1-3] Most patients with *RRAGD* variants suffer from DCM at a young age, requiring heart transplantations in several individuals. To date, there is no treatment available to prevent or delay cardiac complications due to *RRAGD* variants.

RagA-D form a heteromeric complex and function as molecular switches, transitioning between the activation-dictating status of a GTP-bound state and a GDP-bound state, thereby regulating downstream signalling pathways.[4-6] Their activity is crucial for the activation of the mechanistic target of rapamycin complex 1 (mTORC1), a key regulator of cell growth, metabolism, and proliferation.[7,8] The Rag GTPases, along with other associated proteins, form a heterodimeric Ragulator complex, which anchors mTORC1 to the lysosomal surface.[8]

The role of Rag GTPases in cardiomyopathies has been thoroughly studied. Loss of RagA/B in mice cardiomyocytes resulted in cardiac hypertrophy and aberrant lysosomal regulation under transcription factor EB (TFEB).[9] Moreover, a number of *de novo RRAGC* variants caused dilated cardiomyopathy in infants and lead to overactivation of mTORC1 signalling as well as TFEB dysfunctions.[10-12] Previously, DCM-causing gain-of-function *RRAGD* variants have been reported to invoke hyperactivation of mTORC1 signalling in HEK293T cells [1] and inhibition of the MiT/TFE transcription factors family [2]. Altogether, these studies demonstrate the key role of Rag GTPases in maintaining cardiac functions.

mTORC1 play a pivotal role in maintaining heart function throughout pre- and post-natal life (extensively reviewed in [13]), underlining the importance of maintaining physiological mTOR signalling in the heart while avoiding maladaptive mTOR hyperactivity. Due to this, assessment on the potential usage of mTOR inhibitors as a therapy for genetic cardiomyopathies has been done in pre-clinical studies. For example, stimulating autophagy by pharmacological inhibition of mTORC1 using rapamycin proved to be cardioprotective in animal models. This was achieved through reduction of pathological hypertrophy and heart failure, and by limiting ischemic injury and cardiac remodelling after myocardial infarction.[14-16]

Zebrafish (*Danio rerio*) has emerged as a robust model organism for investigating human genetic diseases due to its conserved genetic architecture, accelerated

ontogeny, and optically transparent embryos.[17] With a cardiovascular system exhibiting remarkable parallels to humans, zebrafish offers an exceptional platform for deciphering the genetic foundations of cardiac development and function. Therefore, we aim to further elucidate the effects of *RRAGD* variants on heart phenotypes by injecting human *RRAGD* variants into zebrafish embryos. Moreover, we perform a proof-of-concept study in this zebrafish model by examining the therapeutic potential of mTOR inhibitor rapamycin in preventing RRAGD-induced cardiac dysfunction.

Materials and methods

Ethics statement

All animal experiments conformed to the guidelines from Directive 2010/63/EU of the European Parliament on the protection of animals used for scientific purposes or the current NIH guidelines. Animal experimentation and analysis were therefore restricted to the first five days post-fertilization (dpf). RNA from different tissues of adult zebrafish were previously obtained [18] and was performed in accordance with the national legislation and were approved by the ethical review committee of the Radboud University Nijmegen.

Cloning

h*RRAGD* wild-type (WT) construct was constructed and packaged by VectorBuilder (Vector ID: VB171030-1104zuv; vectorbuilder.com). To obtain mutant constructs, QuikChange Site-Directed Mutagenesis kit (Stratagene) was utilized. For h*RRAGD* S76L (c.227 C>T), forward primer 5′-GAGGAGAAGCGGCAAGTTGTCTATTCAGAAAGTTG and reverse primer 5′-CAACTTTCTGAATAGACAACTTGCCGCTTCTCCTC were used. For h*RRAGD* P119R (c.356 G>C), forward primer 5′-CAGATTTGGGACTTCCGAGGACAGATTGACTTTTTTGACCC and reverse primer 5′-GGGTCAAAAAAGTCAATCTGTCCTCGGAAGTCCCAAATCTG were used.

To generate a zebrafish-suitable expression system, all h*RRAGD* constructs were subcloned into the pT7Ts expression vector using *Asc*I and *Not*I restriction enzymes (New England Biolabs, Massachusetts, USA) with forward primer 5′- CTGGGCGCGCGCCAAGCCAGGTGCTGGGGAAG and reverse primer 5′-GAGCGGCCGCCTACAGCAGCACTCTAGGGG. Afterwards, cRNAs were prepared using the mMESSAGE mMACHINE Kit (Ambion) according to the manufacturer's instructions.

Zebrafish culture and morpholino knockdown

Zebrafish eggs were obtained from natural spawning of Tupfel long-fin zebrafish which were bred and raised under standard conditions in accordance with international and institutional guidelines (28.5°C and 14 hours of light:10 hours of dark cycle).

Morpholino targeting exon 2 of the *rragd* transcript was used: 5'- GATAGATAGTTTCACCTGAGAGTCT (Gene Tools). In parallel, as a control, a standard mismatch morpholino directed (control-MO) against a human β-globin intron mutation, 5'-CCTCTTACCTCAGTTACAATTTATA (Gene Tools) was used. Zebrafish embryos were divided into five groups to carry out a dose-response experiment (doses of 2, 4, 6, and 8 ng/embryo of *rragd*-MO and 8 ng/embryo control-MO, sampling at 120 hpf). MOs were diluted in deionized, sterile water supplemented with 0.5% (w/v) phenol red and injected in a volume of 1 nL into the yolk of one- to two-cell stage embryos using a Pneumatic PicoPump pv280 (World Precision Instruments). After injection, embryos from the same experimental condition were placed in three Petri dishes and cultured at 28.5°C in Mg^{2+}-free E3 medium (5 mM NaCl, 0.17 mM KCl, 0.33 mM $CaCl_2$) or normal E3 medium containing 0.33 mM $MgSO_4$, which was refreshed daily. Animals were anesthetized with tricaine/Tris pH 7.0 solution during samplings. Then, morphologic phenotypes were analysed under the microscope (Leica Microsystems Ltd.). Three morphological phenotypes were distinguished: normal with non-inflated swim bladder in some cases, blood in the intestine, and defects in glomerular filtration. After phenotyping, fish were sampled, each sample constituted of 10 larvae, which were stored at -80 °C until further analyses.

Expression of human *RRAGD* variants in zebrafish embryos

To induce the expression of *RRAGD* variants, the yolks of fertilized zebrafish eggs were injected with 1 nL of 100 ng, *RRAGD*, *RRAGD* S76L, *RRAGD* P119R cRNAs, or phenol red as control vehicle at the one- to two-cell stage embryos using a Pneumatic PicoPump pv280 (World Precision Instruments). Following the injection, embryos were grown at 28.5°C in E3 medium. For rapamycin studies, at 4 hours post-fertilization (hpf), embryos were exposed to either 0.4% (v/v) DMSO or 400 nM rapamycin (and 0.4% (v/v) DMSO, used as a solvent for rapamycin). At 72 hpf, heart phenotype of the zebrafish embryo was analyzed. Subsequently, fish were anaesthetized with tricaine/Tris pH 7.0 solution. Samples for Western blotting was directly processed. Pictures were taken using the Leica Application Suite and a Leica MZFLIII microscope equipped with a DFC450C camera (Leica Microsystems Ltd.). Afterwards, samples were stored at -80°C.

Analysis of heart function in zebrafish embryos

From each experimental group, 12 embryos were randomly selected for heart function analyses (heartbeat, fractional shortening (FS), ejection fraction (EF), and pericardial swelling). For each embryo, 12-13 sec videos of the heart (100x magnification) were taken using Leica Application Suite and a Leica MZFLIII microscope equipped with a DFC450C camera (Leica Microsystems Ltd.). In these videos, the number of heart beats in a 10 sec interval was counted and used to calculate the heartbeat in beats per minute (bpm). Images from the videos were used to measure the long-axis diameter and the area of the ventricle of each embryo during systole and diastole using the ImageJ software. For each embryo, three diastolic and systolic measurements were performed. From these ventricle measurements, the FS of the ventricle, a parameter used regularly to evaluate heart function in zebrafish, was determined using the following formulas:

$$Diameter\ FS\ (\%) = \left(\frac{diastolic\ diameter\ -\ systolic\ diameter}{diastolic\ diameter}\right) \times 100$$

$$Area\ FS\ (\%) = \left(\frac{diastolic\ area - systolic\ area}{diastolic\ area}\right) \times\ 100\%$$

To measure EF, end diastolic volume (EDV) and end systolic volume (ESV) were calculated using the following formula:

$$End\ volume = \frac{(8\ \times\ (area^2))}{3 \times \pi \times diameter}$$

Next, ejection fraction percentage (EF (%)) was calculated:

$$Ejection\ fraction\ (EF\ (\%)) = \frac{EDV - ESV}{EDV} \times 100\%$$

To measure the pericardial swelling, the pericardial cavity during diastole was outlined using the segmented line function and area size was measured in ImageJ software.

Electrolyte measurements in zebrafish larvae

From each experimental group, 8-10 samples were used, of which each constituted by 10 embryos/sample. Samples were quickly washed with nanopure water to avoid contamination of remaining water Mg^{2+} and Ca^{2+}. The washing procedure was repeated twice. Zebrafish embryos were then dried and digested as described previously.[19] The total Mg and Ca content in each sample was quantified with colorimetric assays according to manufacturers' protocols. Total Mg determination was done using a xylidyl blue colorimetric assay kit (Roche Diagnostics) and measured at 600 nm. Total Ca was determined using an o-cresolphthalein

complexone method and read at 570 nm. Within-run precision and accuracy were controlled by means of an internal control Precinorm (Roche Diagnostics). Furthermore, samples were normalized by the protein content, which was determined with the Pierce BCA protein assay kit (Pierce Biotechnology).

Whole embryo lysate and sample preparation

From each experimental group, 2 samples comprising of 10 embryos were prepared. In short, anesthetized embryos were lysed in 100 µL Triton lysis buffer (1 mM EDTA, 1 mM EGTA, 10 mM $C_3H_7Na_2O_6P$, 50 mM NaF, 10 mM $Na_4P_2O_7$, 150 mM NaCl, 270 mM sucrose, 50 mM Tris-HCl pH 7.5, 1% [v/v] Triton X-100) supplemented with protease and phosphatase inhibitors (1.46 nM Pepstatin, 10.5 nM Leupeptin, 1 mM PMSF, 0.154 nM Aprotinin, 1 mM Na_3VO_4) using micropestles until no chunks of tissues were visible. Samples were then clarified by centrifugation at 13000 RPM for 10 minutes at 4°C. Subsequently, supernatants were transferred to new tubes. Protein concentration was measured using the Pierce™ BCA Protein Assay Kit (Thermo Scientific), and 1 µg/µL samples were prepared in 5x Laemmli buffer containing 1 mM dithioterol. Afterwards, samples were denatured at 95°C for 5 minutes and stored in -20°C until further use.

SDS-PAGE and Western blotting

15 µg of lysate was run through 12% SDS-PAGE gel and transferred to a polyvinylidene fluoride (PVDF) membrane. After transfer, similar protein loading was confirmed using Ponceau S staining solution (Thermo Scientific) and imaged (Gel Doc EZ Imager, Bio-Rad). Next, membranes were blocked in 5% (w/v) non-fat dry milk in Tris-buffered saline (TBS) containing 0.1% (v/v) Tween-20 (TBS-T; Sigma-Aldrich) for 1 hour at RT. Subsequently, membranes were incubated in primary antibody diluted in 1% (w/v) non-fat dry milk in TBS-T overnight at 4°C. The following day, membranes were washed 3x in TBS-T for 10 minutes each prior to incubation with secondary antibody diluted in 1% (w/v) non-fat dry milk for 1 hour at RT. Following this, membranes were washed 3x in TBS-T for 10 minutes each and 1x TBS for 10 minutes. To visualize the protein of interests, membranes were incubated with SuperSignal West Pico Chemiluminescent Substrate (Thermo Scientific) or SuperSignal West Femto Maximum Sensitivity Substrate (Thermo Scientific), and then imaged using the ImageQuant™ LAS 4000 (General Electric). Primary antibodies used are from Cell Signaling Technology: p70-S6K (#2708S, 1:1000), p-p70-S6K^{Thr389} (#9234S, 1:1000), p-TFEB^{Ser211} (#37681S**,** 1:1000), and from Invitrogen: GAPDH (#AM4300, 1:4000). Secondary antibodies used were peroxidase (PO) conjugated against IgG mouse (#145-515-035, Brunswig) and IgG rabbit (#A4914, Sigma), both at 1:10000.

Tissue distribution of *RRAGD* expression in adult zebrafish

RNA was previously isolated from tissues of adult zebrafish using TRIzol (Invitrogen) according to the manufacturer's instructions.[18] Tissues from three adult females and three adult males were used. One microgram of RNA was then subjected to reverse transcription using the Moloney Murine Leukaemia Virus Reverse Transcriptase (M-MLV RT; Invitrogen) to obtain the cDNA.

Expression of mRNA was measured using SYBR green (Bio-Rad) using the CFX96 Real-Time PCR Detection System (Bio-Rad). *rragd* gene expression levels in different tissues were normalized to the *elongation factor-1α* (*elf1a*). To calculate relative gene expression, $2^{-\Delta\Delta Ct}$ method was used using *rragd* gene expression in the brain as the control. Primers used to detect *rragd* were forward 5'- CAGTGGACATGCAGACCTATGA and reverse 5'-CCTTCATCTCCAGACAACCCAT. To amplify *elf1a*, forward 5'-GAGGCCAGCTCAAACATGGGC and reverse 5'- AGGGCATCAAGAAGAGTAGTACCGC primers were used.

Statistical analysis

All results are shown as mean ± SEM. When there was only one variable tested, One-way ANOVA was used. When there were at least two variables measured, two-way ANOVA was used. Resulting significant test was followed by Tukey or Šídák post-hoc test. The test used in each experiment is indicated in each figure legend. Statistical significance was described at $P < 0.05$. All statistical tests were performed in GraphPad Prism 10.0.0 for macOS software.

RESULTS

RRAGD S76L and P119R variants compromised heart contractility

Dilated cardiomyopathy is the cardinal symptom of patients with variants in *RRAGD*. In adult zebrafish, *rragd* is highly expressed in the heart compared to other tissues (Supplementary Figure 1A). Moreover, the zebrafish RagD ortholog has a highly similar amino acids sequence compared to human RagD (80%, Supplementary Figure 1B), making it a relevant animal model to study the role of *rragd* in heart. Therefore, morpholino-mediated *rragd* knockdown in zebrafish embryos was done (Supplementary Figure 2). Three different phenotypes, normal, blood in the intestine, and defect glomerular filtration were observed (Supplementary Figure 2A, C). However, no apparent cardiac phenotypes were seen. Moreover, the survival of the embryos was unaffected even with an increasing amount of morpholino (Supplementary Figure 2B).

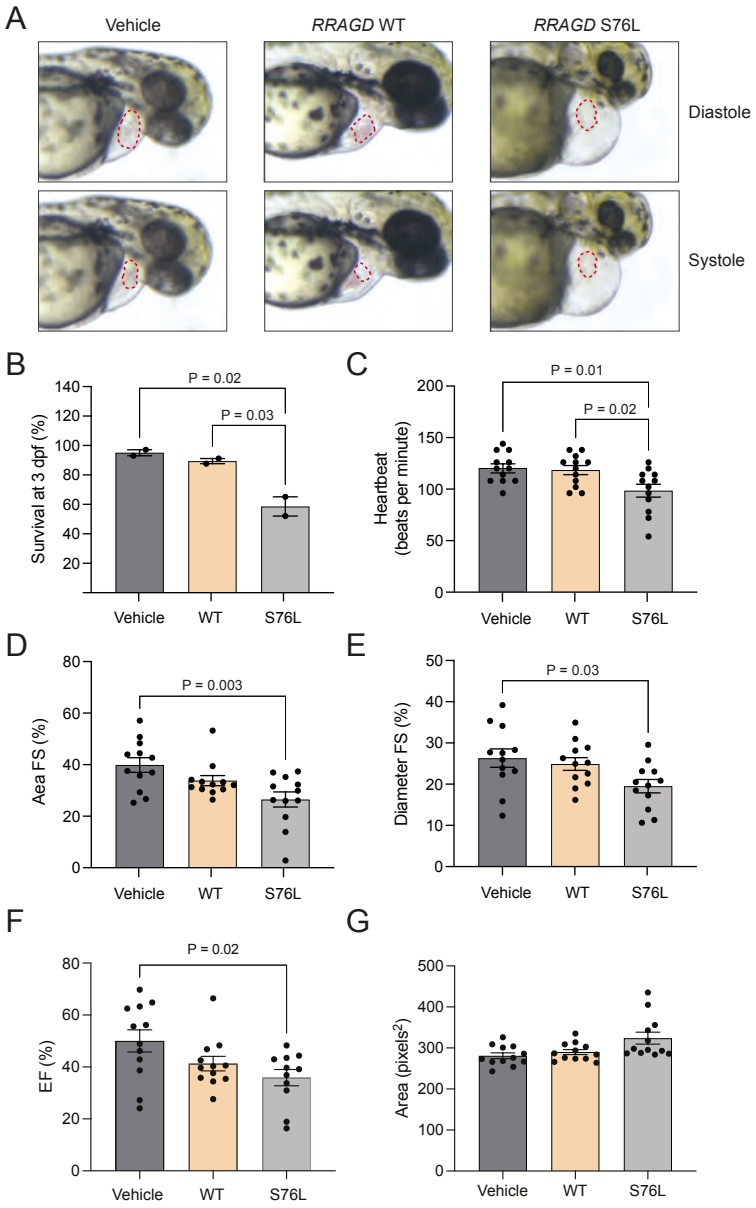

Figure 1. Effects of *RRAGD* S76L cRNA injections in zebrafish embryo. Representative images of the heart ventricles (outlined in red dashed line) of zebrafish vehicle (dark grey bars), human WT *RRAGD* (beige bars), or human S76L *RRAGD* (light grey bars). Magnification: 100x (A). Zebrafish larvae survival during the experiment at 3 dpf compared to the number of viable injected eggs at the beginning of experiment (B). Each condition was divided in two Petri dishes (n = 2). From the surviving population, heartbeat (bpm) (C), percentage of FS considering the ventricle area (D) or the diameter (E), percentage of EF (F), and pericardial cavity area (G) from 12 zebrafish embryos in each condition were measured. Statistical differences between groups were determined using One-way ANOVA followed by Tukey test.

To examine the consequences of *RRAGD* variants in a physiological model, the most common human variants, *RRAGD* S76L (Table 1, Figure 1) and *RRAGD* P119R (Table 1, Figure 2), were injected in zebrafish embryos. Cardiac function was monitored 72 hpf or 3 dpf by determining FS of the ventricle. Hatching of larvae was not affected by the overexpression of any of the variants as also seen in the respective vehicle and WT conditions (Supplementary Figure 3A and B). However, survival of larvae overexpressing *RRAGD* S76L was decreased compared to control groups (Table 1, Fig. 1B) while that of *RRAGD* P119R remains unchanged (Table 1, Figure 2B). Moreover, both variants caused a reduction in heartbeat per minute (Table 1, Figure 1C, 2C). Importantly, in line with our patients' cardiac symptoms, both variants resulted in a decreased FS and EF (Table 1, Figure 1D-F, 2D-F). This was accompanied with fluid retention observed around the heart, which is indicative of heart defects (Figure 1A, 1G, 2A, 2G, Supplementary Video 1, 2). Additionally, heartbeat does not correlate with FS and EF in *RRAGD* WT or mutant animals (Supplementary Figure 4A-D).

To investigate if *RRAGD* variants result in electrolyte disturbance in zebrafish larvae, total Mg^{2+} and Ca^{2+} levels were also measured. Overexpression of *RRAGD* S76L and P119R variants, however, did not change the zebrafish Mg and Ca content (Table 1, Supplementary Figure 3C-F). On a side note, Mg and Ca content in zebrafish embryos decreased in a morpholino dose-dependent manner upon *rragd* knockdown compared to control morpholino (Supplementary Figure 2D, E).

Table 1. Effects of *RRAGD* p.S76L and p.P119R on zebrafish embryos.

	Vehicle	***RRAGD* WT**	***RRAGD* S76L**	**Vehicle**	***RRAGD* WT**	***RRAGD* P119R**
Survival (%)	95 ± 2	90 ± 2	59 ± 7	98 ± 1	98 ± 2	94 ± 1
Heartbeat (bpm)	121 ± 4	119 ± 4	99 ± 6	167 ± 7	170 ± 7	124 ± 7
Area FS (%)	40 ± 3	34 ± 2	27 ± 3	34 ± 2	39 ± 2	29 ± 4
Diameter FS (%)	26 ± 2	25 ± 2	20 ± 2	25 ± 2	22 ± 1	19 ± 3
EF (%)	50 ± 4	41 ± 3	36 ± 3	51 ± 2	51 ± 3	37 ± 5
Pericardial swelling ($pixels^2$)	281 ± 7	290 ± 6	324 ± 15	400 ± 9	396 ± 15	467 ± 33
Total Mg(µg/mg protein)	7 ± 0.3	7 ± 0.1	7 ± 0.4	7.0 ± 2.3	8 ± 0.1	8 ± 0.1
Total Ca(µg/mg protein)	10 ± 0.3	11 ± 0.3	10 ± 0.5	12 ± 0.4	11 ± 0.4	12 ± 0.4
Hatching (%)	98 ± 2	94 ± 0.9	89 ± 3	97 ± 0.9	96 ± 2	90 ± 0.5

FS: fractional shortening, EF: ejection fraction. Values are shown as mean ± SEM.

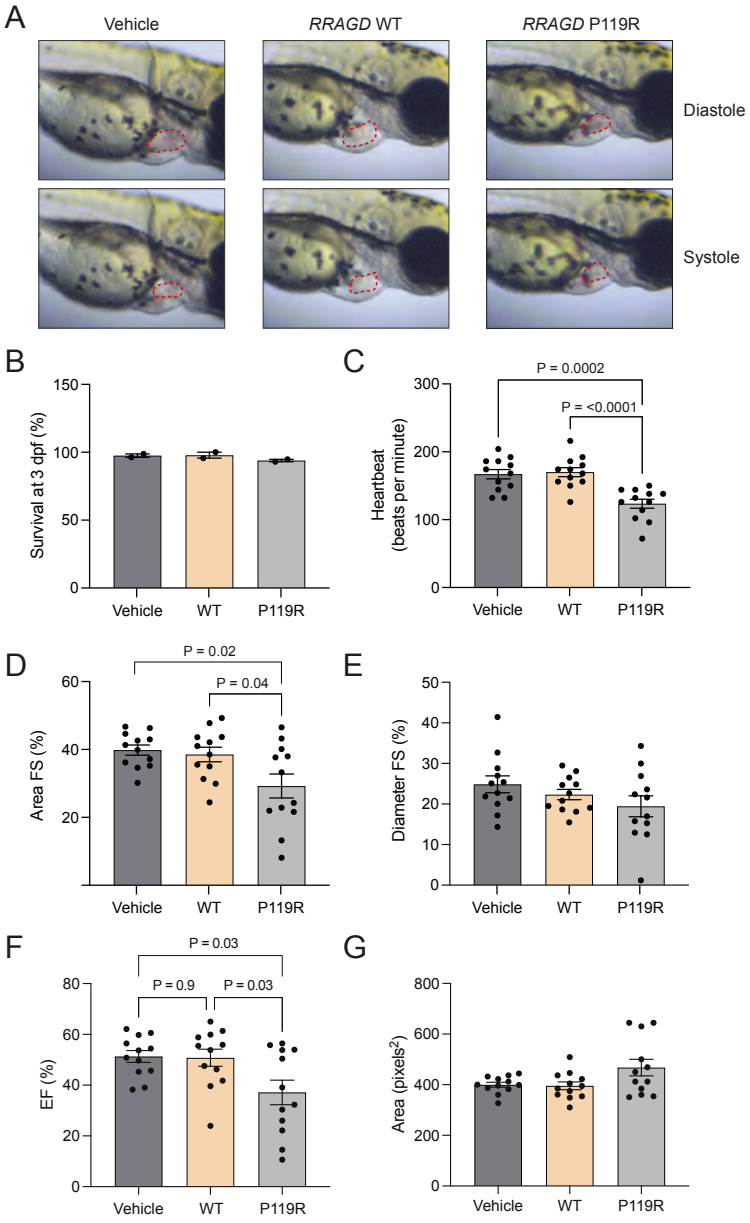

Figure 2. Effects of *RRAGD* P119R cRNA injections in zebrafish embryo. Representative images of the heart ventricles (outlined in red) of zebrafish vehicle (dark grey bars), human WT *RRAGD* (beige bars), or human P119R *RRAGD* (light grey bars). Magnification: 100x (A). Zebrafish larvae survival during the experiment at 3 dpf compared to number of viable injected eggs at the beginning of experiment from two petri dishes (n = 2) (B). From the surviving population, heartbeat (bpm) (C), percentage of FS considering the ventricle area (D) or the diameter (E), percentage of EF (F), and pericardial cavity area (G), from 12 zebrafish embryos in each condition were measured. Statistical differences between groups were determined using One-way ANOVA followed by Tukey test.

Heart malfunction in *RRAGD* S76L and P119R-overexpressing zebrafish is rescued by rapamycin

As we have reported previously, variants found in *RRAGD* patients resulted in overactivation of mTORC1 signalling pathway in HEK293T cells.[1] Here, we investigated the potential therapeutic capability of rapamycin, an mTOR inhibitor, on heart functions (Figure 3, 4, Supplementary Figure 5). Rapamycin treatment improved the survival of S76L-overexpressing larvae compared to vehicle while P119R did not affect survival (Table 2, Figure 3A, 4A). Heart rate was not affected by neither *RRAGD* S76L variant nor rapamycin treatment (Table 1, Figure 3B, Supplementary Video 3). In *RRAGD* P119R-overexpressing larvae, heart rate was lowered, but rapamycin did not rescue this (Table 2, Figure 4B, Supplementary Video 4). Remarkably, cardiac dysfunctions as measured by FS, EF, and pericardial swelling was ameliorated by rapamycin treatment in both variants to the level of that in *RRAGD* WT-overexpressing larvae (Table 2, Figure 3C-G, Figure 4C-G). At the molecular level, rapamycin treatment inhibited mTORC1 activation in all groups as depicted by diminished phosphorylation of mTORC1 targets, S6K and TFEB (Supplementary Figure 6A). No differences in mTORC1 signalling were observed between *RRAGD* mutants and vehicle or *RRAGD* WT groups.

Of note, while *RRAGD* overexpression in zebrafish did not provoke disturbances in electrolyte homeostasis, rapamycin treatment in all groups lowered total Mg and Ca contents compared to the vehicle treatment (Supplementary Figure 6A-D).

Table 2. Effects of rapamycin treatments on zebrafish embryos expressing *RRAGD* p.S76L and p.P119R.

Genotype	*RRAGD* WT		*RRAGD* S76L		*RRAGD* WT		*RRAGD* P119R	
Treatment	**Vehicle**	**Rapamycin**	**Vehicle**	**Rapamycin**	**Vehicle**	**Rapamycin**	**Vehicle**	**Rapamycin**
Survival (%)	96 ± 3	90 ± 2	70 ± 5	83 ± 1	96 ± 2	94 ± 2	95 ± 1	88 ± 11
Heartbeat (bpm)	133 ± 3	121 ± 4	114 ± 11	106 ± 7	158 ± 5	155 ± 5	130 ± 7	124 ± 5
Area FS (%)	44 ± 3	41 ± 3	24 ± 3	47 ± 3	30 ± 3	34 ± 2	23 ± 3	33 ± 2
Diameter FS (%)	29 ± 3	25 ± 2	15 ± 2	25 ± 1	23 ± 2	22 ± 2	18 ± 3	21 ± 2
EF (%)	55 ± 4	54 ± 4	33 ± 4	60 ± 4	50 ± 3	44 ± 4	27 ± 5	42 ± 3
Pericardial swelling (pixels^2)	384 ± 11	417 ± 13	496 ± 29	432 ± 15	381 ± 9	384 ± 14	488 ± 23	423 ± 17
Total Mg(µg/mg protein)	7 ± 0.2	5 ± 0.05	7 ± 0.2	5 ± 0.1	8 ± 0.1	5 ± 0.01	7 ± 0.1	5 ± 0.1
Total Ca(µg/mg protein)	12 ± 0.5	7 ± 0.3	13 ± 0.6	7 ± 0.4	13 ± 0.3	9 ± 0.5	13 ± 0.2	9 ± 0.3

FS: fractional shortening. EF: ejection fraction. Values are shown as mean ± SEM.

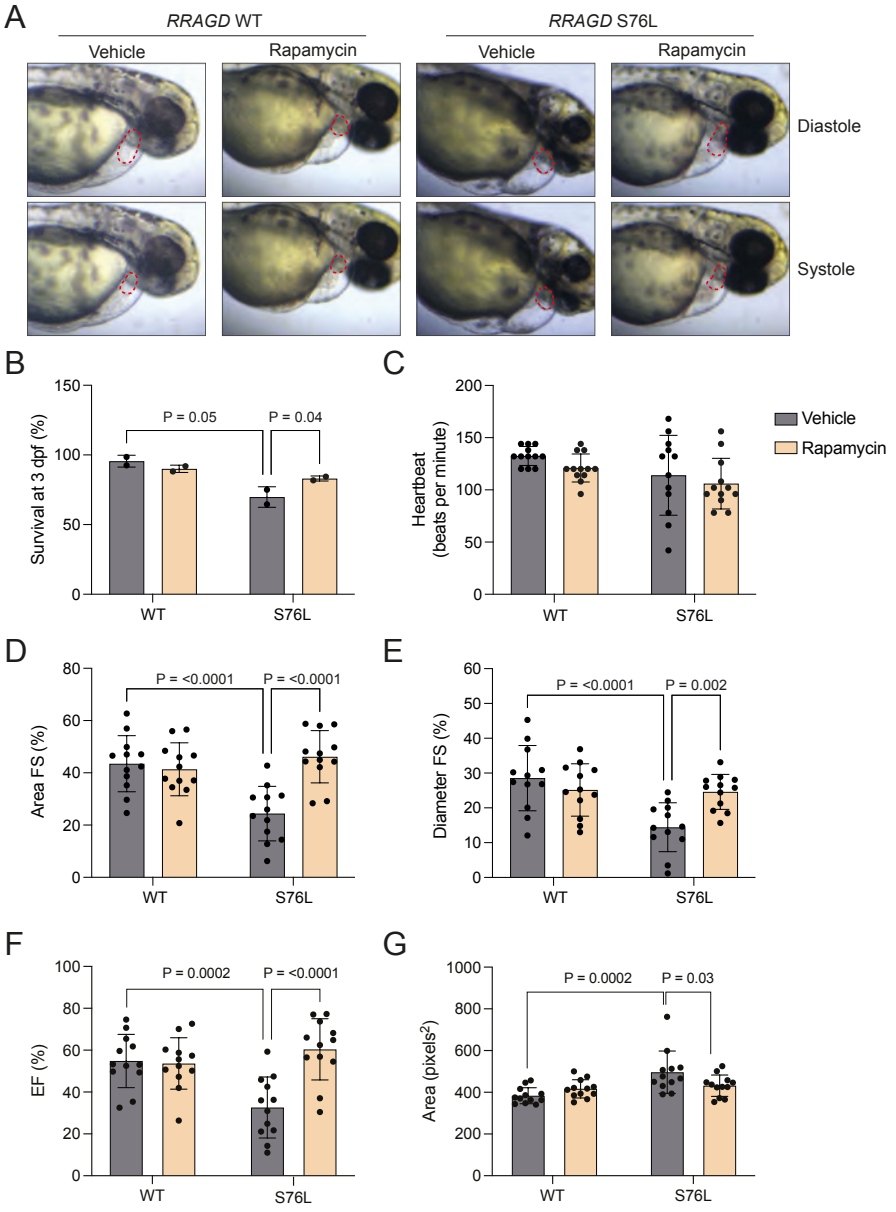

Figure 3. Effects of rapamycin treatment on *RRAGD* S76L expressing zebrafish embryo. Representative images of the heart ventricles (outlined in red) of zebrafish embryo expressing WT or S76L human *RRAGD* upon treatment with 0.4% DMSO as vehicle or 400 nM rapamycin. Magnification 100x (A). Bar graphs of survival percentage at 3 dpf compared to number of viable injected eggs from two petri dishes (n = 2; B), heartbeat (beats per minute; C), FS considering the ventricle area (D) or long-axis diameter (E), EF percentage (F), and pericardial cavity area (G) from 12 zebrafish embryos per experimental group. Statistical differences were determined using Two-way ANOVA followed by Šídák test.

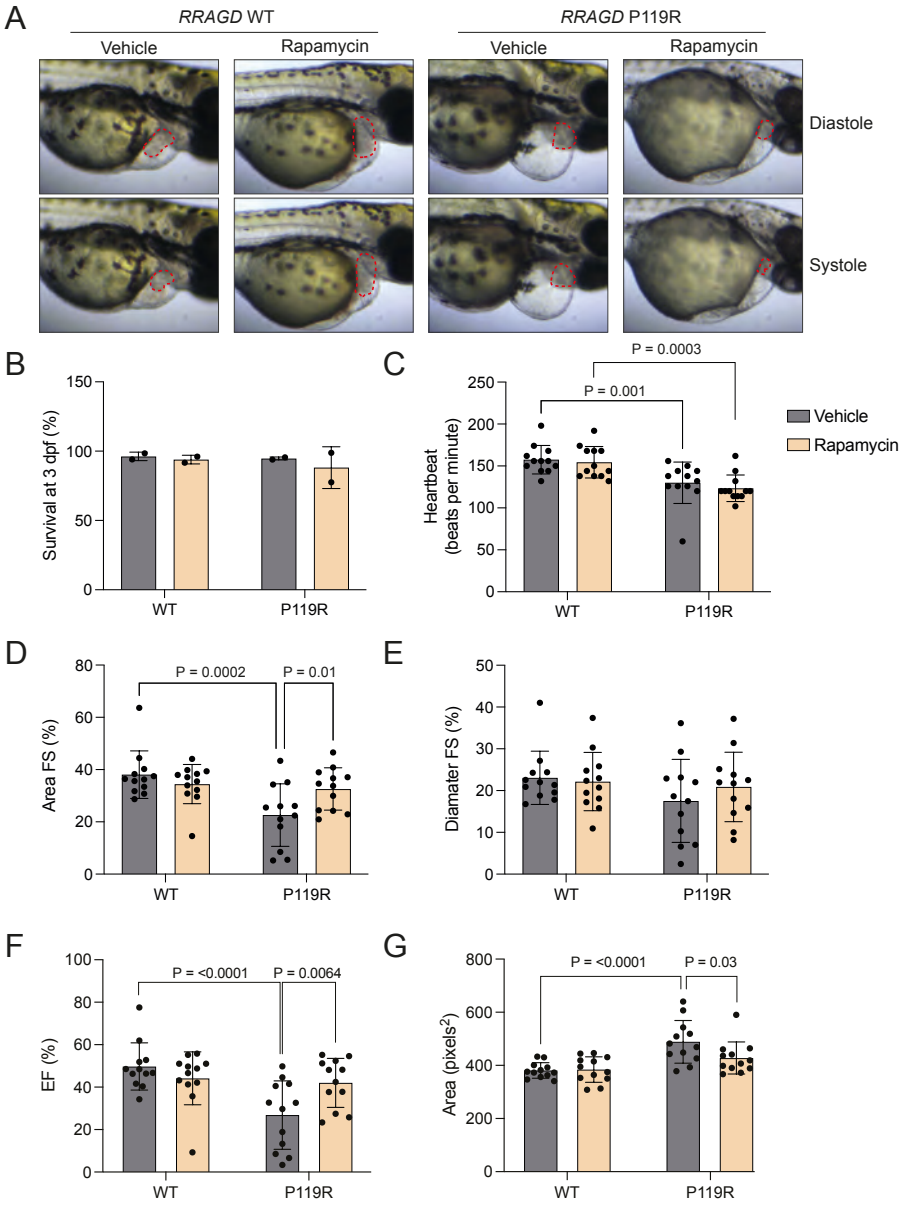

Figure 4. Effects of rapamycin treatment on *RRAGD* P119R expressing zebrafish. Representative images of the heart ventricles (outlined in red) of zebrafish embryos expressing WT or P119R human *RRAGD* upon treatment with 0.4% DMSO as vehicle or 400 nM rapamycin. Magnification 100x (A). Bar graphs of survival at 3 dpf compared to number of viable injected eggs from two petri dishes (n = 2; B), heartbeat (beats per minute; C), FS considering the ventricle area (D) or long-axis diameter (E), EF (F), and pericardial cavity area (G) from 12 zebrafish larvae per experimental group. Statistical differences were determined using Two-way ANOVA followed by Šídák test.

Discussion

In this study, we demonstrate that *RRAGD* variants initially found in ADKH-RRAGD patients result in cardiac dysfunction in zebrafish. Both the p.S76L and p.P119R variants cause reduced FS and EF, lower heartbeat, and fluid retention around the heart. Moreover, we showed that treatment with an mTOR inhibitor, rapamycin, rescued the heart phenotypes seen in *RRAGD* mutants overexpressing embryos.

Using a zebrafish embryo model, the cardiomyopathic phenotypes of *RRAGD* p.S76L and p.P119R variants were demonstrated as pericardial swelling, and lower EF and FS that are independent of heartbeat. To our knowledge, this is the first time that the role of *RRAGD* in the heart is demonstrated *in vivo*. The importance of the other Rag proteins in maintaining cardiac functions were already established previously.[9,10] As Rag GTPases are involved in the recruitment and the activation of mTORC1, we suggest that aberrant mTOR signalling is explaining the phenotypes. Previously, we have demonstrated that overexpression of these variants resulted in increased mTOR activity in HEK293T cells.[1] Moreover, mTOR signalling is well-characterized to be pivotal in heart development and adaptation to stress and mTORC1 hyperactivation has been implicated in DCM.[20] Sambri *et al.*, on the other hand, showed that *RRAGD* variants lead to TFEB dysfunctions independent of mTORC1 activity.[2] Nevertheless, we failed to see changes in mTORC1 signalling, including TFEB phosphorylation, in our model using whole embryo lysates. The effects of RagD on these signalling pathways may be masked by the expression of mTOR in tissues that do not express RagD. To determine the effects of *RRAGD* variants on mTORC1 signalling specifically in the heart, this should be studied in cardiomyocyte cell lines or isolated hearts of adult hearts in future studies. However, the use of adult zebrafish is not compatible with the mRNA injection, which is a limitation of our model. Of note, using morpholino-mediated *rragd* knockdown, loss of *rragd* in zebrafish embryos did not result in cardiac dysfunctions. This is in line with previous findings where *RRAGD* patients' variants have been shown to be a gain-of-function rather than loss-of-function.[2]

Rapamycin treatment rescued FS of the ventricle, EF, pericardial swelling, as well as the survival of the *RRAGD* mutants zebrafish embryos. Our findings are in contrast with *rragc* S75Y adult zebrafish model, in which rapamycin failed to ameliorate heart functions and survival, despite mTOR overactivation.[10] Thus, this raises the question whether rapamycin treatment targeted the pathogenic mTOR dysfunction induced by RagD-variants in our model or whether it represents a general mechanisms to improve cardiac dysfunctions. Indeed, inhibition of mTOR in animals with pressure overload is known to be beneficial as it reduces cardiac hypertrophy and improves

cardiac function.[21-23] Moreover, rapamycin treatment improved cardiac function in various animal models with other (not RagD-related) causes of increased ventricular thickness and reduced FS and EF.[24,25]

Total Mg and Ca contents were undisturbed in zebrafish embryos overexpressing *RRAGD* p.S76L and p.P119R variants. This finding could potentially be explained by anatomical differences between mammalian and zebrafish renal tubules.[26] Because the hallmarks of kidney tubulopathy seen in the Autosomal Dominant Kidney Hypomagnesemia (ADKH)-RRAGD patients are similar to those seen in Familial Hypomagnesemia with Hypercalciuria and Nephrocalcinosis (FHHNC; OMIM: 248250, 248190), we hypothesized that the electrolyte imbalance seen in patients are caused by defect paracellular Mg^{2+} and Ca^{2+} transport in the thick ascending limb (TAL) of the loop of Henle. However, zebrafish embryos and larvae possess a ductal system known as the pronephros that develops into a mesonephros around 12-14 dpf. Therefore, the absence of a metanephric kidney in zebrafish complicates the assessment of kidney physiology.[27]

mTOR inhibition with rapamycin reduced total Mg and Ca contents regardless of the genetic backgrounds. Moreover, loss of *rragd* in zebrafish increased Mg^{2+} and Ca^{2+} levels (Supplementary Figure 3D and E). In rats [28] and renal transplant patients, usage of rapamycin and its derivatives are known to cause hypomagnesemia and renal magnesium wasting. However, the exact pinpointing of the consequences of mTOR inhibition on ion tubular transport, especially in zebrafish, are currently unknown.

In conclusion, this current study demonstrated the effects of *RRAGD* variants in heart functions. Moreover, rapamycin as an mTOR inhibitor was shown to rescue cardiac dysfunctions in our zebrafish model. Future clinical studies should investigate whether mTOR inhibition will benefit patients with *RRAGD* variants. However, the harmful effects of an excessive inhibition of mTOR activity for heart and renal tubular function argue for a controlled restoration of mTOR signalling to physiological levels rather than a suppression of mTOR activity. Moreover, it remains unclear whether *RRAGD* variants lead to mTORC1 overactivation in the heart. Therefore, it is critical that future studies focus on investigating the molecular consequences of *RRAGD* variants in mammalian models to determine the precise therapy for cardiomyopathy ADKH-*RRAGD* patients.

Disclosure

None declared

Acknowledgements

The authors would like to thank Ruud Tilleman for contributing to the collection and analysis of data, miss Caro Bos for statistics support, and Radboud University Zebrafish Facility (www.ru.nl/zebrafish) for their excellent fish husbandry.

Grants

Jeroen de Baaij by the Netherlands Organization of Scientific Research (NWO, Vidi 09150172110040) and the European Research Council (ERC STG 101040682).

References

1. Schlingmann KP, Jouret F, Shen K, et al. mTOR-Activating Mutations in RRAGD Are Causative for Kidney Tubulopathy and Cardiomyopathy. *J Am Soc Nephrol.* 2021;32(11):2885-2899.
2. Sambri I, Ferniani M, Campostrini G, et al. RagD auto-activating mutations impair MiT/TFE activity in kidney tubulopathy and cardiomyopathy syndrome. *Nat Commun.* 2023;14(1):2775.
3. de Frutos F, Diez-Lopez C, Garcia-Romero E, et al. Dilated Cardiomyopathy With Concomitant Salt-Losing Renal Tubulopathy Caused by Heterozygous RRAGD Gene Variant. *Circ Genom Precis Med.* 2024;17(2):e004336.
4. Schurmann A, Brauers A, Massmann S, Becker W, Joost HG. Cloning of a novel family of mammalian GTP-binding proteins (RagA, RagBs, RagB1) with remote similarity to the Ras-related GTPases. *J Biol Chem.* 1995;270(48):28982-28988.
5. Hirose E, Nakashima N, Sekiguchi T, Nishimoto T. RagA is a functional homologue of S. cerevisiae Gtr1p involved in the Ran/Gsp1-GTPase pathway. *J Cell Sci.* 1998;111 (Pt 1):11-21.
6. Sekiguchi T, Hirose E, Nakashima N, Ii M, Nishimoto T. Novel G proteins, Rag C and Rag D, interact with GTP-binding proteins, Rag A and Rag B. *J Biol Chem.* 2001;276(10):7246-7257.
7. Sancak Y, Bar-Peled L, Zoncu R, Markhard AL, Nada S, Sabatini DM. Ragulator-Rag complex targets mTORC1 to the lysosomal surface and is necessary for its activation by amino acids. *Cell.* 2010;141(2):290-303.
8. Sancak Y, Peterson TR, Shaul YD, et al. The Rag GTPases bind raptor and mediate amino acid signaling to mTORC1. *Science.* 2008;320(5882):1496-1501.
9. Kim YC, Park HW, Sciarretta S, et al. Rag GTPases are cardioprotective by regulating lysosomal function. *Nat Commun.* 2014;5:4241.
10. Kim M, Lu L, Dvornikov AV, et al. TFEB Overexpression, Not mTOR Inhibition, Ameliorates RagC(S75Y) Cardiomyopathy. *Int J Mol Sci.* 2021;22(11).
11. Long PA, Zimmermann MT, Kim M, Evans JM, Xu X, Olson TM. De novo RRAGC mutation activates mTORC1 signaling in syndromic fetal dilated cardiomyopathy. *Hum Genet.* 2016;135(8):909-917.
12. Reijnders MRF, Seibt A, Brugger M, et al. De novo missense variants in RRAGC lead to a fatal mTORopathy of early childhood. *Genet Med.* 2023;25(7):100838.
13. Sciarretta S, Forte M, Frati G, Sadoshima J. New Insights Into the Role of mTOR Signaling in the Cardiovascular System. *Circ Res.* 2018;122(3):489-505.
14. Marin TM, Keith K, Davies B, et al. Rapamycin reverses hypertrophic cardiomyopathy in a mouse model of LEOPARD syndrome-associated PTPN11 mutation. *J Clin Invest.* 2011;121(3):1026-1043.
15. Ramos FJ, Chen SC, Garelick MG, et al. Rapamycin reverses elevated mTORC1 signaling in lamin A/C-deficient mice, rescues cardiac and skeletal muscle function, and extends survival. *Sci Transl Med.* 2012;4(144):144ra103.
16. Gao G, Chen W, Yan M, et al. Rapamycin regulates the balance between cardiomyocyte apoptosis and autophagy in chronic heart failure by inhibiting mTOR signaling. *Int J Mol Med.* 2020;45(1):195-209.
17. Dooley K, Zon LI. Zebrafish: a model system for the study of human disease. *Curr Opin Genet Dev.* 2000;10(3):252-256.
18. Arjona FJ, Chen YX, Flik G, Bindels RJ, Hoenderop JG. Tissue-specific expression and in vivo regulation of zebrafish orthologues of mammalian genes related to symptomatic hypomagnesemia. *Pflugers Arch.* 2013;465(10):1409-1421.

19. Arjona FJ, de Baaij JH, Schlingmann KP, et al. CNNM2 mutations cause impaired brain development and seizures in patients with hypomagnesemia. *PLoS Genet.* 2014;10(4):e1004267.

20. Caragnano A, Aleksova A, Bulfoni M, et al. Autophagy and Inflammasome Activation in Dilated Cardiomyopathy. *J Clin Med.* 2019;8(10).

21. McMullen JR, Sherwood MC, Tarnavski O, et al. Inhibition of mTOR signaling with rapamycin regresses established cardiac hypertrophy induced by pressure overload. *Circulation.* 2004;109(24):3050-3055.

22. Shioi T, McMullen JR, Tarnavski O, et al. Rapamycin attenuates load-induced cardiac hypertrophy in mice. *Circulation.* 2003;107(12):1664-1670.

23. Gao XM, Wong G, Wang B, et al. Inhibition of mTOR reduces chronic pressure-overload cardiac hypertrophy and fibrosis. *J Hypertens.* 2006;24(8):1663-1670.

24. Samidurai A, Saravanan M, Ockaili R, et al. Single-Dose Treatment with Rapamycin Preserves Post-Ischemic Cardiac Function through Attenuation of Fibrosis and Inflammation in Diabetic Rabbit. *Int J Mol Sci.* 2023;24(10).

25. Das A, Durrant D, Koka S, Salloum FN, Xi L, Kukreja RC. Mammalian target of rapamycin (mTOR) inhibition with rapamycin improves cardiac function in type 2 diabetic mice: potential role of attenuated oxidative stress and altered contractile protein expression. *J Biol Chem.* 2014;289(7):4145-4160.

26. Desgrange A, Cereghini S. Nephron Patterning: Lessons from Xenopus, Zebrafish, and Mouse Studies. *Cells.* 2015;4(3):483-499.

27. Drummond IA, Davidson AJ. Zebrafish kidney development. *Methods Cell Biol.* 2010;100:233-260.

28. da Silva CA, de Braganca AC, Shimizu MH, et al. Rosiglitazone prevents sirolimus-induced hypomagnesemia, hypokalemia, and downregulation of NKCC2 protein expression. *Am J Physiol Renal Physiol.* 2009;297(4):F916-922.

Supplementary data

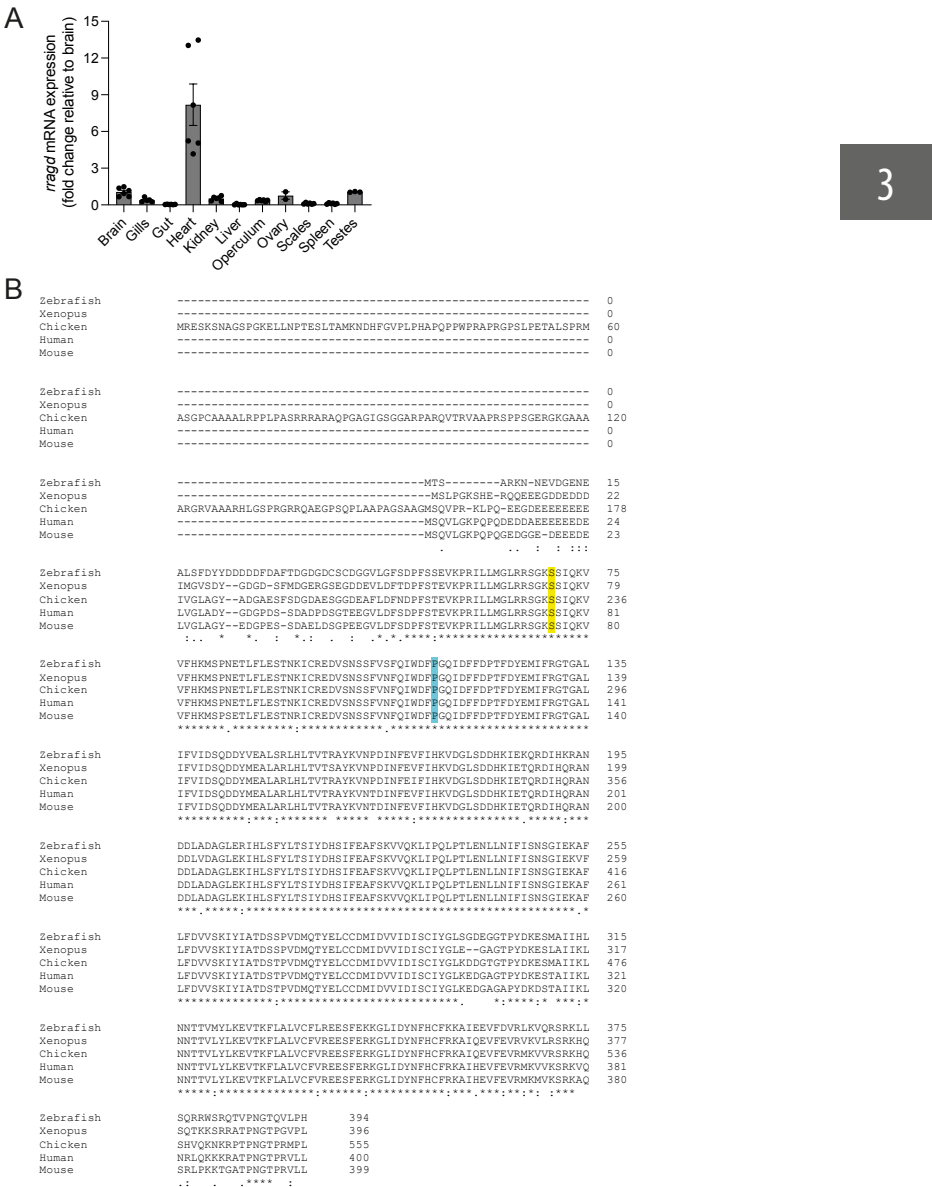

Supplementary Figure 1. Bar graph showing *rragd* mRNA expression across different tissues in adult zebrafish (n = 6, for ovaries and testes n = 2-3, A). Clustal Omega alignment of Human RagD (Homo Sapiens NP_067067.1), Mouse RagD (Mus Musculus NP_081767.2), Chicken RagD Frog RagD (Gallus Gallus XP_015140187.3), Xenopus RagD (Xenopus Tropicalis NP_001072896.1), Zebrafish RagD (Danio Rerio NP_001092894.2) (B). Residue Ser76 affected by mutation is highlighted by yellow while Pro119 residue is highlight by cyan.

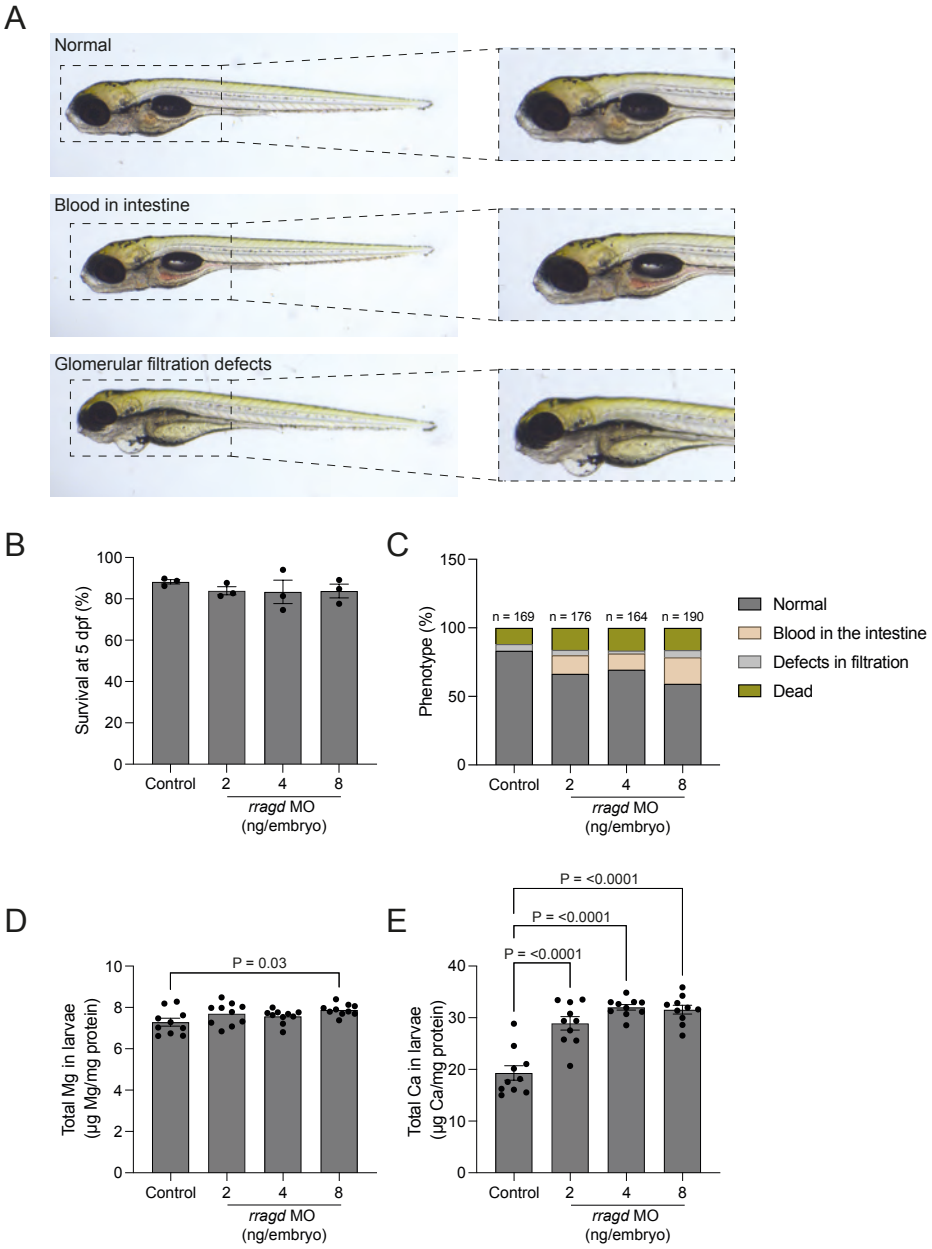

Supplementary Figure 2. Effects of morpholino knockdown of *rragd* in zebrafish embryos. Phenotypes observed in zebrafish embryos injected with control morpholino, 2 ng, 4 ng, or 8 ng *rragd* morpholino at 5 dpf (A). Survival of embryos at 5 dpf compared to viable eggs injected at the beginning of the experiment in three petri dishes (n = 3; B). Percentage of embryos with each phenotype (C). Total Mg (D) and Ca (E) measured in 10 samples consisting of 10 embryos for each sample. Statistical significance was determined using One-way ANOVA followed by Tukey's test.

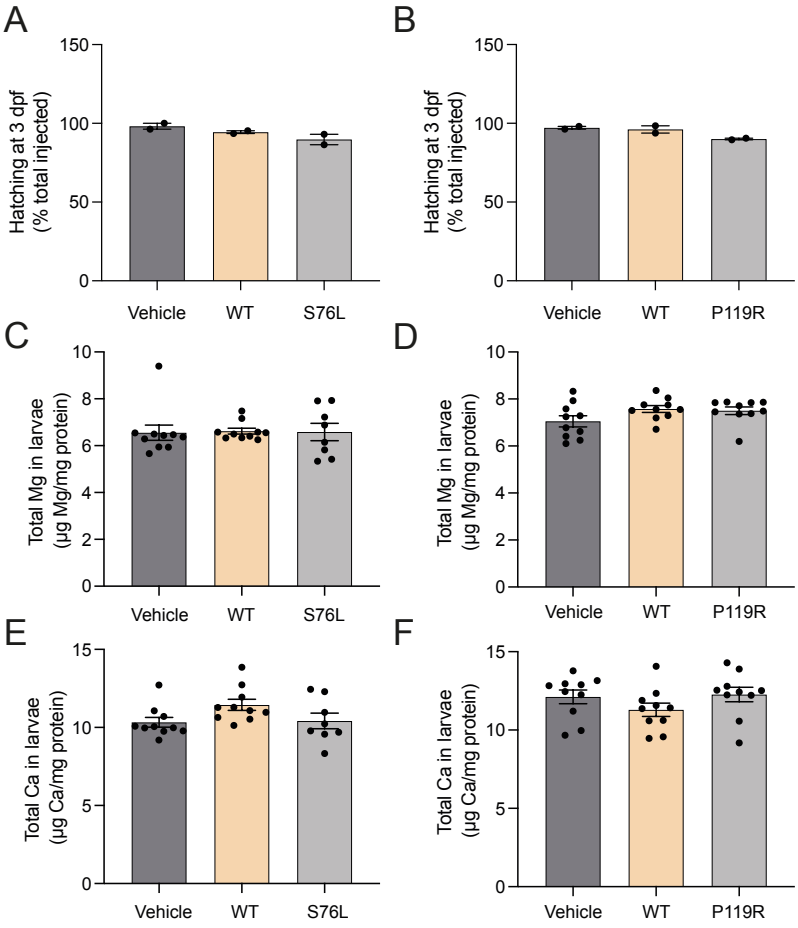

Supplementary Figure 3. Effects of *RRAGD* S76L and P119R on zebrafish embryos hatching and ion homeostasis. Percentage of hatched zebrafish embryos injected with vehicle or human *RRAGD* WT, S76L (A), or P119R (B) cRNAs compared to total viable eggs injected in two petri dishes (n = 2). To measure total Mg (C, D) and Ca (E, F) per embryo, 8-10 samples of pools of ten individual fish were collected. Statistical significance was determined with One-way ANOVA followed by Tukey test.

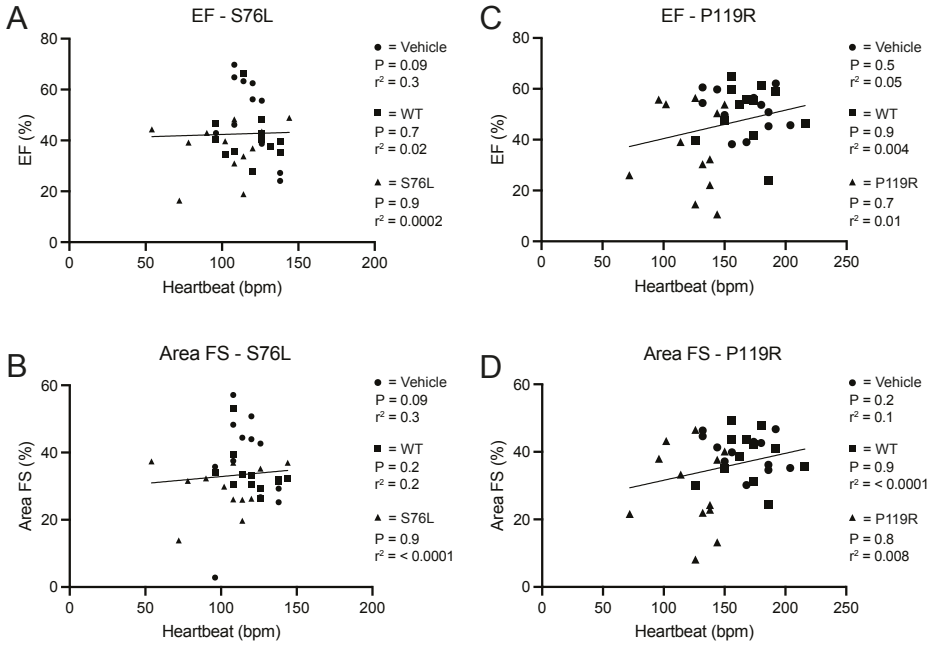

Supplementary Figure 4. Regression analyses between heartbeat and ejection fraction or fractional shortening in zebrafish embryos. Plots depicting correlation between heartbeat and (A, C) ejection fraction (EF) or (B, D) fractional shortening (FS) considering ventricular area.

Supplementary Figure 5. Morphology of zebrafish embryos. Representative images of zebrafish embryos injected with human *RRAGD* WT, S76L (A), or P119R (B) cRNAs, treated with 0.4% DMSO vehicle or 400 nM rapamycin. Images were taken at 3 dpf at 8x or 25x magnification.

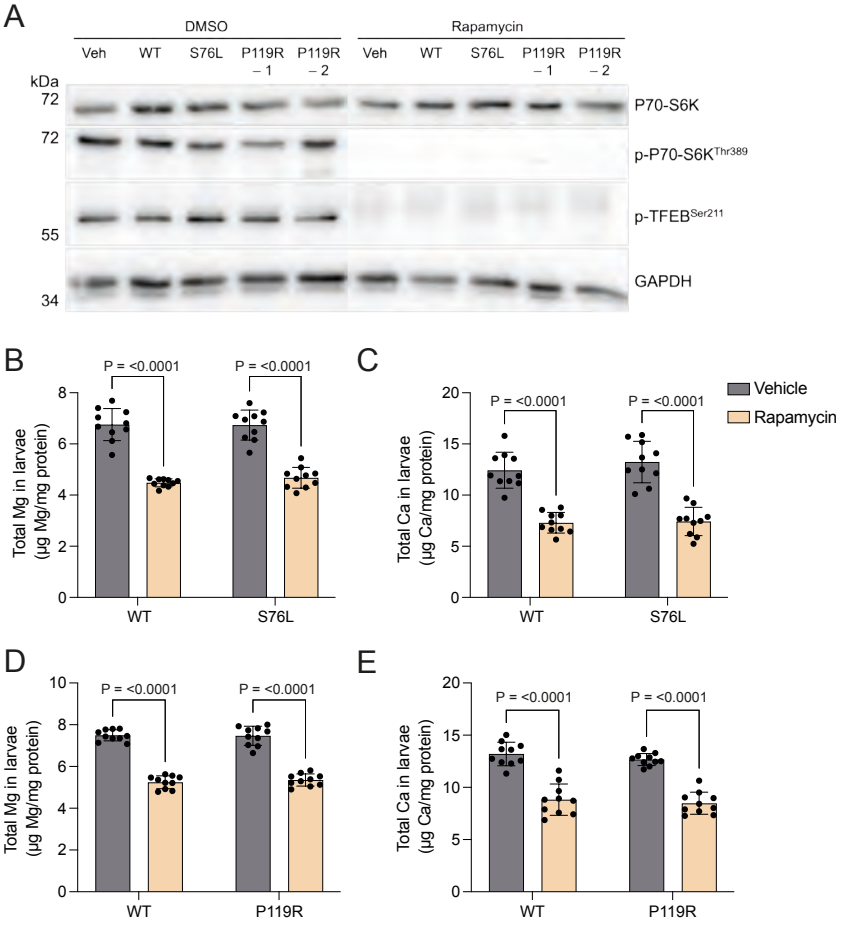

Supplementary Figure 6. Effects of rapamycin treatment on mTORC1 signaling and ion homeostasis in zebrafish embryos. Representative western blots of mTORC1 targets, S6K, and its phosphorylated form (p-p70-S6K) as well as phospho-TFEB from whole zebrafish embryo lysates (n = 2 groups comprising of 10 embryos each in every condition). GAPDH is shown as loading control (A). Total Mg (B, D) and Ca (C, F) contents in 10 samples each consisting of 10 embryos after treatment with vehicle (dark grey bars) or rapamycin (yellow bars). Statistical differences were determined using Two-way ANOVA followed by Šídák test.

Supplementary Video 1. Representative videos of the hearts of zebrafish embryos injected with vehicle, *RRAGD* WT, or *RRAGD* S76L cRNA at 100x magnification.

Supplementary Video 2. Representative videos of the hearts of zebrafish embryos injected with vehicle, *RRAGD* WT, or *RRAGD* P119R cRNA at 100x magnification.

Supplementary Video 3. Representative videos of the hearts of zebrafish embryos injected with *RRAGD* WT or *RRAGD* S76L cRNA, treated with 0.04% (v/v) vehicle or 400 nM rapamycin at 100x magnification.

Supplementary Video 4. Representative videos of the hearts of zebrafish embryos injected with *RRAGD* WT or *RRAGD* P119R cRNA, treated with 0.04% (v/v) vehicle or 400 nM rapamycin at 100x magnification.

CHAPTER 4

RRAGD p.(Ser76Leu) variant causes constitutive activation of mTORC1 and dysregulated expression of muscle development and cytoskeleton genes in cardiomyocytes

Anastasia Adella[1], Pieter A. Leermakers[1], Willem B. van Ham[2], Hesther de Ruiter[3], Judita Ilgutytė[1], Suzanne Hendrickx[1], Levi Nijland[1], Teun P. de Boer[2], Eva van Rooij[3, 4], Joost G.J. Hoenderop[1], Jeroen H.F. de Baaij[1*]

[1] Department of Medical BioSciences, Radboudumc, Nijmegen, The Netherlands
[2] Department of Medical Physiology, University Medical Center Utrecht, Utrecht, The Netherlands
[3] Hubrecht Institute, Royal Netherlands Academy of Arts and Sciences (KNAW) and University Medical Center Utrecht, Utrecht, The Netherlands
[4] Division Heart and Lungs, Department of Cardiology, University Medical Center Utrecht, Utrecht, The Netherlands

Submitted

Abstract

Autosomal dominant kidney hypomagnesemia with *RRAGD* variants (ADKH-*RRAGD*) is a hereditary disorder characterized by kidney tubulopathy and dilated cardiomyopathy (DCM). RagD, encoded by the *RRAGD* gene, is a small GTPase involved in activating the mechanistic target of rapamycin complex 1 (mTORC1) by amino acids. Although several gain-of-function variants in the *RRAGD* gene have been identified, their contributions to DCM remain unclear. Here, we hypothesize that these *RRAGD* variants induce mTORC1 overactivation, thereby contributing to the manifestation of DCM. To investigate this, we established T-REx HeLa cell lines that overexpress the *RRAGD* p.(Ser76Leu) or the wild-type (WT) variant to assess the effects on mTORC1 signaling. Additionally, we developed the first cellular model of ADKH-*RRAGD* utilizing genetically edited human-induced pluripotent stem cell-derived cardiomyocytes (hiPSC-CMs) that express the mutated variant. Our data indicate that the *RRAGD* p.(Ser76Leu) variant maintains the phosphorylation of mTORC1 targets (i.e., S6K, 4E-BP1, and TFEB) during amino acid starvation, in contrast to *RRAGD* WT in T-REx HeLa cells. The pharmacological inhibition of mTOR with Torin1 reversed these changes. In 2D-cultured *RRAGD*$^{WT/p.(Ser76Leu)}$ hiPSC-CMs, mTORC1 remained responsive to amino acid stimulation. Results from bulk RNA sequencing showed an upregulation of pathways associated with cytoskeletal organization and a downregulation of muscle development in *RRAGD*$^{WT/p.(Ser76Leu)}$ hiPSC-CMs. Moreover, a prolonged duration of Ca^{2+} transients was observed in the mutant cardiomyocytes. Altogether, our data demonstrate that gain-of-function variants in *RRAGD* cause mTORC1 constitutive activation. Consequently, cardiomyocytes develop impaired intracellular Ca^{2+} clearance and activation of transcriptional programs, suggesting dedifferentiation.

Keywords: cardiomyocytes, ADKH-*RRAGD*, mTORC1, *RRAGD*, dilated cardiomyopathy

Introduction

Gain-of-function variants in Ras-related GTPase D (RRAGD) are causative for kidney tubulopathy and dilated cardiomyopathy (DCM).[1,2] In patients with pathogenic *RRAGD* variants, cardiomyopathies have been reported in approximately 50% of all cases, requiring heart transplantation in several cases. Other cardiac defects include ventricular arrhythmias, myocardial infarction, and excessive apical trabeculations in a subset of patients.[2,3] Within the spectrum of *RRAGD* variants, the most prevalent variant, p.(Ser76Leu), represents a variant hotspot that is particularly associated with cardiac defects.[1] 80% of the patients with this variant developed cardiomyopathy.[1,3]

RRAGD, encoding the RagD protein, belongs to the family of rag GTPases that act as intracellular amino acid sensors. The Rag GTPases recruit mTORC1 to the lysosomal surface, where it phosphorylates its downstream targets.[4,5] RagC and RagD form heterodimeric complexes with RagA or RagB. Upon amino acid-induced activation, RagA and RagB bind GTP, whereas RagC and RagD are GDP-bound.[6-10] After mTORC1 is activated at the lysosomal surface, mTORC1 phosphorylates canonical substrates such as the S6 kinase (S6K) and the eukaryotic initiation factor 4e binding protein 1 (4E-BP1), and the non-canonical mTORC1 substrates such as the member of the microphthalmia/transcription factor E (MiT/TFE) family, the transcription factor EB (TFEB).[11-17] To date, pathogenic *RRAGD* variants have been demonstrated to disturb both canonical and non-canonical mTORC1 pathways. In HEK293 cells, *RRAGD* variants resulted in constitutive activation of S6K in the absence of amino acids.[1] Moreover, Sambri et al. reported overactivation of only the non-canonical mTORC1 pathway using TFEB as their main read-out.[2]

mTOR signaling is important in maintaining cardiac function (reviewed in [18,19]). Consequently, suppression of mTOR activity has improved cardiac structure and functions in cell and animal models of DCM.[18,19] For example, deletion of *Mtor* in mouse cardiomyocytes suppressed proliferation at early embryonic stages.[20] In adult mice, inducible *Mtor* deletion from the heart caused DCM.[21] The role of Rag GTPases in heart has also been demonstrated. *Rraga* and *Rragb* KO mice develop cardiac hypertrophy.[22] Additionally, gain-of-function variants in *rragc* cause a DCM-like phenotype in cells and zebrafish.[23,24] More recently, we showed that the *RRAGD* p.(Ser76Leu) and p.(Pro119Arg) variants led to cardiac dysfunctions in zebrafish embryos.[25] Although the full molecular mechanisms remain to be elucidated, multiple studies point towards reduced TFEB activity.[2,22-24] Indeed, restoration of TFEB function rescued the *rragc*-induced cardiac dysfunction in zebrafish.[23]

In this study, we examined the cellular consequences of the *RRAGD* p.(Ser76Leu) variant in cardiomyocytes. We hypothesized that the *RRAGD* p.(Ser76Leu) variant leads to constitutive activation of mTORC1, which disrupts cardiomyocyte cellular processes and contributes to the DCM observed in patients. To investigate how this variant affects mTORC1 signaling, we utilized stable T-REx HeLa cell lines overexpressing either *RRAGD* wild-type (WT) or the p.(Ser76Leu) variant. Subsequently, we validated our findings in a more physiologically relevant model using a human-induced pluripotent stem cell-derived cardiomyocyte (hiPSC-CM) model carrying a heterozygous p.(Ser76Leu) variant. Finally, using the hiPSC-CMs, we performed electrophysiological assays and bulk RNA sequencing to systematically analyze the functional consequences of the variant.

Materials and methods

Cloning and plasmids

Human *RRAGD* construct (VectorBuilder GmbH< Neu-Isenburg, Germany (vector ID: VB171030-1104zuv; vectorbuilder.com)) was amplified by PCR and subcloned into the pCINeo IRES mCherry expression vector using AgeI and EcoRI restriction sites. *RRAGD* c.227C>T (p.(Ser76Leu)) mutation was introduced using the QuikChange II XL site-directed mutagenesis kit (Agilent Technologies, California, USA). To make the T-REx HeLa stable cell lines, *RRAGD* WT and p.(Ser76Leu) constructs were subcloned into the pcDNA5/FRT/TO eGFP expression vector using the KpnI and XhoI restriction sites. pcDNA3.1-TFEB-WT-MYC was a gift from James Brugarolas (Addgene plasmid #99955).[26] For CRISPR-Cas9, gRNAs were subcloned into the pSpCas9(BB)-2A-GFP (PX458) vector (Addgene plasmid #48138). All primers and oligonucleotides used are available in Supplementary Table 1.

Antibodies

Primary antibodies from Cell Signaling Technology (Massachusetts, USA): Akt (#4691, WB: 1:1000), p-Akt^{Thr308} (#9275, WB: 1:500), p70-S6K (#2708, WB: 1:1000), p-p70-S6K^{Thr389} (#9234, WB: 1:1000), TFEB (#4240, WB: 1:1000, ICC: 1:200), p-TFEB^{Ser211} (#37681**,** WB: 1:1000), 4E-BP1 (#9452, WB: 1:1000), p-4E-BP1$^{Thr37/46}$ (#2855, WB: 1:1000). From Novius Biologicals (Colorado, USA): RagD (#NBP2-32106, WB: 1:2000, ICC: 200). From Sigma-Aldrich (Missouri, USA): ACTN2 (#A7732, ICC: 1:400, FACS: 1:1000), GFP (#G154, WB: 1:5000), and TAZ (#HPA007415, WB: 1:1000). From Invitrogen (Vilnius, Lithuania): GAPDH (#AM4300, WB: 1:4000). From Santa Cruz Biotechnology (Texas, USA): Vinculin (#sc-25336, WB: 1:1000) and p-TAZ^{Ser89} (#sc-17610, WB: 1:1000). From Bethyl Laboratories (Texas, USA): TFEB (A303-673A, ICC: 1:200). From Abcam (Cambridge,

UK): cTnT (#45932, FACS: 1:1000). For immunoblotting, peroxidase- (PO) conjugated secondary antibodies were used. From Jackson ImmunoResearch Europe Ltd. (Exeter, UK): PO-conjugated anti-IgG mouse (#145-515-035, 1:10000). From Merck Life Sciences (Amsterdam, The Netherlands): PO-conjugated anti-IgG rabbit (#A4914, 1:10000) was used. For immunocytochemistry & FACS experiments, secondary antibodies from Thermo Fisher Scientific (Orlando, USA): anti-IgG rabbit conjugated to Alexa Fluor 488 (#A11008, ICC: 1:300, FACS: 1:1000) and Alexa Fluor 594 (#A11012, ICC: 1:300), and anti-IgG mouse conjugated to Alexa Fluor 488 (#A11029, ICC: 1:300, FACS: 1:1000).

Cell culture

T-REx HeLa cells and HEK293 cells were cultured in culture medium (Dulbecco's Modified Eagle Medium (DMEM) containing 25 mM Hepes, 4.5 g/L glucose, and 4 mM L-glutamine (#42430082, Thermo Fisher Scientific, California, USA), supplemented with 10% FBS (Greiner Bio-One, Alphen aan den Rijn, the Netherlands), 1 mM sodium pyruvate (Thermo Fisher Scientific, California, USA), and 1% v/v MEM non-essential amino acids solution 100x (Capricorn Scientific GmbH, Ebsdorfergrund, Germany)). Human induced pluripotent stem cells (hiPSCs) (American Type Culture Collection (ATCC) #ACS-1026, lot no. 0238, Virginia, USA) were cultured on Geltrex™ lactose dehydrogenase elevating virus-free, human embryonic stem cell-qualified, Reduced Growth Factor Basement Membrane Matrix-coated wells (#A1413302, Thermo Fisher Scientific, California, USA). hiPSCs were kept in Essential 8™ Flex medium (E8 medium) (#A2858501, Thermo Fisher Scientific, California, USA), refreshed every 2 days. After passage, hiPSCs were kept in Essential 8 medium supplemented with 2 µM thiazovivin (#SML1045, Sigma-Aldrich, Missouri, USA) and replaced with plain E8 medium. All cells were kept in a humidified 37°C incubator with 5% CO_2 unless stated otherwise.

T-REx HeLa cell line generation

$1.8x10^6$ T-REx™ HeLa cells (Invitrogen, Massachusetts, USA) were seeded into a 10-cm petri dish and 6 hr later, the cells were co-transfected with 1 µg pOG44 plasmid (Invitrogen, Massachusetts, USA) and 1 µg of either empty pcDNA5/FRT/TO-eGFP (mock), pcDNA5/FRT/TO-eGFP *RRAGD* WT, or p.(Ser76Leu), totaling to 2 µg DNA. As a negative control, cells were transfected with 2 µg of only pOG44 plasmid. For transfection, 2 µL Lipofectamine 2000 (Invitrogen, Massachusetts, USA) was used per 1 µg of DNA. 18 hr later, antibiotics consisting of 3 µg/mL blasticidin (Sigma-Aldrich, Missouri, USA) and 100 µg/mL Hygromycin B (Thermo Fisher Scientific, California, USA) were added to the T-REx HeLa cell culture medium (see cell culture section) to start selection procedure. T-REx HeLa cell culture medium supplemented with antibiotics is now termed T-REx HeLa selection medium. to start the selection procedure. The selection medium was replaced every 2 days until cell sorting.

Nine days after transfection and 24 hr before sorting, expression of GFP or fusion GFP-RagD was induced in the transfected cells by adding 1 µg/mL tetracycline to the selection medium. The following day, the cells were sorted through a fluorescence-activated cell sorting (FACS) machine by the flow cytometry facility at Radboudumc. In short, cells were disassociated from the petri dishes using trypsin-EDTA solution (0.05% (v/v) trypsin, 0.02% (w/v) EDTA) and resuspended in PBS + 2% (w/v) EDTA. Then, individual GFP-positive cells were sorted into a single 96-well plate using a 100 µm nozzle of the Cytek™ Aurora CS System (Cytek, the Netherlands). Cells were next kept in an incubator (37°C incubator with 5% (v/v) CO_2) for 10 days. Thereafter, grown clones from each cell line were expanded and genotyped using the subcloning primers. For each mock, *RRAGD* WT, and p.(Ser76Leu) cell line, one clone was selected and used for subsequent experiments.

T-REx HeLa cells transfection and treatment

For immunoblotting and RT-qPCR experiments, 200,000 T-REx HeLa cells were seeded into a 6-well plate. The next day, expression of GFP or GFP-RagD was induced by adding 1 µg/mL tetracycline to the culture medium. For immunocytochemistry experiments, 300,000 cells were seeded into a 6-well plate. After 6 hr, the cells were transfected with 0.5 µg of pcDNA3.1-WT-TFEB-MYC using FuGENE HD Transfection Reagent (Promega, Shanghai, China) at a 1:2 DNA:FuGENE ratio. The next day, these transfected T-REx HeLa cells were collected, and 20,000 cells were re-seeded on poly-L-lysine-coated 10 mm coverslips in 24-well plates. After 24 hr, 1 µg/mL tetracycline was added to the culture medium to induce the expression of GFP or GFP-RagD. All cells were harvested 24 hr after tetracycline addition.

For drug treatment, 24 hr after tetracycline induction, half of the T-REx HeLa cells were treated with 100 nM rapamycin (#SC-3504A, Santa Cruz Biotechnology, Texas, USA) or 250 nM Torin 1 (#4247, Tocris, Abingdon, UK) for 1 hr. As a control, 0.01% (v/v) solvent DMSO (Sigma-Aldrich, Missouri, USA) was added to the other half of the cells, also for 1 hr.

Genome targeting with CRISPR-Cas9

gRNAs were designed using CRISPOR web tool with no changes to the default parameters.[27] Six gRNAs were selected (Supplementary Figure 2). All six gRNAs were subcloned into the PX458 plasmid (see cloning and plasmids section above) and confirmed by sequencing using the human U6 promoter primer (Supplementary Table 1). Next, a T7 endonuclease assay was performed to assess the cutting efficiency of each gRNA.[28] To do this, HEK293 cells were transfected with 1 µg of gRNA in a 12-well plate using 9 µg of 1 mg/mL polyethylenimine (PEI, Polysciences,

Pennsylvania, USA). After 48 hr, gDNA of HEK293 cells were isolated using proteinase K at 55°C for 2 hr. Next, a PCR was run against *RRAGD*. Next, 1 µL T7 Endonuclease I (New England Biolabs, Massachusetts, USA) was added to the PCR product and incubated for 30 mins at 37°C. Digested products were run on 2% (w/v) agarose gel for analysis. Based on the cutting efficiency and proximity to the region of interest, the most efficient gRNA (i.e., gRNA #5) was selected (Supplementary Table 1).

Next, to introduce the *RRAGD* c.227C>T mutation, hiPSCs were pre-treated with thiazovivin for 1 hr at 37°C. Then, $3x10^6$ hiPSCs suspension was collected and resuspended in 100 µL prewarmed nucleofection mix (Lonza Human Stem Cell Nucleofector™ Kit 1 #VPH-5012, Lonza, Oss, The Netherlands) supplemented with 5 µg PX458 containing gRNA #5 and 1 µg of each WT and p.(Ser76Leu) double-stranded oligonucleotides (gBlocks™ Gene Fragments, IDT, Iowa, USA). These oligonucleotides serve as the template for gene editing. These hiPSCs were then transferred to an electroporation cuvette and nucleofected using the A-203 program of the Nucleofector™ device (Lonza, Oss, The Netherlands). Nucleofected hiPSCs were supplemented with warm E8 medium containing 2 µM thiazovivin and transferred to a Geltrex-coated 6-well, and kept at a 37°C incubator. 48 hr post-nucleofection, hiPSCs were disassociated using Versene Solution (#15040066, Thermo Fisher Scientific, California, USA). Single cells were then sorted into 96-well plates based on GFP signal using FACSJazz (BD Biosciences, Drachten, the Netherlands). The 96-well plates were coated with irradiated mouse embryonic fibroblasts (Thermo Fisher Scientific, California, USA). After sorting, the 96-well plates were centrifuged for 1 min at 200xg and incubated at 37°C.

14 days after the sorting, hiPSC clones were collected using Versene Solution and passaged into two wells of a 96-well plate. With one well, genotyping was performed to check for mutation of interest. In short, the gDNA of the clones was isolated using an ethanol-based precipitation method. Next, a genomic region containing the mutation of interest was amplified with PCR with *RRAGD* genotyping primers (Supplementary Table 1). Subsequently, Sanger sequencing was done to confirm the presence of mutation. Maintenance of the clones was carried out using the other well.

After obtaining a hiPSCs clone with mutation of interest and its isogenic controls, the top three off-target sites predicted by the CRISPOR tool were amplified by PCR and sent for Sanger sequencing (Supplementary Table 1).

Bulk karyo-sequencing

Approximately 1000 hiPSCs were collected and spun down as pellets. Next, the cell pellets were digested in 5 µL of 2 µg Proteinase K (New England Biolabs, Massachusetts, USA) in 1x CutSmart Buffer (New England Biolabs, Massachusetts, USA) for 2 hr at 55°C followed by 10 min at 80°C. To obtain DNA fragments, DNA was digested using 10 µL of 10 U NLAIII (New England Biolabs, Massachusetts, USA) in 1x CutSmart Buffer for 2 hours at 37°C followed by 20 min at 80°C. Following this, the DNA fragments were ligated to adapters by adding 20 µL or 800 U T4 DNA Ligase (New England Biolabs, Massachusetts, USA), 1 mM ATP (Thermo Fisher Scientific), and 50 nM adapter in 1x T4 DNA Ligase Buffer (New England Biolabs, Massachusetts, USA) and incubated at 16°C overnight. The library preparation, sequencing, and analysis were performed as described previously.[29]

Cell growth measurement

2,500 hiPSCs were seeded on a 96-well plate coated with Geltrex. The plates were then placed back in a 37°C incubator to allow the cells to attach. Four hours later, they were transferred to the IncuCyte ZOOM™ live cell imaging system (Essen BioScience, Michigan, USA). Cell growth was recorded every 12 hr for a total duration of 96 hr. The E8 culture medium was refreshed every 2 days. At the end of the experiment, a mask generated in the system program was used to select cell clusters and quantify the cell growth.

Cardiomyocyte differentiation

At the start of the differentiation, hiPSCs were maintained and grown until 80-90% confluency (Day 0). Then, the medium was aspirated, and the cells were rinsed once with HBSS (Thermo Fisher Scientific, California, USA). Differentiation medium (RPMI 1640 with GlutaMAX™ Supplement with HEPES (#72400-021, Thermo Fisher Scientific, California, USA), supplemented with 0.5 mg/mL human recombinant albumin (#A9731, Sigma-Aldrich, Missouri, USA), 0.2 mg/mL L-Ascorbic Acid 2-Phosphate (#681671, Sigma-Aldrich, Missouri, USA) was added with the additional of 4 µm CHIR99021 (#361559, Sigma-Aldrich, Missouri, USA). On day 2, the medium was aspirated, and cells were rinsed once with HBSS. Afterward, the differentiation medium was replaced with fresh differentiation medium supplemented with 5 µM IWP-2 (#681671, Sigma-Aldrich, Missouri, USA). On days 4 and 6, the medium was again refreshed, but with plain differentiation medium. From day 8, or when the cells started beating, the differentiation medium was replaced every 3-4 days with a cardio culture medium. At day 14, hiPSC-derived cardiomyocytes (hiPSC-CMs) were cultured in cardio culture medium (RPMI-1640 Medium with GlutaMAX™ Supplement with HEPES supplemented with B-27 Supplement 50x-serum free

(#17504001, Thermo Fisher Scientific, California, USA)). These hiPSC-CMs were expanded 9-10x the surface area on Geltrex-coated wells and flasks for further applications. 1 and 4 days after expansion, the culture medium was refreshed. After 4 days, the medium was changed once a week.

Cardiomyocyte culture

The hiPSC-CMs used in this study are aged 30 or 80 days post-differentiation. 10 days before the start of the experiment, the hiPSC-CMs were dissociated using 10x TrypLE Select Enzyme without phenol red (#A1217703, Thermo Fisher Scientific, California, USA) for a maximum of 45 minutes at 37°C and replated onto Geltrex-coated surfaces. hiPSC-CMs are kept at a 37°C incubator with 5% (v/v) $CO_{2.}$

For immunoblotting, 250,000 hiPSC-CMs were replated onto a 6-well plate. For immunocytochemistry experiments, 75,000 cells were replated onto a 10 mm coverslip pre-coated with Geltrex. For electrophysiology experiments, 25,000 cells were replated onto a Geltrex-coated 10 mm coverslip.

Cardiomyocyte purity

Approximately $1x10^6$ hiPSC-CMs were disassociated and spun down (300xg for 5 min). The resulting pellets were rinsed once with HBSS and fixed using 1 mL ice-cold 70% EtOH. Next, cells were centrifuged for 4 min at 300xg, and the supernatant was removed. Subsequently, cells were resuspended in blocking buffer (PBS supplemented with 5% (v/v) FBS, 1% (w/v) bovine serum albumin, and 0.5% (v/v) Triton X-100) and incubated for 10 min on ice. Afterward, permeabilized cells were centrifuged for 4 min at 300xg, and the supernatant was removed. The cell pellet was then incubated in a blocking buffer supplemented with anti-cTnT or anti-ACTN2 for 1 hr at 4°C. After 1 hr, 500 µL blocking buffer was added, and cells were centrifuged for 4 min at 300xg. The supernatant was aspirated, and cells were washed with 500 µL blocking buffer before being spun down again. After this, cells were resuspended in 100 µL blocking buffer supplemented with Alexa Fluor 488 anti-rabbit or -mouse. Following a 30-min incubation at RT, cells were washed 2x with 500 µL blocking buffer, each followed by a centrifugation step for 4 min at 300xg. Finally, the supernatant was aspirated, the cells were resuspended in 1 mL PBS, and analyzed using FACSLyric 12 color (BD Biosciences, Drachten, the Netherlands).

Electrophysiology

hiPSC-CMs on coverslips were incubated with either Powerload and FluoVolt (1:1000, Thermo Fisher Scientific, California, USA) or Fluo-4-AM (1:1000, Thermo

Fisher Scientific, California, USA) in cardio culture medium for 20 min at 37°C. Next, the coverslips were placed in FluoroBrite (Thermo Fisher Scientific, California, USA), and kept at 37°C. Cell clusters were imaged using a custom-built microscope (Cairn Research, Kent, UK), and were paced with field stimulation at 1 Hz using an isolated stimulator (Hugo Sachs Stimulator CS). Fluorescent signals were recorded using a 10x water immersion objective (Olympus UMPlanFl 10x/0.30W). Dye excitation was done using an excitation filter of 482/35 nm. Fluorescent signals were captured through a long-pass emission filter (514 nm) by a high-speed camera (Andor Zyla 5.5CL3, Oxford Instruments, Abingdon, UK). Data analysis was performed in FIJI and a custom MATLAB script (DOI 10.17605/OSF.IO/86UFE).

RNA isolation and RT-qPCR

From T-REx HeLa cells, total RNA was extracted using the NucleoSpin RNA Plus kit (Macherey-Nagel, Dueren, Germany) per the manufacturer's protocol. From hiPSC-CMs, Trizol Reagent (Invitrogen, Bleiswijk, The Netherlands) was used according to the manufacturer's protocol. Next, 1 µg of isolated RNA was treated with DNase (Promega, Fitchburg, WI, USA) and reverse transcribed with Moloney Murine Leukemia Virus Reverse Transcriptase (Invitrogen, Bleiswijk, The Netherlands). Obtained samples were stored at -20°C until further use.

Gene expression was quantified using SYBR Green (Bio-Rad, California, USA) on a CFX96 Real-Time PCR Detection System (Bio-Rad, California, USA). The $2^{-\Delta\Delta Ct}$ method was used to calculate relative gene expression, normalized to the geometric mean of the housekeeping genes. For HeLa T-REx cells, the housekeeping genes used were *GAPDH* and *RPLP0*. Values are presented as fold changes against the control group. All primer sequences used are listed in Supplementary Table 1.

Bulk RNA-seq

RNA-Seq libraries were prepared from total RNA using the KAPA RNA HyperPrep Kit with RiboErase (KAPA Biosystems, Massachusetts, USA). Oligo hybridization, rRNA depletion, rRNA depletion cleanup, DNase digestion, DNase digestion cleanup, and RNA elution were performed according to the manufacturer's protocol. Next, fragmentation and priming were performed at 94 °C for 6 min. Synthesis of the first- and second-strands and A-tailing was performed according to the protocol. After that, the adaptor was ligated using NextFlex DNA barcodes (1.5 mM stock; Bio Scientific, Texas, USA), and the first and second post-ligation cleanup was performed according to the protocol. To amplify the library, 11 PCR cycles were performed, and the library was further cleaned up using a 0.8x followed by a 1.0x bead-based cleanup. The size of the library was determined using the High Sensitivity DNA

bioanalyzer kit, and the library concentration was measured using the dsDNA High Sensitivity Assay (DeNovix, Delaware, USA). Finally, paired-end sequencing reads of 50 bp was generated using an Illumina NextSeq 2000.

RNA-seq data analysis

RNA-Seq data were analyzed using the seq2science pipeline (https://vanheeringen-lab.github.io/seq2science/content/workflows/rna_seq.html). In short, reads were aligned to the human GRCh38.p14 reference genome. Next, reads were filtered using SAMtools (RRID: RRID: SCR_002105). Quality score < 20 and PCR duplicates were removed.[30] Reads per gene were counted with the htseq-count script from the Hisat2 software suite using the GTF file corresponding to the transcript assembly. Read counts were further analyzed with DESeq2 (RRID: SCR_002285).[31] Bulk RNA-Seq data will be deposited in the National Center for Biotechnology Information Gene Expression Omnibus (GEO) database (Accession No. not yet available).

Amino acids stimulation

Amino acids (AA) stimulation was performed 24 hr after tetracycline induction in T-REx HeLa cells. Homemade nutrient-rich (+AA) and starvation (-AA) media were made following the culture medium manufacturer's formulation (see the cell culture section for the media). The -AA medium was prepared by omitting the addition of any AA to the medium. To both +AA and -AA media, 1% (v/v) 100x MEM vitamin solution (Thermo Fisher Scientific, USA) was added. The media were then pH-adjusted with 2 M HCl, and sterile filtered through a 0.22 µm filter device. Before use, treatment media were supplemented with 10% (v/v) dialysed FBS (Thermo Fisher Scientific, USA) and 1 mM sodium pyruvate. Specifically to +AA medium, 4 mM L-glutamine (Thermo Fisher Scientific, USA) and 1% (v/v) MEM non-essential amino acids solution 100x (Capricon Scientific, Germany) were added. Prior to the addition of +AA or -AA medium, the cells were washed with PBS. Subsequently, the PBS was replaced with +AA or -AA medium for 1 hr and incubated at 37°C.

For hiPSC-CMs, homemade +AA and -AA media were prepared according to the RPMI 1640 with GlutaMAX™ Supplement with HEPES recipe without AA. Only to +AA medium, 50x RPMI 1640 Amino Acids Solution (Sigma-Aldrich, Missouri, USA) and 2 mM GlutaMAX™ (Sigma-Aldrich, Missouri, USA) were added. The media were then pH-adjusted with 2 M HCl, and sterile filtered through a 0.22 µm filter device. Before use, both +AA and -AA media were supplemented with 50x B-27 Supplement serum free. Prior to treatment media addition, hiPSC-CMs were rinsed once with HBSS. Afterward, HBSS was removed, and +AA or -AA medium was added to the cells and incubated for 1 hr at 37°C.

Immunoblotting

Cells were washed once in the wells with ice-cold PBS prior to lysis in Triton lysis buffer (50 mM Tris-HCl pH 7.5, 1 mM EGTA, 1 mM EDTA, 1% v/v Triton X-100, 10 mM Na-glycerophosphate, 50 mM NaF, 10 mM Na-pyrophosphate, 270 mM sucrose, and 150 mM NaCl) supplemented with phosphatase inhibitor (1 mM Na-orthovanadate) and protease inhibitors (1 mM PMSF, 1 µM aproptin, 0.01 mM leupeptin, 1.4 µM pepstatin) by scraping on ice. Next, samples were centrifuged at 4°C at 13.000 rpm for 10 minutes, and the supernatant was collected. The protein concentration was measured using the Pierce BCA protein assay kit (Thermo Scientific, California, USA) and 1 µg/µL protein samples were prepared in Laemmli + DTT loading buffer. Finally, samples were denatured at 95°C for 5 mins and stored at -20°C until use.

15 µg of proteins were loaded onto a 12% polyacrylamide gel and subjected to SDS-PAGE at 50 V for 30 min, followed by 100 V for 60 min. After SDS-PAGE, the proteins were transferred to polyvinylidene fluoride (PVDF) membranes at 100 V for 120 min. Following the transfer, similar protein loading was confirmed using Ponceau S staining (Thermo Fisher Scientific, California, USA). The membranes were then blocked for 1 hr in 5% (w/v) non-fat dry milk in Tris-buffered saline (TBS) containing 0.1% (v/v) Tween-20 (TBS-T; Sigma-Aldrich, Missouri, USA). After 1 hr, the membranes were incubated in primary antibody diluted in 1% (w/v) non-fat dry milk in TBS-T at 4°C. The following day, the membranes were washed three times in TBS-T for 10 min each and incubated with secondary antibody in 1% milk in TBS-T at room temperature for 1 hr. Afterward, the membranes were washed thrice in TBS-T and once in TBS for 10 min each. To visualize the protein of interest, membranes were incubated with SuperSignal West Pico Chemiluminescent Substrate (Thermo Fisher Scientific, California, USA) or SuperSignal West Femto Maximum Sensitivity Substrate (Thermo Fisher Scientific, California, USA) and then imaged using the ImageQuant™ LAS 4000 (General Electric Healthcare Life Sciences, Uppsala, Sweden).

Immunocytochemistry

Cells on coverslips were fixated with 4% (v/v) paraformaldehyde (Sigma-Aldrich, Missouri, USA) in PBS for 10 min at RT. Subsequently, the cells were permeabilized for 10 min with PBS containing 0.3% (v/v) Triton X-100 and 0.1% (w/v) bovine serum albumin. Next, the coverslips were incubated in 50 mM NH_4Cl in PBS for 10 min. Following 2x rinsing with PBS, the coverslips were blocked in goat serum dilution buffer (GSDB) containing 16% (v/v) goat serum and 0.3% Triton X-100 in PBS for 30 min. Subsequently, the coverslips were incubated in primary antibodies diluted in GSDB overnight at 4°C. The next day, the coverslips were washed 3x with PBS

for 10 min each and incubated with secondary antibodies diluted in GSDB for 45 min at RT. The samples were then washed 3x with PBS for 10 min each. During the second wash, DAPI was added to the PBS to a final concentration of 300 nM. Finally, samples were mounted with Fluoromont-G (Southern Biotech, Alabama, USA). Images were taken with an SP8 confocal microscope with a tunable pulsed white light laser (WLL) and a fixed 405 nm diode laser (Leica Microsystems, Amsterdam, the Netherlands). A 63x water-based objective (NA 1.20) was used. DAPI was excited with the 405 nm laser with 5% laser intensity and detected with a PMT detector (432-474 nm) with a 1000 volt gain. GFP was excited with the WLL at 488 nm with 25% laser intensity and detected with a HyD (493-560 nm) with a 50% gain. Alexa Fluor 594 was excited with the WLL at 594 nm with 3% laser intensity and detected with a HyD (600-668 nm) with a 10% gain. Appropriate notch filters were used to limit noise from reflection light.

To quantify TFEB nuclear translocation, automated scripts were created in ImageJ2 version 2.14.0. For T-REx HeLa cells, using the TFEB channel, TFEB-transfected cells were manually selected using the free-shape function. The DAPI channel was used to determine the location and outline of the nuclei. Next, a ratio of the TFEB signal in the nuclei over the total TFEB signal in cells per image was calculated, thus depicting the TFEB translocation to the nuclei. For hiPSC-CMs, z-stacks consisting of 5 to 7 z-plane images per stack were acquired. Next, a similar automated script was applied to calculate DAPI intensity, the TFEB signal in the nuclei, and in total cells, but without manually selecting cells as endogenous TFEB expression was analyzed. Afterward, within each stack, the z-plane image with the brightest DAPI signal (i.e., the middle plane of the nuclei) was selected and used for quantification. In each experiment, 10 images from 10 independent fields were obtained per condition. In the end, the average of the 10 images per genotype was calculated.

Statistics

All results are depicted as individual values and mean ± SEM. When there are only two experimental groups, a one- or two-tailed unpaired *t*-test was used. If more than two groups are being compared, one-way ANOVA followed by a post-hoc test was used. When there were more than two experimental groups with two variables, two-way ANOVA followed by a post-hoc test was used. The post-hoc test used in each experiment is indicated in each figure legend. Statistical significance was described at $p < 0.05$. All graphs and statistical tests were run in GraphPad Prism version 10.4.1 (532) for macOS (GraphPad Software, Boston, MA, USA).

Results

RRAGD p.(Ser76Leu) variant impairs mTORC1 signaling response to amino acids

To study the effect of the *RRAGD* p.(Ser76Leu) variant on amino-acid-induced mTORC1 signaling, T-REx HeLa cell lines overexpressing GFP (mock) or GFP-*RRAGD* WT or p.(Ser76Leu) were stimulated with amino acids for 1 hr. Upon stimulation (+AA), S6K phosphorylation was not significantly different between *RRAGD* WT and p.(Ser76Leu) cells (Figure 1A-B).

On the other hand, TFEB phosphorylation, when corrected to GAPDH, was significantly higher in *RRAGD* p.(Ser76Leu) cells compared to *RRAGD* WT cells (mean ± SEM; 1.48 ± 0.08 vs. 0.64 ± 0.19; Figure 1C). In amino acids deprived conditions (-AA), S6K and TFEB phosphorylation was significantly higher in *RRAGD* p.(Ser76Leu) cells compared to *RRAGD* WT cells (p-S6K: 0.50 ± 0.05 vs. 0.22 ± 0.03; p-TFEB/GAPDH: 1.25 ± 0.14 vs. 0.36 ± 0.08; p-TFEB/TFEB: 1.47 ± 0.22 vs. 0.62 ± 0.16; Figure 1B-D). Of note, overexpression of *RRAGD* p.(Ser76Leu) resulted in significantly higher TFEB expression than mock and WT cells (Figure 1E). Endogenous TFEB mRNA expression, however, was not different between all three cell lines (Figure 1F). To examine the effects of *RRAGD* p.(Ser76Leu) on nuclear translocation of TFEB, cells were stained for TFEB after exposure to +AA or -AA conditions for 1 hr. *RRAGD* p.(Ser76Leu) cells had a significantly lower relative nuclear TFEB signal compared to *RRAGD* WT cells under -AA conditions (0.11 ± 0.02 vs. 0.27 ± 0.03; Figure 1G-H).

To assess whether the constant phosphorylation of S6K, 4E-BP1, and TFEB depends on mTORC1 activity, the cells were treated with the pharmacological mTORC1 inhibitors Torin1 (Figure 2) and rapamycin (Supplementary Figure 1). In line with S6K phosphorylation (Figure 1A-B), 4E-BP1 phosphorylation seemed to persist in -AA + DMSO conditions in *RRAGD* p.(Ser76Leu) cells, unlike in mock and *RRAGD* WT cells (Figure 2A). Inhibition of mTOR by Torin1 diminished S6K and 4E-BP1 phosphorylation, and significantly lowered TFEB phosphorylation in both +AA and -AA conditions in p.(Ser76Leu) cells compared to DMSO treatment (Torin1 vs. DMSO; +AA p-TFEB/GAPDH: 0.01 ± 0.01 vs. 1.01 ± 0.14; +AA p-TFEB/TFEB: 0.34 ± 0.03 vs. 1.09 ± 0.01; -AA p-TFEB/GAPDH: 0.01 ± 0.02 vs. 0.9 ± 0.21; -AA p-TFEB/TFEB: 0.31 ± 0.30 vs. 1.24 ± 0.30; Figure 2A-C). Moreover, immunofluorescence on TFEB indicated that Torin1 treatment significantly increased the nuclear re-localization of TFEB compared to DMSO treatment under both +AA and -AA conditions in *RRAGD* p.(Ser76Leu) cells that were transiently transfected with TFEB (Torin1 vs. DMSO; +AA 0.78 ± 0.06 vs. 0.08 ± 0.01; -AA 0.74 ± 0.04 vs. 0.19 ± 0.05; Figure 2D & E). Inhibition

of mTORC1 signaling by rapamycin abolished the phosphorylation of S6K and 4E-BP1 but did not affect phosphorylated TFEB (Supplementary Figure 1A-C).

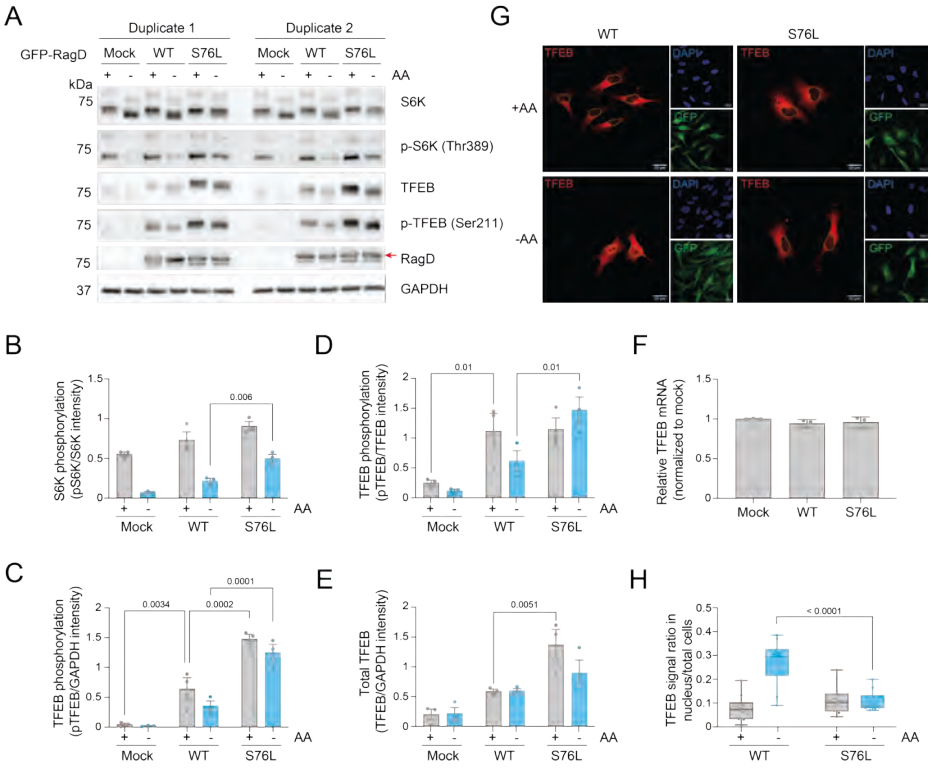

Figure 1. *RRAGD* p.(Ser76Leu) variant constitutively activate mTORC1 in T-REx HeLa cells. (A-E) T-REx HeLa cells stably overexpressing GFP (mock), GFP-*RRAGD* WT (WT), and GFP-*RRAGD* p.(Ser76Leu) (S76L) were exposed amino acids-containing medium (+AA, grey bars) or amino acids-deprived medium (-AA, blue bars) for one hr. (A) Representative immunoblots of S6K, p-S6K, TFEB, p-TFEB, GFP, and GAPDH after amino acids stimulation. (B-E) Quantification of (B) phosphorylated S6K, (C) phosphorylated TFEB corrected to GAPDH, (D) phosphorylated TFEB corrected to total TFEB, and (E) total TFEB expression (mean ± SEM from 3 independent experiments). (F) mRNA levels of TFEB in mock, *RRAGD*-WT, and *RRAGD*-p.(Ser76Leu) T-REx HeLa cell lines. (G, H) mock, *RRAGD*-WT, and *RRAGD*-p.(Ser76Leu) T-REx HeLa cell lines transiently transfected with TFEB and exposed to 1 hr amino acids stimulation. (F) Representative images of TFEB staining (red), GFP-RagD (green), and DAPI (blue). The nuclei of cells that were transfected with TFEB are outlined in yellow. (H) quantification of TFEB signal in the nucleus/in the total cells. (F) Scale bars indicate 20 µm. (H) Boxes indicate the 25th to 75th quartile; middle lines indicate the median, and whiskers extend from maximum to minimum 1 independent experiment with images from 10 independent fields per condition. For statistical analyses, the following tests were done. (B-E) Two-way ANOVA comparison between mock or p.(Ser76Leu) cells and WT cells within treatment (i.e., +AA and -AA), followed by Dunnett's test. (G) One-way ANOVA and Tukey's test. (H) Two-way ANOVA, where the effects of genotypes within each treatment were compared, followed by Sidak's test.

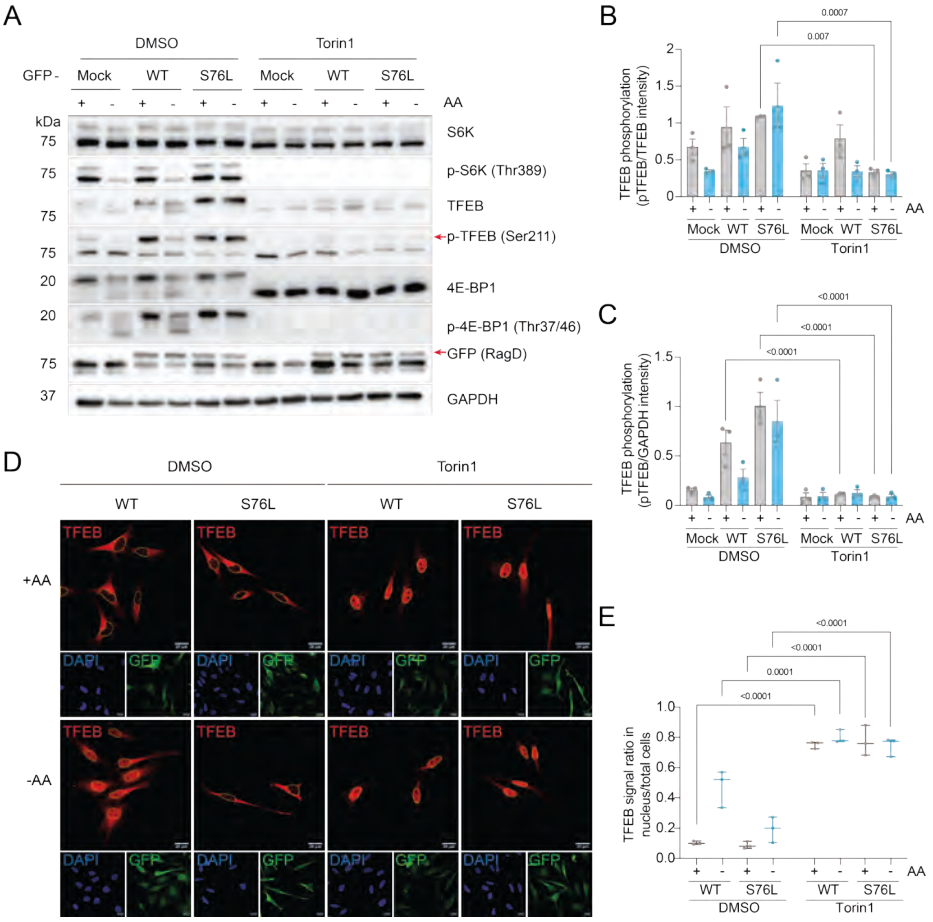

Figure 2. mTOR inhibition by Torin1 restored mTORC1 signaling *RRAGD* p.(Ser76Leu) T-REx HeLa cells. (A-E) T-REx HeLa cells stably overexpressing GFP (mock), GFP-*RRAGD* WT (WT), and GFP-*RRAGD* p.(Ser76Leu) (S76L) were exposed to amino acids stimulation using amino acids-containing medium (+AA, grey bars) or amino acids-deprived medium (-AA, blue bars) and 250 nm Torin1 or 0.01% DMSO for 1 hr. (A) Representative immunoblots of S6K, p-S6K, TFEB, p-TFEB, 4E-BP1, p-4E-BP1, GFP, and GAPDH following treatment mentioned above. (B, C) Quantification of (B) TFEB phosphorylation corrected to total TFEB and (C) TFEB phosphorylation corrected to GAPDH (mean ± SEM from 3 independent experiments). (D-E) Mock, *RRAGD*-WT, and *RRAGD*-p.(Ser76Leu) T-REx HeLa cell lines transiently transfected with TFEB and exposed to 1 hr amino acids stimulation and 250 nM Torin1 or 0.01% DMSO. (F) Representative immunofluorescence images of TFEB staining (red), GFP-RagD (green), and DAPI (blue). TFEB-positive nuclei are outlined in yellow. Scale bars indicate 20 µm. (H) Quantification of TFEB signal in the nucleus/in the total cells. Vertical lines indicate the 25th to 75th quartile, horizontal lines indicate the median, and whiskers extend from maximum to minimum from 3 independent experiments with images from 10 independent fields per condition. For statistical analyses, Two-way ANOVA was performed in which a comparison between DMSO and Torin1 treatment within the genotypes and +AA or -AA was made, followed by Sidak's test.

Generation of *RRAGD*$^{WT/p.Ser76Leu}$ induced-pluripotent stem cell-derived cardiomyocytes

To validate the effects of the *RRAGD* p.(Ser76Leu) variant in a more physiologically relevant model, we generated a human induced pluripotent stem cell (hiPSC) model with an endogenous heterozygous expression of the *RRAGD* p.(Ser76Leu) variant (hereafter referred to as *RRAGD*$^{WT/p.(Ser76Leu)}$), mediated by the CRISPR-Cas9 system (Figure 3A, Supplementary Figure 2A). *RRAGD*$^{WT/WT}$ hiPSCs are isogenic controls of *RRAGD*$^{WT/p.(Ser76Leu)}$ hiPSCs, obtained from a clone that also underwent the CRISPR-Cas9 gene editing, but no mutation was introduced. Characterization of the hiPSCs indicated that cell growth of *RRAGD*$^{WT/p.Ser76Leu}$ and *RRAGD*$^{WT/WT}$ hiPSCs were not significantly different (Figure 3B). Furthermore, Sanger sequencing of the top three predicted off-targets revealed no mistargeting by the sgRNA following CRISPR-Cas9 gene editing (Supplementary Figure 2B). Additional quality controls through immunofluorescence confirmed that both *RRAGD*$^{WT/p.Ser76Leu}$ and *RRAGD*$^{WT/WT}$ hiPSCs remain pluripotent, as evidenced by the positive nuclear staining of pluripotent markers SOX-2, OCT3/4, and NANOG (Supplementary Figure 2C & D). Finally, karyo-sequencing of these hiPSC clones demonstrated a normal chromosome copy number (Supplementary Figure 2E & F).

Next, these hiPSCs were differentiated into cardiomyocytes (hiPSC-CMs) (Figure 3C). To determine whether the p.(Ser76Leu) variant affects RagD subcellular localization, we performed immunofluorescence, which showed that in both *RRAGD*$^{WT/p.Ser76Leu}$ and *RRAGD*$^{WT/WT}$ hiPSC-CMs, RagD predominantly localized in the cytoplasm but was also found in the nucleus (Figure 3D). We then employed electrophysiological assays (*i.e.,* Ca^{2+} transient and action potential measurements) to functionally characterize *RRAGD*$^{WT/p.Ser76Leu}$ hiPSC-CMs. Our findings indicated that in Ca^{2+} transient measurements (Figure 3E), Ca^{2+} transient duration (CTD_{90}) was significantly prolonged in *RRAGD*$^{WT/p.Ser76Leu}$ hiPSC-CMs compared to *RRAGD*$^{WT/WT}$ hiPSC-CMs (mean ± SEM *RRAGD*$^{WT/p.Ser76Leu}$ vs. *RRAGD*$^{WT/WT}$ hiPSC-CMs; CTD_{90}: 782 ± 9.1 ms vs. 717.3 ± 20.5 ms; Figure 3F). Relative Ca^{2+} amplitude was similar between the two cell lines (Figure 3G). The action potential duration (APD; Figure 3H), as measured by the APD_{50} and APD_{90}, was not significantly different between *RRAGD*$^{WT/p.Ser76Leu}$ and *RRAGD*$^{WT/WT}$ hiPSC-CMs (Figure 3I & J).

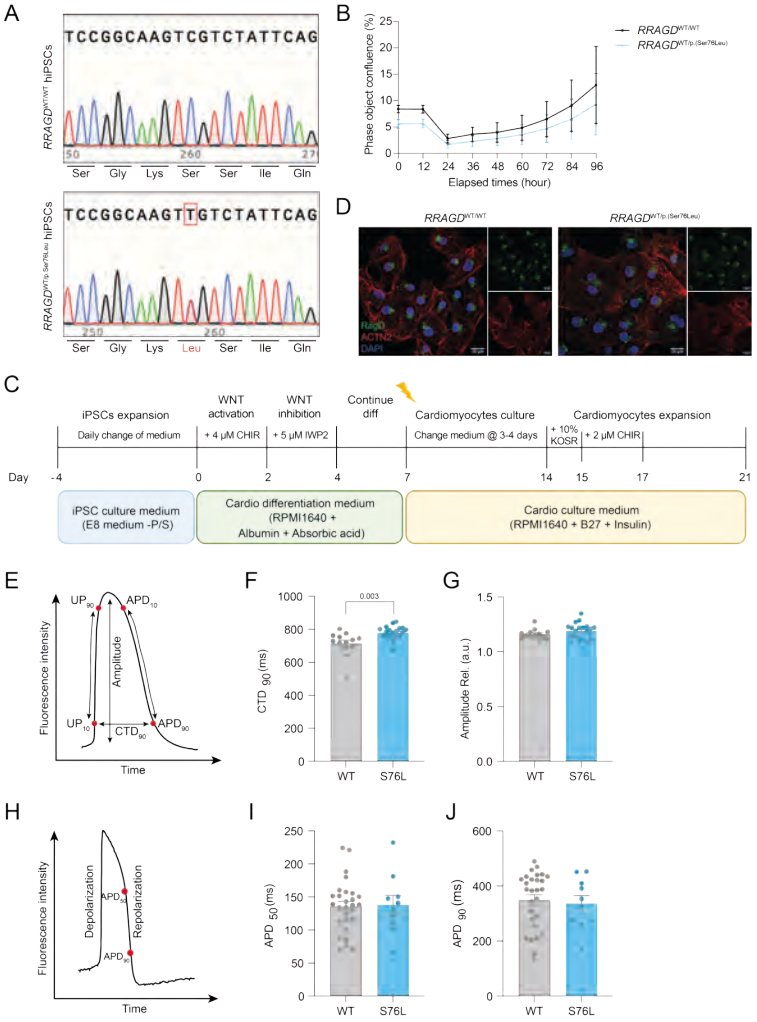

Figure 3. Generation of *RRAGD*$^{WT/p.(Ser76Leu)}$ human induced pluripotent stem cell-derived cardiomyocytes (hiPSC-CMs). (A) Sequencing results of *RRAGD*$^{WT/WT}$ (top) and *RRAGD*$^{WT/p.(Ser76Leu)}$ (bottom) hiPSCs clones. The red box highlights *RRAGD* c.227C>T (p.(Ser76Leu) mutation. (B) Representative growth curve of *RRAGD*$^{WT/WT}$ (black line) and *RRAGD*$^{WT/p.(Ser76Leu)}$ (blue line) hiPSCs (mean ± SD). (C) hiPSC-CMs differentiation scheme. (D) Representative immunofluorescence image of *RRAGD*$^{WT/WT}$ *RRAGD*$^{WT/p.(Ser76Leu)}$ hiPSC-CMs stained with RagD (green), sarcomere ACTN2 (red), and DAPI (blue). Scale bars = 20 µm. (E-J) Electrophysiological assays of *RRAGD*$^{WT/WT}$ (grey bar) and *RRAGD*$^{WT/p.(Ser76Leu)}$ (blue bar) hiPSC-CMs. (E) Illustration of Ca^{2+} transient assay parameters depicting the amplitude, 10% and 90% upstroke (UP) and downstroke (APD), and the 90% Ca^{2+} transient duration (CTD). (F) CTD_{90} represents the total duration of the Ca^{2+} transient. (G) Relative amplitude represents the amount of Ca^{2+} in the initial release. Data are mean ± SEM from 13-20 cell clusters from 1 differentiation round. (H) Illustration of action potential parameters depicting 50% and 90% of the downstroke of the fluorescence intensity, also known as action potential duration (APD). (G) 50% and (H) 90% of APD (APD 50 and 90, respectively). Data are mean ± SEM from 10-28 cell clusters from 1 differentiation round. (F, G, I, and J) Two-tailed unpaired T-test statistical test was performed. (E and H) Adapted from van Ham et al.[32]

Heterozygous *RRAGD* p.(Ser76Leu) expression does not affect mTORC1 signalling in 2D-cultured hiPSC-CMs

To validate our findings in HeLa cells in 2D-cultured cardiomyocytes, *RRAGD*$^{WT/p.(Ser76Leu)}$ and *RRAGD*$^{WT/WT}$ hiPSC-CMs were exposed to 1 hr of amino acid starvation, followed by 30 min of re-supplementation (i.e., -/+AA). Immunoblotting showed that phosphorylation of S6K, 4E-BP1, and TFEB was not statistically different in *RRAGD*$^{WT/p.(Ser76Leu)}$ and *RRAGD*$^{WT/WT}$ hiPSC-CMs, also under -/+AA conditions (**Figure 4A-C**). Accordingly, TFEB subcellular localization was not statistically different in *RRAGD*$^{WT/p.(Ser76Leu)}$ than that in *RRAGD*$^{WT/WT}$ hiPSC-CMs (**Figure 4D-E**).

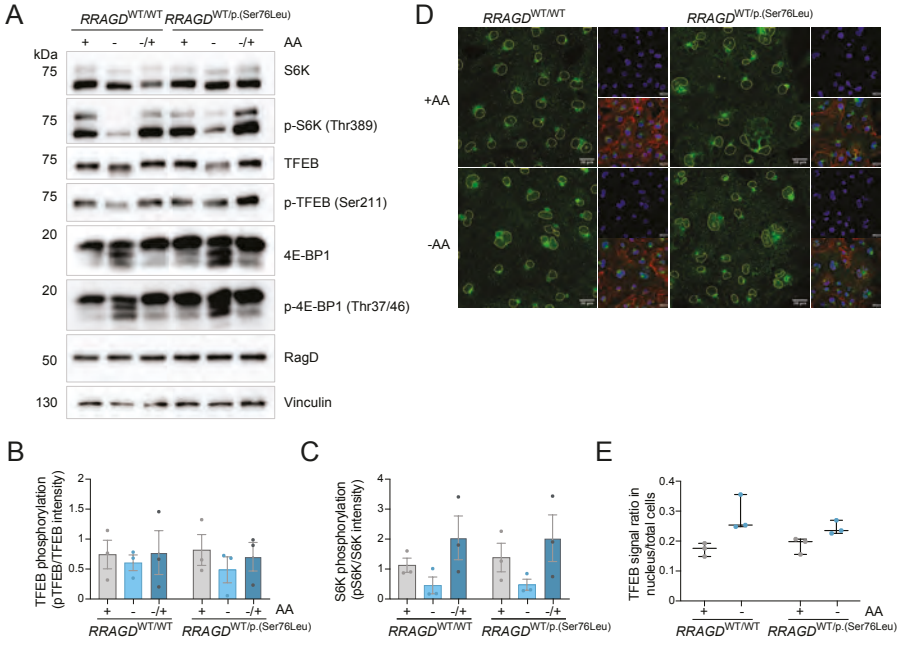

Figure 4. Heterozygous *RRAGD* p.(Ser76Leu) variant did not alter mTORC1 signaling in 2D-cultured hiPSC-CMs. (A-E) *RRAGD*$^{WT/WT}$ and *RRAGD*$^{WT/p.(Ser76Leu)}$ hiPSC-CMs were exposed to amino acids stimulation, which are culture medium containing amino acids (+AA), deprived from amino acids (-AA) for 1 hr, or -AA for 1 hr followed by re-supplementation of +AA medium (-/+AA) for 0.5 hr. (A) Immunoblots of S6K, p-S6K, TFEB, p-TFEB, 4E-BP1, p-4E-BP1, RagD, and vinculin. (B-C) Quantification of (B) phosphorylated TFEB and (C) S6K (mean ± SEM from 3 independent hiPSC-CMs differentiations). Grey bars = +AA, light blue bars = -AA, dark blue bars = -/+AA. (D) Representative immunofluorescence image of *RRAGD*$^{WT/WT}$ and *RRAGD*$^{WT/p.(Ser76Leu)}$ hiPSC-CMs exposed to 1 hr of +AA or -AA and stained for TFEB (green), sarcomeric ACTN2 (red), and DAPI (blue). On the TFEB images, the quantified nuclei area is outlined in yellow. Scale bars = 20 µm. (E) Quantification of TFEB signal ratio in the nucleus over TFEB in total cells. Vertical lines span from the minimum to the maximum point, and horizontal lines depict the median. Grey = *RRAGD*$^{WT/WT}$ hiPSC-CMs and blue = *RRAGD*$^{WT/p.(Ser76Leu)}$ hiPSC-CMs. (B-E) The statistical test used was two-way ANOVA followed by Sidak's multiple comparison test, comparing the effects of genotypes within the treatment group (i.e., +AA, -AA, or -/+AA).

Bulk RNA-seq revealed enriched pathways in *RRAGD*$^{WT/p.(Ser76Leu)}$ hiPSC-CMs

To obtain a more complete overview of the cellular consequences of *RRAGD* p.(Ser76Leu) variant in hiPSC-CMs, bulk RNA-seq was performed (Figure 5A). In *RRAGD*$^{WT/p.(Ser76Leu)}$ hiPSC-CMs, 172 genes were differentially expressed (Supplementary Table 2). Of these 172 genes, 48 were downregulated, and 124 were upregulated compared to *RRAGD*$^{WT/WT}$ hiPSC-CMs (adjusted p-value < 0.1; Figure 5B). Among these differentially expressed genes (DEGs), 39 genes overlapped with a published RNA-seq dataset from the ventricles of DCM patients,[33] which includes key genes (log2 fold change; log2fc to *RRAGD*$^{WT/WT}$) such as *ALPK3* (-2.64), *BMP4* (1.43), *MYL3* (-0.91), *MYO1D* (0.78), and *NPPA* (-0.83) (Figure 5C, Supplementary Table 3).

> Figure 5. Gene expression profile of 2D-cultured *RRAGD*$^{WT/p.(Ser76Leu)}$ hiPSC-CMs with bulk RNA-seq. (A) Principal component analysis plot showing the clustering of samples based on genotypes *RRAGD*$^{WT/WT}$ (WT; grey) and *RRAGD*$^{WT/p.(Ser76Leu)}$ (S76L; blue) hiPSC-CMs. Samples are from 4 differentiations. (B) Volcano plot of differentially expressed genes (DEGs; adjusted (adj.) p < 0.1) in *RRAGD*$^{WT/p.(Ser76Leu)}$ hiPSC-CMs from *RRAGD*$^{WT/WT}$ hiPSC-CMs. In total, 172 genes comprising 124 upregulated (red) and 48 downregulated (turquoise) are differentially expressed in *RRAGD*$^{WT/p.(Ser76Leu)}$ hiPSC-CMs. Grey dots indicate insignificant DEGs (adj. p > 0.1), and black dots indicate fold change of genes > -0.5 and < 0.5. Triangles indicate genes with $-\log_{10}$ p-value > 10. Grey dotted lines indicate the cut-off marks. Genes labeled are significant DEGs overlapping with a previously published RNA-seq dataset of genes specific to DCM patients (see Supplementary Table 3).[33] (C) In the Venn diagram of 172 DEGs with DCM-specific genes in Sweet et al. [33], 39 genes overlapped. (D-E) Bubble plots showing enriched pathways in *RRAGD*$^{WT/p.(Ser76Leu)}$ hiPSC-CMs. (D) Top enriched biological function gene ontology (GO) pathways based on false discovery rate (FDR). Filtered for pathways relevant in cardiomyocytes. (E) Enriched Kyoto Encyclopedia of Genes and Genomes (KEGG) pathways. The intensity of the bubble color is based on -log10FDR; red shows upregulated pathways, and blue shows downregulated pathways. The bubble size indicates the number of DEGs in each pathway (count). (F-H) Box plots of DEGs in (F) muscle developmental pathways, (G) Hippo pathway, and (H) PI3K-Akt pathway, displaying the log transcripts per million (TPM) of the genes in *RRAGD*$^{WT/WT}$ (WT; grey) and *RRAGD*$^{WT/p.(Ser76Leu)}$ (S76L; blue) hiPSC-CMs samples. The boxes indicate the 1st to 3rd quartile, the middle lines indicate the median, whiskers extend from 1st to 3rd quartile, and black dots indicate the outlier.

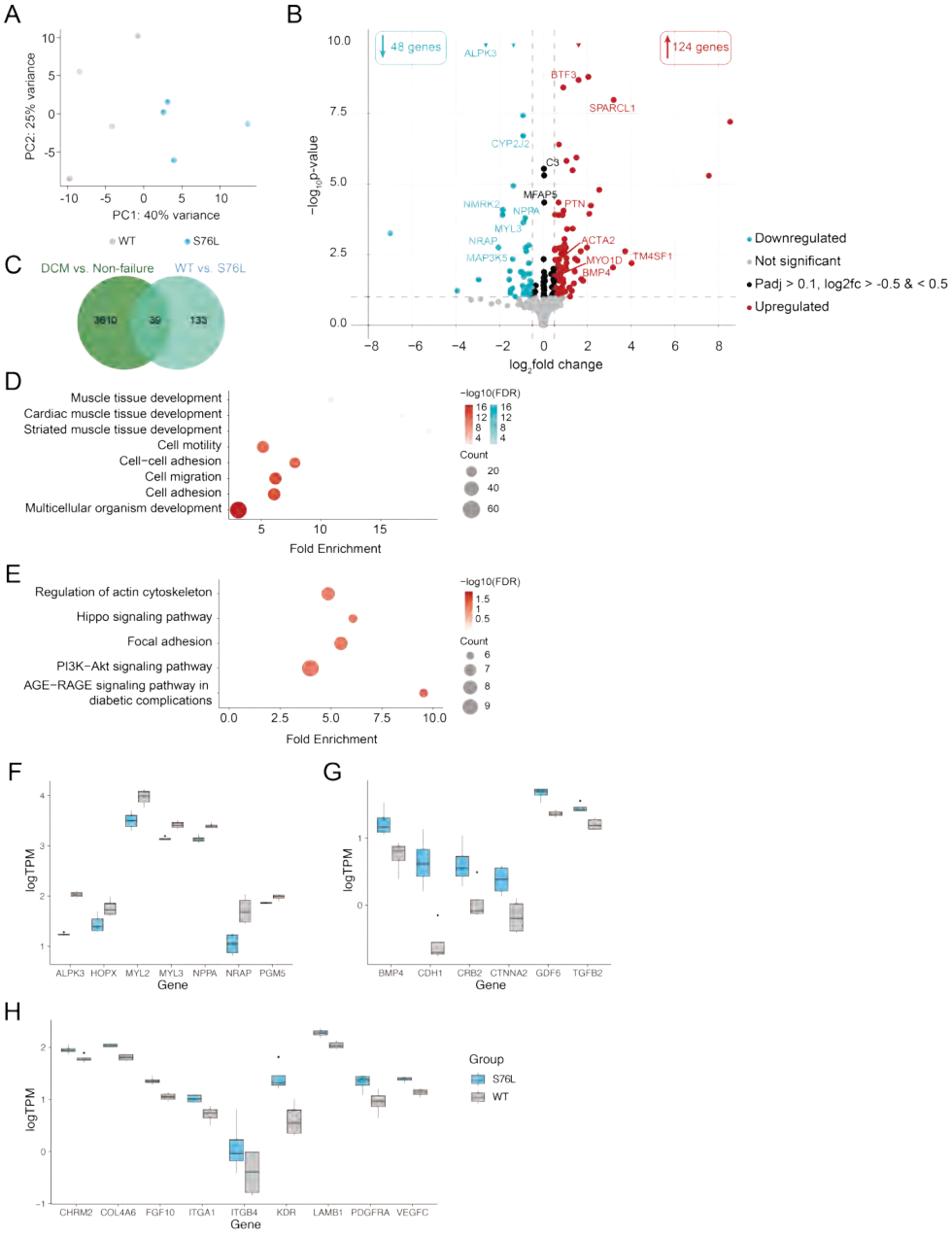
A
PC2: 25% variance
PC1: 40% variance
WT
S76L
B
48 genes
124 genes
ALPK3
BTF3
SPARCL1
CYP2J2
C3
MFAP5
PTN
NMRK2
NPPA
MYL3
NRAP
ACTA2
MAP3K5
MYO1D
TM4SF1
BMP4
−log10 p-value
log2fold change
Downregulated
Not significant
Padj > 0.1, log2fc > -0.5 & < 0.5
Upregulated
C
DCM vs. Non-failure
WT vs. S76L
3610
39
133
D
Muscle tissue development
Cardiac muscle tissue development
Striated muscle tissue development
Cell motility
Cell−cell adhesion
Cell migration
Cell adhesion
Multicellular organism development
Fold Enrichment
−log10(FDR)
Count
E
Regulation of actin cytoskeleton
Hippo signaling pathway
Focal adhesion
PI3K−Akt signaling pathway
AGE−RAGE signaling pathway in diabetic complications
Fold Enrichment
−log10(FDR)
Count
F
logTPM
ALPK3 HOPX MYL2 MYL3 NPPA NRAP PGM5
Gene
G
logTPM
BMP4 CDH1 CRB2 CTNNA2 GDF6 TGFB2
Gene
H
logTPM
CHRM2 COL4A6 FGF10 ITGA1 ITGB4 KDR LAMB1 PDGFRA VEGFC
Gene
Group
S76L
WT

Afterwards, pathway analysis was conducted to investigate the functions of the DEGs. Gene ontology (GO) enrichment analysis indicated that pathways related to muscle tissue development were downregulated, while those linked to cell adhesion and extracellular matrix organization were upregulated in *RRAGD*$^{WT/p.(Ser76Leu)}$ hiPSC-CMs (Figure 5D, Supplementary Figure 3A-C). Further examination using the Kyoto Encyclopedia of Genes and Genomes (KEGG) pathway revealed that pathways such as focal adhesion, actin cytoskeleton regulation, Hippo signaling, and PI3K-Akt signaling were upregulated in *RRAGD*$^{WT/p.(Ser76Leu)}$ hiPSC-CMs (Figure 5E). Upon closer inspection, genes specific to DCM patients,[33] including *ALPK3, NPPA, MYL2,* and *MYL3,* were identified within the muscle tissue development pathways (Figure 5F). Furthermore, genes such as *CTNNA2*, *COL4A6*, *ITGA1*, *ITGB4*, and *LAMB1* were present in the upregulated pathways, including cell adhesion, Hippo signaling, and PI3K-Akt signaling (Figure 5G, H). No mTOR or TFEB-related pathways or genes were among the significant DEGs in *RRAGD*$^{WT/p.(Ser76Leu)}$ hiPSC-CMs when compared to *RRAGD*$^{WT/WT}$ hiPSC-CMs.

Because Hippo and PI3K-Akt signaling activities were upregulated in *RRAGD*$^{WT/p.(Ser76Leu)}$ hiPSC-CMs, we examined the phosphorylation of TAZ and Akt as a measure of pathway activation through immunoblotting (Supplementary Figure 4A). We showed that Akt phosphorylation at the Thr-308 site was significantly lowered in *RRAGD*$^{WT/p.(Ser76Leu)}$ hiPSC-CMs while TAZ phosphorylation at the Ser-89 site was unchanged (*RRAGD*$^{WT/p.(Ser76Leu)}$ vs. *RRAGD*$^{WT/WT}$; p-Akt: 0.58 ± 0.02 vs. 0.79 ± 0.06; Supplementary Figure 4B and C).

Discussion

Pathogenic variants in *RRAGD* cause DCM. Here, we demonstrate that the cardiomyocytes carrying the *RRAGD* p.(Ser76Leu) variant display signs of dedifferentiation and malfunction. These conclusions are based on electrophysiological analysis demonstrating a longer Ca^{2+} transient duration, downregulation of pathways related to muscle development, and upregulation of pathways linked to actin cytoskeleton, extracellular matrix organization, and cell-cell adhesion. We propose that these changes can be attributed to increased canonical and non-canonical mTORC1 signaling. Taken together, these results provide evidence for cardiomyocyte dysfunction in ADKH-*RRAGD*.

DCM is a genetically and phenotypically heterogeneous disease with over 50 known causative genes. The mechanisms leading to the manifestation of DCM also

differ widely depending on the underlying genetic cause. For example, the most common cause of DCM is genetic variations in genes encoding the sarcomeric components such as titin, myosin, and troponin lead to cardiomyocyte-impaired force generation, while variants in genes encoding desmosomal proteins, which are responsible for cell-cell adhesion, are also found in a DCM cohort.[34,35] Additionally, variants in genes that lead to cytoskeleton disorganization, Ca^{2+} cycling abnormalities, and ion channel dysfunctions have also been associated with DCM.[34] The diversity highlights the need for a thorough understanding of each DCM form and, ultimately, a precision medicine approach to manage it. To understand how *RRAGD* p.(Ser76Leu) variant influences cardiomyocyte gene expression, we utilized bulk RNA-seq. Among the DEGs, genes associated with muscle development pathways were downregulated, while genes involved in actin cytoskeleton, extracellular matrix, and cell-cell adhesion pathways were upregulated in *RRAGD*$^{WT/p.Ser76Leu}$ hiPSC-CMs. Previous transcriptomic studies with DCM subjects have identified dysregulated mitochondria, cell adhesion, cytoskeleton, and extracellular matrix components.[33,36]

Interestingly, our electrophysiological assay showed the Ca^{2+} transient duration in *RRAGD*$^{WT/p.Ser76Leu}$ hiPSC-CMs were significantly longer than those in *RRAGD*$^{WT/WT}$ hiPSC-CMs, suggesting impaired Ca^{2+} handling in mutant cardiomyocytes. Of note, this Ca^{2+} transient measurement was performed on 1 batch of differentiation and warrants to be repeated in the future. In previous DCM models, TAB2 deficiency in hiPSC-CMs caused an increased time to peak (representing the time of calcium release into the cytosol) and prolonged Ca^{2+} transient duration (representing the time to release and remove calcium from the cytosol), while p.(Arg173Trp) variant in *TNNT2* gene in patient-specific hiPSC-CMs caused smaller Ca^{2+} amplitude without a change in timing. [37,38] In both studies, reduced contractility was observed.[37,38] We did not investigate if the cardiomyocyte contractility was compromised in our cells. Nevertheless, due to the changes in the expression of genes related to cytoskeleton organization, muscle development, and impaired Ca^{2+} handling, we hypothesize the *RRAGD* p.(Ser76Leu) variant is causing the cardiomyocytes to undergo either remodeling or dedifferentiation to less muscle-like cells.

To uncover the consequences of the *RRAGD* p.(Ser76Leu) variant on mTORC1 signaling, we used HeLa cell lines that stably overexpress *RRAGD* WT or p.(Ser76Leu) and demonstrated that both canonical and non-canonical mTORC1 responses to amino acid signaling are impaired in the mutant cell line. These results confirm that the *RRAGD* p.(Ser76Leu) variant diminishes the mTORC1 response to amino acid starvation, leading to its constitutive activation.[1,2] Furthermore, we showed

that this entire process relies on mTOR, as inhibiting mTOR with Torin1 completely reduced the phosphorylation levels of S6K, 4E-BP1, and TFEB and resulted in TFEB nuclear localization. Interestingly, we also observed higher total TFEB expression in *RRAGD* WT and p.(Ser76Leu) cells than in mock cells, as did Sambri *et al*.[2] In our currennt study, we showed that this increase was not due to changes in TFEB mRNA levels and suggested an increased protein expression. Indeed, this could be due to increased TFEB interactions with 14-3-3 protein, which was previously observed when ADKH-*RRAGD* variants are expressed in cells.[2] TFEB phosphorylation at the Ser-211 site increases TFEB interaction with 14-3-3 protein, thus preventing its nuclear translocation.[16]

Our findings in *RRAGD*$^{WT/p.(Ser76Leu)}$ hiPSC-CMs showed normal mTORC1 signaling to amino acids stimulation, which included normal TFEB phosphorylation and subcellular localization. In line with these data, no genes involved in mTOR, lysosomal biogenesis, autophagy, or mitochondrial pathways were enriched in our *RRAGD*$^{WT/p.Ser76Leu}$ cardiomyocytes based on the bulk RNA-seq results. Interestingly, the same *RRAGD* variant had previously been shown to impair TFEB's response to pharmacologically induced lysosomal damage in hiPSC-CMs.[2] Moreover, *RRAGC* variants have been associated with DCM in patients; at the cellular level, TFEB dysfunctions were reported.[23,24] The normal mTORC1 signaling response to amino acid removal in our mutant cardiomyocyte model is, however, as expected, given the immature nature of 2D-cultured hiPSC-CMs.[39] During development, the level of mTORC1 activation in cardiomyocytes changes, with its activity being high during fetal stages and low after birth.[40-42] This might be due to the role of mTORC1 signaling in supporting cell proliferation and regeneration, and postnatally, it is known that cardiomyocytes have limited capacity to proliferate and regenerate.[20,43-45] Considering that 2D-cultured hiPSC-CMs are early embryonic-like and our findings suggest a dedifferentiating phenotype in the mutant cardiomyocytes, we hypothesized that the *RRAGD* variants maintain cardiomyocytes in an immature state, and this causes cardiac dysfunction after birth in our ADKH-*RRAGD* patients. Indeed, 80% of ADKH-*RRAGD* patients with the p.(Ser76Leu) variant who developed DCM exhibited symptoms between the ages of 3 and 32, when cardiomyocytes are generally considered mature.[1,3] Although it is not known if cardiac dysfunction already manifests during prenatal development, our results indicate that cardiomyocyte maturity is an important factor to consider for future research.

In ADKH-*RRAGD*, mTOR inhibition has been proposed as a potential therapy.[1,25] However, the specificity and efficacy of mTOR inhibition in managing this disease remain the primary concern in prescribing this drug to patients.[46,47] Indeed, while

we have previously demonstrated that rapamycin treatment improved cardiac function in zebrafish embryos overexpressing *RRAGD,* we could not confirm if mTORC1 overactivation was present.[25] Regardless, the critical function of mTOR in DCM progression has been demonstrated in mice as cardiomyocyte-specific inducible deletion of *Mtor* or *Raptor* induced DCM and reduced mortality. [20,21,48,49] Lower phosphorylation of 4E-BP1 and S6K, increased autophagy, and increased apoptosis were thought to be causative of the compromised cardiac functions in these models. [20,21,48,49] In mouse models with preexisting DCM, pharmacological inhibition of mTORC1 improved cardiac function.[50,51] However, this could mean that mTOR inhibition can improve DCM symptoms even in cases where mTOR dysregulation is not observed, suggesting symptomatic relief rather than targeting the cause. Previously, rapamycin treatment has been shown to benefit a DCM patient with severe heart failure due to reduced ejection fraction carrying *LMNA* p.(Glu161Lys) variant.[52] In the patient's cardiac biopsies, a higher mTOR phosphorylation compared to a healthy control was observed.[52] Six months of rapamycin treatment improved ejection fraction and the New York Heart Association (NYHA) functional classification from class IV to class II in this patient.[52] In this case, using rapamycin as a last resort was justified within the framework of personalized medicine.[52] Therefore, for ADKH-*RRAGD* patients, it is essential to first elucidate the molecular etiology of the disease to determine whether constitutive mTORC1 activation is the primary pathogenic driver before evaluating the potential benefits of mTOR inhibition.

This study has several strengths and limitations. We are the first to generate an ADKH-*RRAGD* hiPSC-CMs model. In these cardiomyocytes, bulk RNA-seq and Ca^{2+} transient assay results suggested that the 2D-cultured *RRAGD*$^{WT/p.(Ser76Leu)}$ hiPSC-CMs were less differentiated than *RRAGD*$^{WT/WT}$hiPSC-CMs. In cardiomyocytes, dedifferentiation signifies a cellular event where cardiomyocytes revert to a less differentiated state accompanied by cytoskeletal and contractile apparatus reorganization, the re-expression of fetal genes, and changes in energy metabolism.[53,54] Therefore, future studies should aim to evaluate if *RRAGD*$^{WT/p.(Ser76Leu)}$ hiPSC-CMs are dedifferentiated, for example, by measuring the proliferating population and confirming if the changes in cytoskeleton gene expression are followed by cytoskeletal reorganization in these cardiomyocytes. An important limitation of our experiments is the immaturity of the hiPSC-derived cardiomyocyte model, a well-known issue in the field.[55,56] To address this, future investigations should focus on enhancing the maturity of *RRAGD*$^{WT/p.Ser76Leu}$ hiPSC-CMs, for instance, by utilizing 3D cultures such as engineered heart tissue (EHT), cardiac microtissues, or organoids, which more accurately mimic adult *in vivo* cardiomyocytes

(reviewed in [57]). Advancing the maturation of hiPSC-CMs through 3D cultures will be a valuable next step for investigating the molecular mechanisms underlying ADKH-*RRAGD* and how variants in this gene contribute to DCM development in patients. Alternatively, cultured human myocardial slices are a fully mature model that can be very useful, although studying the effects of variants requires either successful genetic modification of the slices, or the availability of patient tissue obtained during cardiac surgeries such as heart transplantion or LVAD implantation.

In conclusion, this study demonstrated that the *RRAGD* p.(Ser76Leu) variant, the most prevalent ADKH-*RRAGD* variant identified to date, induces constitutive mTORC1 activity resulting in dysregulation of both non-canonical and canonical targets. Bulk RNA-seq and Ca^{2+} transient measurement indicate less differentiated cardiomyocyte due to this variant, hinting at early cardiac dysfunction in ADKH-*RRAGD* patients. Future studies should examine how *RRAGD* variants affect mTORC1 signaling and cellular processes in animal models or patient biopsies to further confirm the molecular mechanisms underlying DCM in ADKH-*RRAGD*. Understanding the molecular mechanisms of ADKH-*RRAGD* would be of utmost value in providing treatment options for patients.

Disclosure

None declared

Acknowledgements

The authors thank Dr. Joost Martens and the Molecular Biology department at Radboud University for their help and assistance in performing bulk RNA-seq, Kops's group at Hubrecht Institute for performing bulk karyo-seq, and the FACS facilities at Hubrecht Institute and Radboudumc for cell-sorting. Additionally, the authors thank the Radboudumc Technology Center Microscopy for the use of their microscopy facilities.

Grants

This work was funded by the European Research Council grant 101040682 (IN-THE-KIDNEY) and Netherlands Organization for Scientific Research grants OCENW.M.21.022 and VIDI 391 09150172110040 (IMAGE-THE-KIDNEY).

References

1. Schlingmann KP, Jouret F, Shen K, et al. mTOR-Activating Mutations in RRAGD Are Causative for Kidney Tubulopathy and Cardiomyopathy. *J Am Soc Nephrol.* 2021;32(11):2885-2899.
2. Sambri I, Ferniani M, Campostrini G, et al. RagD auto-activating mutations impair MiT/TFE activity in kidney tubulopathy and cardiomyopathy syndrome. *Nat Commun.* 2023;14(1):2775.
3. de Frutos F, Diez-Lopez C, Garcia-Romero E, et al. Dilated Cardiomyopathy With Concomitant Salt-Losing Renal Tubulopathy Caused by Heterozygous RRAGD Gene Variant. *Circ Genom Precis Med.* 2024;17(2):e004336.
4. Anandapadamanaban M, Masson GR, Perisic O, et al. Architecture of human Rag GTPase heterodimers and their complex with mTORC1. *Science.* 2019;366(6462):203-210.
5. Rogala KB, Gu X, Kedir JF, et al. Structural basis for the docking of mTORC1 on the lysosomal surface. *Science.* 2019;366(6464):468-475.
6. Kim E, Goraksha-Hicks P, Li L, Neufeld TP, Guan KL. Regulation of TORC1 by Rag GTPases in nutrient response. *Nat Cell Biol.* 2008;10(8):935-945.
7. Sancak Y, Peterson TR, Shaul YD, et al. The Rag GTPases bind raptor and mediate amino acid signaling to mTORC1. *Science.* 2008;320(5882):1496-1501.
8. Sekiguchi T, Hirose E, Nakashima N, Ii M, Nishimoto T. Novel G proteins, Rag C and Rag D, interact with GTP-binding proteins, Rag A and Rag B. *J Biol Chem.* 2001;276(10):7246-7257.
9. Hirose E, Nakashima N, Sekiguchi T, Nishimoto T. RagA is a functional homologue of S. cerevisiae Gtr1p involved in the Ran/Gsp1-GTPase pathway. *J Cell Sci.* 1998;111 (Pt 1):11-21.
10. Schurmann A, Brauers A, Massmann S, Becker W, Joost HG. Cloning of a novel family of mammalian GTP-binding proteins (RagA, RagBs, RagB1) with remote similarity to the Ras-related GTPases. *J Biol Chem.* 1995;270(48):28982-28988.
11. Holz MK, Ballif BA, Gygi SP, Blenis J. mTOR and S6K1 mediate assembly of the translation preinitiation complex through dynamic protein interchange and ordered phosphorylation events. *Cell.* 2005;123(4):569-580.
12. Fingar DC, Blenis J. Target of rapamycin (TOR): an integrator of nutrient and growth factor signals and coordinator of cell growth and cell cycle progression. *Oncogene.* 2004;23(18):3151-3171.
13. Gingras AC, Gygi SP, Raught B, et al. Regulation of 4E-BP1 phosphorylation: a novel two-step mechanism. *Genes Dev.* 1999;13(11):1422-1437.
14. Kim J, Kundu M, Viollet B, Guan KL. AMPK and mTOR regulate autophagy through direct phosphorylation of Ulk1. *Nat Cell Biol.* 2011;13(2):132-141.
15. Martina JA, Chen Y, Gucek M, Puertollano R. MTORC1 functions as a transcriptional regulator of autophagy by preventing nuclear transport of TFEB. *Autophagy.* 2012;8(6):903-914.
16. Roczniak-Ferguson A, Petit CS, Froehlich F, et al. The transcription factor TFEB links mTORC1 signaling to transcriptional control of lysosome homeostasis. *Sci Signal.* 2012;5(228):ra42.
17. Settembre C, Zoncu R, Medina DL, et al. A lysosome-to-nucleus signalling mechanism senses and regulates the lysosome via mTOR and TFEB. *EMBO J.* 2012;31(5):1095-1108.
18. Sciarretta S, Volpe M, Sadoshima J. Mammalian target of rapamycin signaling in cardiac physiology and disease. *Circ Res.* 2014;114(3):549-564.
19. Sciarretta S, Forte M, Frati G, Sadoshima J. New Insights Into the Role of mTOR Signaling in the Cardiovascular System. *Circ Res.* 2018;122(3):489-505.

20. Zhu Y, Pires KM, Whitehead KJ, et al. Mechanistic target of rapamycin (Mtor) is essential for murine embryonic heart development and growth. *PLoS One.* 2013;8(1):e54221.
21. Zhang D, Contu R, Latronico MV, et al. MTORC1 regulates cardiac function and myocyte survival through 4E-BP1 inhibition in mice. *J Clin Invest.* 2010;120(8):2805-2816.
22. Kim YC, Park HW, Sciarretta S, et al. Rag GTPases are cardioprotective by regulating lysosomal function. *Nat Commun.* 2014;5:4241.
23. Kim M, Lu L, Dvornikov AV, et al. TFEB Overexpression, Not mTOR Inhibition, Ameliorates RagC(S75Y) Cardiomyopathy. *Int J Mol Sci.* 2021;22(11).
24. Reijnders MRF, Seibt A, Brugger M, et al. De novo missense variants in RRAGC lead to a fatal mTORopathy of early childhood. *Genet Med.* 2023;25(7):100838.
25. Adella A, Tengku F, Arjona FJ, et al. RRAGD variants cause cardiac dysfunction in a zebrafish model. *Am J Physiol Heart Circ Physiol.* 2024;327(5):H1187-H1197.
26. Vega-Rubin-de-Celis S, Pena-Llopis S, Konda M, Brugarolas J. Multistep regulation of TFEB by MTORC1. *Autophagy.* 2017;13(3):464-472.
27. Concordet JP, Haeussler M. CRISPOR: intuitive guide selection for CRISPR/Cas9 genome editing experiments and screens. *Nucleic Acids Res.* 2018;46(W1):W242-W245.
28. Sentmanat MF, Peters ST, Florian CP, Connelly JP, Pruett-Miller SM. A Survey of Validation Strategies for CRISPR-Cas9 Editing. *Sci Rep.* 2018;8(1):888.
29. Bolhaqueiro ACF, Ponsioen B, Bakker B, et al. Ongoing chromosomal instability and karyotype evolution in human colorectal cancer organoids. *Nat Genet.* 2019;51(5):824-834.
30. Li H, Handsaker B, Wysoker A, et al. The Sequence Alignment/Map format and SAMtools. *Bioinformatics.* 2009;25(16):2078-2079.
31. Love MI, Huber W, Anders S. Moderated estimation of fold change and dispersion for RNA-seq data with DESeq2. *Genome Biol.* 2014;15(12):550.
32. van Ham WB, Meijboom EEM, Ligtermoet ML, et al. An hiPSC-CM approach for electrophysiological phenotyping of a patient-specific case of short-coupled TdP. *Stem Cell Res Ther.* 2024;15(1):470.
33. Sweet ME, Cocciolo A, Slavov D, et al. Transcriptome analysis of human heart failure reveals dysregulated cell adhesion in dilated cardiomyopathy and activated immune pathways in ischemic heart failure. *BMC Genomics.* 2018;19(1):812.
34. De Paris V, Biondi F, Stolfo D, Merlo M, Sinagra G. Pathophysiology. In: Sinagra G, Merlo M, Pinamonti B, eds. *Dilated Cardiomyopathy: From Genetics to Clinical Management.* Cham (CH)2019:17-25.
35. Elliott P, O'Mahony C, Syrris P, et al. Prevalence of desmosomal protein gene mutations in patients with dilated cardiomyopathy. *Circ Cardiovasc Genet.* 2010;3(4):314-322.
36. Verdonschot JAJ, Wang P, Derks KWJ, et al. Clustering of Cardiac Transcriptome Profiles Reveals Unique: Subgroups of Dilated Cardiomyopathy Patients. *JACC Basic Transl Sci.* 2023;8(4):406-418.
37. Sun N, Yazawa M, Liu J, et al. Patient-specific induced pluripotent stem cells as a model for familial dilated cardiomyopathy. *Sci Transl Med.* 2012;4(130):130ra147.
38. Sun W, Zhang J, Li S, et al. TAB2 deficiency induces dilated cardiomyopathy by promoting mitochondrial calcium overload in human iPSC-derived cardiomyocytes. *Mol Med.* 2025;31(1):42.
39. Karbassi E, Fenix A, Marchiano S, et al. Cardiomyocyte maturation: advances in knowledge and implications for regenerative medicine. *Nat Rev Cardiol.* 2020;17(6):341-359.
40. Garbern JC, Lee RT. Mitochondria and metabolic transitions in cardiomyocytes: lessons from development for stem cell-derived cardiomyocytes. *Stem Cell Res Ther.* 2021;12(1):177.

41. Garbern JC, Helman A, Sereda R, et al. Inhibition of mTOR Signaling Enhances Maturation of Cardiomyocytes Derived From Human-Induced Pluripotent Stem Cells via p53-Induced Quiescence. *Circulation.* 2020;141(4):285-300.
42. Paltzer WG, Aballo TJ, Bae J, et al. mTORC1 regulates the metabolic switch of postnatal cardiomyocytes during regeneration. *J Mol Cell Cardiol.* 2024;187:15-25.
43. Bergmann O, Bhardwaj RD, Bernard S, et al. Evidence for cardiomyocyte renewal in humans. *Science.* 2009;324(5923):98-102.
44. Bergmann O, Zdunek S, Felker A, et al. Dynamics of Cell Generation and Turnover in the Human Heart. *Cell.* 2015;161(7):1566-1575.
45. Miklas JW, Levy S, Hofsteen P, et al. Amino acid primed mTOR activity is essential for heart regeneration. *iScience.* 2022;25(1):103574.
46. Trepiccione F, Sambri I, Ruggiero B, et al. RRAGD-Associated Autosomal Dominant Kidney Hypomagnesemia with Cardiomyopathy: A Review on the Clinical Manifestations and Therapeutic Options. *Kidney Blood Press Res.* 2024;49(1):637-645.
47. Sambri I, Trepiccione F. A zebrafish model to study RRAGD variants associated cardiomyopathy. *Am J Physiol Heart Circ Physiol.* 2024;327(6):H1343-H1344.
48. Shende P, Plaisance I, Morandi C, et al. Cardiac raptor ablation impairs adaptive hypertrophy, alters metabolic gene expression, and causes heart failure in mice. *Circulation.* 2011;123(10):1073-1082.
49. Mazelin L, Panthu B, Nicot AS, et al. mTOR inactivation in myocardium from infant mice rapidly leads to dilated cardiomyopathy due to translation defects and p53/JNK-mediated apoptosis. *J Mol Cell Cardiol.* 2016;97:213-225.
50. Jin B, Shi H, Zhu J, Wu B, Geshang Q. Up-regulating autophagy by targeting the mTOR-4EBP1 pathway: a possible mechanism for improving cardiac function in mice with experimental dilated cardiomyopathy. *BMC Cardiovasc Disord.* 2020;20(1):56.
51. Wu W, Jin Q, Ostlund C, et al. mTOR Inhibition Prolongs Survival and Has Beneficial Effects on Heart Function After Onset of Lamin A/C Gene Mutation Cardiomyopathy in Mice. *Circ Heart Fail.* 2024;17(4):e011110.
52. Neupane B, Pradhan K, Ortega-Ramirez AM, et al. Personalized Medicine Approach in a DCM Patient with LMNA Mutation Reveals Dysregulation of mTOR Signaling. *J Pers Med.* 2022;12(7).
53. Zhu Y, Do VD, Richards AM, Foo R. What we know about cardiomyocyte dedifferentiation. *J Mol Cell Cardiol.* 2021;152:80-91.
54. Szibor M, Poling J, Warnecke H, Kubin T, Braun T. Remodeling and dedifferentiation of adult cardiomyocytes during disease and regeneration. *Cell Mol Life Sci.* 2014;71(10):1907-1916.
55. Goversen B, van der Heyden MAG, van Veen TAB, de Boer TP. The immature electrophysiological phenotype of iPSC-CMs still hampers in vitro drug screening: Special focus on I(K1). *Pharmacol Ther.* 2018;183:127-136.
56. Shead KD, Huethorst E, Burton F, Lang NN, Myles RC, Smith GL. Human Induced Pluripotent Stem Cell-Derived Cardiomyocytes for Preclinical Cardiotoxicity Screening in Cardio-Oncology. *JACC CardioOncol.* 2024;6(5):678-683.
57. Campostrini G, Windt LM, van Meer BJ, Bellin M, Mummery CL. Cardiac Tissues From Stem Cells: New Routes to Maturation and Cardiac Regeneration. *Circ Res.* 2021;128(6):775-801.

Supplementary data

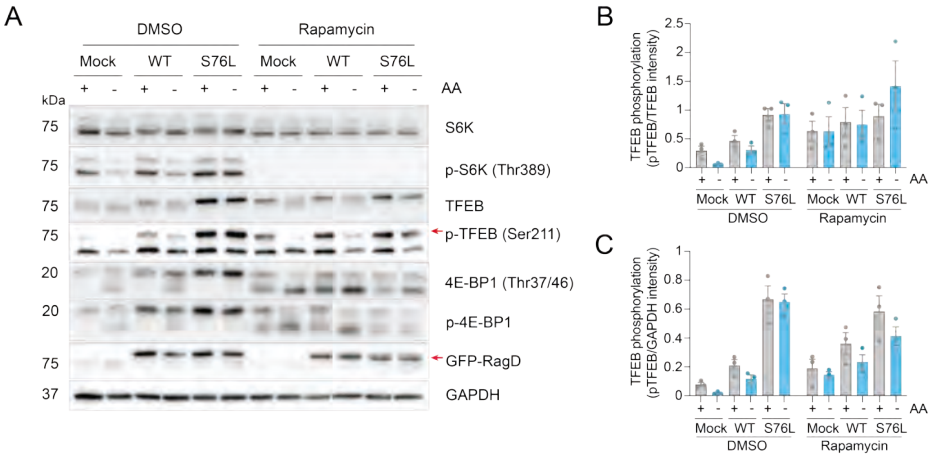

Supplementary Figure 1. mTOR inhibition by rapamycin suppressed S6K and 4E-BP1 phosphorylation but not TFEB in *RRAGD* p.(Ser76Leu) T-REx HeLa cells. (A-E) T-REx HeLa cells stably overexpressing GFP (mock), GFP-*RRAGD* WT (WT), and GFP-*RRAGD* p.(Ser76Leu) (S76L) were exposed to amino acids stimulation using amino acids-containing medium (+AA, grey bars) or amino acids-deprived medium (-AA, blue bars) and 100 nm rapamycin or 0.01% DMSO for 1 hr. (A) Representative immunoblots of S6K, p-S6K, TFEB, p-TFEB, 4E-BP1, p-4E-BP1, GFP, and GAPDH following treatment mentioned above. (B, C) Quantification of (B) TFEB phosphorylation corrected to total TFEB and (C) TFEB phosphorylation corrected to GAPDH (mean ± SEM from 3 independent experiments). Two-way ANOVA followed by Sidak's multiple comparison test where the effects of DMSO and Torin1 treatment were compared within each genotype, and each amino acids treatment group.

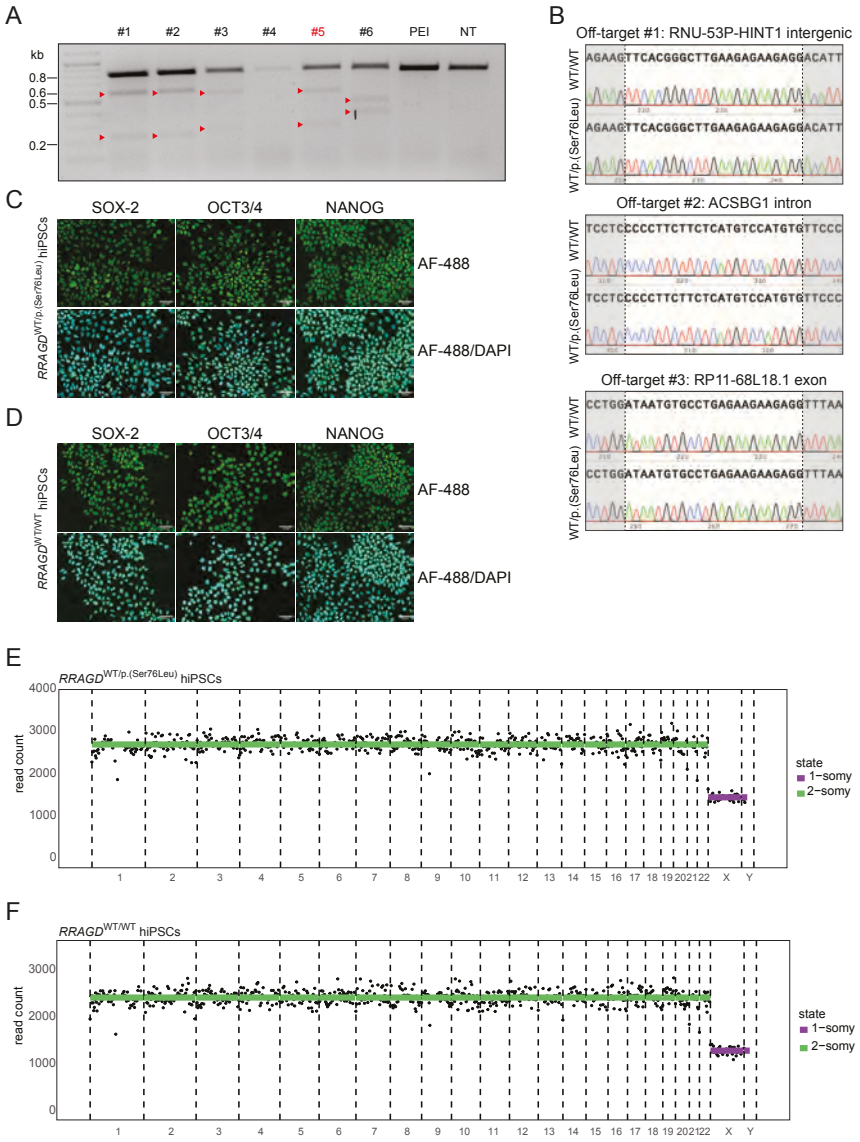

Supplementary Figure 2. CRISPR-Cas9-mediated generation of *RRAGD*$^{WT/WT}$ and *RRAGD*$^{WT/p.(Ser76Leu)}$ hiPSCs. (A) T7 endonuclease assay in HEK293 cells gDNA transiently transfected with either one of the six gRNAs, only transfection agent (i.e., polyethylenimine or PEI), or cells without any treatment (non-treated or NT). gRNA #5 was picked for subsequent steps. Red arrows indicate DNA fragments cut by T7 endonuclease. (B) Sanger sequencing results of the top three predicted off-target sites on gRNA #5. (C-D) Representative immunofluorescence images of pluripotency markers SOX-2, OCT3/4, and NANOG (green), and DAPI counterstain (blue) in (C) *RRAGD*$^{WT/p.(Ser76Leu)}$ and (D) *RRAGD*$^{WT/WT}$ hiPSCs clones. Scale bars indicate 20 µm. (E-F) Karyo-sequencing profiles of (E) *RRAGD*$^{WT/p.(Ser76Leu)}$ and (F) *RRAGD*$^{WT/WT}$ hiPSCs clones.

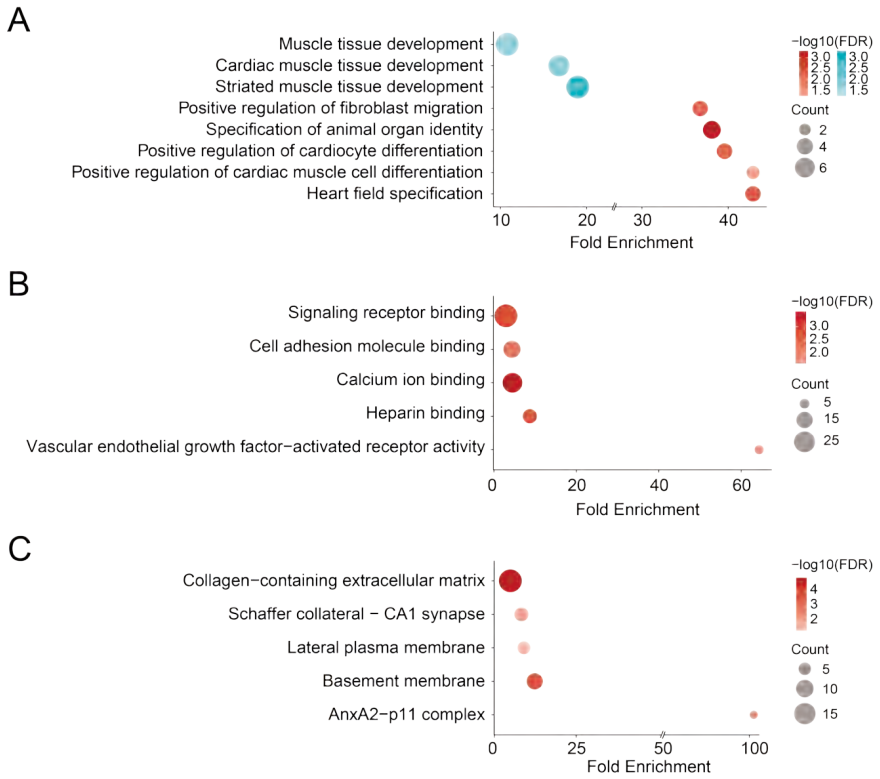

Supplementary Figure 3. Enriched gene ontology (GO) terms within the bulk RNA-seq differentially expressed gene list. (A-C) Bubble plots of top enriched (A) biological process, (B) molecular function, and (C) cellular component GO terms in *RRAGD*$^{WT/p.(Ser76Leu)}$ hiPSC-CMs. The terms have been filtered for those relevant in cardiomyocytes. The ranking of the terms was based on fold enrichment. The intensity of the bubble color is based on -$\log_{10}$ false discovery rate (FDR); red shows upregulated pathways, and blue shows downregulated pathways. The bubble size indicates the number of genes in each pathway (count).

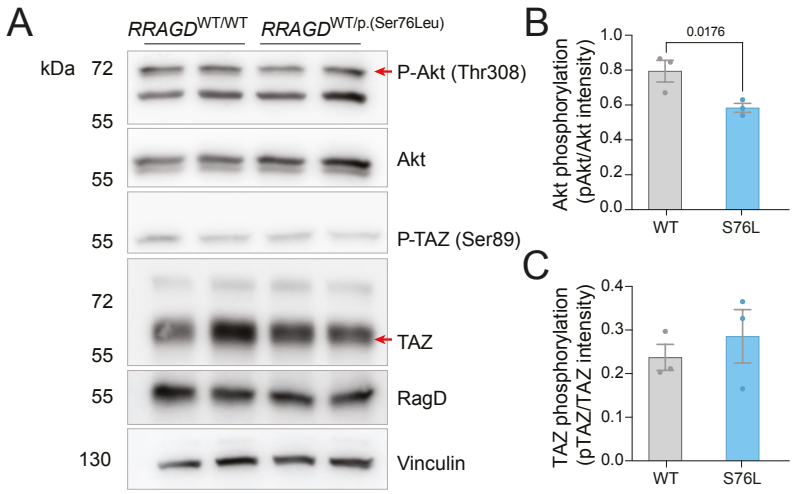

Supplementary Figure 4. Validation of bulk RNA-seq. (A) Representative immunoblots of p-Akt, Akt, p-TAZ, TAZ, RagD, and vinculin in *RRAGD*$^{WT/WT}$ and *RRAGD*$^{WT/p.(Ser76Leu)}$ hiPSC-CMs. (B-C) Quantification of (B) Akt phosphorylation and (C) TAZ phosphorylation immunoblots in *RRAGD*$^{WT/WT}$ (WT; grey bars) and *RRAGD*$^{WT/p.(Ser76Leu)}$ (S76L; blue bars) hiPSC-CMs. Mean ± SEM from three independent differentiations. One-tailed unpaired T-test was performed.

Supplementary Table 1. List of primers. [$]DNA template for CRISPR-Cas9. Mutation site (*RRAGD* c.227C>T) is underlined. *Primers were used to amplify amplicons through PCR, and the forward primers were also used for Sanger sequencing.

Usage	Target	Direction	Sequence (5'-3')
Subcloning to pCINeo	All h*RRAGD* variants	Forward	GCACCGGTTGCCACCATGTACCCATACGATGTTCC
		Reverse	GTGAATTCCTACAGCAGCACTCTAGGGGTCC
Subcloning to pcDNA5	All h*RRAGD* variants	Forward	GCCGGTACCAGCCAGGTGCTGG
		Reverse	GCCCTCGAGCTACAGCAGCACTCTAGG
Mutagenesis	h*RRAGD* p.(Ser76Leu)	Forward	GAGGAGAAGCGGCAAGTTGTCTATTCAGAAAGTTG
		Reverse	CAACTTTCTGAATAGACAACTTGCCGCTTCTCCTC
RT-qPCR	h*GAPDH*	Forward	GGAGTCAACGGATTTGGTCGTA
RT-qPCR		Reverse	GGCAACAATATCCACTTTACCAGAGT
RT-qPCR	h*RPLP0*	Forward	ACTCTGCATTCTCGCTTCCT
RT-qPCR		Reverse	AGGACTCGTTTGTACCCGTT
RT-qPCR	h*TFEB*	Forward	GGTGCAGTCCTACCTGGAG
RT-qPCR		Reverse	GTGGGCAGCAAACTTGTTCC
Cloning gRNA #5 to PX458	h*RRAGD* p.(Ser76Leu)	Forward	CACCGCTCATGGGCCTGAGGAGAAG
		Reverse	AAACCTTCTCCTCAGGCCCATGAGC
DNA template WT[$]	h*RRAGD* WT		ATTCTCATTTTGTGGTTTCTCCAGTTCTG-GACTTCAGTGACCCCTTCAGCACTGAAGTGAAGC-CGAGAATTCTG*CTCA*TGGGCCTGAGGAGATCCGG-CAAGTCGTCTATTCAGAAAGTTGTCTTTCA
DNA template KI[$]	h*RRAGD* p.(Ser76Leu)		ATTCTCATTTTGTGGTTTCTCCAGTTCTG-GACTTCAGTGACCCCTTCAGCACTGAAGTGAAGC-CGAGAATTCTGCTCATGGGCCTGAGGAGATCCGG-CAAGTTGTCTATTCAGAAAGTTGTCTTTCA
Genotyping*	All h*RRAGD* variants	Forward	TGGGAAGTATAGACCAGCGG
		Reverse	TTTGTAGATGTTGACTAGCGGT
Off-target #1*	RNU-53P-HINT1 intergenic	Forward	CCACACATTGGGACACTCTAG
		Reverse	GGAAAGCTTGGATGTGGATAC
Off-target #2*	ACSBG1 intron	Forward	GAGGACACAGGACACATTGTGC
		Reverse	CTACAGGGAGCACTCCCACTG
Off-target #3*	RP11-68L18.1 exon	Forward	GAACTACATGACATGTTCTCCG
		Reverse	GCTCTGGAACTGGCTTATATTC

Supplementary Table 2. Differentially expressed genes between *RRAGD*$^{WT/p.(Ser76Leu)}$ and *RRAGD*$^{WT/WT}$ hiPSC-CMs following bulk RNA-seq. Log2FC: Log2 fold change. Padj: adjusted p-value.

Gene ID	hgnc_ symbol	Mean count WT	Mean count S76L	Log2FC	p-value	padj
ENSG00000136383	ALPK3	2056.75	500	-2.643519469	4.45E-97	7.02E-93
ENSG00000112936	C7	726.5	3799.75	1.768109681	1.04E-43	8.23E-40
ENSG00000135842	NIBAN1	1397.5	897.25	-1.287690259	2.04E-17	1.07E-13
ENSG00000153993	SEMA3D	22.25	148.25	2.055427677	4.01E-13	1.58E-09
ENSG00000251129	WWC2-AS1	46	236.25	1.612113228	6.51E-13	2.05E-09
ENSG00000145741	BTF3	494	1435.75	0.91179882	1.44E-12	3.78E-09
ENSG00000152583	SPARCL1	9.25	132.25	3.213681219	4.61E-12	1.04E-08
ENSG00000186073	CDIN1	516	400.75	-0.927229837	1.87E-11	3.68E-08
ENSG00000167785	ZNF558	0	50	8.536510024	3.54E-11	6.21E-08
ENSG00000134716	CYP2J2	756.75	590.75	-0.920794414	1.23E-10	1.94E-07
ENSG00000197565	COL4A6	814.5	2071.5	0.711896709	2.75E-10	3.95E-07
ENSG00000005108	THSD7A	36.5	172.25	1.513620955	8.76E-10	0.00000115
ENSG00000266472	MRPS21	119.25	391.25	1.058511994	1.25E-09	0.00000152
ENSG00000125730	C3	3.25	152.5	0.02475256	2.54E-09	0.00000287
ENSG00000272674	PCDHB16	33.25	138.25	1.339431262	3.09E-09	0.00000325
ENSG00000039068	CDH1	3.25	83.25	0.037477287	5.02E-09	0.00000496
ENSG00000278318	ZNF229	0	29.25	7.565604678	5.44E-09	0.00000505
ENSG00000108439	PNPO	75	41.5	-1.371997047	1.35E-08	0.0000118
ENSG00000120729	MYOT	5.25	53.25	2.55456972	1.93E-08	0.0000161
ENSG00000173406	DAB1	342.5	866.25	0.698018873	5.99E-08	0.000045
ENSG00000197614	MFAP5	8	113	0.040310508	5.85E-08	0.000045
ENSG00000189221	MAOA	11.5	94.75	2.174514026	8.05E-08	0.0000577
ENSG00000101638	ST8SIA5	43	17	-1.844412851	0.00000012	0.000082
ENSG00000156466	GDF6	160.5	490	0.922341612	0.000000134	0.0000881
ENSG00000052850	ALX4	8.5	62.5	2.099268331	0.000000178	0.00011245
ENSG00000153707	PTPRD	1167.25	2682.75	0.536064543	0.000000201	0.00012219
ENSG00000105894	PTN	706.75	1772.25	0.694591229	0.000000214	0.0001251
ENSG00000070193	FGF10	135.75	390.5	0.878072087	0.000000235	0.0001259
ENSG00000077009	NMRK2	59.75	23.25	-1.859605883	0.000000239	0.0001259
ENSG00000091136	LAMB1	1335.5	3626.5	0.710194041	0.000000235	0.0001259
ENSG00000175206	NPPA	3996	3282.5	-0.82921057	0.000000316	0.00016114
ENSG00000160808	MYL3	9677.5	7296.25	-0.913395877	0.000000473	0.00023326
ENSG00000171617	ENC1	40.5	180.25	1.34376473	0.000000793	0.00037931
ENSG00000137261	KIAA0319	44	151.25	1.080629249	0.000000846	0.00039276
ENSG00000156253	RWDD2B	9.5	0	-7.002290045	0.00000123	0.00055596

Supplementary Table 2. Continued

Gene ID	hgnc_ symbol	Mean count WT	Mean count S76L	Log2FC	p-value	padj
ENSG00000113248	PCDHB15	53.5	174.75	0.967307135	0.00000204	0.00089297
ENSG00000125266	EFNB2	168	556.75	0.967528846	0.00000322	0.00137355
ENSG00000100461	RBM23	273.75	249.25	-0.66031649	0.0000035	0.00145271
ENSG00000075340	ADD2	355.5	278	-0.820680109	0.00000439	0.00176707
ENSG00000197893	NRAP	514	186.75	-2.053327933	0.00000448	0.00176707
ENSG00000079691	CARMIL1	81.5	232.75	0.837448415	0.00000486	0.00178361
ENSG00000118257	NRP2	222	795	1.029828025	0.00000477	0.00178361
ENSG00000206579	XKR4	6.5	48	1.994779843	0.00000466	0.00178361
ENSG00000108950	FAM20A	141.75	388.25	0.714175641	0.00000533	0.00186866
ENSG00000213949	ITGA1	102.25	315.75	0.866639512	0.00000528	0.00186866
ENSG00000163430	FSTL1	3320.5	8044.25	0.538837039	0.00000562	0.00192687
ENSG00000184347	SLIT3	742.25	1702	0.523442118	0.00000658	0.00220959
ENSG00000091972	CD200	24	132.5	1.708332817	0.00000748	0.00240674
ENSG00000112414	ADGRG6	95.5	299.75	0.961147358	0.00000778	0.00240674
ENSG00000164764	SBSPON	1.5	47.25	3.738610914	0.00000768	0.00240674
ENSG00000185847	LINC01405	347.75	293.5	-0.779167998	0.00000773	0.00240674
ENSG00000182732	RGS6	102	291	0.815191095	0.00000987	0.00299523
ENSG00000145808	ADAMTS19	94.5	315.25	1.057161754	0.0000143	0.00426327
ENSG00000024422	EHD2	47	240.5	1.451674842	0.0000152	0.00442837
ENSG00000111245	MYL2	13368	7567.75	-1.397615899	0.0000159	0.00457028
ENSG00000264230	RNU4ATAC	0	17.25	0.013456511	0.0000163	0.00458404
ENSG00000092969	TGFB2	179	458.75	0.659455094	0.0000174	0.00479514
ENSG00000146530	VWDE	97.25	260	0.717416965	0.0000179	0.00479514
ENSG00000288941		280.75	654.75	0.547647829	0.0000177	0.00479514
ENSG00000187210	GCNT1	9	48.5	1.561675717	0.0000197	0.00517896
ENSG00000132470	ITGB4	1	38	4.031167734	0.0000252	0.00635819
ENSG00000134853	PDGFRA	101	397.25	1.059677657	0.000025	0.00635819
ENSG00000197442	MAP3K5	129.5	118	-0.669065101	0.0000254	0.00635819
ENSG00000067798	NAV3	267.5	669.25	0.682043487	0.0000298	0.0073531
ENSG00000137936	BCAR3	68	221.25	1.00976701	0.0000355	0.00861396
ENSG00000107796	ACTA2	5196.5	14601.75	0.823175334	0.0000385	0.00909285
ENSG00000169908	TM4SF1	1.5	32	3.184117602	0.0000386	0.00909285
ENSG00000099337	KCNK6	394.75	963.5	0.594298132	0.0000423	0.00982376
ENSG00000145934	TENM2	200.25	620.75	0.930421415	0.000044	0.01006199
ENSG00000153820	SPHKAP	1687.75	3747	0.461337379	0.000045	0.01014548

Supplementary Table 2. Continued

Gene ID	hgnc_ symbol	Mean count WT	Mean count S76L	Log2FC	p-value	padj
ENSG00000173068	BNC2	56	199.5	1.048056067	0.0000467	0.01039191
ENSG00000270112	CELF2-DT	28.75	13	-1.53411202	0.0000551	0.01207769
ENSG00000125378	BMP4	20.5	102	1.436529449	0.0000588	0.01271258
ENSG00000147872	PLIN2	78.5	53.25	-0.980635223	0.0000599	0.01278257
ENSG00000171357	LURAP1	55	37	-1.03736431	0.0000623	0.01311028
ENSG00000275342	FGD5P1	13	101	0.030981633	0.0000635	0.01318154
ENSG00000181744	DIPK2A	477.75	1099.5	0.470782684	0.0000683	0.01400128
ENSG00000109472	CPE	87	257.5	0.763555619	0.0000726	0.01468722
ENSG00000143382	ADAMTSL4	246.25	234.5	-0.641285613	0.0000751	0.0150015
ENSG00000151892	GFRA1	139.5	381.75	0.766987407	0.0000786	0.01514495
ENSG00000176658	MYO1D	96.25	271.75	0.777440437	0.0000771	0.01514495
ENSG00000178031	ADAMTSL1	132.25	392	0.789229725	0.0000787	0.01514495
ENSG00000127824	TUBA4A	204	170.75	-0.721186064	0.0000797	0.0151505
ENSG00000138193	PLCE1	879.5	1819.5	0.360986041	0.0000826	0.01552484
ENSG00000186314	PRELID2	253.25	574	0.513774196	0.0000966	0.0179461
ENSG00000112379	ARFGEF3	26.75	102.75	0.061517791	0.000100053	0.01836205
ENSG00000171476	HOPX	329.5	262	-0.896944836	0.000108619	0.01970495
ENSG00000150782	IL18	1.75	34.25	0.016769967	0.000118228	0.02120454
ENSG00000163347	CLDN1	7.25	47.5	1.731030719	0.000131309	0.02328602
ENSG00000137571	SLCO5A1	87.75	265.5	0.900635082	0.000137016	0.02376408
ENSG00000150630	VEGFC	57.75	156.25	0.68261445	0.000136908	0.02376408
ENSG00000131016	AKAP12	684.25	1912.5	0.732734873	0.00014048	0.02409989
ENSG00000111816	FRK	38.25	17.75	-1.566147006	0.000142154	0.02412494
ENSG00000101871	MID1	278.25	632	0.456905427	0.000144528	0.02426682
ENSG00000276476	LINC00540	10.75	1.5	-2.958512337	0.000146546	0.02434663
ENSG00000105926	PALS2	132.5	351.25	0.663754862	0.000149914	0.02443134
ENSG00000162630	B3GALT2	290	692.75	0.597237949	0.000150151	0.02443134
ENSG00000055813	CCDC85A	38.75	115.25	0.779462381	0.000161567	0.02602046
ENSG00000173175	ADCY5	500.25	494	-0.606844376	0.000168917	0.0269294
ENSG00000088992	TESC	103.75	283.75	0.730063748	0.000175301	0.02695263
ENSG00000111110	PPM1H	15.5	87.25	0.035016604	0.000171766	0.02695263
ENSG00000140575	IQGAP1	105.5	403.25	0.074202542	0.000176457	0.02695263
ENSG00000165323	FAT3	1016.5	2370.5	0.487761079	0.000177287	0.02695263
ENSG00000289309		5.5	35.75	1.817452461	0.000177601	0.02695263
ENSG00000116396	KCNC4	280	274.75	-0.573567763	0.000183283	0.0275501

Supplementary Table 2. Continued

Gene ID	hgnc_ symbol	Mean count WT	Mean count S76L	Log2FC	p-value	padj
ENSG00000108797	CNTNAP1	188.75	437	0.485654881	0.000193971	0.0288816
ENSG00000243566	RN7SL838P	0	12.75	0.009931416	0.000200826	0.02962273
ENSG00000136943	CTSV	72	256	0.915463818	0.000216084	0.03157834
ENSG00000144278	GALNT13	12.75	66.5	1.39670771	0.000230862	0.03342833
ENSG00000108691	CCL2	0.75	20.25	0.016806722	0.000258345	0.03706785
ENSG00000154330	PGM5	727.5	830.75	-0.345460931	0.000277396	0.0392433
ENSG00000205038	PKHD1L1	0.75	72.5	0.006449277	0.000280966	0.0392433
ENSG00000272079	AC004233.3	44	31.75	-0.944015201	0.0002792	0.0392433
ENSG00000068976	PYGM	451.75	406.5	-0.592041896	0.000284168	0.03934234
ENSG00000011201	ANOS1	167.5	392.25	0.481138439	0.000304804	0.04136784
ENSG00000171812	COL8A2	1.5	20.25	0.020768549	0.000306661	0.04136784
ENSG00000175093	SPSB4	174.25	163.5	-0.652000477	0.000303225	0.04136784
ENSG00000132199	ENOSF1	245.75	229	-0.604052852	0.00032828	0.04390891
ENSG00000167363	FN3K	114.25	97.5	-0.695779904	0.000335468	0.04449327
ENSG00000143324	XPR1	1325.5	2871.5	0.420704421	0.000345806	0.04502721
ENSG00000180957	PITPNB	277.25	597.25	0.420053028	0.000348053	0.04502721
ENSG00000182197	EXT1	537.25	1268	0.506944262	0.000342806	0.04502721
ENSG00000013016	EHD3	745.75	1661.25	0.394671886	0.000357693	0.04523757
ENSG00000156140	ADAMTS3	64.25	203.25	0.858117354	0.000358278	0.04523757
ENSG00000169181	GSG1L	16.75	75	0.038361062	0.000357992	0.04523757
ENSG00000198075	SULT1C4	12.5	50.75	1.193267385	0.000373053	0.04672937
ENSG00000165186	PTCHD1	116	301	0.59937543	0.000390971	0.04858816
ENSG00000231811	RPL36AP35	72	30.5	-1.410768434	0.000397497	0.04901325
ENSG00000129675	ARHGEF6	300	288.5	-0.523660143	0.000402461	0.04924062
ENSG00000106565	TMEM176B	74.75	56.25	-0.880674525	0.000424806	0.05157466
ENSG00000128052	KDR	66	517.5	0.017549658	0.000432156	0.0520666
ENSG00000125848	FLRT3	82.75	223.5	0.634538969	0.000446319	0.05336556
ENSG00000111859	NEDD9	85	260.25	0.761798286	0.000458592	0.05442074
ENSG00000148204	CRB2	11.75	79.75	0.026431803	0.000465466	0.05482423
ENSG00000280285	AC108215.1	30.75	15.25	-1.494701227	0.000480114	0.05613063
ENSG00000184216	IRAK1	65.75	54	-0.731070399	0.000489958	0.05686031
ENSG00000087245	MMP2	38	174.25	0.043401601	0.000503278	0.05797982
ENSG00000100815	TRIP11	122.75	303.25	0.513601324	0.00054065	0.06113562
ENSG00000146833	TRIM4	5.5	0.25	-3.927054485	0.000540401	0.06113562
ENSG00000241644	RPS23P6	7.75	39	1.301122224	0.000542291	0.06113562

Supplementary Table 2. Continued

Gene ID	hgnc_ symbol	Mean count WT	Mean count S76L	Log2FC	p-value	padj
ENSG00000105290	APLP1	53.75	186.5	0.993973783	0.000580278	0.06486219
ENSG00000142089	IFITM3	202.25	569.25	0.74077742	0.000587676	0.06486219
ENSG00000143416	SELENBP1	53.25	38.75	-0.878599546	0.000587546	0.06486219
ENSG00000165238	WNK2	1143.25	1279.75	-0.372300109	0.000598594	0.06560835
ENSG00000198846	TOX	111.75	257.75	0.465106829	0.000670077	0.07282824
ENSG00000286039		202.25	177.75	-0.620889169	0.000673695	0.07282824
ENSG00000287661		32	12.25	-1.506911004	0.000687284	0.07379184
ENSG00000113805	CNTN3	3	27	0.019646465	0.000694462	0.07405877
ENSG00000119900	OGFRL1	52.75	168.25	0.834263969	0.000736648	0.07803032
ENSG00000016082	ISL1	56.75	156.75	0.678196945	0.00076597	0.08059531
ENSG00000168824	NSG1	12.75	72.75	0.026775494	0.000778814	0.08140416
ENSG00000065320	NTN1	46.5	32.25	-0.909427523	0.000790509	0.08154647
ENSG00000181072	CHRM2	704	1503.75	0.410718536	0.000785416	0.08154647
ENSG00000179862	CITED4	62.75	50.25	-0.742624485	0.000796283	0.08160869
ENSG00000157827	FMNL2	94.5	252	0.601179854	0.000817612	0.08325401
ENSG00000170381	SEMA3E	4.5	33.5	0.020796257	0.000860267	0.08703584
ENSG00000197747	S100A10	41	301.5	0.019160701	0.000883571	0.08882419
ENSG00000141756	FKBP10	216.75	493.5	0.449848569	0.000921307	0.09203158
ENSG00000107521	HPS1	147.5	153.75	-0.450522184	0.000930536	0.09236749
ENSG00000155966	AFF2	29.25	103.25	0.040805948	0.000936374	0.09236749
ENSG00000054938	CHRDL2	2.25	28.25	0.01447017	0.000974478	0.09536758
ENSG00000156381	ANKRD9	184.75	178	-0.518224936	0.000978873	0.09536758
ENSG00000240583	AQP1	845.25	2169.5	0.548704979	0.000993507	0.09619956
ENSG00000123689	G0S2	140.75	378.5	0.696420022	0.001020407	0.09765018
ENSG00000165300	SLITRK5	7.75	36.75	1.225115597	0.001020863	0.09765018
ENSG00000158258	CLSTN2	564.25	1409.5	0.571027493	0.001036613	0.09797347
ENSG00000172201	ID4	22.5	75.25	0.049580782	0.001036658	0.09797347
ENSG00000157600	TMEM164	401	430.25	-0.410838656	0.001045955	0.09826377
ENSG00000066032	CTNNA2	5	33	0.021327659	0.00106546	0.0984061
ENSG00000157680	DGKI	502.75	1132	0.467273908	0.001066175	0.0984061
ENSG00000173376	NDNF	26	14.25	-1.282081645	0.00106447	0.0984061
ENSG00000182718	ANXA2	1541.75	3309.25	0.356936405	0.001089411	0.09996616

Supplementary Table 3. *RRAGD*$^{WT/p.S76L}$ hiPSC-CMs differentially expressed genes vs. DCM. List of genes differentially expressed in our bulk RNA-seq data that overlapped with genes specific to DCM patients in Sweet et al. Log2FC: Log2 fold change, padj: adjusted p-value).

Gene ID	hgnc_ symbol	Mean count WT	Mean count S76L	Log2FC	p-value	padj
ENSG00000136383	ALPK3	2056.75	500	-2.6435195	4.45E-97	7.02E-93
ENSG00000145741	BTF3	494	1435.75	0.91179882	1.44E-12	3.78E-09
ENSG00000152583	SPARCL1	9.25	132.25	3.21368122	4.61E-12	1.04E-08
ENSG00000134716	CYP2J2	756.75	590.75	-0.9207944	1.23E-10	1.94E-07
ENSG00000125730	C3	3.25	152.5	0.02475256	2.54E-09	0.00000287
ENSG00000197614	MFAP5	8	113	0.04031051	5.85E-08	0.000045
ENSG00000105894	PTN	706.75	1772.25	0.69459123	2.14E-07	0.0001251
ENSG00000077009	NMRK2	59.75	23.25	-1.8596059	2.39E-07	0.0001259
ENSG00000175206	NPPA	3996	3282.5	-0.8292106	3.16E-07	0.00016114
ENSG00000160808	MYL3	9677.5	7296.25	-0.9133959	4.73E-07	0.00023326
ENSG00000100461	RBM23	273.75	249.25	-0.6603165	0.0000035	0.00145271
ENSG00000197893	NRAP	514	186.75	-2.0533279	0.00000448	0.00176707
ENSG00000197442	MAP3K5	129.5	118	-0.6690651	0.0000254	0.00635819
ENSG00000137936	BCAR3	68	221.25	1.00976701	0.0000355	0.00861396
ENSG00000169908	TM4SF1	1.5	32	3.1841176	0.0000386	0.00909285
ENSG00000125378	BMP4	20.5	102	1.43652945	0.0000588	0.01271258
ENSG00000109472	CPE	87	257.5	0.76355562	0.0000726	0.01468722
ENSG00000176658	MYO1D	96.25	271.75	0.77744044	0.0000771	0.01514495
ENSG00000171476	HOPX	329.5	262	-0.8969448	0.00010862	0.01970495
ENSG00000162630	B3GALT2	290	692.75	0.59723795	0.00015015	0.02443134
ENSG00000088992	TESC	103.75	283.75	0.73006375	0.0001753	0.02695263
ENSG00000154330	PGM5	727.5	830.75	-0.3454609	0.0002774	0.0392433
ENSG00000068976	PYGM	451.75	406.5	-0.5920419	0.00028417	0.03934234
ENSG00000143324	XPR1	1325.5	2871.5	0.42070442	0.00034581	0.04502721
ENSG00000182197	EXT1	537.25	1268	0.50694426	0.00034281	0.04502721
ENSG00000106565	TMEM176B	74.75	56.25	-0.8806745	0.00042481	0.05157466
ENSG00000128052	KDR	66	517.5	0.01754966	0.00043216	0.0520666
ENSG00000111859	NEDD9	85	260.25	0.76179829	0.00045859	0.05442074
ENSG00000184216	IRAK1	65.75	54	-0.7310704	0.00048996	0.05686031
ENSG00000087245	MMP2	38	174.25	0.0434016	0.00050328	0.05797982
ENSG00000105290	APLP1	53.75	186.5	0.99397378	0.00058028	0.06486219
ENSG00000142089	IFITM3	202.25	569.25	0.74077742	0.00058768	0.06486219
ENSG00000143416	SELENBP1	53.25	38.75	-0.8785995	0.00058755	0.06486219

Supplementary Table 3. Continued

Gene ID	hgnc_ symbol	Mean count WT	Mean count S76L	Log2FC	p-value	padj
ENSG00000165238	WNK2	1143.25	1279.75	-0.3723001	0.00059859	0.06560835
ENSG00000179862	CITED4	62.75	50.25	-0.7426245	0.00079628	0.08160869
ENSG00000197747	S100A10	41	301.5	0.0191607	0.00088357	0.08882419
ENSG00000141756	FKBP10	216.75	493.5	0.44984857	0.00092131	0.09203158
ENSG00000123689	G0S2	140.75	378.5	0.69642002	0.00102041	0.09765018
ENSG00000182718	ANXA2	1541.75	3309.25	0.35693641	0.00108941	0.09996616

CHAPTER 5

General discussion

Partly adapted from:
mTOR signaling in renal ion transport

Anastasia Adella[1] and Jeroen H.F. de Baaij[1]

[1] Department of Medical BioSciences, Radboudumc, Nijmegen, The Netherlands

Acta Physiologica, 2023

Introduction

The overarching goals of this thesis were to identify the cellular consequences of the Ras-related GTPase D (*RRAGD*) variants found in patients with *RRAGD*-associated autosomal dominant kidney hypomagnesemia (ADKH-*RRAGD*) and to investigate potential therapies for the patients. In **chapter 2**, we described a large cohort of newly identified ADKH-*RRAGD* patients (n=12) with three novel *RRAGD*-associated variants. Using HeLa cells, we confirmed that most of the new variants resulted in a constitutively active mechanistic target of rapamycin complex 1 (mTORC1) non-canonical signaling. In **chapter 3**, we generated the first *in vivo* model of ADKH-*RRAGD* using zebrafish embryos. We demonstrated that overexpression of the *RRAGD* p.(Ser76Leu) and p.(Pro119Arg) variants led to cardiac dysfunctions. By looking further into the molecular mechanisms underlying dilated cardiomyopathy (DCM) due to the *RRAGD* p.(Ser76Leu) variant in **chapter 4**, we revealed that pathways previously shown to be altered in DCM patients, such as actin cytoskeleton, cell-cell adhesion, and extracellular matrix, were affected in human induced pluripotent stem cells (hiPSC-CMs) carrying the heterozygous *RRAGD* p.(Ser76Leu) variant ($RRAGD^{WT/p.(Ser76Leu)}$ hiPSC-CMs). However, no mTOR- and TFEB-related pathways were enriched. Finally, we investigated potential therapeutic options for ADKH-*RRAGD* patients in **chapters 2 and 3**. We validated the potential use of dapagliflozin to elevate serum Mg^{2+} levels in ADKH-*RRAGD* patients in **chapter 2** and demonstrated the beneficial effects of mTORC1 inhibition with rapamycin in rescuing cardiac dysfunctions in **chapter 3**. In this discussion, the current state of mTORC1 signaling in ADKH-*RRAGD* will be first addressed. Second, we will discuss the common hallmarks in ADKH-*RRAGD* patients, which are DCM and kidney tubulopathy. Third, the correlation between genotype and phenotype in this disease and their role in the clinical manifestations will be discussed. Lastly, the clinical implications of this study will be explored, followed by a discussion of potential therapeutic perspectives.

mTORC1 signaling in ADKH-*RRAGD*: the current state

Since the initial report of ADKH-*RRAGD* patients in 2020, multiple studies have examined the molecular mechanisms underlying this novel rare disease.[1-4] In ADKH-*RRAGD*, clinical manifestations of this disease vastly vary among patients, with some experiencing the full spectrum of phenotypes (i.e., kidney tubulopathy and DCM) and others displaying only kidney tubulopathy.[1-4] As RagD functions in aiding mTORC1 activation at the lysosomal surface, and the *RRAGD* variants are known to keep RagD in its active form,[1,2] we hypothesized that *RRAGD* variants cause mTORC1

constitutive activation. In the earliest studies, we first showed that mTORC1 canonical signaling (i.e., S6 kinase (S6K) phosphorylation) was constitutively active in the absence of amino acids due to *RRAGD* variants, while Sambri *et al*. reported in 2023 that at the basal level (amino acid-rich conditions), only mTORC1 non-canonical signaling (i.e., transcription factor EB (TFEB) phosphorylation) was overactivated.[2] To address the disparity between these studies, we investigated how *RRAGD* variants influence mTORC1 response to amino acid stimulation in **chapters 2 and 4**. Using stable HeLa cell lines, we showed in **chapter 4** that the most common ADKH-*RRAGD* variant so far (i.e., *RRAGD* p.(Ser76Leu)) did not affect mTORC1 signaling at the basal level. Instead, our data suggested that the *RRAGD* variant caused constitutive activation of mTORC1, as both its canonical (i.e., S6K and 4E-BP1) and non-canonical (i.e., TFEB) targets remained phosphorylated in the absence of amino acid. **Chapter 2** describes how three novel *RRAGD* variants, p.(Ser77Phe), p.(Thr91Ile), and p.(Ile100Arg), affect mTORC1 signaling. We found that the p.(Ser77Phe) and p.(Ile100Arg) *RRAGD* variants cause the constitutive activation of only the mTORC1 non-canonical signaling pathway. Moreover, the expression of these variants resulted in a slightly more activated canonical mTORC1 signaling compared to the expression of *RRAGD* wild type (WT), but this was not statistically significant. Of note, the *RRAGD* p.(Thr91Ile) variant did not induce either mTORC1 overactivation or constitutive activation. Therefore, the results of these chapters suggest that *RRAGD* variants can induce mTORC1 activation differently.

TFEB requires the active GDP-bound RagC/D for its lysosomal surface recruitment and the subsequent phosphorylation by mTORC1.[5] Because of this, RagC/D play an important role in TFEB activation.[6,7] Interestingly, RagC has been shown to stimulate TFEB activity independently of mTORC1.[8] A previous study on the effects of a RagC p.(Ser75Tyr) variant in zebrafish and cardiomyocytes showed increased interaction with TFEB and TFEB cytoplasmic retainment due to this mutation.[8] While rapamycin treatment was able to rescue TFEB phosphorylation, pull-down assay revealed that RagC p.(Ser75Tyr) binding to TFEB was not abrupted, and TFEB remained retained in the cytoplasm, suggesting an mTORC1 independent effect of the mutation on TFEB.[8] Therefore, one of the key questions surrounding the *RRAGD* variants is whether their effects on TFEB are mediated by mTORC1. In **chapter 4**, we showed that the effects of *RRAGD* variants on constant TFEB phosphorylation depended on mTOR, as pharmacological mTOR inhibition with Torin1 abolished the phosphorylation of TFEB. These results are in line with the findings by Sambri *et al*.[2] Moreover, our data is indicative of a functional restoration of TFEB upon Torin1 treatment, as TFEB translocated to the nuclei was clearly observed in this condition. Taken together, these results suggest that aberrant TFEB activation due to *RRAGD* variants is mediated by mTORC1.

Another important question surrounding the molecular mechanistic avenue of ADKH-*RRAGD* is: what is the role of the other Rag GTPases in this disease? Raptor, the catalytic subunit of mTORC1, can extensively interact with active GTP-bound RagA/B, and, to a much lesser extent, with RagC/D.[9,10] Moreover, it is known that the nucleotide-binding state of RagA/B is important in regulating mTORC1 activity, while that of RagC/D plays a minor role in this.[5,11] As RagA/B activity is important for mTORC1 recruitment and activation, it is intriguing how mutant RagD leverages the activation of the RagA/B in ADKH-*RRAGD*. Previous studies suggested that dysregulation of the individual Rag GTPases may be sufficient in driving disease pathogenesis.[12-15] For example, recurrent somatic mutations in *RRAGC* are frequently found in follicular lymphoma patients [12], missense *RRAGC* variants have been associated with pediatric DCM, hepatopathy, and brain abnormalities [13,14], and a *RRAGA* p.(Leu60Arg) variant in autosomal dominant cataracts [15]. As to our knowledge, the status of the other Rag GTPases in these diseases has never been studied, whether the variants change the active conformation of the remaining Rags or if they override the nucleotide-binding status of the other Rags remains to be elucidated.

In summary, *RRAGD* variants cause the aberrant regulation of mTORC1 canonical and non-canonical signaling pathways. Moreover, the different variants affect mTORC1 activation levels differently. In the next sections, we will discuss the cellular consequences of the variants and how they are associated with DCM and kidney tubulopathy in ADKH-*RRAGD*.

Dilated cardiomyopathy in ADKH-*RRAGD*

DCM was present in one-third of all identified ADKH-*RRAGD* patients. To confirm the pathogenicity of *RRAGD* variants, in **chapter 3**, we used zebrafish embryos injected with *RRAGD* wild-type (WT), p.(Ser76Leu), or p.(Pro119Arg) mRNA to model ADKH-*RRAGD* and studied the effects of the variants on heart and pronephros functions. While the pronephros functioned normally compared to the WT control, overexpression of the two *RRAGD* variants resulted in cardiac dysfunctions, as shown by pericardial edema and reduced fractional shortening and ejection fraction. Although the mechanisms that lead to cardiac dysfunction remain elusive, we confirmed the pathogenicity of the *RRAGD* variants in the heart. Previously, *rragc* p.(Ser75Tyr) mutation was found to cause cardiac dysfunction in a zebrafish model, where the fish heart displayed lower fractional shortening and ejection fraction, among other cardiac function measurements, indicative of impaired cardiac function.[8] Additionally, double deletion of RagA and RagB in mouse cardiomyocytes caused heart enlargement and dilatation

of the left ventricle.[16] Taken together, all members of the Rag GTPase family play a critical role in maintaining cardiac function and integrity.

The molecular mechanisms

At the molecular level, TFEB overactivation and the subsequent lysosomal dysregulation are responsible for impaired cardiac function in the RagA-C studies.[8,13,14,16] In **chapter 3**, we investigated if there was mTORC1 and TFEB overactivation in our RagD mutant zebrafish model and found a comparable signaling activity as seen in RagD WT zebrafish. We speculate this was due to the whole embryo lysates we were looking at rather than only at cardiomyocytes. To address this, we generated *RRAGD*$^{WT/p.(Ser76Leu)}$ hiPSC-CMs in **chapter 4**. We did not observe changes in mTORC1 or TFEB signaling in this model, which can likely be attributed to the early embryonic cardiomyocyte-like properties of 2D cultured hiPSC-CMs. During early embryonic stages, mTORC1 signaling has been shown to support cardiomyocyte proliferation and its inhibition results in the maturation of cardiomyocytes with postnatal-like properties.[17,18] Thus, mTORC1 activity shows a temporal profile in the cardiomyocytes, which is high during fetal development and low in the post-natal stage.[17,18] Interestingly, Sambri *et al*. showed that 2D cultured hiPSC-CMs with ectopic expression of *RRAGD* variants displayed reduced TFEB nuclear translocation compared to WT *RRAGD*.[2]

Due to the normal mTORC1 and TFEB signaling activities in our immature zebrafish and hiPSC-CMs models (**chapters 3 and 4**), we suggest that the pathogenicity of *RRAGD* variants in the heart occurs postnatal when cardiomyocytes are mature and limitedly proliferating. Indeed, the bulk RNA-seq results in **chapter 4** suggest a dedifferentiating phenotype in our *RRAGD*$^{WT/p.(Ser76Leu)}$ hiPSC-CMs. In mammalian embryonic and fetal stages, cardiomyocytes are highly proliferative and regenerative to support development and survival. For example, the absence of *Rheb* from mice embryos is lethal and results in impaired heart development [19]. Moreover, cardiomyocyte-specific *Mtor* deletion (*cMtor*KO) causes consequential suppressed proliferation and increased apoptosis at the early stages of embryonic development [20]. After birth, classical views describe heart growth as a process mediated by volume expansion of cardiomyocytes rather than cardiomyocyte cellular division. Recent studies have unveiled that mature cardiomyocytes do have limited regenerative capability [21,22]. Thus, mTOR signaling is essential for maintaining cardiac structure and overall function in a physiological state and during adaptation to pressure overload in postnatal and adult hearts [23]. In the c*Mtor*KO mice study, mice that survived *in utero* phase developed cardiac hypertrophy and died by 10 weeks of age due to heart failure [20]. During adulthood, inducible cardiac

deletion of *Mtor* in mouse model results in a fatal DCM [24]. When exposed to pressure overload, mice models lacking *Mtor* and *Raptor* in the heart, often display failure to adapt to pressure overload, eventually leading to heart failure [24,25]. In a zebrafish injured heart model, amino acid activation of mTORC1 is enhanced, stimulating cardiomyocyte proliferation and supporting regeneration [26]. Altogether, these studies emphasize the critical role of mTOR signaling in promoting cardiomyocyte proliferation and regeneration, with its activity being high during development and diminished in the postnatal period. For ADKH-*RRAGD*, this means that future studies should focus on how the *RRAGD* variants affect the transition of cardiomyocytes from fetal to postnatal state, as well as how these variants influence mTORC1 activity in the context of cardiac stress and adaptation.

In addition to inactivation of mTORC1, multiple studies have explored the implications of mTORC1 hyperactivation on cardiac function and demonstrated that sustained and chronic mTORC1 hyperactivation is maladaptive to the heart.[27-29] mTORC1 hyperactivation was induced through cardiac-specific deletion of tuberous sclerosis complex 2 (*Tsc2*) or muscle-specific deletion of folliculin (*Flcn*) genes, resulting in cardiac hypertrophy.[27-29] In these studies, the transgenic mice displayed impaired cardiac function and developed DCM,[27,28] except in the study conducted by Davogustto et al., wherein mice lacking cardiomyocyte *Tsc2* presented with non-lethal concentric left ventricular hypertrophy.[29] At the molecular level, alterations such as inhibited autophagic flux, elevated ATP levels, increased mitochondrial function, and metabolic shifts towards glycolysis have been demonstrated.[27-29] These investigations hinted at how constitutive mTORC1 activation due to *RRAGD* variants might result in DCM.

Future perspectives

In this thesis, we confirmed the importance of RagD in maintaining cardiac function and integrity and showed the pathogenicity of *RRAGD* variants in the heart. However, the mechanisms that underlie DCM remain elusive. Our RNA sequencing results showed dysregulation of genes related to non-sarcomere cytoskeleton organization and muscle development pathways, indicative of a less differentiated phenotype than *RRAGD* WT expressing cardiomyocytes. Therefore, we hypothesize that mTORC1 constitutive activation due to *RRAGD* variants maintains the cardiomyocytes in an immature state. This ultimately drives the DCM progression in the patients (Figure 1). Due to the necessity of mTORC1 activation during heart development, it is possible that the pathogenicity of the variants is not yet apparent. However, in the postnatal stage, when mTORC1 activity should be low, we speculate that the constant activation of mTORC1 impairs the cardiomyocyte maturation process by keeping the

fetal genes expression, glycolytic metabolism, and cellular proliferation. To confirm this, future studies should investigate whether cardiomyocyte dedifferentiation occurs, for example, by measuring proliferating cell populations, looking at the cellular ultrastructure, and measuring metabolism in these cells.

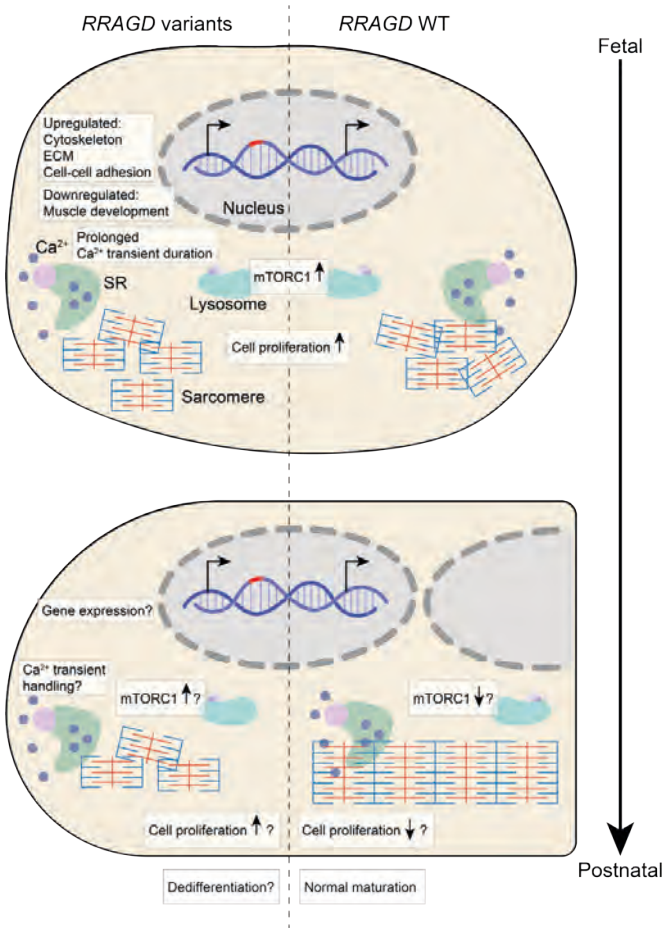

Figure 1. Proposed molecular mechanisms underlying cardiomyocyte defects in ADKH-*RRAGD*. In hiPSC-CMs, *RRAGD* variants caused prolonged Ca^{2+} transient duration and changes in the expression of genes related to muscle development, actin cytoskeleton, extracellular matrix, and cell-cell adhesion. We proposed that these phenotypes are suggestive of less differentiated cardiomyocytes. During the fetal stage, mTORC1 activity is maintained high in cardiomyocytes to support growth and proliferation. Postnatally, mTORC1 activity is reduced in cardiomyocytes. However, as *RRAGD* variants induce the constitutive activation of mTORC1, we hypothesized that this retains the cardiomyocytes in an immature, early embryonic-like state. ECM: extracellular matrix, mTORC1: mechanistic target of rapamycin complex 1, SR: sarcoplasmic reticulum, WT: wild type.

A clear limitation of the studies in **chapters 3 and 4** is the immaturity of the models, which prevents further investigation into the molecular mechanisms underlying DCM in ADKH-*RRAGD*. Uncovering these mechanisms will be essential for designing targeted therapeutic strategies in patients. Nevertheless, we understand now that development and aging have roles in this disease. Therefore, future research should carefully control these factors to fully understand how *RRAGD* variants cause DCM. This can be done, for example, by creating a transgenic zebrafish line or a mammalian model for ADKH-*RRAGD*. Moreover, due to rapid development in the field, it is now possible to study this in more human-based cell models, such as 3D cultured cardiac organoids, which will reflect human physiology more closely (reviewed in [30]).

Kidney tubulopathy in ADKH-*RRAGD*

Among the 36 identified ADKH-*RRAGD* patients, kidney tubulopathy characterized by hypomagnesemia, hypercalciuria, hypokalemia, and nephrocalcinosis remains the most prominent hallmark of this disease (**chapter 2**). These symptoms resemble familial hypomagnesemia with hypercalciuria and nephrocalcinosis (FHHNC), where impaired Mg^{2+} and Ca^{2+} transport in the thick ascending limb (TAL) occurs.[31,32] Paracellular transport of Mg^{2+} and Ca^{2+} in the TAL is mediated by the tight junction proteins Claudin-16 and -19. Loss-of-function mutations in genes encoding these proteins are associated with FHHNC.[31,32] Moreover, a subset of ADKH-*RRAGD* patients presented with hypomagnesemia and hypokalemic alkalosis without hypercalciuria and nephrocalcinosis, resembling a mix of Bartter type III and Gitelman syndrome, in which impaired electrolyte transport distal convoluted tubule (DCT) occurs.[33-35] Bartter syndrome type III is associated with loss-of-function mutations in the chloride channel Kb (*CLCNKB*), encoding the basolateral TAL and DCT Cl^- exporter ClC-Kb.[36] Gitelman syndrome is attributed to inactivating mutations in the apical Na^+-Cl^- cotransporter (NCC), which is localized in the DCT.[33] The observed hypokalemia is suggested to be multifactorial, potentially including K^+ wasting resulting from increased Na^+ delivery and reabsorption by the distal nephron.[37] This causes an increase in the apical renal outer medullary K^+ channel (ROMK) activity, which facilitates K^+ efflux into the pro-urine. The etiology of hypomagnesemia remains a subject of debate, though it has been proposed to be linked to K^+ loss.[38] Additionally, mice lacking NCC had a reduced abundance of the transient receptor potential melastatin type 6 (TRPM6).[39] This suggests that TRPM6 downregulation is involved in Gitelman syndrome. Due to the similarities between ADKH-*RRAGD* and FHHNC, as well as Bartter type III and Gitelman syndrome, we hypothesized that kidney tubulopathy in ADKH-*RRAGD* originates from defects in

the paracellular Mg^{2+} and Ca^{2+} transport in the TAL and DCT. This can be due to the direct impact of mTORC1 constitutive activation on Mg^{2+} and Ca^{2+} transport or secondary via impaired Na^+ transport in these segments. In the TAL, the Na^+ reabsorption mediated by the Na^+-K^+-$2Cl^-$ cotransporter 2 (NKCC2) influences the permeability of Claudin-16 and Claudin-19 by the positive lumen membrane potential. Indeed, in the murine kidney, *RRAGD* is predominantly expressed in the TAL and DCT segments. [1,40]

The underlying mechanisms: the hypotheses

One of the most important questions surrounding kidney tubulopathy in ADKH-*RRAGD* is how mTORC1 and Rag GTPases regulate electrolyte transport in the TAL and the DCT. In the TAL, most studies showed that inhibition of mTOR activity with pharmacological intervention or deletion of mTORC1 components in the kidney, such as the *Raptor* gene, reduces the protein expression of NKCC2.[41,42] Mice with kidney-specific *Raptor* deletion experienced polyuria, polydipsia, and an elevated urinary excretion of Ca^{2+} and Mg^{2+}.[41] Response to furosemide, a loop diuretic that blocks NKCC2 activity, was blunted in these animals and was accompanied by loss of mTORC1 activity and reduced protein expression of NKCC2.[41] Interestingly, Wistar rats treated with sirolimus, also known as rapamycin, experienced a lowering of serum K^+ and Mg^{2+} and greater urinary excretion of K^+ and Mg^{2+}, as well as polyuria and polydipsia.[42] This was accompanied by less NKCC2 protein expression.[42] In the DCT, data on how mTOR activity affects NCC and TRPM6 are conflicting. In mice lacking kidney *Raptor*, NCC expression at the protein level is decreased.[41] However, mTORC1 inhibition by rapamycin treatment in WT rats demonstrated normal NCC protein expression.[43] TRPM6 protein expression in sirolimus-treated rats is enhanced, while rapamycin treatment in NRK-52e cells reduced TRPM6 mRNA expression.[42,44] Thus, mTORC1 inhibition dysregulates the expression of NKCC2, NCC, and TRPM6, and causes Ca^{2+}, Mg^{2+}, and K^+ wasting. Indeed, in renal transplant recipients, prolonged consumption of mTOR inhibitors as immunosuppression has been linked to hypomagnesemia. Interestingly, *RRAGD* variants result in mTORC1 constitutive activation instead of inhibition and still cause kidney tubulopathy in the patients. We speculate that this disparity might be similar to that seen in the heart, where both inactivation and hyperactivation of mTORC1 lead to detrimental effects, suggesting that the balance in the signaling pathway activation is needed for electrolyte homeostasis. Therefore, based on these previous studies, we hypothesized that *RRAGD* variants induced kidney tubulopathy by reducing the expression of NKCC2 and NCC, thereby causing the phenotypes seen in ADKH-*RRAGD* patients (Figure 2). In **chapter 2**, we assessed the functions of NKCC2 and NCC in ADKH-*RRAGD* patients carrying the p.(Thr97Pro) variant to identify the

origin of kidney tubulopathy in ADKH-*RRAGD* patients. To do this, we assessed the patients' renal response to the furosemide and hydrochlorothiazide (HCT; NCC inhibitor) diuretics. In this thesis, we demonstrated that the patients' responses to furosemide and HCT diuretics were preserved, as indicated by the fractional excretion of Cl^- comparable to that of healthy controls.[45] This suggests that NKCC2 and NCC function normally in these patients. However, this study was only conducted in one family and therefore, should be confirmed in other patients with different *RRAGD* variants.

Given the phenotypic similarities between FHHNC and ADKH-*RRAGD*, it is also possible that mTORC1 constitutive activation affects Claudin-16 and -19 activity. Currently, it is unknown whether mTOR affects the expression and/or activity of Claudin-16 and -19. Nonetheless, mTOR activity has been shown to be influenced by Ca^{2+} sensing receptor (CaSR) activation in proximal tubule cell lines that exhibit reduced expression of polycystin 1 (*PKD1*).[46] In the TAL, CaSR regulates the activity of Claudin-16 and -19 in response to high intracellular Ca^{2+} levels by increasing *CLDN14* transcription.[47] Claudin-14, which is encoded by the *CLDN14* gene, is a tight junction protein that interacts with Claudin-16 within the Claudin-16 and -19 complex.[47] Through this interaction, Claudin-14 reduces the cation permeability of the Claudin-16 and -19 complex, thereby decreasing Mg^{2+} and Ca^{2+} reabsorption in the TAL.[47] Therefore, it would be important to investigate whether Claudin-16 and -19 function is inhibited via the CaSR-Claudin-14 axis in ADKH-*RRAGD* (Figure 2).

Future perspectives

Chapter 2 of this thesis provides insight into kidney tubulopathy in ADKH-*RRAGD,* with many opportunities still available for future research. First, a diuretic challenge was conducted on one ADKH-*RRAGD* family carrying the *RRAGD* p.(Thr97Pro) variant. In this family, hypercalciuria and nephrocalcinosis are absent.[1] It would also be beneficial to carry out this challenge on patients displaying the full spectrum of kidney tubulopathy for a thorough phenotypic characterization, including those with p.(Ser76Leu) and p.(Ser77Phe) *RRAGD* variants. Further testing in more patients will aid in fully characterizing the NKCC2 and NCC functionalities in ADKH-*RRAGD*. Second, it is important to investigate how *RRAGD* variants affect the expression and functionality of the electrolyte transporters suspected to be involved in kidney tubulopathy (i.e., NKCC2, NCC, TRPM6, TRPV5, Claudin-16, and Claudin-19) in experimental models. Lastly, several patients who have undergone heart transplants are currently receiving immunosuppressant therapies. One patient with the *RRAGD* p.(Ser77Phe) variant is being treated with everolimus, a rapamycin derivative. Given that chronic use of rapamycin in transplant recipients

is recognized to induce hypomagnesemia, it would be intriguing to determine whether hypomagnesemia is alleviated or worsened in this patient.

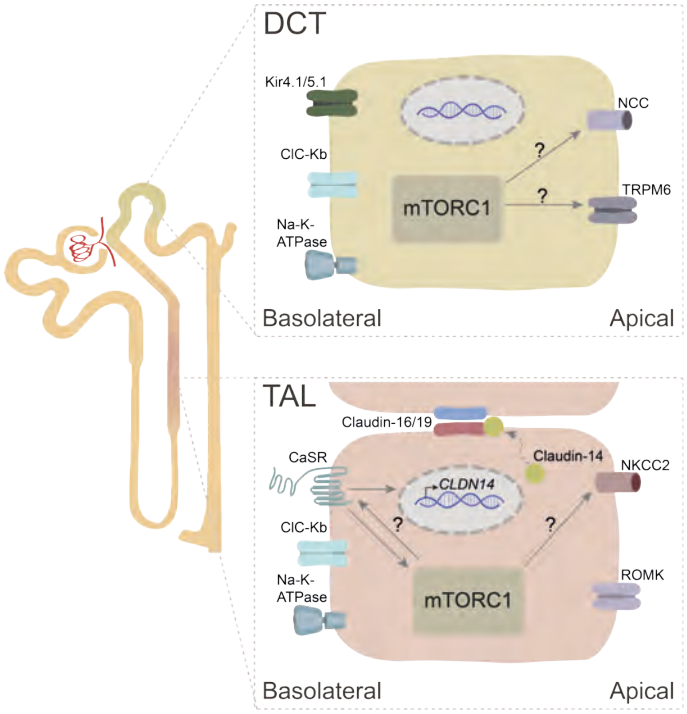

Figure 2. Hypothesized molecular mechanisms of kidney tubulopathy in ADKH-*RRAGD*. In the nephron, mTORC1 constitutive activation due to *RRAGD* variants impairs electrolyte transports in the TAL and DCT segments. In the TAL, mTORC1 activity is known to influence NKCC2 protein expression. NKCC2 activity drives the paracellular transport of Mg^{2+} and Ca^{2+} via the tight junction proteins Claudin-16 and -19. How *RRAGD* variants and mTORC1 activity affect NKCC2 in ADKH-*RRAGD* remains elusive. Moreover, CaSR activation has been linked to mTORC1 activation. CaSR activation induces the transcription of *CLDN14*, which encodes for Claudin-14. Claudin-14 interacts with Claudin-16 and blocks Mg^{2+} and Ca^{2+} paracellular transport in this manner. We hypothesized that mTORC1 activity affects Claudin-16 and -19 function via the CaSR-Claudin-14 axis. In the DCT, loss of mTORC1 lowered the protein expression of NCC and mRNA of TRPM6. CaSR: Ca^{2+} sensing receptor, ClC-Kb: Cl^- channel Kb, Kir4.1/5.1: inwardly rectifying K^+ channel 4.1 and 5.1, mTORC1: mechanistic target of rapamycin 1, NCC: Na^+-Cl^- cotransporter, NKCC2: Na^+-K^+-$2Cl^-$ cotransporter 2, ROMK: renal outer medullary K^+ channel, TRPM6: transient receptor potential melastatin 6.

Functional studies and investigations into the molecular mechanisms of ADKH-*RRAGD* in the kidney have been hampered by the absence of an appropriate study model. Since Mg^{2+} and Ca^{2+} transport in the TAL occurs paracellularly, a fully polarized cell model with tight junction formation is essential for accurately

mimicking *in vivo* conditions. One approach is to utilize animal models, such as a mouse line carrying one of the *RRAGD* variants, and perform electrophysiological measurements using microdissected TAL tubules [48] along with metabolic and molecular parameters. Another strategy is to develop kidney organoids and tubuloids from iPSCs derived from patients or using the *RRAGD*$^{WT/p.(Ser76Leu)}$ iPSCs generated in **chapter 4,** and perform functional assays to measure electrolyte transport capabilities in these organoids. The advantage of kidney organoids and tubuloids over a mouse model is that the source of cells can be human, making them more comparable to the patients (reviewed in [49]).

Genotype-phenotype correlation

One challenge in understanding the molecular mechanism of ADKH-*RRAGD* is the allelic heterogeneity of this disease. In our initial study, we described patients with varying degrees of clinical manifestations and mTORC1 activation.[1] Cells overexpressing the *RRAGD* p.(Ser76Leu) variant exhibited the strongest mTORC1 activation compared to other variants, and most patients with this variant display kidney tubulopathy and DCM (**chapters 2 and 4**). Conversely, cells overexpressing the *RRAGD* p.(Thr97Pro) variant induce mTORC1 activation to a lesser extent, while patients with this mutation primarily experience hypomagnesemia without hypercalciuria and nephrocalcinosis, and do not exhibit DCM.[1] Thus, we hypothesized that the level of mTORC1 activation correlates with the severity of clinical manifestations. Indeed, in **chapters 3 and 4**, we demonstrated that the p.(Ser76Leu) variant caused cardiac dysfunctions in zebrafish embryos and resulted in the strongest mTORC1 constitutive activation compared to other variants. Additionally, 5 out of 8 patients containing this variant experienced the full phenotypic spectrum of ADKH-*RRAGD* (i.e., kidney tubulopathy and DCM), making this variant the most prevalent and causing the most severe phenotype. Furthermore, we investigated the effects of three novel *RRAGD* variants (i.e., p.(Ser77Phe), p.(Thr91Ile), and p.(Ile100Arg)) on mTORC1 activity (**chapter 2**). We found that, similar to other *RRAGD* variants [2], the p.(Ser77Phe) and p.(Ile100Arg) variants cause constitutive activation of mTORC1 non-canonical signaling. In contrast, the *RRAGD* p.(Thr91Ile) variant did not alter mTORC1 activation, in line with the milder phenotypes, as in p.(Thr97Pro) variant in our previous study. Therefore, data from this thesis suggest that *RRAGD* variants-induced mTORC1 constitutive activation correlates with disease severity. Interestingly, patients with the *RRAGD* p.(Ile100Arg) exhibit the same range of symptoms as the patients carrying the p.(Thr91Ile) variant (i.e., kidney tubulopathy without DCM), suggesting

more factors other than the genotype itself play a role in determining patients' phenotype. Which factors are at play need to be elucidated in future investigations.

Clinical implications

With 24 patients initially identified worldwide, the characterization of ADKH-*RRAGD* patients' phenotypes remains limited. As a more comprehensive characterization is crucial for understanding the disease pathogenesis and developing therapeutic approaches, **chapter 2** expanded the patient cohort to 36 patients, enabling a more thorough characterization of the patients' phenotypes. The onset of the disease is mainly during childhood, with some adult cases. For patient management, it is most interesting for healthcare providers and families to understand whether patients who currently display kidney tubulopathy will develop DCM. For now, because DCM onset in both childhood and adulthood is observed, it is best to continue monitoring the cardiac functions of the patients. Furthermore, currently, 40% of all female patients and 21% of all male patients developed DCM. Whether sex is a factor at play in the clinical manifestations should be investigated when more patients are diagnosed and a long-term follow-up. Additionally, in more than half of the identified patients, kidney tubulopathy occurs without DCM, suggesting that the two phenotypes can be independent of each other. For future patient diagnosis, it would be important to also screen idiopathic DCM patient cohorts in addition to idiopathic tubulopathy cohorts. Thus, the results of the studies in this thesis raise awareness of this rare disease and will ultimately assist in diagnosing more patients.

Therapeutic perspectives

Currently, ADKH-*RRAGD* patients are receiving magnesium and potassium supplementation to manage kidney tubulopathy, and are receiving RAS and ACE inhibitors for heart failure. Due to a lack of understanding of the disease pathogenesis, a more directed therapy that targets the root cause of the problem is currently unavailable. In **chapter 2**, we demonstrated the benefits of taking dapagliflozin, a drug belonging to the Na^+-glucose cotransporter 2 (SGLT2) inhibitor class, in alleviating hypomagnesemia in ADKH-*RRAGD* patients. Prior to our study, a few ADKH-*RRAGD* patients were prescribed SGLT2 inhibitors to manage heart failure.[1,2] However, whether hypomagnesemia was alleviated in these patients was not investigated. Dapagliflozin is currently approved for clinical use for patients with heart failure and mildly reduced ejection fraction and to treat patients with refractory hypomagnesemia.[50-53] Interestingly, SGLT2 inhibitors also displayed

mTORC1 inhibitory properties *in vitro*.[54-56] In **chapter 3**, inhibition of mTORC1 with rapamycin rescued cardiac dysfunctions in zebrafish embryos overexpressing p.(Ser76Leu) and p.(Pro119Arg) *RRAGD* variants. However, we were not able to show that mTORC1 overactivation was present in these fish. This prompts the question of whether rapamycin treatment specifically addresses the pathogenic mTOR dysfunction caused by *RRAGD* variants in our model or if it acts through a broader mechanism to improve cardiac dysfunctions, as demonstrated in numerous studies.[57-59] Regardless, it would be interesting to study if the increased serum Mg^{2+} is due to mTORC1 inhibition.

Several more targeted therapeutic approaches remain to be explored. One approach would be the restoration of the microphthalmia/transcription factor E (MiT/TFE) members function, which includes TFEB. TFEB dysfunction has been proposed as the root cause of ADKH-*RRAGD*, particularly the DCM. In other studies, the loss of RagA/B and the *RRAGC* p.(Ser75Tyr) variant resulted in TFEB's inability to translocate to the nucleus, ultimately causing cardiac dysfunction in mice and zebrafish models.[8,16] Interestingly, restoring functional TFEB through ectopic expression of *tfeb* in *rragc* p.(Ser75Tyr) transgenic zebrafish re-established cardiac function and improved the survivability of the fish.[8] For the patients, the fastest available treatment option would be to use clinically approved TFEB agonists, digoxin, ikarugamycin, and alexidine dihydrochloride.[60] However, side effects of these drugs should be carefully evaluated before prescribing them to patients. For example, although digoxin has been prescribed for the management of systolic dysfunction in patients with congestive heart failure (CHF), its toxicity due to long-term use results in life-threatening side effects such as ventricular arrhythmias.[61] Another potential therapeutic approach that has been used in clinics is adeno-associated virus (AAV) vector-based gene therapy.[62,63] Using such an AAV vector, delivery of functional TFEB would be possible, but this would require safety and efficacy testing to obtain clinical approval. Another potential therapeutic approach for ADKH-*RRAD* is restoring RagD functions through gene therapy. Unlike loss-of-function diseases, gain-of-function or dominant-negative diseases like ADKH-*RRAGD* are more challenging to address with gene therapy. Simply introducing a functional copy of the gene is insufficient, as the pathological effects of the mutant protein persist. Antisense oligonucleotide (ASO)-based therapies are promising for such diseases due to their target specificity and ability to degrade specific mRNA or even remove a specific protein domain (reviewed in [64]). Before exploring this option, it is crucial to evaluate how *RRAGD* mRNA knockdown is tolerated by the cell to avoid introducing further harm. For instance, if *RRAGD* haploinsufficiency is tolerated in the organism or if it could lead to more complications, which were

seen previously in other genetic diseases.[65,66] Alternatively, Jones *et al*. recently combined two approaches called knockdown-replace gene therapy in a dynamin-1 (*DNM1*) developmental and epileptic encephalopathy mouse model.[67] In these mice, the expression of the mutant *Dnm1* gene was knocked down using interfering RNA (RNAi), while simultaneously providing *Dnm1* cDNA, both encoded in an AAV9 vector.[67] However, this approach is still in the pre-clinical stage and would require more evidence before the combination of knockdown-replace gene therapy can be brought into the clinic.

In summary, each therapeutic approach discussed here has its own advantages and disadvantages. From the disease mechanisms perspective, restoring RagD functions by means of knockdown would be the ideal therapeutic approach because it directly targets the main cause of the disease. However, once the mechanisms that drive ADKH-*RRAGD* pathogenesis have been confirmed, dampening mTORC1 activation with its clinically approved inhibitors and restoring TFEB function using the clinically approved TFEB agonists would offer the most immediate and accessible therapeutic strategy. Therefore, this indicates a need for a more thorough investigation of the underlying molecular mechanisms of ADKH-*RRAGD*. Ultimately, a deeper understanding of ADKH-*RRAGD* mechanisms will assist in developing more targeted therapies and also aid in identifying biomarkers that can guide treatment decisions.

Conclusion

In conclusion, this thesis sheds light on the pathogenesis and therapeutic prospects of ADKH-*RRAGD*. Future research should further clarify the molecular mechanisms underlying ADKH-*RRAGD* in more physiologically relevant models. Understanding how *RRAGD* variants disrupt protein function and contribute to kidney tubulopathy and DCM is essential for enhancing our knowledge of the disease and identifying therapeutic strategies.

References

1. Schlingmann KP, Jouret F, Shen K, et al. mTOR-Activating Mutations in RRAGD Are Causative for Kidney Tubulopathy and Cardiomyopathy. *J Am Soc Nephrol.* 2021;32(11):2885-2899.
2. Sambri I, Ferniani M, Campostrini G, et al. RagD auto-activating mutations impair MiT/TFE activity in kidney tubulopathy and cardiomyopathy syndrome. *Nat Commun.* 2023;14(1):2775.
3. Trepiccione F, Sambri I, Ruggiero B, et al. RRAGD-Associated Autosomal Dominant Kidney Hypomagnesemia with Cardiomyopathy: A Review on the Clinical Manifestations and Therapeutic Options. *Kidney Blood Press Res.* 2024;49(1):637-645.
4. Adella A, Tengku F, Arjona FJ, et al. RRAGD variants cause cardiac dysfunction in a zebrafish model. *Am J Physiol Heart Circ Physiol.* 2024;327(5):H1187-H1197.
5. Cui Z, Napolitano G, de Araujo MEG, et al. Structure of the lysosomal mTORC1-TFEB-Rag-Ragulator megacomplex. *Nature.* 2023;614(7948):572-579.
6. Napolitano G, Di Malta C, Esposito A, et al. A substrate-specific mTORC1 pathway underlies Birt-Hogg-Dube syndrome. *Nature.* 2020;585(7826):597-602.
7. Gollwitzer P, Grutzmacher N, Wilhelm S, Kummel D, Demetriades C. A Rag GTPase dimer code defines the regulation of mTORC1 by amino acids. *Nat Cell Biol.* 2022;24(9):1394-1406.
8. Kim M, Lu L, Dvornikov AV, et al. TFEB Overexpression, Not mTOR Inhibition, Ameliorates RagC(S75Y) Cardiomyopathy. *Int J Mol Sci.* 2021;22(11).
9. Rogala KB, Gu X, Kedir JF, et al. Structural basis for the docking of mTORC1 on the lysosomal surface. *Science.* 2019;366(6464):468-475.
10. Anandapadamanaban M, Masson GR, Perisic O, et al. Architecture of human Rag GTPase heterodimers and their complex with mTORC1. *Science.* 2019;366(6462):203-210.
11. Acharya A, Demetriades C. mTORC1 activity licenses its own release from the lysosomal surface. *Mol Cell.* 2024;84(22):4385-4400 e4387.
12. Okosun J, Wolfson RL, Wang J, et al. Recurrent mTORC1-activating RRAGC mutations in follicular lymphoma. *Nat Genet.* 2016;48(2):183-188.
13. Long PA, Zimmermann MT, Kim M, Evans JM, Xu X, Olson TM. De novo RRAGC mutation activates mTORC1 signaling in syndromic fetal dilated cardiomyopathy. *Hum Genet.* 2016;135(8):909-917.
14. Reijnders MRF, Seibt A, Brugger M, et al. De novo missense variants in RRAGC lead to a fatal mTORopathy of early childhood. *Genet Med.* 2023;25(7):100838.
15. Chen JH, Huang C, Zhang B, et al. Mutations of RagA GTPase in mTORC1 Pathway Are Associated with Autosomal Dominant Cataracts. *PLoS Genet.* 2016;12(6):e1006090.
16. Kim YC, Park HW, Sciarretta S, et al. Rag GTPases are cardioprotective by regulating lysosomal function. *Nat Commun.* 2014;5:4241.
17. Garbern JC, Helman A, Sereda R, et al. Inhibition of mTOR Signaling Enhances Maturation of Cardiomyocytes Derived From Human-Induced Pluripotent Stem Cells via p53-Induced Quiescence. *Circulation.* 2020;141(4):285-300.
18. Paltzer WG, Aballo TJ, Bae J, et al. mTORC1 regulates the metabolic switch of postnatal cardiomyocytes during regeneration. *J Mol Cell Cardiol.* 2024;187:15-25.
19. Goorden SM, Hoogeveen-Westerveld M, Cheng C, et al. Rheb is essential for murine development. *Mol Cell Biol.* 2011;31(8):1672-1678.
20. Zhu Y, Pires KM, Whitehead KJ, et al. Mechanistic target of rapamycin (Mtor) is essential for murine embryonic heart development and growth. *PLoS One.* 2013;8(1):e54221.

21. Bergmann O, Bhardwaj RD, Bernard S, et al. Evidence for cardiomyocyte renewal in humans. *Science.* 2009;324(5923):98-102.

22. Bergmann O, Zdunek S, Felker A, et al. Dynamics of Cell Generation and Turnover in the Human Heart. *Cell.* 2015;161(7):1566-1575.

23. Sciarretta S, Volpe M, Sadoshima J. Mammalian target of rapamycin signaling in cardiac physiology and disease. *Circ Res.* 2014;114(3):549-564.

24. Zhang D, Contu R, Latronico MV, et al. MTORC1 regulates cardiac function and myocyte survival through 4E-BP1 inhibition in mice. *J Clin Invest.* 2010;120(8):2805-2816.

25. Shende P, Plaisance I, Morandi C, et al. Cardiac raptor ablation impairs adaptive hypertrophy, alters metabolic gene expression, and causes heart failure in mice. *Circulation.* 2011;123(10):1073-1082.

26. Miklas JW, Levy S, Hofsteen P, et al. Amino acid primed mTOR activity is essential for heart regeneration. *iScience.* 2022;25(1):103574.

27. Hasumi Y, Baba M, Hasumi H, et al. Folliculin (Flcn) inactivation leads to murine cardiac hypertrophy through mTORC1 deregulation. *Hum Mol Genet.* 2014;23(21):5706-5719.

28. Taneike M, Nishida K, Omiya S, et al. mTOR Hyperactivation by Ablation of Tuberous Sclerosis Complex 2 in the Mouse Heart Induces Cardiac Dysfunction with the Increased Number of Small Mitochondria Mediated through the Down-Regulation of Autophagy. *PLoS One.* 2016;11(3):e0152628.

29. Davogustto GE, Salazar RL, Vasquez HG, et al. Metabolic remodeling precedes mTORC1-mediated cardiac hypertrophy. *J Mol Cell Cardiol.* 2021;158:115-127.

30. Campostrini G, Windt LM, van Meer BJ, Bellin M, Mummery CL. Cardiac Tissues From Stem Cells: New Routes to Maturation and Cardiac Regeneration. *Circ Res.* 2021;128(6):775-801.

31. Praga M, Vara J, Gonzalez-Parra E, et al. Familial hypomagnesemia with hypercalciuria and nephrocalcinosis. *Kidney Int.* 1995;47(5):1419-1425.

32. Simon DB, Lu Y, Choate KA, et al. Paracellin-1, a renal tight junction protein required for paracellular Mg2+ resorption. *Science.* 1999;285(5424):103-106.

33. Simon DB, Nelson-Williams C, Bia MJ, et al. Gitelman's variant of Bartter's syndrome, inherited hypokalaemic alkalosis, is caused by mutations in the thiazide-sensitive Na-Cl cotransporter. *Nat Genet.* 1996;12(1):24-30.

34. Jeck N, Konrad M, Peters M, Weber S, Bonzel KE, Seyberth HW. Mutations in the chloride channel gene, CLCNKB, leading to a mixed Bartter-Gitelman phenotype. *Pediatr Res.* 2000;48(6):754-758.

35. Zelikovic I, Szargel R, Hawash A, et al. A novel mutation in the chloride channel gene, CLCNKB, as a cause of Gitelman and Bartter syndromes. *Kidney Int.* 2003;63(1):24-32.

36. Simon DB, Bindra RS, Mansfield TA, et al. Mutations in the chloride channel gene, CLCNKB, cause Bartter's syndrome type III. *Nat Genet.* 1997;17(2):171-178.

37. Moes AD, van der Lubbe N, Zietse R, Loffing J, Hoorn EJ. The sodium chloride cotransporter SLC12A3: new roles in sodium, potassium, and blood pressure regulation. *Pflugers Arch.* 2014;466(1):107-118.

38. Huang CL, Kuo E. Mechanism of hypokalemia in magnesium deficiency. *J Am Soc Nephrol.* 2007;18(10):2649-2652.

39. Nijenhuis T, Vallon V, van der Kemp AW, Loffing J, Hoenderop JG, Bindels RJ. Enhanced passive Ca2+ reabsorption and reduced Mg2+ channel abundance explains thiazide-induced hypocalciuria and hypomagnesemia. *J Clin Invest.* 2005;115(6):1651-1658.

40. Karlsson M, Zhang C, Mear L, et al. A single-cell type transcriptomics map of human tissues. *Sci Adv.* 2021;7(31).
41. Grahammer F, Haenisch N, Steinhardt F, et al. mTORC1 maintains renal tubular homeostasis and is essential in response to ischemic stress. *Proc Natl Acad Sci U S A.* 2014;111(27):E2817-2826.
42. da Silva CA, de Braganca AC, Shimizu MH, et al. Rosiglitazone prevents sirolimus-induced hypomagnesemia, hypokalemia, and downregulation of NKCC2 protein expression. *Am J Physiol Renal Physiol.* 2009;297(4):F916-922.
43. Cui Y, Huang Q, Auman JT, et al. Genomic-derived markers for early detection of calcineurin inhibitor immunosuppressant-mediated nephrotoxicity. *Toxicol Sci.* 2011;124(1):23-34.
44. Ikari A, Sanada A, Sawada H, Okude C, Tonegawa C, Sugatani J. Decrease in transient receptor potential melastatin 6 mRNA stability caused by rapamycin in renal tubular epithelial cells. *Biochim Biophys Acta.* 2011;1808(6):1502-1508.
45. Bech AP, Wetzels JFM, Nijenhuis T. Reference values of renal tubular function tests are dependent on age and kidney function. *Physiol Rep.* 2017;5(23).
46. Di Mise A, Tamma G, Ranieri M, et al. Activation of Calcium-Sensing Receptor increases intracellular calcium and decreases cAMP and mTOR in PKD1 deficient cells. *Sci Rep.* 2018;8(1):5704.
47. Gong Y, Renigunta V, Himmerkus N, et al. Claudin-14 regulates renal Ca(+)(+) transport in response to CaSR signalling via a novel microRNA pathway. *EMBO J.* 2012;31(8):1999-2012.
48. Plain A, Wulfmeyer VC, Milatz S, et al. Corticomedullary difference in the effects of dietary Ca(2)(+) on tight junction properties in thick ascending limbs of Henle's loop. *Pflugers Arch.* 2016;468(2):293-303.
49. Dilmen E, Orhon I, Jansen J, Hoenderop JGJ. Advancements in kidney organoids and tubuloids to study (dys)function. *Trends Cell Biol.* 2024;34(4):299-311.
50. Authors/Task Force M, McDonagh TA, Metra M, et al. 2023 Focused Update of the 2021 ESC Guidelines for the diagnosis and treatment of acute and chronic heart failure: Developed by the task force for the diagnosis and treatment of acute and chronic heart failure of the European Society of Cardiology (ESC) With the special contribution of the Heart Failure Association (HFA) of the ESC. *Eur J Heart Fail.* 2024;26(1):5-17.
51. Zannad F, Ferreira JP, Pocock SJ, et al. SGLT2 inhibitors in patients with heart failure with reduced ejection fraction: a meta-analysis of the EMPEROR-Reduced and DAPA-HF trials. *Lancet.* 2020;396(10254):819-829.
52. Arbelo E, Protonotarios A, Gimeno JR, et al. 2023 ESC Guidelines for the management of cardiomyopathies. *Eur Heart J.* 2023;44(37):3503-3626.
53. Ray EC, Boyd-Shiwarski CR, Liu P, Novacic D, Cassiman D. SGLT2 Inhibitors for Treatment of Refractory Hypomagnesemia: A Case Report of 3 Patients. *Kidney Med.* 2020;2(3):359-364.
54. Schaub JA, AlAkwaa FM, McCown PJ, et al. SGLT2 inhibitors mitigate kidney tubular metabolic and mTORC1 perturbations in youth-onset type 2 diabetes. *J Clin Invest.* 2023;133(5):e164486.
55. Tuttle KR. Digging deep into cells to find mechanisms of kidney protection by SGLT2 inhibitors. *J Clin Invest.* 2023;133(5).
56. Li X, Lu Q, Qiu Y, et al. Direct Cardiac Actions of the Sodium Glucose Co-Transporter 2 Inhibitor Empagliflozin Improve Myocardial Oxidative Phosphorylation and Attenuate Pressure-Overload Heart Failure. *J Am Heart Assoc.* 2021;10(6):e018298.
57. Kushwaha S, Xu X. Target of rapamycin (TOR)-based therapy for cardiomyopathy: evidence from zebrafish and human studies. *Trends Cardiovasc Med.* 2012;22(2):39-43.

58. Jin B, Shi H, Zhu J, Wu B, Geshang Q. Up-regulating autophagy by targeting the mTOR-4EBP1 pathway: a possible mechanism for improving cardiac function in mice with experimental dilated cardiomyopathy. *BMC Cardiovasc Disord.* 2020;20(1):56.

59. Wu W, Jin Q, Ostlund C, et al. mTOR Inhibition Prolongs Survival and Has Beneficial Effects on Heart Function After Onset of Lamin A/C Gene Mutation Cardiomyopathy in Mice. *Circ Heart Fail.* 2024;17(4):e011110.

60. Wang C, Niederstrasser H, Douglas PM, et al. Small-molecule TFEB pathway agonists that ameliorate metabolic syndrome in mice and extend C. elegans lifespan. *Nat Commun.* 2017;8(1):2270.

61. Cummings ED, Swoboda HD. Digoxin Toxicity. In: *StatPearls.* Treasure Island (FL)2025.

62. Naso MF, Tomkowicz B, Perry WL, 3rd, Strohl WR. Adeno-Associated Virus (AAV) as a Vector for Gene Therapy. *BioDrugs.* 2017;31(4):317-334.

63. Au HKE, Isalan M, Mielcarek M. Gene Therapy Advances: A Meta-Analysis of AAV Usage in Clinical Settings. *Front Med (Lausanne).* 2021;8:809118.

64. Lauffer MC, van Roon-Mom W, Aartsma-Rus A, Collaborative N. Possibilities and limitations of antisense oligonucleotide therapies for the treatment of monogenic disorders. *Commun Med (Lond).* 2024;4(1):6.

65. Ben-Shalom R, Keeshen CM, Berrios KN, An JY, Sanders SJ, Bender KJ. Opposing Effects on Na(V)1.2 Function Underlie Differences Between SCN2A Variants Observed in Individuals With Autism Spectrum Disorder or Infantile Seizures. *Biol Psychiatry.* 2017;82(3):224-232.

66. Wagnon JL, Barker BS, Ottolini M, et al. Loss-of-function variants of SCN8A in intellectual disability without seizures. *Neurol Genet.* 2017;3(4):e170.

67. Jones DJ, Soundararajan D, Taylor NK, et al. Effective knockdown-replace gene therapy in a novel mouse model of DNM1 developmental and epileptic encephalopathy. *Mol Ther.* 2024;32(10):3318-3330.

CHAPTER 6

Summary

Mechanistic target of rapamycin (mTOR) kinase is the key regulator of cell growth and proliferation. The two mTOR protein complexes, mTORC1 and mTORC2, work together to ensure cell growth, metabolism, and survival. Due to this central role of mTOR, its regulation is tightly controlled by a series of metabolic cues, including growth factors and amino acids. The Rag GTPase family serves as the intracellular amino acid sensor that can activate mTORC1. There are four members of the Rag GTPases: RagA, B, C, and D. Upon a series of upstream signaling due to amino acid presence, RagA and RagB bind to GTP, while Rag C and RagD bind to GDP. Then, RagA or RagB form a heterodimeric complex with RagC or RagD. In these nucleotide-binding states and heterodimers, the Rag GTPases recruit mTORC1 to the lysosomal surface. Subsequently, mTORC1 becomes activated and proceeds to prime its downstream targets to regulate protein synthesis, transcription, lipid synthesis, and inhibit autophagy. Due to this central role of Rag GTPases in mTORC1 activation, pathogenic variants in these genes have been associated with human diseases. Recently, heterozygous missense variants in *RRAGD* have been demonstrated that cause kidney tubulopathy and dilated cardiomyopathy (DCM) in a novel rare disease called autosomal dominant kidney hypomagnesemia with *RRAGD* variants (ADKH-*RRAGD*).

ADKH-*RRAGD*

ADKH-*RRAGD* was initially described in 2020, and key disease hallmarks include kidney tubulopathy, which comprises hypomagnesemia, hypokalemia, hypercalciuria, and nephrocalcinosis, as well as DCM. Despite this, the clinical and molecular etiology of this disease remains largely unidentified. Early studies on ADKH-*RRAGD* have shown that the variants in patients impair RagD's ability to bind GTP, resulting in a constitutively active nucleotide-free or constantly GDP-bound RagD. However, how the *RRAGD* variants influence the mTORC1 signaling pathway and contribute to disease pathogenesis is poorly understood. Moreover, allelic and phenotypic heterogeneity are evident among patients. Consequently, it is important to understand what factors influence disease outcomes. In this thesis, we focused on understanding the pathogenesis of ADKH-*RRAGD*. Specifically, we aimed to identify the cellular consequences of *RRAGD* variants and to investigate potential therapies for patients.

RRAGD variants constitutively activate mTORC1 signaling

In previous studies, *RRAGD* variants were shown to over-activate mTORC1 signaling. However, the disparity in findings prompted us to clarify how *RRAGD* variants affect

mTORC1 signaling. In **chapters 2 and 4**, we investigated the effects of *RRAGD* variants p.(Ser76Leu), p.(Ser77Phe), p.(Thr91Ile), and p.(Ile100Arg) on mTORC1 response to amino acid stimulation. We found that in the presence of amino acids, mTORC1 signaling in cells overexpressing the *RRAGD* variants was comparable to *RRAGD* wild-type (WT) cells. When depleted of amino acids, transcription factor EB (TFEB) phosphorylation (i.e., non-canonical mTORC1 signaling) prevailed in *RRAGD* p.(Ser76Leu), p.(Ser77Phe), and p.(Ile100Arg) cells. Only the p.(Ser76Leu) variant caused a significantly higher S6 kinase (S6K) phosphorylation (i.e., canonical mTORC1 signaling) than *RRAGD* WT, while p.(Ser77Phe) and p.(Ile100Arg) variants only caused a minor increase. This is in line with the fact that the p.(Ser76Leu) variant is the most prevalent variant so far, and it is also the variant that is most strongly associated with DCM. Interestingly, the *RRAGD* p.(Thr91Ile) variant did not affect mTORC1 signaling, which might fit the milder phenotype in the patients. Thus, we confirmed that *RRAGD* variants cause the constitutive activation of the mTORC1 signaling pathway. Moreover, we suggest that how *RRAGD* variants affect the level of mTORC1 activation may correlate with the disease severity.

RRAGD variants are the main driver of cardiac dysfunction in ADKH-*RRAGD*

To understand how the *RRAGD* variants cause cardiac dysfunction in ADKH-*RRAGD* patients, we used a zebrafish embryo model in **chapter 3**. We injected these embryos with mRNA of *RRAGD* WT, p.(Ser76Leu), or p.(Pro119Arg). Three days post-fertilization, zebrafish larvae overexpressing *RRAGD* variants developed pericardial edema and lowered cardiac function, which was measured by lowered fractional shortening and ejection fraction. Therefore, we have confirmed the pathogenicity of the *RRAGD* variants in the heart. To further understand the molecular mechanisms underlying the DCM in the patients, we generated human induced pluripotent stem cells (hiPSCs) carrying heterozygous *RRAGD* p.(Ser76Leu) variant in **chapter 4**. Next, these hiPSCs were differentiated into cardiomyocytes (hiPSC-CMs). Although mTORC1 signaling was undisturbed, electrophysiological assays revealed that the mutant hiPSC-CMs displayed a prolonged Ca^{2+} transient duration compared to WT hiPSC-CMs. This suggests that there is a delay in Ca^{2+} release and clearance from the cytosol due to the variant. Bulk RNA-seq further showed that the *RRAGD* p.(Ser76Leu) variant caused changes in gene expression; pathways related to cytoskeleton organization, such as the actin cytoskeleton, extracellular matrix, and cell-cell adhesion, were upregulated, while pathways related to muscle development were downregulated. Taken together, our results indicate a less

differentiated cardiomyocyte phenotype due to the *RRAGD* p.(Ser76Leu) variant. We speculate that this is due to the role of mTORC1 in cardiomyocytes, which is maintaining the balance between cell proliferation and differentiation.

The role of NKCC2 and NCC in ADKH-*RRAGD*

Kidney tubulopathy in ADKH-*RRAGD* resembles familial hypomagnesemia with hypercalciuria and nephrocalcinosis (FHHNC), as well as a mix of Bartter type III and Gitelman syndrome. This indicates that pathogenic RagD variants cause a defect in the thick ascending limb (TAL) and distal convoluted tubule (DCT). Indeed, RagD is mainly expressed in these two segments in mouse nephrons. In these segments, Mg^{2+}, Ca^{2+}, and K^+ transport is influenced by Na^+ reabsorption. In the TAL, Na^+ reabsorption is carried out by Na^+ -K^+-$2Cl^-$ cotransporter 2 (NKCC2). In the DCT, the Na^+ -Cl^- cotransporter (NCC) facilitates the influx of Na^+. To assess if NKCC2 and NCC functions are compromised in ADKH-*RRAGD*, patients from a family carrying the p.(Thr97Pro) were prescribed furosemide and hydrochlorothiazide (HCT) diuretics in **chapter 2**. Furosemide inhibits NKCC2, while HCT inhibits the NCC. We found that the fractional excretions of Cl^- and Mg^{2+} in the patients were comparable to those in healthy controls. This suggests that NKCC2 and NCC function normally in these patients.

Clinical implications and therapeutic perspectives

This work expanded the characterization of ADKH-*RRAGD* patients' phenotypes with **chapter 2**. Here, we described a new cohort of twelve ADKH-*RRAGD* patients carrying already identified variants and three new variants, p.(Ser77Phe), p.(Thr91Ile), and p.(Ile100Arg). In this cohort, kidney tubulopathy was also the most prominent phenotype. Taken together with previous reports, 36 ADKH-*RRAGD* patients have been identified so far. Aside from kidney tubulopathy, DCM is present in half of the patients. So far, the p.(Ser76Leu) variant is the most prevalent, as it is present in 8 patients. Moreover, this variant represents a mutation hotspot that is particularly associated with DCM, with 5 out of 8 patients carrying this variant developing DCM. Additionally, we found that while DCM primarily develops during childhood, several patients developed it in their second decade of life. This indicates that for patients with kidney tubulopathy, monitoring cardiac function is important. In future studies, identifying more patients will help determine other factors affecting disease outcomes, such as sex. Finally, all current patients were genetically diagnosed after the diagnosis of kidney tubulopathy. However, the

existence of patients with isolated kidney tubulopathy (i.e., no DCM) indicates that kidney tubulopathy and DCM may occur independently of each other. Therefore, *RRAGD* should be included not only in the kidney tubulopathy gene panel but also in cardiomyopathies of idiopathic origin to help more patients receive genetic diagnoses.

ADKH-*RRAGD* patients currently receive magnesium and potassium supplementation to manage hypomagnesemia and hypokalemia, as well as RAS, SGLT2, and ACE inhibitors for heart failure, which highlights the absence of targeted therapy. This thesis also evaluates therapeutic options for ADKH-*RRAGD* patients. In **chapter 2**, a 15-day treatment with dapagliflozin alleviated hypomagnesemia in these patients. **Chapter 3** describes how treatment with mTORC1 inhibitor rapamycin prevented cardiac dysfunction in zebrafish embryos overexpressing *RRAGD* variants. However, this thesis did not further investigate the molecular mechanisms by which dapagliflozin and rapamycin alleviated symptoms. Therefore, future research should aim to uncover the molecular etiology of this disease to provide targeted therapeutic options for patients.

CHAPTER 7

Samenvatting

Het mechanistisch target van rapamycine (mTOR)-eiwit is de centrale regelaar van celstofwisseling. Het eiwit komt voor in twee eiwitcomplexen, genaamd mTORC1 en mTORC2, die samenwerken om de groei, energiehuishouding, en overleving van cellen te waarborgen. Vanwege deze belangrijke rol wordt de activiteit van mTOR nauwkeurig gereguleerd door verschillende signalen, waaronder groeifactoren en aminozuren.

De Rag GTPase-familie werkt als een sensor die detecteert of er aminozuren aanwezig zijn. De Rag-familie bestaat uit vier leden: RagA, B, C en D. Wanneer aminozuren aanwezig zijn, bindt RagA of RagB aan GTP, terwijl RagC of RagD aan GDP bindt. Ze vormen dan samen een complex dat mTORC1 naar het lysosoom brengt en activeert. Na activatie stimuleert mTORC1 eiwitsynthese, transcriptie en vertstofwisseling, terwijl het autofagie (celafbraak) remt.

Recent zijn negen families gevonden met een genetische afwijking in het RagD eiwit. Patiënten met deze ziekte hebben afwijkingen aan de nierbuisjes en gedilateerde cardiomyopathie (dilated cardiomyopathy; DCM). Hierdoor verliezen de patiënten te veel magnesium in de urine (hypermagnesiurie) en ontstaat een tekort in het bloed (hypomagnesiëmie). De ziekte heeft hieraan zijn naam te danken: autosomaal dominante nierhypomagnesiëmie door *RRAGD*-mutaties (ADKH-*RRAGD*)

ADKH-*RRAGD*

ADKH-*RRAGD* werd voor het eerst beschreven in 2020. Kenmerkende symptomen zijn niertubulopathie, bestaande uit hypomagnesiëmie, hypokaliëmie, hypercalciurie en nefrocalcinose, evenals DCM. De oorzaken van deze ziekte zijn nog onbekend. Eerdere studies hebben aangetoond dat de GTP-binding van RagD verstoord is, waardoor RagD voortdurend actief blijft. Er is nog onvoldoende kennis over hoe deze *RRAGD*-varianten de mTORC1 signalering beïnvloeden. Daarom is het belangrijk om te begrijpen welke factoren van invloed zijn op het ziekteverloop. In deze thesis richten we ons op het begrijpen van het pathomechanisme van ADKH-*RRAGD*. Een specifiek doel was om de cellulaire gevolgen van *RRAGD*-varianten te identificeren en mogelijke therapieën te onderzoeken.

RRAGD-varianten veroorzaken permanente activatie van mTORC1-signalering

Eerdere studies tonen aan dat RRAGD-varianten overactiviteit van mTORC1-signalering veroorzaken. Omdat de literatuur hierover tegenstrijdig is, hebben wij onderzocht hoe deze varianten mTORC1-signalering beïnvloeden. In **hoofdstuk 2 en 4** onderzochten we de effecten van *RRAGD*-varianten p.(Ser76Leu), p.(Ser77Phe), p.(Thr91Ile) en p.(Ile100Arg) op de reactie van mTORC1 na stimulatie met aminozuren. Na stimulatie was mTORC1-signalering in cellen met *RRAGD*-varianten vergelijkbaar met wildtype (WT) cellen. Bij afwezigheid van aminozuren bleef transcriptiefactor EB (TFEB) gefosforyleerd (alternatieve mTORC1-signalering) in cellen met varianten p.(Ser76Leu), p.(Ser77Phe) en p.(Ile100Arg). S6 kinase (S6K)-fosforylatie was alleen verhoogd in de p.(Ser76Leu)-variant ten opzichte van WT. Slechts een bepekte verhoging werd veroorzaakt door de p.(Ser77Phe) en p.(Ile100Arg)-varianten. S6K is onderdeel van de klassieke mTORC1-signalering. De p.(Ser76Leu)-variant is de meest voorkomende variant en het sterkst geassocieerd met DCM. De p.(Thr91Ile) mutatie beïnvloedde de mTORC1-signalering niet. Hiermee bevestigden wij dat RRAGD-varianten leiden tot permanente activatie van mTORC1 signalering. Daarnaast suggereren onze bevindingen dat de mate van mTORC1-activatie mogelijk samenhangt met de ernst van het ziektebeeld.

RRAGD-varianten veroorzaken verminderde hartfunctie in ADKH-*RRAGD*

Om te begrijpen hoe *RRAGD*-varianten een verminderde hartfunctie veroorzaken, gebruikten we in **hoofdstuk 3** een zebravismodel. Zebravis embryo's werden geïnjecteerd met mRNA van *RRAGD* WT, p.(Ser76Leu) of p.(Pro119Arg). Na drie dagen vertoonde de zebravis embryo's geïnjecteerd met *RRAGD*-varianten hartfunctiestoornis. Dit kwam tot uiting als pericardiaal oedeem, gemeten door lagere fractionele verkorting en ejectiefractie. Hiermee tonen we aan dat *RRAGD*-varianten daadwerkelijk bijdragen aan de ontwikkeling van hartafwijkingen. Om de moleculaire mechanismen van DCM verder te begrijpen, genereerden we in **hoofdstuk 4** humane geïnduceerde pluripotente stamcellen (hiPSC's) met een heterozygote *RRAGD* p.(Ser76Leu) mutatie en differentieerden deze tot cardiomyocyten (hiPSC-CMs). mTORC1-signalering was onverstoord in deze cellen. Echter, mutant-hiPSC-CM vertoonden een verlengde duur van de Ca^{2+}-transiënt. Dit suggereert een vertraagde afgifte en verwijdering van Ca^{2+} uit het cytosol. Bulk RNA-sequencing resultaten lieten veranderingen in genexpressie zien: verhoogde

expressie van genen betrokken bij de organisatie van het cytoskelet en verminderde expressie van genen betrokken bij de spierontwikkeling. Dit wijst erop dat cardiomyocyten met de *RRAGD* p.(Ser76Leu)-variant een minder gedifferentieerd fenotype vertonen. We vermoeden dat dit komt door de rol die mTORC1 speelt bij het in balans houden van proliferatie en differentiatie van cardiomyocyten.

De rol van NKCC2 en NCC in ADKH-*RRAGD*

De niertubulopathie bij ADKH-*RRAGD* vertoont overeenkomsten met familiale hypomagnesiëmie met hypercalciurie en nefrocalcinose (FHHNC), evenals met een combinatie van Bartter type III en het syndroom van Gitelman. Dit wijst erop dat pathogene RagD-varianten leiden tot een defect in de dikke stijgende buis van de lus van Henle (thick ascending limb; TAL) en het distaal convoluut (distal convoluted tubule; DCT). RagD komt vooral voor in deze nefronsegmenten van de muis. In deze segmenten wordt het transport van Mg^{2+}, Ca^{2+} en K^{+} beïnvloed door de Na^{+}-reabsorptie. In de TAL wordt Na^{+}-reabsorptie gefaciliteerd door de Na^{+}-K^{+}-$2Cl^{-}$-cotransporteur 2 (NKCC2). In de DCT wordt dit gedaan door de Na^{+}-Cl^{-}-cotransporteur (NCC). Om de werking van NKCC2 en NCC te evalueren, kregen ADKH-*RRAGD*-patiënten uit een familie met de p.(Thr97Pro)-variant in **hoofdstuk 2** de diuretica furosemide en hydrochloorthiazide (HCT) voorgeschreven. Furosemide remt de NKCC2 in de TAL, terwijl HCT de NCC in de DCT remt. De fractionele excreties van Cl^{-} en Mg^{2+} bij patiënten was vergelijkbaar met gezonde controles, wat suggereert dat NKCC2 en NCC normaal functioneren in deze patiënten.

Klinische implicaties en therapeutische perspectieven

Het onderzoek beschreven in **hoofdstuk 2** heeft geleid tot een betere karakterisering van het fenotype van ADKH-*RRAGD*-patiënten. Hierin onderzochten we een nieuw cohort van twaalf ADKH-*RRAGD*-patiënten met bekende varianten en drie nieuwe varianten, p.(Ser77Phe), p.(Thr91Ile) en p.(Ile100Arg). In dit cohort was niertubulopathie het meest prominente fenotype. In combinatie met eerdere rapportages zijn er tot nu toe 36 ADKH-*RRAGD*-patiënten geïdentificeerd. Naast niertubulopathie is bij de helft van de patiënten sprake van DCM. De variant p.(Ser76Leu) komt het meest voor en werd aangetroffen bij acht patiënten. Bovendien vertegenwoordigt deze variant een mutatie-hotspot die vooral geassocieerd is met DCM. In 5 van de 8 patiënten met deze variant ontwikkelde DCM. Verder zagen we dat, hoewel DCM meestal al tijdens de kindertijd ontstaat,

er ook patiënten zijn bij wie dit pas in het tweede levensdecennium optrad. Dit geeft aan dat het monitoren van de hartfunctie bij patiënten met niertubulopathie ook op volwassen leeftijd nog belangrijk is. In toekomstige studies zal het identificeren van meer patiënten helpen om andere factoren die het ziekteverloop beïnvloeden in kaart te brengen, zoals geslacht. Tot slot kregen alle huidige patiënten pas een genetische diagnose nadat de niertubulopathie klinisch was vastgesteld. Het bestaan van patiënten met geïsoleerde niertubulopathie (zonder DCM) suggereert echter dat niertubulopathie en DCM onafhankelijk van elkaar kunnen optreden. Daarom zou *RRAGD* niet alleen in het diagnostische genenpanel voor niertubulopathieën, maar ook voor cardiomyopathieën van idiopathische oorsprong opgenomen moeten worden, zodat meer patiënten een genetische diagnose kunnen ontvangen.

ADKH-*RRAGD*-patiënten krijgen momenteel magnesium- en kaliumsupplementen voorgeschreven om hypomagnesiëmie en hypokaliëmie te behandelen. Om hartfalen te manegen, worden RAS-, SGLT2- en ACE-remmers voorgeschreven. Dit benadrukt dat er momenteel geen gerichte therapie beschikbaar is. Deze dissertatie evalueert therapeutische opties voor ADKH-*RRAGD*-patiënten. In **hoofdstuk 2** zorgde een behandeling van 15 dagen met dapagliflozine voor een vermindering van hypomagnesiëmie bij patiënten. **Hoofdstuk 3** beschrijft hoe de mTORC1-remmer rapamycine een vermindering van de hartfunctie kan voorkomen in zebravis embryo's die *RRAGD*-varianten tot expressie brengen. Deze dissertatie onderzocht echter niet via welke moleculaire mechanismen dapagliflozine en rapamycine deze symptomen verminderden. Toekomstig onderzoek zou zich daarom moeten richten op het verder ophelderen van de moleculaire mechanismen achter deze ziekte, met als doel om gerichte therapeutische interventies voor patiënten te ontwikkelen.

CHAPTER 8

Kesimpulan

Target mekanistik dari rapamycin (mTOR) merupakan regulator utama pertumbuhan dan proliferasi sel. Dua kompleks protein mTOR, yaitu mTORC1 dan mTORC2, bekerja sama untuk memastikan pertumbuhan sel, metabolisme, serta kelangsungan hidup sel. Karena peran sentralnya, mTOR diregulasi secara ketat oleh berbagai sinyal metabolik, seperti faktor pertumbuhan dan asam amino. Famili protein Rag GTPase berfungsi sebagai sensor asam amino intraseluler untuk aktivasi mTORC1. Rag GTPase terdiri dari empat anggota: RagA, RagB, RagC, dan RagD. Keberadaan asam amino dalam sel memicu rentetan proses proses yang melibatkan protein-protein Rag GTPase; RagA dan RagB mengikat GTP, sedangkan RagC dan RagD mengikat GDP. Selanjutnya, RagA atau RagB membentuk kompleks heterodimer bersama RagC atau RagD. Kompleks Rag GTPase ini berperan untuk merekrut mTORC1 ke permukaan lisosom. Proses ini memicu aktivasi mTORC1, mengakibatkan rentetan aktivasi dari protein-protein yang ada di bawah kendali mTORC1. Jalur persinyalan mTORC1 menginduksi perubahan dalam regulasi sintesis protein, transkripsi, sintesis lipid, serta menghambat autofagi. Karena peran sentral Rag GTPase dalam aktivasi mTORC1, varian patogenik pada gen-gen ini diasosiasikan dengan berbagai penyakit manusia; Studi-studi terbaru menunjukkan bahwa varian *missense* heterozigot pada *RRAGD* menyebabkan tubulopati ginjal dan kardiomiopati dilatasi. Penyakit langka yang baru ini sekarang disebut hipomagnesemia ginjal dominan autosomal dengan varian *RRAGD* (*autosomal dominant kidney hypomagnesemia with RRAGD variants*; ADKH-*RRAGD*).

ADKH-*RRAGD*

Kasus pertama ADKH-*RRAGD* dilaporkan pada tahun 2020. Manifestasi klinis utama penyakit ini berupa kardiomiopati dilatasi dan tubulopati ginjal. Tubulopati ginjal pada ADKH-*RRAGD* dicirikan dengan keberadaan hipomagnesemia, hipokalemia, hiperkalsiuria, dan nefrokalsinosis. Meskipun manifestasi klinis dari ADKH-*RRAGD* telah dimengerti, mekanisme klinis dan molekuler penyakit ini masih belum dipahami. Studi awal mengenai ADKH-*RRAGD* menunjukkan bahwa varian yang ditemukan pada pasien mengacaukan kemampuan protein RagD untuk mengikat GTP. Hal ini dapat menyebabkan dua perubahan pada RagD: RagD yang tidak mengikat nukleotida, dan RagD yang terus berikatan dengan GDP. Kedua perubahan ini menyebabkan aktivasi RagD secara konstitutif. Akan tetapi, bagaimana variasi dari gen *RRAGD* memengaruhi sinyal mTORC1 dan berkontribusi pada patogenesis penyakit masih belum dipahami sepenuhnya. Terlebih lagi, studi menunjukkan keberadaan heterogenitas alelik dan fenotipik antar pasien. Oleh karena itu, faktor-faktor yang mempengaruhi perkembangan penyakit ini perlu

dipahami lebih lanjut. Dalam disertasi ini, kami berfokus memahami patogenesis ADKH-*RRAGD*. Fokus utama studi ini adalah mengidentifikasi konsekuensi seluler dari varian *RRAGD* serta mengeksplorasi potensi terapi bagi pasien.

Varian dari gen *RRAGD* mengaktifkan pensinyalan mTORC1 secara konstitutif

Studi sebelumnya menunjukkan bahwa varian *RRAGD* menyebabkan hiperaktivasi mTORC1. Namun, hasil yang bervariasi mendorong kami untuk mengklarifikasi bagaimana varian *RRAGD* mempengaruhi sinyal mTORC1. Dalam **bab 2 dan 4**, kami menyelidiki bagaimana mTORC1 merespons stimulasi asam amino dibawah kendali varian p.(Ser76Leu), p.(Ser77Phe), p.(Thr91Ile), dan p.(Ile100Arg) dari gen *RRAGD*. Kami menemukan bahwa dalam kondisi kaya asam amino, sinyal mTORC1 pada sel yang mengekspresikan varian *RRAGD* mirip dengan sel yang mengekspresiken tipe-liar (*wild type*; WT) *RRAGD*. Namun, saat sel kekurangan asam amino, varian p.(Ser76Leu), p.(Ser77Phe), dan p.(Ile100Arg) menyebabkan tetap berlangsungnya fosforilasi terhadap faktor transkripsi EB (*transcription factor EB*; TFEB), atau dikenal juga sebagai sinyal mTORC1 non-kanonik. Selain itu, hanya varian p.(Ser76Leu) yang menunjukkan peningkatan signifikan dalam fosforilasi S6 kinase (S6K). S6K merupakan bagian dari sinyal mTORC1 kanonik. Sementara itu, varian p.(Ser77Phe) dan p.(Ile100Arg) hanya menunjukkan peningkatan minor terhadap fosforilasi S6K. Di sel WT, tidak adanya asam amino menyebabkan hilangnya fosforilasi TFEB dan S6K. Temuan ini selaras dengan fakta bahwa p.(Ser76Leu) merupakan varian paling umum sejauh ini. Terlebih lagi, pasien dengan varian ini paling banyak mengalami kardiomiopati dilatasi dibandingkan dengan varian-varian lainnya. Menariknya, varian *RRAGD* p.(Thr91Ile) tidak mengubah sinyal mTORC1. Hal ini sesuai dengan fenotip pasien yang lebih ringan. Dengan demikian, kami mengonfirmasi bahwa varian-varian dari gen *RRAGD* menyebabkan aktivasi jalur pensinyalan mTORC1 secara konstitutif. Selain itu, tingkat aktivasi mTORC1 kemungkinan berkorelasi dengan keparahan penyakit.

Varian *RRAGD* sebagai penyebab disfungsi jantung pada ADKH-*RRAGD*

Untuk memahami bagaimana varian *RRAGD* menyebabkan disfungsi jantung pada pasien, kami menggunakan model embrio ikan zebra dalam **Bab 3**. Kami menyuntikkan embrio dengan RNA duta atau *messenger* RNA (mRNA) *RRAGD* WT, p.(Ser76Leu), atau p.(Pro119Arg). Tiga hari pasca fertilisasi, larva ikan zebra yang

mengekspresikan varian *RRAGD* menunjukkan pembengkakan perikardium dan penurunan fungsi jantung. Hal ini bisa dilihat dari penurunan *fractional shortening* dan *ejection fraction*. Hasil ini mengonfirmasi patogenisitas varian *RRAGD* di jantung. Di **bab 4**, kami juga menggunakan sel induk pluripoten diinduksi dari manusia (*human induced pluripotent stem cells*; hiPSCs) yang mengekspresikan heterozigot p.(Ser76Leu). Lalu, sel-sel ini didiferensiasi lebih jauh menjadi kardiomiosit (*hiPSC-derived cardiomyocytes*; hiPSC-CMs). Di model ini, meskipun sinyal mTORC1 tidak berubah, uji elektrofisiologi menunjukkan bahwa hiPSC-CMs mutan memiliki durasi transien Ca^{2+} lebih lama dibandingkan hiPSC-CMs WT. Ini menandakan bahwa varian *RRAGD* menyebabkan gangguan pelepasan dan pembersihan Ca^{2+} intraseluler. Analisis RNA-seq menunjukkan perubahan ekspresi beberapa gen. Gen-gen yang terkait dengan organisasi sitokeleton, matriks ekstraseluler, dan adhesi sel-sel mengalami peningkatan regulasi. Sementara gen-gen terkait perkembangan otot mengalami penurunan regulasi. Ini menandakan bahwa varian p.(Ser76Leu) menyebabkan fenotip kardiomiosit yang kurang berdiferensiasi, kemungkinan akibat gangguan keseimbangan proliferasi dan diferensiasi yang diatur oleh mTORC1.

Peran NKCC2 dan NCC dalam ADKH-*RRAGD*

Tubulopati ginjal pada pasien ADKH-*RRAGD* menunjukkan kemiripan dengan hipomagnesemia familial dengan hiperkalsiuria dan nefrokalsinosis (*familial hypomagnesemia with hypercalciuria and nephrocalcinosis*; FHHNC) serta campuran antara Bartter sindrom tipe III dan Gitelman sindrom. Ini mengindikasikan bahwa varian patogenik RagD menyebabkan disfungsi pada cabang asenden tebal dari lengkung Henle (*thick ascending limb*; TAL) dan tubulus kontortus distal (*distal convoluted tubule*; DCT). Memang, di nefron tikus, protein RagD diekspresikan di dua segmen tersebut. Di TAL dan DCT, transport Mg^{2+}, Ca^{2+}, dan K^{+} dipengaruhi oleh reabsorpsi Na^{+}. Untuk mengevaluasi status reabsorpsi Na^{+} di TAL dan DCT, sejumlah pasien ADKH-*RRAGD* dari satu keluarga yang membawa varian p.(Thr97Pro) diberikan diuretik furosemide dan hydrochlorothiazide (HCT) pada **bab 2**. Furosemide menghambat Na^{+}-K^{+}-$2Cl^{-}$ cotransporter 2 (NKCC2) di TAL, sementara HCT menghambat Na^{+}-Cl^{-} cotransporter (NCC) di DCT. Kami menemukan bahwa fraksi ekskresi Mg^{2+} pada para pasien tersebut sebanding dengan populasi kontrol sehat. Ini menunjukkan bahwa fungsi NKCC2 dan NCC di pasien-pasien tersebut adalah normal.

Implikasi klinis dan perspektif terapi

Disertasi ini memperluas karakterisasi fenotipe pasien ADKH-*RRAGD* pada **bab 2**. Di sini, kami mendeskripsikan satu kohor baru yang terdiri dari dua belas pasien. Pasien-pasien tersebut membawa beberapa varian yang telah teridentifikasi sebelumnya, dan tiga varian baru, yaitu p.(Ser77Phe), p.(Thr91Ile), dan p.(Ile100Arg). Dalam kohor ini, tubulopati ginjal tetap menjadi fenotipe yang paling menonjol pada semua pasien. Hingga saat ini, total 36 pasien ADKH-*RRAGD* telah teridentifikasi. Di seluruh pasien tersebut, kardiomiopati dilatasi ditemukan pada setengah dari pasien. Sampai sekarang, varian p.(Ser76Leu) merupakan varian yang paling sering ditemukan, yaitu pada 8 pasien. Selain itu, varian ini juga merupakan *hotspot* mutasi yang paling dikaitkan dengan kardiomiopati dilatasi, di mana 5 dari 8 pasien yang membawa varian ini mengalaminya. Menariknya, kami menemukan bahwa meskipun kardiomiopati dilatasi umumnya berkembang pada masa kanak-kanak, beberapa pasien baru mengalaminya pada dekade kedua kehidupan. Hal ini menunjukkan bahwa pada pasien dengan tubulopati ginjal, pemantauan fungsi jantung saat dewasa sangatlah penting. Pada penelitian mendatang, identifikasi lebih banyak pasien akan membantu menentukan faktor-faktor lain yang mempengaruhi perkembangan penyakit, seperti jenis kelamin. Selain itu, semua pasien saat ini didiagnosis secara genetik setelah diagnosis tubulopati ginjal. Namun, keberadaan pasien hanya dengan tubulopati ginjal (tanpa kardiomipati dilatasi) menunjukkan bahwa tubulopati ginjal dan kardiomipati dilatasi dapat terjadi secara independen satu sama lain. Oleh karena itu, *RRAGD* harus dimasukkan tidak hanya dalam panel gen tubulopati ginjal, tetapi juga dalam panel kardiomiopati idiopatik untuk membantu lebih banyak pasien mendapatkan diagnosis genetik.

Saat ini, pasien ADKH-*RRAGD* menerima suplementasi magnesium dan kalium untuk mengatasi hipomagnesemia dan hipokalemia, serta inhibitor RAS, SGLT2, dan ACE untuk gagal jantung. Hal ini menyoroti ketiadaannya terapi yang spesifik dan tertarget. Disertasi ini juga mengevaluasi opsi terapeutik untuk pasien ADKH-*RRAGD*. Pada **bab 2**, pengobatan dengan dapagliflozin selama 15 hari berhasil memperbaiki hipomagnesemia pada pasien. **Bab 3** menunjukkan bahwa pengobatan dengan inhibitor mTORC1, rapamycin, pada embrio ikan zebra yang mengekspresikan varian *RRAGD* secara berlebih mencegah disfungsi jantung. Namun, disertasi ini tidak mengeksplorasi lebih lanjut mekanisme molekuler bagaimana dapagliflozin dan rapamycin meredakan gejala. Oleh karena itu, penelitian di masa depan harus bertujuan untuk mengungkap etiologi molekuler penyakit ini agar dapat menyediakan pilihan terapi yang tertarget bagi pasien.

CHAPTER 9

Appendices

List of abbreviations

Research data management

About the author

List of publications

PhD portfolio

List of abbreviations

#	
2D	2-dimentional
3D	3-dimentional
4E-BP1	Eukaryotic initiation factor 4E-binding protein 1
A	
AA	Amino acid
AAV	Adeno-associated virus
ACMG-AMP	American College of Medical Genetics and Genomics and the Association for Molecular Pathology
ADKH-RRAGD	Autosomal dominant kidney hypomagnesemia with *RRAGD* variants
AF	Atrial fibrillation
AGC	A, G, and C kinases
AKI	Acute kidney injury
Akt	Protein kinase B
AMPK	5' adenosine monophosphate-activated protein kinase
ANOVA	Analysis of variance
APD	Action potential duration
ASO	Antisense oligonucleotide
ATP	Adenosine triphosphate
B	
Bp	Base pair
Bpm	Beats per minute
BSA	Bovine serum albumin
C	
Ca^{2+}	Calcium ion
Cas9	CRISPR-associated protein 9
CaSR	Ca^{2+} sensing receptor
CASTOR1	Cellular arginine sensor of mTORC1
cDNA	Complementary DNA
CKD	Chronic kidney disease
Cl^-	Chloride ion
CLDN14	Claudin-14
ClC-KB	Chloride channel Kb
CLEAR	Coordinated Lysosomal Expression and Regulation
cRNA	Complementary RNA
CRISPR	Clustered regularly interspaced short palindromic repeats
CRT-D	Cardiac resynchronization therapy-defibrillator
CTD	Ca^{2+} transient duration
D	
Dapa	Dapagliflozin
DAPI	4',6-diamidino-2-phenylindole
DCM	Dilated cardiomyopathy
DCT	Distal convoluted tubule
DEG	Differentially expressed gene
DEPTOR	DEP domain containing mTOR interacting protein
DMEM	Dulbecco's Modified Eagle Medium
DMSO	Dimethyl sulfoxide
DNA	Deoxyribonucleic acid
DNM1	Dynamin-1
Dpf	Day post-fertilization
DTT	Dithiothreitol
E	
E8	Essential 8
ECM	Extracellular matrix
EDTA	Ethylenediaminetetraacetic acid
EDV	End diastolic volume
EF	Ejection fraction
EHT	Engineered heart tissue

ES	Exome sequencing
ESV	End systolic volume
Erk	Extracellular signal-regulated kinase

F

FACS	Fluorescence-activated cell sorting
FBS	Fetal bovine serum
FDR	False discovery rate
FE	Fractional excretion
FHHNC	Familial hypomagnesemia with hypercalciuria and nephrocalcinosis
FKBP12	12-kilo Dalton FK506-binding protein
FLCN	Folliculin
FNIP1	FLCN-interacting protein 1
FNIP2	FLCN-interacting protein 2
FS	Fractional shortening

G

GAP	GTPase-activating protein
GAPDH	Glyceraldehyde-3-phosphate dehydrogenase
GATOR1	GAP towards TOR complex 1
GATOR2	GAP towards TOR complex 2
GDP	Guanosine diphosphate
GEF	Guanosine-nucleotide exchange factor
GEO	Gene Expression Omnibus
GFP	Green fluorescent protein
GO	Gene ontology
gRNA	Guide RNA
GRCh38.p14	Genome Reference Consortium Human Build 38 patch release 14
GSDB	Goat serum dilution buffer
GTP	Guanosine triphosphate

H

HBSS	Hanks' Balanced Salt Solution
HCT	Hydrochlorothiazide
HEK293	Human embryonic kidney 293 cells
HeLa	Henrietta Lacks cells
HGNC	HUGO Gene Nomenclature Committee
hiPSC	Human induced pluripotent stem cell
hiPSC-CM	hiPSC-derived cardiomyocyte
Hpf	Hour post-fertilization
HT	Heart transplantation

I

IB	Immunoblotting
ICC	Immunocytochemistry
IF	Immunofluorescence
IRS	Insulin receptor substrate

J

K

K^+	Potassium ion
Kb	Kilobase
kDa	Kilodalton
KEGG	Kyoto Encyclopedia of Genes and Genomes
Kir4.1	Inwardly rectifying K^+ channel 4.1
Kir5.1	Inwardly rectifying K^+ channel 5.1
KO	Knockout
KT	Kidney tubulopathy

L

LA	Left atrium
LV	Left ventricle
LVEDD	Left ventricle end diastolic dimension
LVEF	Left ventricle ejection fraction

M

MAPK	Mitogen-activated protein kinase
Mg^{2+}	Magnesium ion
MiT/TFE	Microphthalmia/transcription factor E
mLST8	Mammalian lethal SEC13 protein 8
MO	Morpholino
mRNA	Messenger RNA
mTOR	Mechanistic target of rapamycin
mTORC1	Mechanistic target of rapamycin complex 1
mTORC2	Mechanistic target of rapamycin complex 2

N

Na^+	Sodium ion
NA	Numerical aperture
NANOG	Homeobox protein NANOG
NCC	Na^+-Cl^- cotransporter
NKCC2	Na^+-K^+-2Cl cotransporter 2
NYHA	New York Heart Association

O

OCT3/4	Octamer-binding transcription factor 4
OMIM	Online Mendelian Inheritance in Man

P

p-4E-BP-1	Phosphorylated 4E-BP1
p-Akt	Phosphorylated Akt
PBS	Phosphate buffered saline
PCR	Polymerase chain reaction
PDB	Protein data bank
PDK1	Pyruvate dehydrogenase kinase 1
PI3Ks	Phosphoinositide 3 kinases
PIP_3	Phosphatidylinositol-3, 4, 5-triphosphate
PIP_2	Phosphatidylinositol-4, 5-bisphosphate
PKCα	Protein kinase Cα
PKD1	Polycystin 1
PMSF	Phenylmethylsulfonyl fluoride
P.o.	*Per os*
PO	Peroxidase
PRAS40	Akt substrate of 40-kilo Dalton
Protor1	Protein observed with RICTOR 1
Protor2	Protein observed with RICTOR 2
p-S6K	Phosphorylated S6K
p-TAZ	Phosphorylated TAZ
p-TFEB	Phosphorylated TFEB
PVDF	Polyvinylidene fluoride

Q

R

RA	Right atrium
RRAGA/ RagA	Ras-related GTP binding protein A
RRAGB/ RagB	Ras-related GTP binding protein B
RRAGC/ RagC	Ras-related GTP binding protein C
RRAGD/ RagD	Ras-related GTP binding protein D
Rapa	Rapamycin
Raptor	Regulatory-associated protein of mTOR
RAS	Renin-angiotensin system

Rheb	RAS homologue enriched in brain
Rictor	Rapamycin-insensitive companion of mTOR
RNA	Ribonuleic acid
RNA-seq	RNA sequencing
ROMK	Renal outer medullary K^+ channel
RPMI	Roswell Park Memorial Institute medium
RSK	Ribosomal s6 kinase
RT	Room temperature
RT-qPCR	Reverse transcriptase quantitative PCR
RV	Right ventricle

S

S6K	S6 kinase
SCNA8	Na^+ voltage-gated channel alpha subunit 8
SCNA2	SCNA subunit 2
SDS	Sodium dodecyl sulfate
SDS-PAGE	SDS-polyacrylamide gel electrophoresis
SEM	Standard error of the mean
SGK1	Serum and glucocorticoid-induced protein kinase 1
SGLT2	Na^+-glucose cotransporter 2
Sin1	Stress-activated protein kinase-interacting protein 1
SNV	Single nucleotide variant
SOX-2	SRY box-2
SR	Sarcoplasmic reticulum
SREBPs	Sterol regulatory element binding proteins

T

TAL	Thick ascending limb
TAZ	Tafazzin
TBS	Tris buffered saline
TBS-T	TBS + 0.1% v/v Tween-20
TFEB	Transcription factor EB
TRPM6	Transient receptor potential melastatin type 6
TRPV5	Transient receptor potential cation channel subfamily V member 5
TSC1	Tuberous sclerosis complex 1
TSC2	Tuberous sclerosis complex 2

U

ULK1	Unc-51 like autophagy activating kinase 1
US	Ultrasound

V

V-ATPase	Vacuolar H^+-ATPase
v/v	Volume per volume
v/w	Volume per weight
VUS	Variants of uncertain significance

W

WB	Western blotting
WLL	White light laser
WT	Wild type

X

Y

Z

Research data management

All data presented in this thesis were collected and archived in compliance with the Findable, Accessible, Interoperable, and Reusable (FAIR) guidelines.[1]

Data for chapters 2 and 4 was obtained through laboratory experiments. Data for chapter 3 was from an animal experiment on zebrafish embryos, which conformed to the guidelines from Directive 2010/63/EU of the European Parliament on the protection of animals used for scientific purposes or the current NIH guidelines.

In chapter 2, patients' data and healthy controls (healthy controls were from a published dataset PMID: 29212860) were included. The studies followed relevant national and international legislation and regulations, guidelines, codes of conduct, and Radboudumc policy. We received only pseudonymized data from the clinicians involved. Therefore, the privacy of the participants in this chapter was warranted. Moreover, informed consents were obtained from the clinicians to collect and process their data for this research project. To preserve patients' confidentiality and privacy, data containing pseudonymized patient information and blood test results will be archived in a closed section on the departmental H-drive, which can only be accessed by the PI and project team members.

For all chapters, the experimental procedures, data, and analyses are stored in an electronic lab journal, Labguru. These materials are available and accessible to all lab members. Additionally, the data are also available on the internal Radboudumc H- and I-drives, as well as the Data Sharing Collections (DSC's) in the Radboud Data Repository. For the H- and I-drives, the file names correspond to the experimental numbering in Labguru, following the group's experimental numbering order. This is in accordance with the Findable principle. Digital experimental data are stored for a minimum of 10 years. Samples from *in vitro* data are kept until publication. Patient materials in chapter 2 were processed by the hospitals where the patients received care, and no materials were transferred or kept in our laboratory.

This thesis will be made publicly available through the Radboud University Thesis Repository. Chapter 3 has been published in the American Journal of Physiology Heart and Circulatory Physiology journal. Chapter 2 has been submitted to Kidney International Reports journal, which is an open access journal. Chapter 4 is in preparation and will be submitted to an open access journal. RNA sequencing raw data from chapter 4 will be published in an online open access database for high throughput sequencing results, Gene Expression Omnibus (GEO).

The table below details where the data and research documentation for each chapter can be found on the RDR. All data archived as a Data Sharing Collection remain available for at least 10 years after termination of the studies.

Chapter	Database	Data type	DOI/Identifier	Access
2	RDR	Raw data	10.34973/wmax-xv61	CC0-1.0
3	RDR	Raw data	10.34973/j6as-sj51	CC0-1.0
4	RDR	Raw data	10.34973/gy6d-7692	CC0-1.0
4	GEO	RNA-seq raw data		Open acess

GEO: gene expression omnibus

References

1. Wilkinson, M.D., et al., *The FAIR Guiding Principles for scientific data management and stewardship.* Sci Data, 2016. **3**: p. 160018.

About the author

Anastasia Adella was born in Jakarta, Indonesia, on September 7, 1996. Her passion for biology led her to pursue the G30 International Bachelor's Program in Biological Sciences at the University of Tsukuba in Tsukuba, Japan, from 2014 to 2018, where she was awarded the Tsukuba Scholarship. For her graduation research, she joined Dr. Hidekazu Kuwayama's laboratory, investigating the role of a potential Mg^{2+} transporter, MRS2, in *Dictyostelium discoideum*. In 2018, she continued her studies in the Research Master's Molecular Mechanisms of Disease at Radboud University in Nijmegen, the Netherlands. During her master's studies, she received both the Radboudumc Study Fund and the Radboud Scholarship. During her first master's internship, she investigated the mechanisms that couple sodium and magnesium transport in the distal convoluted tubule at Radboudumc, under the supervision of Dr. Gijs Franken and Dr. Jeroen de Baaij. Her second master's internship took place within the Mandrup-Poulsen group at the University of Copenhagen, where she examined the role of Clec16a as a master regulator of mitophagy in pancreatic β-cells, supported by the Erasmus+ Traineeship Grant. Adella actively participated in the Indonesian Student Associations in Tsukuba and Nijmegen throughout her studies.

Following the completion of her master's studies in 2020, Adella commenced her doctoral research at Radboudumc under the guidance of Prof. Dr. Joost Hoenderop and Dr. Jeroen de Baaij, co-supervised by Dr. Pieter A. Leermakers. Her doctoral research integrates her interests in rare diseases and cellular signaling pathways, focusing specifically on the role of the mTORC1 signaling pathway in the pathogenesis of autosomal dominant kidney hypomagnesemia linked to *RRAGD* variants. The findings of her doctoral research are compiled within this thesis. During this period, she had the opportunity to present her results at the Dutch Physiology Days held in Amsterdam, the Netherlands, as well as at an EMBO workshop on New Cardiobiology in Heidelberg, Germany. Throughout her trajectory, Adella has provided research internship supervision to four master's students from the Medical Biology and Biomedical Sciences programs.

List of publications

ORCID-ID: 0000-0001-5712-6112

Included in this thesis

1. **Adella A,** Jouret F, Madariaga L, Leermakers PA, Arango P, Ariceta G, Bjerre A, Bockenhauer D, Coccia P, Dhamija R, de Frutos F, Garcia-Castano A, van Katwijk SB, Lucas J, Möller T, Müller D, e Vairo FP, Raki M, Venselaar H, Wilke MVMB, Nijenhuis T, Hoenderop JGJ, de Baaij JHF. Novel RRAGD variants in autosomal dominant kidney hypomagnesemia and therapeutic perspectives. KI Reports.
2. **Adella A**, Tengku F, Arjona FJ, Broekman S, de Vrieze E, van Wijk E, Hoenderop JGJ, and de Baaij JHF. RRAGD variants cause cardiac dysfunction in a zebrafish model. Am J Physiol Heart Circ Physiol 327: H1187-H1197, 2024.
3. **Adella A**, and de Baaij JHF. mTOR signaling in renal ion transport. Acta Physiol (Oxf) 238: e13960, 2023.
4. **Adella A**, Leermakers PA, van Ham WB, de Ruiter H, Ilgutytė J, Hendrickx S, Nijland L, de Boer TP, van Rooij E, Hoenderop JGJ, de Baaij JHF. *RRAGD* p.(Ser76Leu) variant causes constitutive activation of mTORC1 and dysregulated expression of muscle development and cytoskeleton genes in cardiomyocytes. *Submitted*.

Not included in this thesis

1. **Adella A**, Gommers LMM, Bos C, Leermakers PA, de Baaij JHF, and Hoenderop JGJ. Characterization of intestine-specific TRPM6 knockout C57BL/6 J mice: effects of short-term omeprazole treatment. Pflugers Arch 477: 99-109, 2025.
2. Gommers LMM, Leermakers PA, van der Wijst J, Roig SR, **Adella A**, van de Wal MAE, Bindels RJM, de Baaij JHF, and Hoenderop JGJ. Butyrate reduces cellular magnesium absorption independently of metabolic regulation in Caco-2 human colon cells. Sci Rep 12: 18551, 2022.
3. Franken GAC*, **Adella A***, Bindels RJM, and de Baaij JHF. Mechanisms coupling sodium and magnesium reabsorption in the distal convoluted tubule of the kidney. Acta Physiol (Oxf) 231: e13528, 2021.

* Authors have contributed equally

PhD portfolio

PhD candidate:	Anastasia Adella
Department:	Medical BioSciences
PhD period:	15/10/2020-14/10/2024
PhD Supervisors:	Dr. Jeroen H.F. de Baaij and Prof. dr. Joost G.J. Hoenderop
PhD Co-supervisor:	Dr. Pieter A. Leermakers

Training activities	**Year(s)**	**Hour(s)**
Courses and workshops		
• Career development: "The Next Step in My Career"	2024	17.0
• R basics for data preparation and presentation	2023	20.0
• Radboudumc Scientific Integrity	2022	20.0
• Dutch Kidney Foundation Summer School	2022	28.0
• Project Management for PhD Candidates	2021	56.0
• Radboudumc Introduction Day	2021	14.0
• RIMLS - Introduction course "In the lead of my PhD"	2021	21.0
Lectures and seminars		
• Journal Club	2022-2024	28.0
• Research Integrity Rounds	2021-2024	3.5
• Renal disorders theme meetings	2020-2022	28.0
• Meet the Expert sessions	2021	5.6
• Radboud Research Rounds	2020-2021	5.6
Conferences		
• EMBO New Cardiobiology#	2024	35.0
• Dutch Physiology Days*	2022	14.0
• PhD retreats#	2021-2023	80.0
Teaching activities		
Supervision of internship students		
• Master Biomedical Sciences student Suzanne Hendrickx	2024	60.0
• Master Medical Biology student Levi Nijland	2023-2024	60.0
• Master Medical Biology student Judita Ilgutytė	2023	60.0
• Master Medical Biology student Sara B. van Katwijk	2022-2023	60.0
Teaching		
• Research Project – Faculty of Medical Sciences	2021-2023	98.0
• Meet the PhD – Faculty of Medical Sciences	2021	28.0
Total		**741.7**

* Oral presentation, # Poster presentation

ACKNOWLEDGEMENTS

Writing this section of my thesis now would not have been possible without the people who were there at the beginning, whom I met along the way, and who stayed with me until the end.

To my promotors, **Jeroen** and **Joost**, and co-promotor, **Pieter**.

Jeroen, you are the first person I would like to thank. Thank you for everything. Thank you for the valuable lessons you have taught me; it was a great pleasure to work with you over the past six years. I'm sorry that I thought you were French when you taught the MMD introduction course (because de Baaij is a very French name...). But in all seriousness, without you, I would not have done a PhD. After my very fun internship with the Goose, we wrote a grant proposal for my PhD project. Although we did not get the grant, I was somehow still able to infiltrate your group as a PhD candidate (yay!). The PhD journey was not easy, but I thoroughly enjoyed working with you. I'm sad that we no longer work together. I will miss you and our shenanigans talking about Willem (not so) behind his back. But don't worry, I will stick around and bother you with all my dogs and food stories!

Joost, you always had my back throughout my PhD journey. Whenever I needed support, you always ensured that I received it and encouraged me to move forward. You are busy with all your activities, but somehow, you always make time for me. I appreciate your support throughout my PhD journey, Joost. Without you, I would not have such an amazing PhD project 😀

Pieter, my co-promotor!!! It was a great pleasure having you join my project as my daily-daily supervisor. You were first added to my project because I was experiencing issues with project management. You taught me how to plan my week, making it more efficient. However, I clearly needed you beyond project management due to your extensive knowledge and expertise. My PhD journey was not always a smooth sail, but together we pushed through, and we became a wonderful team! You are also always positive about me, so talking with you gives me confidence. I'm so glad that you could stay in the lab, as it would have been a great loss if you had to leave us. So, thank you for adopting me as your first PhD candidate! 😊

To all **collaborators** with whom I worked during my PhD, within and outside of Radboudumc.

Eva, thank you for being very open and helpful when we initially approached you to create a cardiomyocyte model. I would also like to thank you for sharing your

knowledge and allowing me to join your lab temporarily. It was a great experience to visit your lab almost every day to generate the cell model and meet your lab members. **Hesther**, thank you for taking the time to work with me intensively at the beginning of our project. I enjoyed working with you for the several months that I was coming back and forth to Hubrecht. **Eirini**, **Suji**, **Thomas**, and other Eva's group members, thank you for welcoming me into your lab. It was also nice to attend the EMBO together in Heidelberg.

Teun, thank you for welcoming me to your lab in Utrecht for the functional measurements of the cardiomyocytes. **Willem**, although we only worked together a couple of times, it was nice working with you. Thank you for measuring my cardiomyocytes, analyzing the data, and explaining to me all the other sides of physiology.

Paco, together with Jeroen, you initiated the *RRAGD* in the zebrafish project and basically laid the foundation for this thesis. I must say, I am impressed and inspired by the way you managed your research data! It was very tidy, and I could locate all the data easily, which I also must thank you for.

Erwyn, Erik, and **Sanne,** our work together is included in chapter 3 and has been published! Thank you for making the rebuttal possible. **Sanne**, thank you for taking the time to inject zebrafish embryos for this project! It was a great experience working with you.

My time at the physiology lab would not have been memorable without my **colleagues**. I had a great time with everyone.

First and foremost, my dearest paranymphs, **Caro** and **Willem**. I hope the way I "proposed" to you guys is forever etched in your memory.

Caro, CB!!! I remember the first time we met; I was visiting the lab for the second time as a future student of Gijs (it was fixed, but I had not started yet). You guys were having a coffee break, and Gijs introduced us. We did not immediately become friends as I was a student of the lowest rank, and you were of the highest rank as a technician, according to Wouter's lab hierarchy. And then I started my PhD, and we started to vibe together. Shenanigans in and outside of the lab, our love for (dark) jokes and food and dogs and good music, and the rest is history. Thank you for always being there for me. I know you always have my back. I am so glad to have you in my life and be friends with you! 💜

Willem, where do I even begin? I honestly do not remember how we became close. I just remember talking with you during MMD, and suddenly, we were friends. Maybe I initially forced you into becoming friends with me. I don't know. But I am very happy to have you in my life 💙. No words can explain. I'm also happy to serve as a memory box for you, haha. Thank you for always listening to all my complaints and uploading all those sequencing forms. Ah, we had so much fun together! It's sad that we don't work together anymore. However, we will stay in touch! You better start telling me stories without me asking 😊

PhDs gang, **Teodora, Emre,** and **Willem.** You guys were there since the beginning! We were there for each other from the start 😉. We had to change our group name several times, from 'New PhDs Gang' to 'Intermediate PhDs', and then to 'Senior PhDs'. Now, we are officially called the 'Retired PhDs Gang'. I would like to congratulate all of us for finishing this PhD journey at the same time (more or less). **Teodora**, my fellow girly PhD! You are a kind person, and your loyalty to those you care about is inspiring. Additionally, I'm always impressed by your organizational and negotiation skills. I'm happy to see that your small family has grown since you and Vlad welcomed Dana into the world. We stay in touch!!! P.S. You are one of the funniest people in the lab 💖. **Emre**, e-dawg, future CEO of a biotech company. Seeing you in the lab, working on 10 different projects simultaneously, supervising students, and securing grants was an everyday scene for most of us. Thank you for all the memeing moments we shared, silly jokes, and shared love for random comedy series. Good luck with your Postdoc journey, and also with Azar Innovations! Parkour for life!

Janneke, thank you for being a support system, not only to me, but also to the whole lab (now department!). Your calmness, efficiency, and organizational skills are top-notch, and I take you as an example 😀

Jojanneke, I remember our shared love for Indonesian food! Thank you for giving me the opportunity to teach bachelor's students during my PhD 😀 It was a great learning experience for me.

Femke, master of cloning, cell culture, database, and many more! You were always so helpful and made time for everyone who approached you for help. I'm glad that I could return the favor by helping you a little bit with CRISPR-Cas9 during my last months as a PhD candidate. I also enjoyed our coffee break conversations, and I found out you are a bit of a funny rebel yourself. Thank you, Femke!

Charlotte OH, we first met when I was a student and you had just started your PhD. When I joined the group, I was glad that you were still working on the same project. We were part of the Organoids team (although I did not work with organoids), but you made an effort to understand the entire mTORC1 pathway. I always admire your perseverance, cheerfulness, and assertiveness 💛

Idil, having you in the lab was like a miracle because you were our master of autophagy. Additionally, you are a very fun person, and we could connect on many different levels, beyond just science. I enjoyed our discussions not only about science, but also about food and TV series. I'm glad I could see you in Istanbul earlier this year and experience the amazing culinary and culture based on your recommendations. I wish you all the best with your future career!

Esra, we met when you were a student of Wouter, and then you became a member of the lab. I enjoyed our conversations together, your unexpectedly dark humor, all the reel sharing, food trips, and the Efteling trip! I wish you good luck with finishing your cool PhD project 😀

Lara, I must thank you for encouraging me to be vulnerable during my first PhD year! Because of this, I was able to allow myself to make mistakes and be imperfect. I wish you all the best for your future and with little Meike 😀

Charlotte (H), it was nice to have you join our lab! Thank you for providing me with valuable advice during my final year of the PhD. Good luck with the remaining of your Postdoc journey.

Lotte, my neighbor! I think you were one of the most helpful people in the lab to me. I always asked you so many questions, even how to do some calculations, and you kindly explained it all to me. Thank you for making my first PhD years easier. I also enjoyed our talks, your growing interests in Indonesian food, and more. Good luck with your new job! 😀

Eveline!!! You became my new neighbor after Lotte left, and you were the best neighbor I could have asked for. Us monopolizing the speaker to play pop, Disney, and theatrical songs was a fantastic time! And don't forget to turn the volume up when it's after 5 pm. Not only that, you were also a foodie, followed pop culture heavily, and a Harry Potter fan. Oh, amazing! The fact that you are a LOTR fan who occasionally plays chess did not bother me (grappig). I treasured the friendship we built in such a short time, and I know we will stay friends long after this. Not only

are you a cool person, but you are also a great scientist. I know you're on the right track, girl. Good luck with the rest of your PhD and your amazing career!

Guido, Guidi, my unit mate! How does it feel to be the most senior PhD in the lab now? Big responsibility, right? Thank you for being a great unit mate, Guido. I cherished our time together, sharing our lives, and thank you for sharing your wisdom with me. Also, your social skills will always inspire me haha. For the last time, I will finally say, Unit Five!

Heidi, my buddy! Thank you for guiding me through the initial phase of my PhD, although you were also new and still navigating it yourself. I enjoyed working with you, including the complaining and troubleshooting, as well as the ChIP-seq!

Faris, you have joined our lab as a Postdoc and started on the RRAGD project. I was very happy to know that I was no longer alone; moreover, you came from Malaysia, which is closer to home! I'm happy that you have grown comfortable living in the Netherlands with your little family. I enjoyed working with you on the RRAGD project and in the Organoids team! Good luck with the rest of your Postdoc journey 😀

Barnabas, when you first came to the lab I was still a student of Gijs. I remember you were an expert in physiology, but you were new to many of the techniques we use in the lab. But when I came back several months later, you'd mastered them! I always enjoyed talking with you about many things. Thank you for sharing your wisdom, pipette tips, and also your tips and tricks with me.

Valentina, Vale! Taking a Dutch course at the STEP together with you and Teodora was a fond memory! I think most of our memories together revolve around surviving the Netherlands post-PhD life. I'm happy we stayed in touch and checked in on each other every now and then. I know we will make it. We should not give up! ✨

Sylvia, your project management skills are top-notch. I secretly took an example from you, so I must thank you for that! It was also a lot of fun hanging out together, chatting, and sharing food. Good luck with your Postdoc!

Sara, my first student ever, and this is how I will remember you 😉. Thank you for teaching me early on how to be more organized, and thank you for always consistently following my ideas, even when they may have been boring. I'm happy you joined us as a PhD candidate! I always appreciate your sharp and witty humor. Good luck with the rest of your PhD! You will do great!

Gijs, Gidjes, Goose! Thank you for adopting me as your student and showing me what it's like to be a PhD student. Your dark humor and sarcasm never failed to make me laugh 😀 Thanks to you, I became the master of Western blotting. Just like the saying goes, something like "the student has become the master".

Jana, I want to thank you for being a helpful person in the lab. You are always ready to give someone a helping hand, really. You also took care of my cardiomyocytes during my vacation, so, thank you for that! I enjoyed spending time with you, going out for food, and visiting Efteling, Paris, and Disneyland. Let's go to Europapark for real! 😆 Good luck with the remaining of your PhD!

Wouter, Popeees! Thank you for making my PhD life more fun with all your shenanigans! I was really impressed that you've become such an adventurous person when it comes to food. I'm happy that you are living the life in Zurich. We meet again soon!

Lynette, Malou, Daan, Mark, and Maria, thank you for being a part of my PhD journey 😀 I enjoyed the conversations we have exchanged and the lessons learned.

Sem, Jopp, and Brenda, the new generation of PhDs 😀 I enjoyed hanging out with you during the last months of my PhD. Good luck with your PhD journeys, you guys are in good hands 🥰

To my students: **Sara, Judita, Levi, and Suzanne**. Working with you guys was definitely a highlight in my PhD journey! I truly enjoyed the experience, and thank you guys for joining my little project 😊 **Judita**, we started a bit messy, and you got a bit bored because of all the cloning you had to do. You also had little lab experience at the beginning, which made you less confident. But you pushed yourself and ultimately became the master of cloning, cell culture, cell line generation, and many more by the end of your internship! The cells you worked so hard for became the very solid foundation of my PhD thesis. P.S. Thank you for teaching me to be more organized, haha. **Levi**, I must again applaud you for your dedication, as you travel every day from Utrecht to Nijmegen for the internship. That was no easy feat! On top of all the traveling, you also managed to do like 100 Western blots and lots of qPCR. We achieved good results, but you were not satisfied, so you embarked on an exploration to perform immunofluorescence. We had to get used to each other at first, but in the end, it worked out well. I'm happy to know that you could do more translational research during your second internship (in Utrecht, too!). Good luck on your future endeavors! **Suzanne**, you were my last student! I remember

asking you if you could be a bit independent, since I was finishing up my PhD. You confidently said that you could, and you indeed could! As always, the project started a bit messy and was more on the exploratory side, but you didn't give up and made it work. I could leave you alone while you brainstorm with Pieter about how to develop the macro and take the best microscopic images for our project. I am happy to know that you became interested in cardiomyocytes and your second internship in Barcelona also used cardiomyocytes (in a more cardiology-focused lab, even!). We worked together very well, and there were also things I learned from you. So, thank you for that 😀 I wish you the best of luck for your future!

To **my family and friends**, who may not have a science background but have tried to understand my project and never stopped supporting me along the way.

Mba Yoyen, guru bahasa Belanda ku yang terkeren. Dankzij jou was ik ook bezig met Nederlandse les naast mijn onderzoek! Terima kasih sudah meluangkan waktu untuk ngajarin aku bahasa Belanda dan juga kumpul-kumpul mba. Semoga ke depannya kita tetap keep in touch 😀☺️

My MMD family, **Maren, Sadiksha, Alex, and Ajie**. I am grateful that we crossed paths. Thank you for the fun we had during MMD and PhD time. I hope to stay in touch with all of you.

Anes, Aqil, Ariq, Bella, teh Dina, Gytha, Livia, Shania, and Thiya makasih atas semua kebadutan kita yang menghibur gue di masa-masa sulit PhD. Next time jangan kapok main ke Nijmegen lagi dan jadi mbak nya Bilbi yaaa 🤡

Vrienden en vriendinnen van D'n Bult: **Dirk, Dirkje, Freek, Geert, Glenn, Iris, Lieke, Loet, Marly, Matia, Renske, Roel, Wessel, en Yorim**. Ik ben blij dat ik samen met jullie een gezellige tijd kan hebben, even pauze van mijn onderzoek. Bedankt voor het warme welkom!

Friends that I met in high school, **Chika, Cut, Dela, and Echa.** Teman-temanku yang selalu menginspirasi, mantra-mantra manifestasi, tapi ga lupa buat seneng-seneng. Makasih udah selalu dukung gue dan nyempetin buat ketemu tiap gue pulang ke Indo. You guys have made more impact in my life than you think 🥰

My oldest friends from middle school, **Aliq, Bunga, Carina, Dani, Dinda, Fraya, Ratih, Raras, Ruth, and Sastia**, yang nama grup nya berubah terus. Dan **Nisa,** temen SMA yang jatohnya kok geng SMP. Makasih buat selalu ngasih semangat,

memotivasi, dan suportif satu sama lain. Walaupun kalian susah ngerti apa yang gue kerjain tapi kalian tetep dukung gue! Love you, girls 🥰❤️

Dogo-dogo Nijmegen, **Ajie, Caecil, Daniel, Dennis, Mumu, Sabil, Vania, dan mas Iwap. Caecil, Sabil, mas Iwap**, walaupun kalian udah pindah dari Nijmegen/ Belanda, kalian tetap jadi bagian dari PhD gue. Makasih guys seru-seruannya. Lebih sering ketemu kali yaa 🤓. **Ajie, Daniel, Dennis, Mumu, dan Vania**, teman-teman daycare kuu! Tanpa kalian hidup ku di Belanda bagaikan makan sandwich pake keju setiap hari. Terima kasih support nya selama ini, semoga kita temenan terus sampai tua nanti. Beli rumah sebelahan yaa next.

Mijn liefste schoonfamilie: **Anja, Peter, Stijn, Loes, Jelle, en Lotte**. Dankzij jullie voel ik me hier in Nederland thuis. **Anja en Peter**, bedankt dat jullie mij in jullie familie hebben verwelkomd en voor de eindeloze steun voor Jesper en mij tijdens onze PhD's. Ik ben blij dat we nu wat meer tijd hebben om samen te zijn! 🥰

Ko Aarona, seneng deh kita deket lagi apalagi pas masa-masa PhD lomoi. Semoga kita ketemu lebih sering ya kohh, lav u 💖.

Papi, makasih ya pi udah selalu doain Adell!

My beloved, **Jesper Bergmans**. Meeting you was the best thing that happened during my PhD. Thank you for making half of my PhD journey even more wonderful. Thank you for encouraging me to step out of my comfort zone again and again (and I was comfortable). Thank you for pushing our little rascal, **Bilbo Barkins**, into our lives. I also cherished the memories we shared with **Sammie, Kevin, Scrappy, Coco, and Patches**. Thank you for showing me that life has more meaning. We are very different people, but our differences make us strong. Your coolheadedness and my high energy, that's a perfect combination. Ik hou van jou, and I am looking forward to our future together 💖.

To the two who were there since the beginning of it all, **Mami and kak Odre**. **Kak**, as much as I did not want to admit it, you are my role model. Dari jaman TK udah ngejar-ngejar ceceh sampe jatoh, maunya ngikutin terus. Makasih udah jadi role model terbaik buat lomoi! Your perseverance, creativity, and kindness inspire me to keep going. Walaupun dulu kita berantem terus, sekarang kita jadi the bestest of friends. Here's to many, many, many more adventures ahead, until we're old and grey. I'm happy that you're with **Sergio,** and I wish you two the best in life. P.S. Thank you for the beautiful thesis cover, you two! Proves my point about your creativity.

Mami, tanpa Mami, Adell ga bakal sampai di titik ini. Without a strong mother like you, we would not have made it this far. Mami bener-bener jadi role model Adell. Dari dulu Mami selalu dukung semua yang Adell mau, berusaha provide semua nya, walaupun ga gampang. Setiap Adell lagi merasa kesusahan, Adell selalu inget kata-kata Mami and that keeps me going. Everything I have achieved in life, I owe it all to you, Mami. Terima kasih Mami. Mami akan selalu jadi bagian dari semua yang Adell lakukan. Semoga Adell bisa terus buat mami bangga, dan bisa bahagiain Mami lebih lagi ya Mi. I will always keep you close in my heart, in every step of the way, forever.

Finally, to everyone I might have forgotten to mention, I would like to extend my sincere gratitude.

Thank you. Dank jullie wel. Terima kasih.

9 789465 151229 >

Radboudumc university medical center

IN·DEI·NOMINE·FELICITER

Radboud University